DEVELOPMENT OF AQUEOUS ATRP FOR BIOMEDICAL APPLICATIONS

Antonina Alekseyevna Simakova

Department of Chemistry

Carnegie Mellon University

September 2015

In partial fulfillment of the requirements for the Ph.D. degree in Chemistry

Acknowledgements

I would like to dedicate this dissertation to my family. I wouldn't be able to reach this point without the love and support from my parents, Alexey and Elizaveta Simakov. They have always taught me to be a curious and ambitious scientist, challenge myself and never give up. My brother Nikolay Simakov, being a true big brother, has been always a great example and paved the way for me to come here to get my PhD. I am so thankful to my husband Jacob Mohin for his incredible love and care for me. Going hand in hand during our PhD made it one of the greatest experiences in my life.

I would like to express my deepest and sincerest gratitude to my advisor Prof. Krzysztof Matyjaszewski. His incredible passion for science and knowledge guided and encouraged me throughout my time as a PhD student. I want to thank him for teaching me how be a good scientist: thinking critically and creatively, being dedicated to your work, and always think what you can do better.

Special thank you goes to Dr. Jim Spanswick for his great insights into my work and his tireless help in editing my papers, presentations, and dissertation.

I would like to thank all my committee members: Prof. Newell Washburn and Prof. Robert Tilton for their great feedback during all my PhD study milestones, Prof. Kevin Noonan and Prof. Brent Sumerlin for joining my committee for my final examination.

I am very grateful to all my collaborators on all my projects, who are mentioned in the Preface section to each Chapter.

I would like to thank my mentors and collaborators Dr. Andrew Magenau and Dr. Dominik Konkolewicz for the great discussions and productive and creative work together.

Dr. Saadyah Averick has been a great collaborator, officemate and a friend – we discussed and worked together on so many research ideas, problems and solutions. Being a member of a Matyjaszewski Group was a great experience and I was very lucky to meet so many amazing people. I would like to thank all former and present Matyjaszewski Group members. I am especially thankful to Dr. Hong Cho, Dr. Kristin Schroeder, Melissa Lamson, Dr. Katarzyna Wegner, Sangwoo Park, Dr. Mingjiang Zhong, Seiji Okada, Dr. Hangjun Ding, Dr. Valerie Williams, Dr. Maciek Kopec, Dr. Amir Khabibulin, Dr. Penglin Ye, Dr. Antoine Beziau, Matthew Mackenzie, Tom Ribelli, Pawel Krys, Sipei Li and Sushil Lathwal.

I also would like to thank Prof. Roberto Gil, Dr. Gayathri Withers, and Prof. Mark Bier for their help and expertise, Dr. Rea Freeland for her support and advice, and all my Chemistry PhD grad school classmates.

Abstract

Preparation of functional bio-responsive polymer-based materials is the subject of increasing research efforts. Such type of materials could find broad applications in biology and medicine due to their promising performance in the areas of drug and biomolecule delivery, tissue engineering and diagnostic systems. The preparation of such materials has significantly advanced over last 20 years due to the development of reversible deactivation radical polymerization (RDRP) methods. Atom transfer radical polymerization (ATRP), the most often used RDRP procedure, is a versatile and powerful technique for preparation of various functional polymers.

Even though ATRP showed great potential for design and synthesis of materials for biomedical applications, there are still many improvements and innovations that should be made in order to effectively utilize this method for production of useful biomaterials. This dissertation seeks to obtain the information required for improving the understanding of several aspects of ATRP, primarily focusing on controlling the polymerization in aqueous media, and how this contributes to the preparation of materials relevant to the biomedical field. Accordingly, this dissertation is divided into VIII chapters, where **Chapter I** is an introduction to the ATRP in aqueous media and reviews state of the art of aqueous ATRP and materials prepared by this method.

Protein-polymer hybrids (PPH) are commercially available therapeutics for treatment of various diseases. Over the last decade the traditional procedure employed for preparation of PPHs had been “grafting-to”, i.e. attaching a preformed polymer to a biomolecule. This technique was challenged by a new approach “grafting-from”, where a well-defined polymer can be grown directly from a specific site on a biomolecule. This

method significantly improves purification procedures and yield, which can potentially bring the cost down. Grafting-from requires performing the polymerization under aqueous conditions, optimally under biocompatible conditions. However, conducting ATRP in homogeneous aqueous media is inherently difficult due to multiple side reactions and high reaction rates.

Chapter II introduces the first approach on controlling ATRP in aqueous media utilizing one of the most active catalytic systems and how it was applied to growing a well-defined polymer from a protein.

In **Chapter III** another method for conducting an ATRP under aqueous conditions was investigated. This method addressed the primary disadvantage of the first method, namely high concentrations of a catalyst, which can affect protein stability and efficiency of purification of a bioconjugate.

In **Chapter IV** a further advance in ATRP in aqueous media is discussed and introduces a novel catalytic system. A series of new bioinspired iron porphyrin-based complexes were synthesized and successfully applied to ATRP in water.

In addition to chemical composition, size and degradation behavior are among the important characteristics of polymeric materials targeted for biologically relevant applications. The size of a polymer can define its circulation time and delivery efficiency. A significant number of studies have suggested that polymers of higher molecular weight and consequently increased size are more efficient in drug delivery applications. However polymer accumulation, due to more difficult natural removal from a biological system, can result in subsequent negative effects. This is exacerbated by the fact that most of the polymers prepared by radical polymerization consist of a carbon-carbon backbone, which

is not easily degraded under physiological conditions. Thus, **Chapter V** is focused on preparation of copolymers with hydrolytically degradable moieties within the polymer backbone, which facilitates utilization of higher molecular weight polymers for drug delivery, as the polymers can degrade below the renal threshold thereby facilitating removal from a body.

Another class of polymers that have gained attention for drug delivery applications are nanosized crosslinked polymer networks, called nanogels, due to their high stability and high cargo loading capacity. Previous studies showed that positively charged nanogels can be efficient carriers for nucleic acids, which had been shown to be very challenging to internalize into a cell. However, even low concentrations cationic polymers can be toxic to cells. One solution to this problem is the generation of core-shell particles where the cationic charge is shielded by a non-toxic shell. **Chapter VI** investigates how well-defined core-shell cationic nanogels can be prepared in a one-pot method to overcome this limitation in an economical fashion.

Macroscopic gels can be used for several applications such as slow release devices and soft actuators. However, there are a limited number of approaches on how to efficiently fuse two macroscopic gels with drastically different properties and chemical compositions. In **Chapter VII**, the preparation of heterogeneous hydrophilic-hydrophobic gels is studied and supported by a computational model.

Overall, this dissertation investigates the limitation of current procedures for synthesis of materials targeting biomedical applications and seeks to provide procedures for synthesis of well-defined polymers and PPH by ATRP under biocompatible aqueous conditions. The developed methods include preparation of degradable polymers by ATRP,

the design and synthesis of core-shell cationic nanogels that are applied to delivery of nucleic acids, and finally how heterogeneous macroscopic gels can be fused together to provide materials with a desired combination of properties. **Chapter VIII** summarizes the main achievements of the work described in this thesis and provides an outlook on future developments.

Table of Contents

List of Abbreviations

Monomers

BA	*n*-Butyl acrylate
DMAEMA	2-(Dimethylamino)ethyl methacrylate
DVB	Divinyl benzene
FMA	Fluorescein *o*-methacrylate
MAA	Methacrylic acid
OEOMA	Oligo(ethylene oxide) methyl ether methacrylate
$PEOMA_{2k}$	Poly(ethylene oxide) methyl ether methacrylate (M_n= 2 080)
QDMAEMA	Quaternized DMAEMA
OEODMA	Oligo(ethylene oxide) dimethacrylate
OEODMA-SS	Oligo(ethylene oxide) dimethacrylate disulfide (cross-linker)
*t*BA	*tert*-Butyl acrylate

Corresponding polymers are represented with a "p" in front of the monomer

ATRP Initiators

EBiB	Ethyl 2-bromoisobutyrate
EBPA	Ethyl α-bromophenylacetate
PEO_{2k}iBBr	Poly(ethylene oxide) isobutyryl bromide
PEO_{2k}BPA	Poly(ethylene oxide) bromophenyl acetate

Ligands for Cu Based ATRP Catalyst

bpy	2,2′-Bipyridine
Me_6TREN	Hexamethylated tris(2-aminoethyl)amine
TPMA	Tris(2-pyridylmethyl)amine

Other Abbreviations

AFM	Atomic force microscopy
AGET	Activators generated by electron transfer
ARGET	Activators regenerated by electron transfer
ATRP	Atom transfer radical polymerization
CRP	Controlled radical polymerization
DMF	Dimethylformamide
DMSO	Dimethyl sulfoxide
DP	Degree of polymerization
*e*ATRP	Electrochemically mediated ATRP
GPC	Gel permeation chromatography

GSH	Glutathione
HEK cell	Human Embryonic Kidney cells
M	Monomer
MALLS	Multi-angle lager light scattering
MI	Macroinitiator
MM	Macromonomer
NA	Nucleic acid
NMP	Nitroxide mediated polymerization
NMR	Nuclear magnetic resonance
PEG (= PEO)	Poly(ethylene glycol) (= poly(ethylene oxide)
pDNA	Plasmid deoxyribonucleic acid
RAFT	Reversible addition-fragmentation chain transfer
RDRP	Reversible-deactivation radical polymerization
RI	Reflective index
RNA	Ribonucleic acid
RNAi	RNA interference
SARA	Supplementary activator and reducing agent
siRNA	Small interfering RNA
$Sn(EH)_2$	Tin(II) bis(2-ethyl-hexanoate)
THF	Tetrahydrofuran

Symbols

$[M]_0$	Initial monomer concentration
conv	Conversion
D_h	Hydrodynamic diameter
k_a	Rate coefficient of activation
K_{ATRP}	ATRP equilibrium constant
k_d	Rate coefficient of deactivation
M_n or $M_{n,RI}$	Number average molecular weight
$M_{n,MALLS}$	Absolute molecular weight measured by
$M_{n,theo}$	Theoretical molecular weight
pH	Acidity of aqueous solution
$R\text{-}P_n^{\bullet}$	Propagating polymeric radicals with α-R group from the initiator RX
$R\text{-}P_n\text{-}X$	Living polymer chains with both α-R group and ω-X group from the initiator R-X
R-X	Small molecule initiator with a X functional group (in ATRP it is an alkyl halide)

List of Schemes

List of Figures

List of Tables

Chapter I. Performing Atom Transfer Radical Polymerization in Water: Challenges, Developments, and Applications

I.1. Introduction

Radical polymerization (RP) is one of the most versatile polymerization methods which provides a significant share of the commercial polymer production.[1] However, its application for preparation of materials with complex macromolecular structure is limited due to side reactions such as transfer and termination.[2] That is why ever since the discovery of living anionic polymerization there was a constant interest in suppressing termination in RP process in order to obtain polymers with control over molecular weight, dispersity and architecture. The discovery of reversible deactivation radical polymerization (RDRP) methods[3-7] led to an exponential increase in research focused on preparation of tailored functional materials via radical polymerization. Advantages of free radical polymerization, such as tolerance to impurities and polar groups, became available for synthesis of polymers with various composition, topologies and architecture.

The essence of control over radical polymerization via available RDRP methods, previously known as "living" or controlled radical polymerization (CRP), lies in the development of procedures where most of the radical precursors are present in their dormant state and only small fraction of potential radicals can propagate at any instance.[8] Currently, several RDRP methods have been reported and utilized including nitroxide mediated polymerization (NMP),[6,7] reversible addition-fragmentation chain transfer (RAFT) polymerization,[4] atom transfer radical polymerization (ATRP)[9] and some others.

Among them, ATRP gained popularity since its discovery in 1995[3,5] and currently remains the most often utilized RDRP technique. The main advantages of ATRP include commercial availability of almost all polymerization components, such as initiators and catalysts, use of catalytic amounts of metal complexes, ease of chain end modification, the ability to polymerize a wide range of radically copolymerizable monomers and incorporate macromolecules prepared by other polymerization procedures.[10]

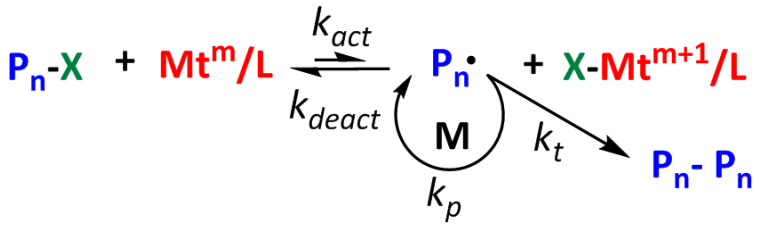

Scheme I.1. General mechanism of atom transfer radical polymerization (ATRP).

During an ATRP reaction, the carbon-halogen bond in an alkyl halide is reversibly cleaved by a reaction with a transition metal complex in its lower oxidation state, which results in the formation of a radical and a metal complex in its higher oxidation state (**Scheme I.1**).[9] The resultant carbon radical can propagate, terminate or react with the metal-halide complex to reform a dormant species.[8] Specific conditions are selected such that active radicals are rapidly deactivated, making the dormant state the majority species. Due to the high fraction of dormant chains, termination usually does not exceed 1 – 10 %, depending on conditions.[11] In this way, ATRP, similar to other living polymerization methods, allows for precise control over macromolecular composition, architecture and functionality (**Figure I.1**).[2]

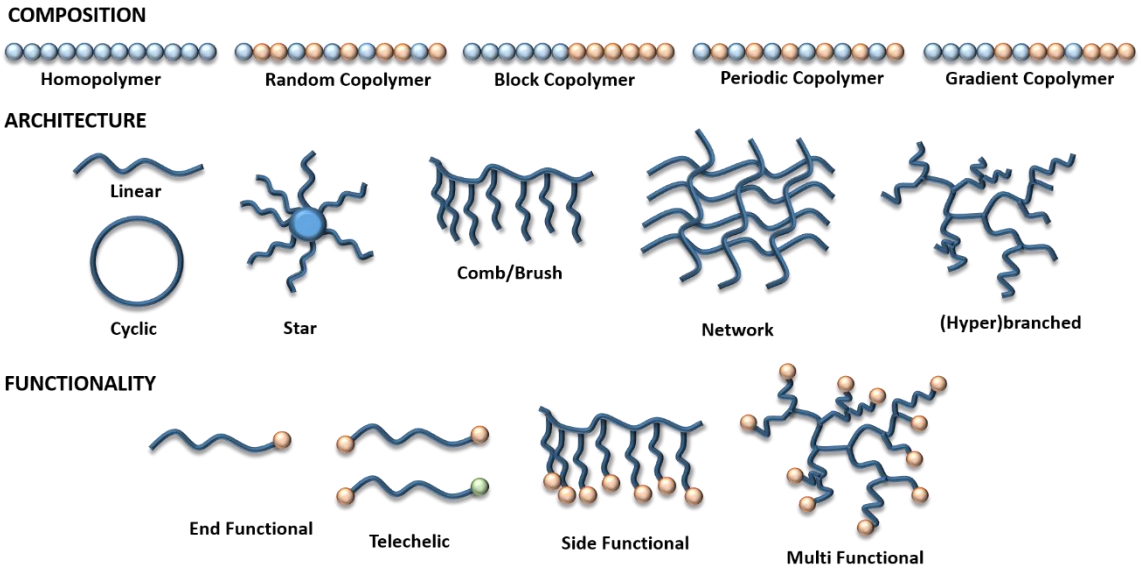

Figure I.1. Control over composition, architecture and functionality of materials prepared by ATRP.

Many initiators and catalysts were developed for polymerization of various monomers.[12] Depending on the activity of a monomer, one has to use an appropriate initiator and select a proper catalyst to produce a well-defined polymer. **Figure I.2a** shows different initiators characterized by different activation rate constants depending on their structure.[12] Among reported transition metal complexes catalyzing ATRP, copper complexes are the most studied and used and the activity of the catalyst corresponds to its redox potential (**Figure I.2b**).[12,13] The more active catalysts are characterized by an increasingly negative redox potential. The initially developed ATRP catalysts, including those with 2,2'-bipyridine (bpy), 1,1,4,7,10,10-hexamethyltriethylenetetramine (HMTETA) or N,N,N',N',N''-pentamethyldiethylenetriamine (PMDETA) ligands, display moderate activity but are inexpensive, and are often utilized to perform polymerization.[12,13] More active catalysts formed with ligands such as tris[(2-pyridyl)methyl]amine (TPMA) and Tris(2-(dimethylamino)ethyl)amine (Me_6TREN) became popular with the

implementation of low catalyst concentration ATRP methods,[14] which will be discussed further in this Chapter.

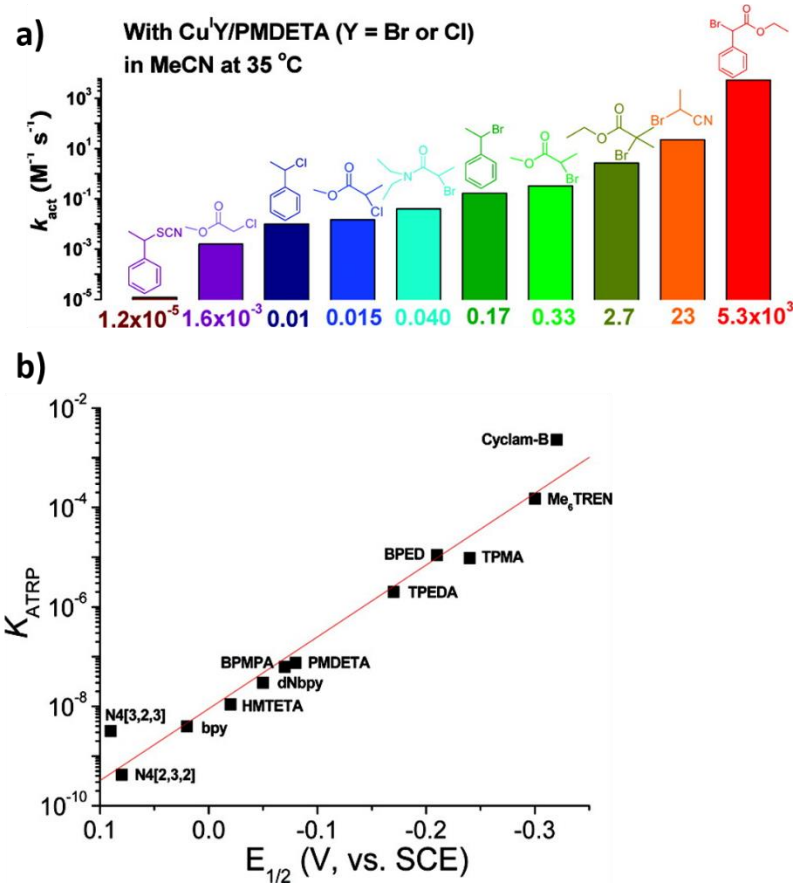

Figure I.2. a) k_{act} for Cu^{I}/PMDETA with various initiators at 35 °C in acetonitrile; **b)** Plot of K_{ATRP} (measured with EtBriB) vs $E_{1/2}$ for 12 $Cu^{II}Br_2$/L complexes. Reprinted with permission from references.[12,15] Copyright © 2007, 2008 American Chemical Society.

Even though ATRP has many advantages and is a well-developed method, it still has certain limitations. Some monomers are not easily polymerized by ATRP or polymerization results do not produce a well-defined product with high chain-end functionality.[10,16-19] Performing ATRP in water was once included among other limitations of this polymerization method due to noticeable difference in reactions rate and quality of prepared polymer compared to polymerizations conducted in organic media.[20-26] Soon after the first publication disclosing an ATRP in water[27] it was discovered that performing the

polymerization in the presence of water can be compromised due to the occurrence of side reactions and fast polymerization as compared to organic solvents.[10,20,22,24,28-33]

Nevertheless, using water as the polymerization media provides a number of advantages. First, water is an inexpensive, non-hazardous, non-volatile and non-flammable solvent. There is a wide range of water soluble monomers of interest that can be polymerized in aqueous media (**Figure I.3**).[20-23,25,27,28,33-45] Additionally, polymerization in aqueous media creates an option of growing synthetic polymers from biomolecules,[46-50] which require aqueous conditions to maintain their stability and solubility. Thus, many studies targeted various approaches to perform well-controlled polymerization in water, thereby providing many mechanistic insights to increase control over the reactions.

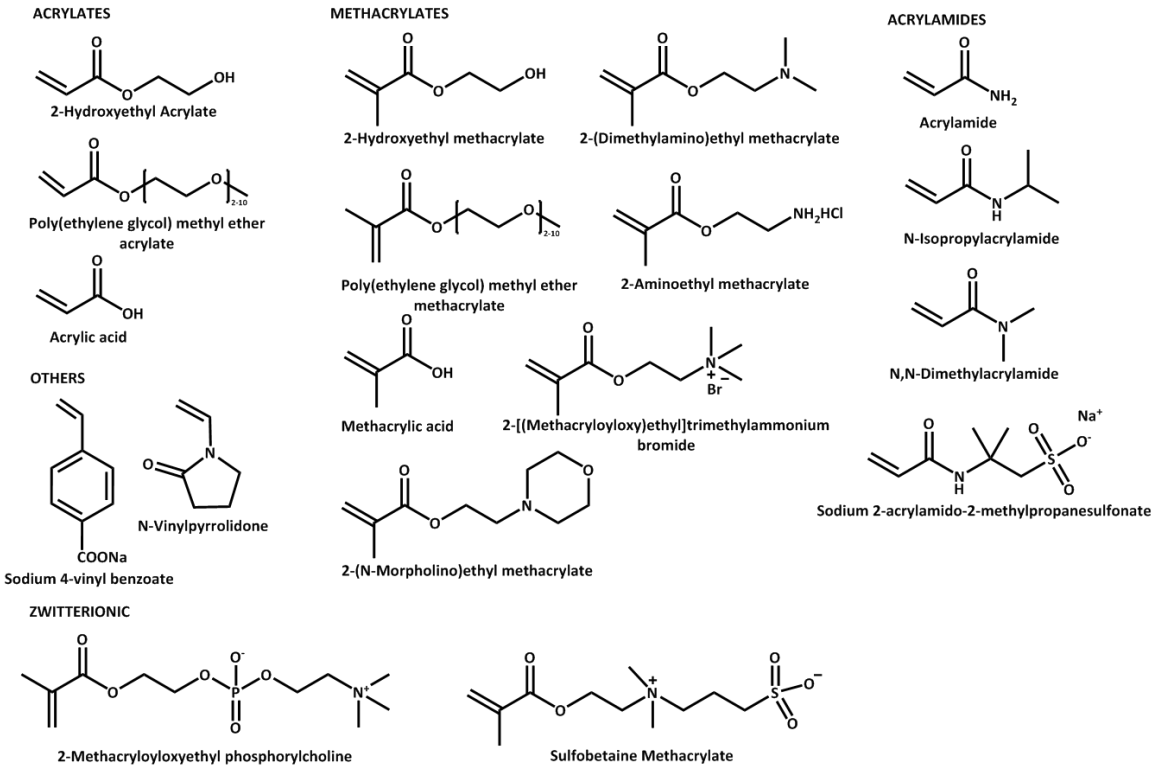

Figure I.3. Water-soluble monomers that were reported to be polymerized by aqueous ATRP

I.2. Thesis goal

Polymer use in biomedicine has remained of high interest for many decades. It was validated by commercialization of various materials, starting from polymers for drug delivery applications and ending with bulk materials and components for tissue engineering, instrumentation, care devices and implants.[51-58] With the discovery of RDRP methods a large body of research is targeting application of these methods to create well-defined functional materials for biomedicine.[46] Drug and biomolecule delivery became one the major focuses due to its promising results in improving efficiencies of treatment for many life impactful diseases including cancers, genetic and autoimmune disorders, and viral infections.[53,59-71]

As mentioned previously, aqueous ATRP can be beneficially applied to generate a wide range of materials if one can develop conditions to fully control the reaction. The goal of this thesis was to investigate how to control ATRP in aqueous media and prepare biomedicine relevant materials by these improved procedures. Research results obtained during my PhD were split between six Chapters (Chapters II – VII), and are focused on studying and preparing well-defined bioresponsive materials such as water-soluble polymers, protein-polymer hybrids, degradable materials (linear polymers and nanogels), and macrogels by means of ATRP.

This Chapter will discuss why it is challenging to conduct ATRP in the presence of water, how the well-controlled polymerization can be achieved, and discuss several interesting applications of this method relevant to the scope of the Thesis.

I.3. The effect of water on ATRP

Soon after the discovery of ATRP, it was quickly recognized that while the polymerization of water soluble monomers can be successfully conducted in water, there were many drastic differences and hurdles compared to organic media. One of the most noticeable differences was the significant acceleration of the reaction rate upon addition of water.[34,36,72] It was reported that the rate of polymerization increases upon addition of water to an organic solvent, and for polymerizations conducted with water as the only solvent, monomer conversions could reach more than 90% within an hour even at room temperature.[22,23,35,36,72] While faster reaction can be an advantageous polymerization feature, the final polymers were often characterized by broader molecular weight distributions and reduced livingness of the system (**Figure I.4**). Several groups conducted fundamental studies in order to understand how to control ATRP in aqueous media. This section will summarize their findings on the fundamental effects of water on the nature of ATRP.

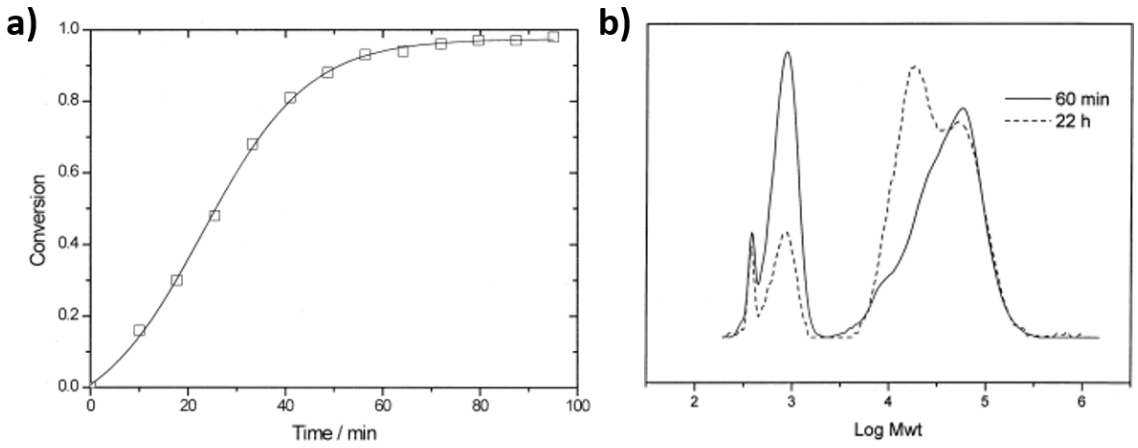

Figure I.4. a) Conversion-time plot for the polymerization of MeO(PEG)-MA in D_2O solvent at 25 °C, [M]/[I]/[CuBr]/[L] = 10/1/0.01/0.03; b) SEC traces for the polymerization of MeO(PEG)-MA in D_2O at 25 °C, [2]/[Cu(I)Br]/[Cu(II)Br_2]/[4] = 1/0.009/0.001/0.03. Reprinted with permission from the reference. [23] Copyright © 2001 WILEY-VCH Verlag GmbH & Co.

Initial investigation into the nature of the influence of water on an ATRP (monomer/water) showed that for many copper complexes apparent ATRP rate constant k_p^{app} increased on average by 3 orders of magnitude when compared to reactivity in organic systems (acetonitrile/bulk).[73] Taking into account differences in k_p due to monomer and solvent effect, the remaining differences in reaction rate can be explained by the higher radical concentration [R•]. From the ATRP rate equation (1) it is evident that several factors can contribute to generation of a higher polymerization rate and poorer control during polymerization in the presence of water:

$$R_p = k_p K_{ATRP} \frac{[RX][Cu^I L_n]}{[Cu^{II} L_n X]} [M] \quad (1)$$

where $K_{ATRP} = k_{act}/k_{deact}$ – ATRP equilibrium constant, k_{act} – activation rate constant, k_{deact} – deactivation rate constant, k_p – propagation rate constant, [RX] – initiator concentration, $[Cu^I L_n]/[Cu^{II} L_n X]$ – ratio of activator to deactivator, [M] – monomer concentration.

The ATRP equilibrium constant, K_{ATRP}, defines the catalytic activity of a specific ATRP system (metal complex/initiator). The initial investigation on the effect of solvents on ATRP were based on thermodynamic contributions and predicted that K_{ATRP} value in water should be significantly higher than in any other organic solvents (**Figure I.5a**).[74] Further investigations demonstrated that the activation rate constant k_{act} is well-correlated with solvent polarity (except for alcohols) due to increased stabilization of the Cu^{II} complexes (**Figure I.5b**).[75] In another publication an estimate for the value of K_{ATRP} for Cu/TPMA complex in water was based on the thermodynamic data and provided a value for $K_{ATRP} = 1.49\times10^{-1}$, which is 4 orders of magnitude higher than equilibrium constant in MeCN: $K_{ATRP} = 9.6\times10^{-6}$.[76] In the same paper k_{act} was measured by cyclic voltammetry to be $\geq 2.46\text{x}10^6$ $M^{-1}s^{-1}$, which indicated that activation was significantly faster in water.[76]

The most recent study on the value of K_{ATRP} in water for Cu/bpy complex by on-line vis/NIR spectroscopy confirmed that the increase in ATRP equilibrium constant in water was consistent with previous reports and was mainly due to higher k_{act} .[77] Therefore in the presence of the same amount of active Cu(I) species in aqueous media there will be significantly more radicals generated, resulting in faster polymerization, but also a higher fraction of termination and transfer reactions.

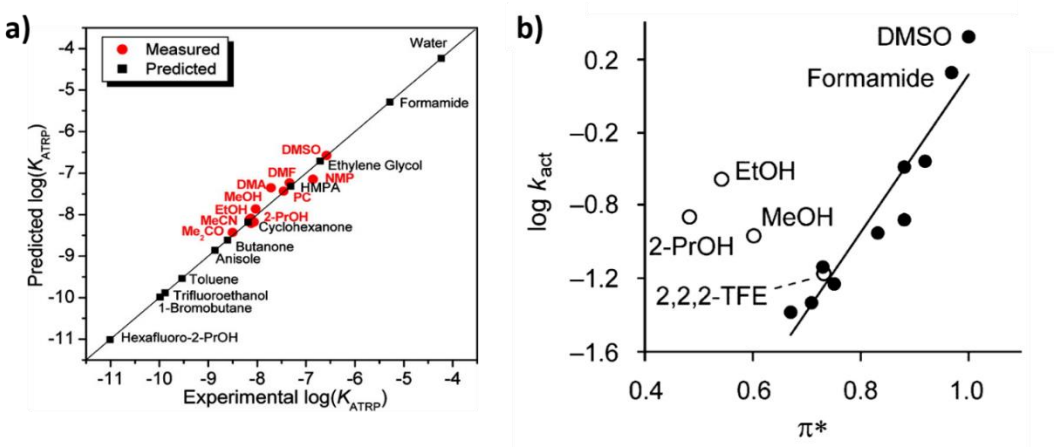

Figure I.5. a) Calculated Log(K_{ATRP}) values for CuIBr/HMTETA + MBriB are plotted against values predicted by the Kamlet−Taft relationship relationship; **b)** Plot of log k_{act} vs π*. Reprinted with permission from references.[74,75] Copyright © 2009 American Chemical Society.

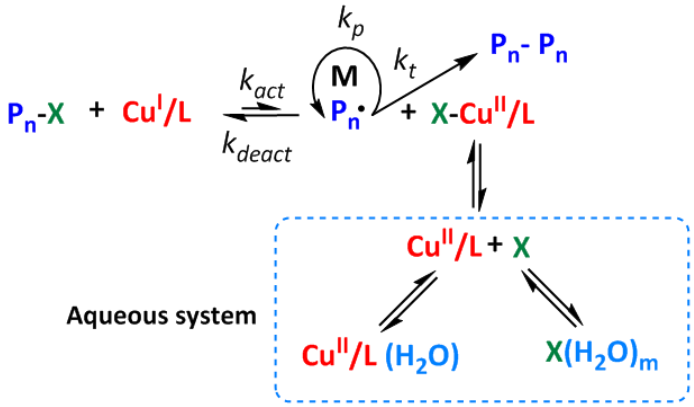

Scheme I.2. Basic equilibria in aqueous ATRP system.

ATRP equilibrium is dependent on the ratio between Cu^{I} and Cu^{II} species formed in the polymerization medium. An ATRP, employing medium activity catalysts, in organic solvents is quite slow and can be performed with high ratios of Cu^{I}:Cu^{II} complexes, often created by addition of only the Cu^{I} complex to the reaction. However, in water fast rates of polymerization were reported even in the presence of high amounts of deactivator. This result is not only due to a high ATRP equilibrium constant, but also because of dissociation of Cu-Br bond in the deactivator in water (**Scheme I.2**). In aqueous environments the halide ligand dissociates from the Cu^{II} species, and a water molecule takes its place. This reaction reduces the effective concentration of deactivator in the polymerization medium yielding polymers with broad MWD. This can be resolved by starting with a high concentration of Cu^{II} species (≥80%), which results in slower and better controlled polymerization (**Figure I.6**). Another solution is addition of an extra halide salt, which pushes the equilibrium in the dissociation reaction (**Scheme I.2**) back to a higher concentration of the functional deactivator, resulting in slower reaction and formation of polymers with narrower MWDs, indicating more efficient deactivation. This approach is especially important for polymerizations carried out in the presence of low concentrations of catalyst, and is investigated in Chapter III.

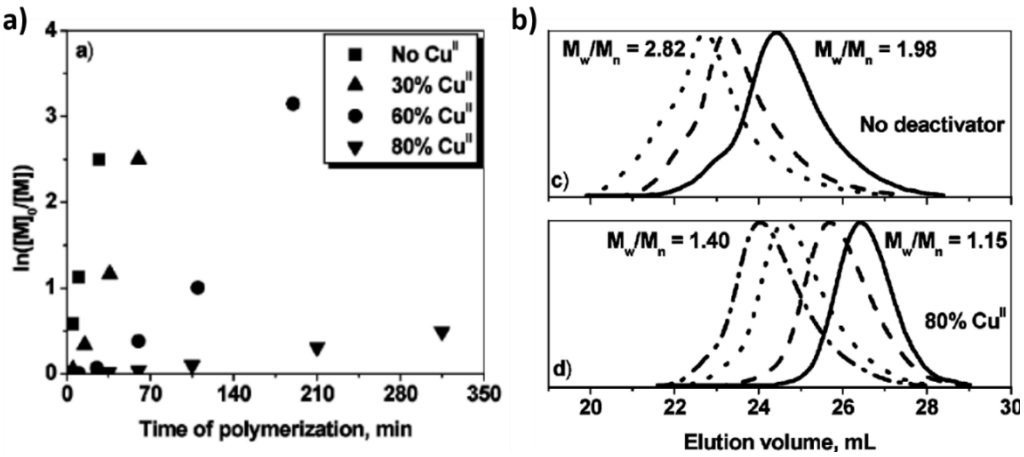

Figure I.6. Cu^{I}/Cu^{II} ratio effect on polymerization. Reprinted with permission from the reference. [24] Copyright © 2009 American Chemical Society.

High K_{ATRP} and dissociation of the halide from the deactivator are among major reasons for poor control during ATRP in water. However, other side reactions, such as ligand displacement by monomers, polymers or solvent, and Cu^{I} disproportionation, also contribute to reduced control. Catalyst dissociation is clearly illustrated by significantly improved polymerization results if the complex was formed before addition to the reaction compared to the formation of the complex in the presence of a monomer, particularly a basic monomer such as 2-(dimethylamino)ethyl methacrylate.[22] Another possible side reaction occurring is the substitution reactions of the alkyl halide in the polymer chain-end, especially at higher temperatures and in the presence of basic monomers, but they can be addressed by performing the polymerization at room temperatures or lower, and by making appropriate pH adjustments.[78,79]

I.4. Various ATRP methods in water and their application

Despite multiple side reactions, discussed above, and an inherently high K_{ATRP} it is possible to achieve well-controlled polymerization in water utilizing multiple ATRP methods, (**Scheme I.3**). Various ATRP procedures were applied to synthesize well-defined polymers, block copolymers, hybrid materials, functionalized surfaces and bioconjugates in water.

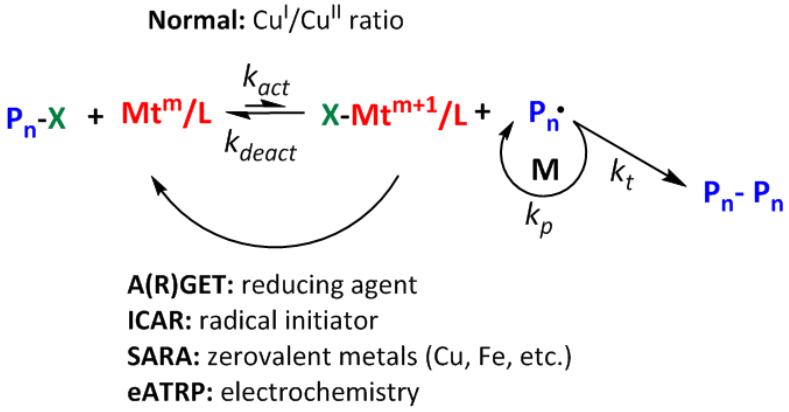

Scheme I.3. Various ATRP methods.

I.4.1. Normal copper mediated ATRP.

Copper based catalyst complexes are the most developed and studied ATRP catalysis.[8,10,12] Most of the original reports on polymerization in water utilized the initially developed normal ATRP catalyzed by copper complexes. Under Normal ATRP conditions, relatively high concentrations of both Cu^{I} and Cu^{II} complexes are added at the beginning of the reaction. 2, 2'-Bipyridine (bpy) is commercially available and forms a water soluble copper complex of modest activity (**Figure I.7**).[12] A number of publications reported successful polymerizations utilizing this type of copper complex. Very fast polymerizations were reported, however the prepared polymers were characterized by rather broad MWDs (**Figure I.4**).[23] Control over the polymerization was improved by

addition of up to 80% of the Cu^{II} deactivating species compared to Cu^{I} species (**Figure I.6**).[24,80] Use of more active ligands such as HMTETA for normal ATRP resulted in a less well-controlled polymerization due to presence of higher concentrations of the higher activity Cu^{I} species.[22] Therefore in the presence of more active catalyst an even lower fraction of Cu^{I} species should be added to the reaction.

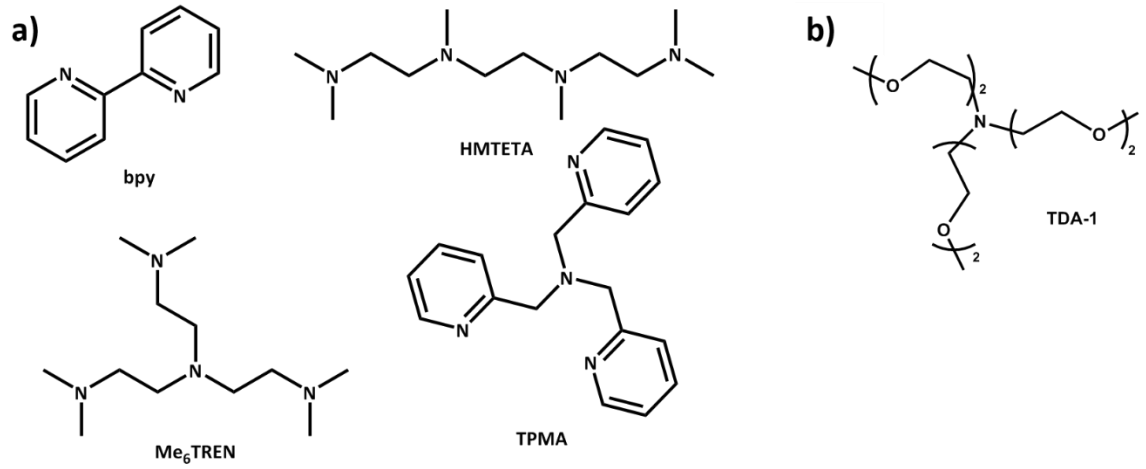

Figure I.7. Ligands utilized for ATRP in water for copper (a) and iron (b).[21-24,33,34,45,49,73,81,82]

Normal aqueous ATRP can be applied to the preparation of a wide range of materials. It is particularly attractive for a synthesis of bioconjugates by grafting from a biomolecule (**Figure I.8**).[39,47,83-86] Bioconjugates are currently used in various applications including pharmaceuticals, sensing technologies and catalysis.[71,87,88] The development of the "grafting from" method emerged as a procedure which could significantly improve both efficiency of conjugation and simplification of purification procedures when compared to traditionally used "grafting to" method, where a preformed polymer is coupled to a biomolecule.[25,26,39,43,49,50,83,84,89-91] Application of "grafting from" method requires polymerization under biocompatible conditions, which would not degrade or modify the

biomolecule. The main requirement is that the reaction is carried out in predominately aqueous media, especially for polymerization from proteins and peptides.

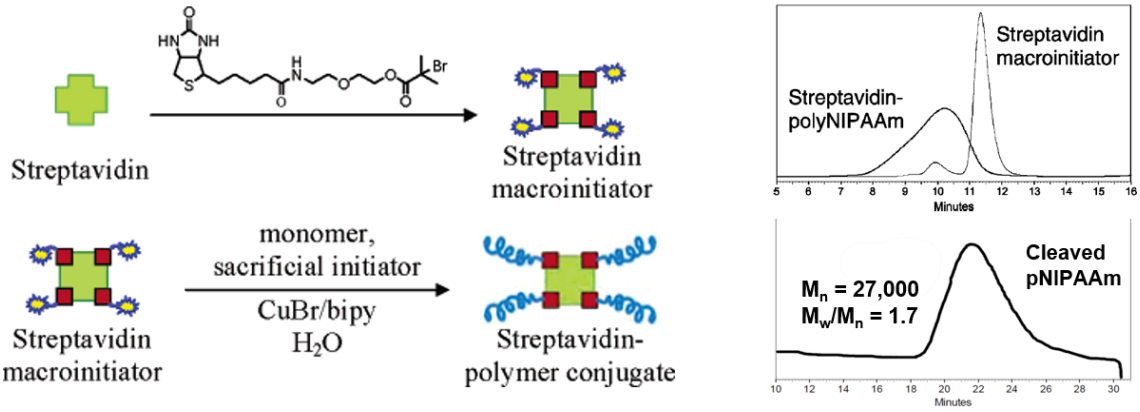

Figure I.8. Grafting pNIPAAm from a streptavidin macroinitiator. Reprinted with permission from the reference. [83] Copyright © 2005 American Chemical Society.

Reports on grafting from a protein by normal ATRP were published as early as 2005,[25,39,83] and showed promising polymerization results. Proteins in such hybrid materials preserved their function and were often characterized by higher stability under physiological conditions. However, often the formed protein-polymer hybrids were characterized by relatively broad MWD and inefficient initiation (**Figure I.8, Figure I.**9).

A broad range of proteins were used in a grafting from ATRP despite difficulties with polymerization conditions yielding materials with preserved protein functionality and new properties provided by polymer. Polymers were grafted from proteins such as myoglobin,[26] GFP,[50] and human growth hormone[49] by ATRP in water. The obtained protein-polymer hybrids were shown to have improved stability under various conditions, limited loss of activity, and significantly better pharmacokinetics and tumor accumulation profiles. Russel et al. reported temperature and pH-sensitive systems to regulate enzymes stability and activity within a range of biologically relevant conditions (**Figure I.10**).[92,93]

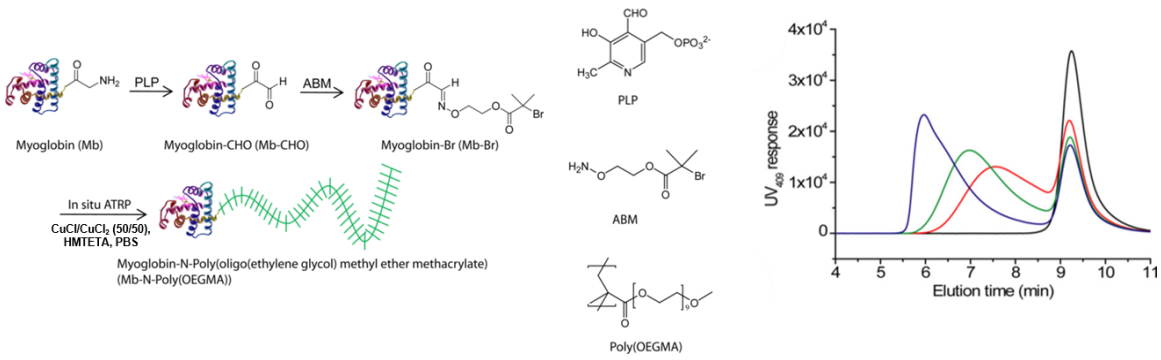

Figure I.9. Grafting poly(OEOMA) from myoglobin. Reprinted with permission from the reference.[26]

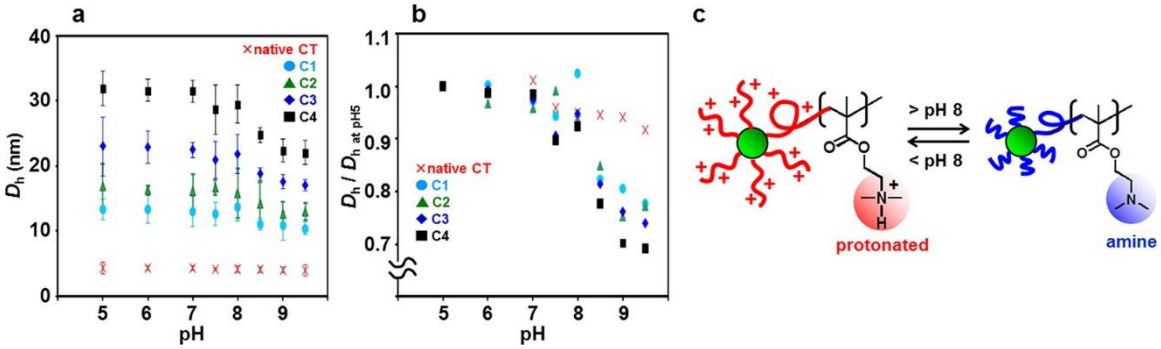

Figure I.10. Hydrodynamic diameter (*D*h) of native and polymer-modified chymotrypsin as a function of pH. (a) pH-dependence of the hydrodynamic diameter of native CT and conjugates; (b) hydrodynamic diameter (for native and modified enzyme) relative to those at pH 5; (c) schematic representation of the impact of pH on the conformation of the grafted PDMAEMA chains below and above pH 8. Reprinted with permission from the reference.[92] Copyright © 2013 American Chemical Society.

ATRP is among the most frequently used RDRP methods for preparation of surfaces with a high density of grafted polymers.[94-98] The simple procedures for modification of surfaces with initiating moieties and consequent grafting from polymerization provides a uniform, highly dense concentration, of polymer brushes attached to the surface.[94-96,99] Aqueous ATRP is particularly suitable for modification of flat surfaces and particles with water-soluble neutral and ionic polymers. Modified particles included silica particles, polystyrene latexes, gold nanoparticles, carbon nanotubes and some others formed by grafting water-soluble polymers from silica,

polystyrene latexes, or carbon nanotubes in aqueous media results in a fast and efficient polymerization that improves the colloidal stability of the formed particles in aqueous solutions (**Figure I.11**).[100-104] Grafting from surfaces by aqueous ATRP can be very fast and efficient.[105] Stimuli-responsive surfaces can be synthesized by grafting from polymers such as pDMAEMA or pNIPAAM (**Figure I.12**).[105,106] "Grafting from" approach generates particles and surfaces with densely grafted polymer brushes.

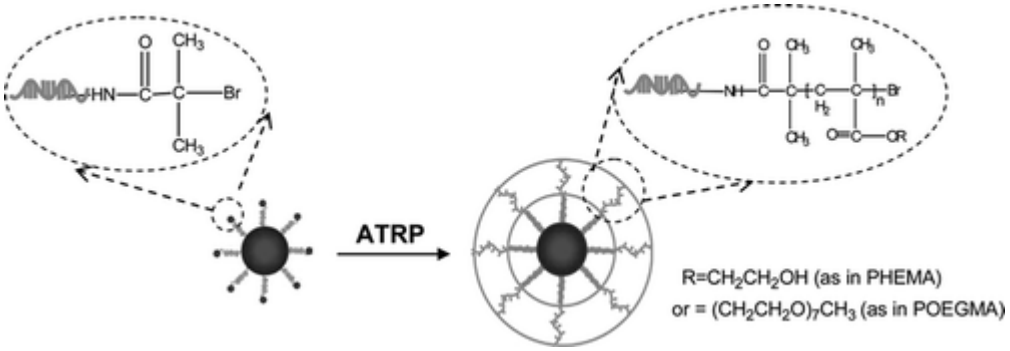

Figure I.11. Grafting from a gold nanoparticle with immobilized initiator. Reprinted with permission from the reference.[102] Copyright © 2007 American Chemical Society.

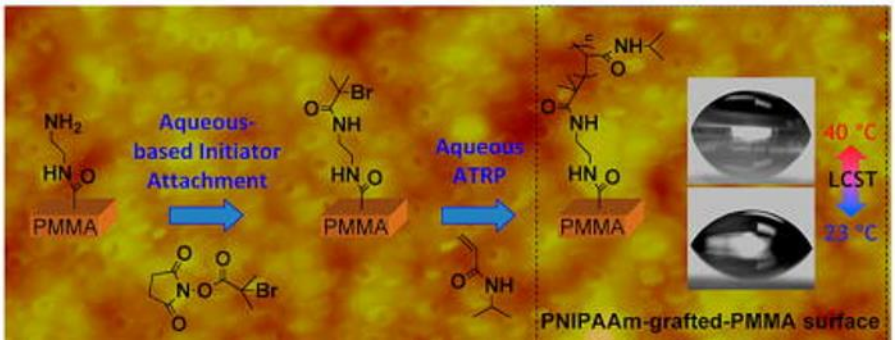

Figure I.12. Grafting from surfaces by aqueous ATRP to generate temperature sensitive surface. Reprinted with permission from the reference.[106] Copyright © 2013 American Chemical Society.

Normal ATRP was initially utilized for preparation of many materials due to its simplicity. However, on the laboratory scale, it is difficult experimentally to add small

amounts of active Cu^{I} species to the reaction medium without oxidizing them. Such difficulties can be resolved by other methods, where Cu^{I} species are generated *in situ*.

I.4.2. *In situ* Cu^{I} generation methods.

AGET ATRP. In activator generated by electron transfer (AGET) ATRP the Cu^{I} species are generated *in situ* from Cu^{II} species by addition of various reducing agents.[107] Reducing agents such as hydrazine, ascorbic acid and glucose are particularly relevant for aqueous ATRP due to their solubility. Ascorbic acid is the most commonly used reducing agent because it is not toxic compared to hydrazine, and more efficient than glucose.[26,30,44,49,82,108,109] This method eliminates use of easily oxidized Cu^{I} species, and thus results in more convenient setup and provides reproducible results. It was shown that even very active catalysts, such as Cu/TPMA, (**Figure I.2, Figure I.**7) can provide well-defined polymers when only small amount of ascorbic acid are used.[30,49] For instance, decreasing amount of ascorbic acid from 30 mol. % to only 8 mol. % relative to Cu^{II} will result in formation of a polymer with significantly lower polydispersity, but monomer conversion was also lower.[30]

The convenience of this approach was utilized to generate various types of materials including bioconjugates,[49,110] grafted particles[111] and surfaces. Recent report on p(St-AA)/iron oxide composite microspheres modified with poly(acrylic acid) brushes showed that complex hybrid materials can be synthesized by post-polymerization modification including synthesis of gold nanoparticles for interaction with proteins (**Figure I.13**).[111]

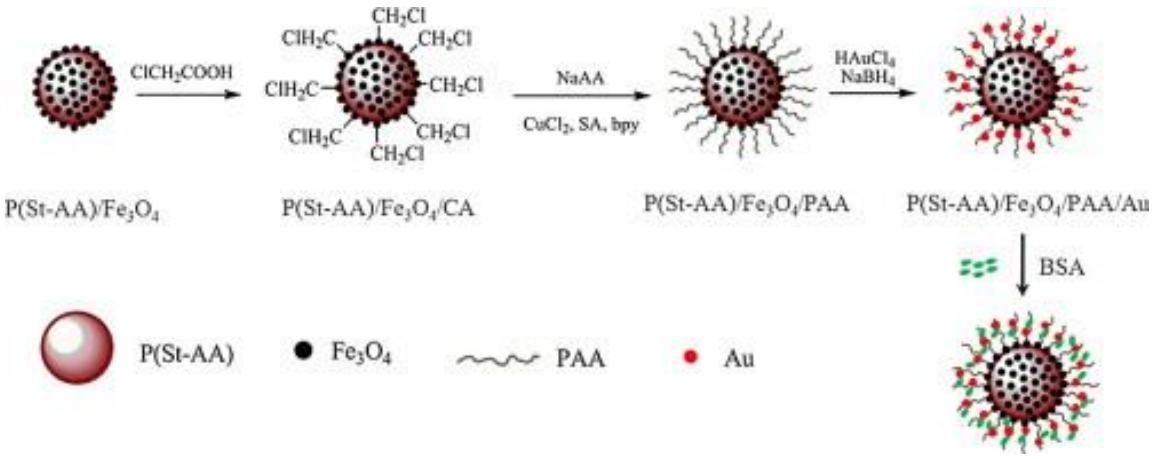

Figure I.13. The synthesis of PAA brushes modified magnetic particles for immobilizing gold nanoparticles. Reprinted with permission from the reference.[111] Copyright © 2014 Elsevier.

eATRP. Another method to generate the activator species in controlled way is the electrochemical ATRP (eATRP) procedure, where a sufficient electrical potential can be applied to the cathode in an electrochemical cell so that a controlled reduction of $Cu^{II}L$ to $Cu^{I}L$ occurs at the working electrode.[76,112,113] One advantage of this method is that byproducts are not produced as in AGET ATRP. However eATRP requires complex equipment to operate. Depending on the applied potential E_{app} one can control amount of Cu^{I} generated and consequently control the amount of radicals formed. It was reported that with E_{app} higher than redox potential E_0 one can achieve excellent control of polymerization in water, but with more negative E_{app} (more Cu) < E_0 the reaction was much faster and polymers MWD were >1.5 (**Figure I.14**).[76] In comparison, when conducting an eATRP in organic media, like acetonitrile, when the applied potential is equal to or more negative than the redox potential, this is a good choice for carrying out a well-controlled polymerization within a reasonable time of reaction.[114]

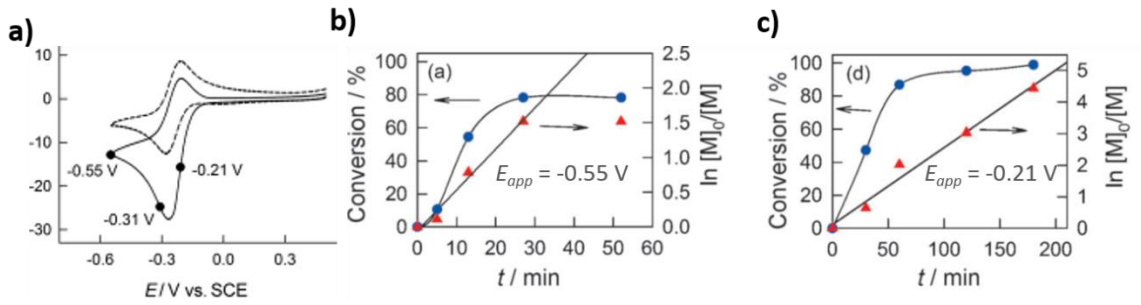

Figure I.14. Cyclic voltammograms of 1 mM $Cu^{II}L^{2+}$ in H_2O/$OEOMA_{475}$ (9:1 v/v) + 0.1 M Et_4NBF_4 recorded at v=0.1 V s^{-1} in the absence (- - - -) and presence (—) of 1 mM HEBriB; the three dots on the CV trace correspond to the E_{app} values used in the polymerization experiments. Reprinted with permission from the reference.[76] Copyright © 2011 WILEY-VCH Verlag GmbH & Co.

ARGET and ICAR ATRP. One of the criticisms of ATRP was the presence of a high concentration of the catalyst and difficulty of its removal after polymerization completion. If one decreased the amount of catalyst added under normal ATRP conditions then polymerization would not reach high monomer conversion and would stop at an early point due to the persistent radical effect. Thus, new methods were invented based on the regeneration of Cu^{II} species formed by termination reactions (**Scheme I.3**). Activator regenerated by electron transfer (ARGET) ATRP is based on regeneration of Cu^{II} species in the presence of reducing agents.[14] Another low ppm catalyst procedure is initiators for continuous activator regeneration (ICAR) ATRP which utilizes radical initiators for the same purpose.[14]

High activity stable catalysts like copper complexes formed with TPMA or Me_6TREN ligands provide the best performance in these ATRP methods in organic media, but can be considered to be too active for aqueous media, generating high concentration of radicals leading to high levels of termination (**Figure I.7**). Chapter III describes the first example of how to control ARGET ATRP method in aqueous media, where radicals are continuously generated at very low amounts by feeding of reducing agent or slow thermal

decomposition of the radical initiator. Further publications utilizing such low catalyst methods support the idea that in addition to producing well-defined polymers they simplify purification procedures. ARGET ATRP can be efficiently applied to the polymerization of various functional water soluble monomers like OEOMA or DMAEMA.[105,115] Not only does purification becomes easier, but overall cost and environmental impact are also decreased. In the recent publication, it was estimated that formation of polymer brushes from a surface can be very efficient and inexpensive if one utilizes ARGET ATRP in water with low monomer and low concentration of catalyst in the presence of excess reducing agent **(Figure I.15)**.[105] Due to the high activity of the system, it is still possible to grow polymer from a surface in a scalable procedure, and the final cost was estimated to be more than 800 times lower compared the cost of a normal ATRP.[105]

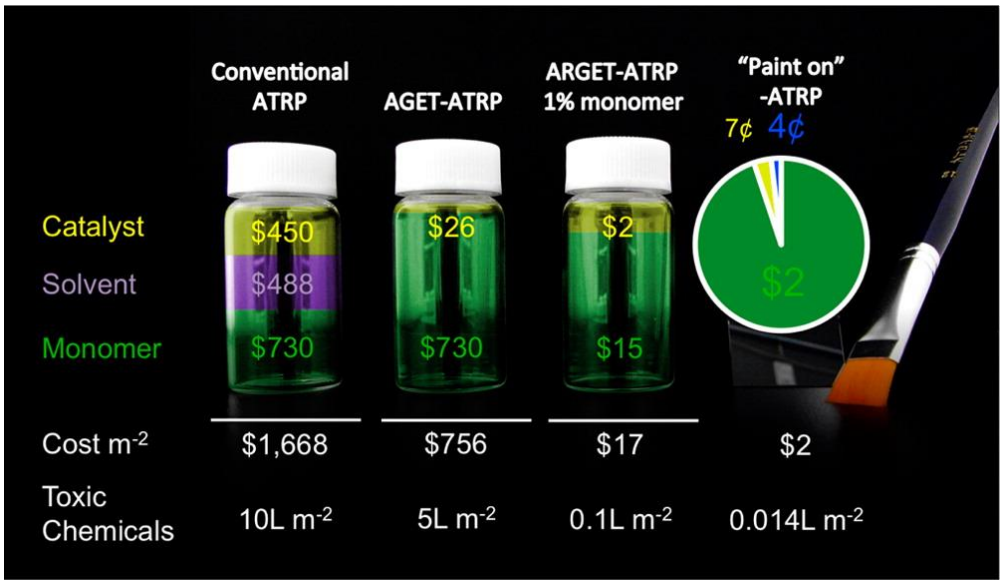

Figure I.15. Costs of polymer brushes created using conventional ATRP, AGET-ATRP, ARGET-ATRP and "paint on"-ATRP. Green indicates cost of monomer, purple cost of organic solvent, yellow cost of catalyst, and blue cost of ascorbic acid. The total cost per square meter is shown at the bottom, along with the amount of toxic chemicals used. Reprinted with permission from the reference. [105] Copyright © 2013 American Chemical Society.

Another advantage of using aqueous ATRP is when an organic substrate is used and its swelling or dissolution is undesirable. For instance, it was reported that a shape memory material poly(octylene diazoadipate-*co*-octylene adipate) immobilized on the surface can be grafted with p(OEOMA) brush in water by ARGET ATRP at ambient temperatures in order to inhibit material swelling and prevent triggering a shape memory transition (**Figure I.16**).[115] Upon heating such materials experience uniaxial wrinkling behavior due to differences in strain between the substrate and polymer brush.

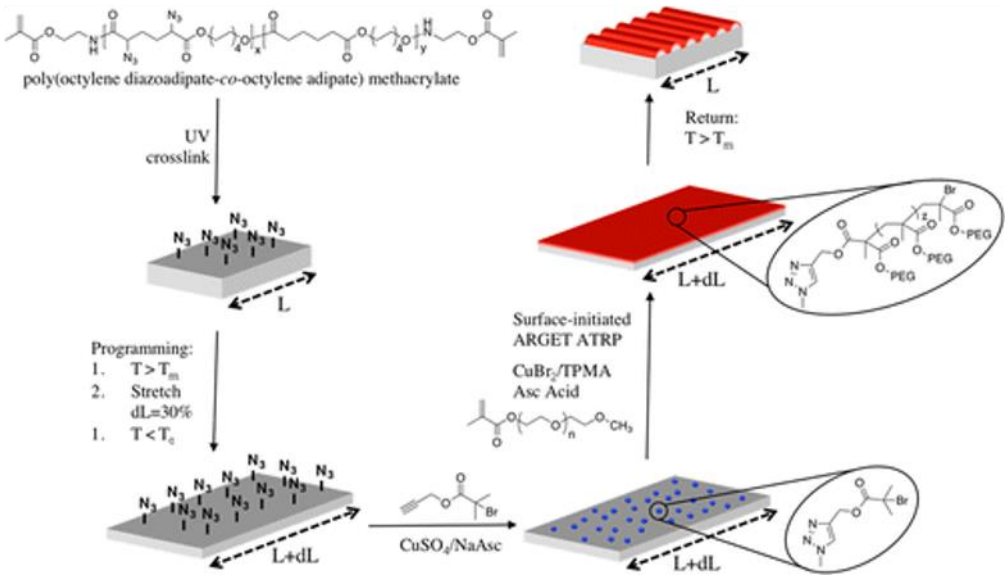

Figure I.16. Grafting from surfaces by aqueous ATRP to generate shape memory material. Reprinted with permission from the reference. [115] Copyright © 2015 American Chemical Society.

SARA ATRP. A slightly different pathway occurs when a zero-valent metal (Cu^0) is used to reduce the added Cu^{II} complex. In addition to participating in a redox reaction the Cu^0 is capable of direct activation of the alkyl halide.[116] However, activation by the Cu^I complex is still prevalent, and this is why this method is called supplemental activator and reducing agent (SARA) ATRP.[116] An alternative name for this approach, which can be found in the literature, is single electron transfer living radical polymerization (SET-LRP),

which implies a different mechanism of activation.[117] These two descriptions were a source of an extensive debate in the literature due to contrasting theories on the activation role of Cu^0 versus Cu^I. According to SET-LRP mechanism Cu^0 is exclusively reacts with alkyl halide, which occurs by outer sphere electron transfer (OSET), and Cu^I instantaneously undergoes disproportionation.[117,118] But in SARA ATRP Cu^I is a principle activator and activation of alkyl halide occurs by inner sphere electron transfer.[116] According to this mechanism Cu^0 only acts as supplemental activator as well as reducing agent.[116] Recently, several experimental and theoretical studies demonstrated the validity of SARA ATRP mechanism over SET LRP.[116,119] It was shown that alkyl halides primarily react with Cu^I complexes rather than Cu^0.[116,119] Furthermore, Cu^0 preferentially comproportionates with Cu^{II}, while only minor disproportionation occurs for certain complex/solvent systems.[116,119] Finally, according to Marcus analysis it was calculated that alkyl halide activation proceeds through ISET ~10^{10} times faster than through OSET.[120] Overall, experimental and theoretical evaluations indicated that Cu^I species are highly active (>100 times than Cu^0), and reaction of Cu^I complexes with alkyl halides is at least 2 orders of magnitude faster than their disproportionation.[121] These findings on polymerization in the presence of zero-valent copper showed that mechanism in this case is in agreement with SARA ATRP, and not SET-LRP.

Various monomers were successfully polymerized by SARA ATRP including (meth)acrylates and acrylamides in either pure water or mixtures with polar solvents.[32,33,122-125] Well-controlled PEG-based polyacrylates can be produced by addition of Cu^0 together with stable Cu^{II} deactivator to create conditions with reduced concentration of radicals (Error! Reference source not found.).[45] Polymerization proceeded much faster

than when the reaction was conducted in organic solvents (DMSO), but was still as well-controlled. There were a few reports on unsuccessful polymerization of methacrylamides. Most of the time the polymerizations resulted in low monomer conversion and broad MWD due to low activity of the monomer and side reactions. However very fast polymerization of methacrylamides, such as N-(2-hydroxypropyl)methacrylamide, was reported when using Cu^0 with an active ligand, Me_6TREN, yielding polymers with mediocre dispersities, lowest ~1.5 (Error! Reference source not found.).[33] Polymerization of acrylamides (NIPAAM) however were quite successful and provided polymers with narrow MWD (~1.1) within minutes of initiation of polymerization (Error! Reference source not found.).[124]

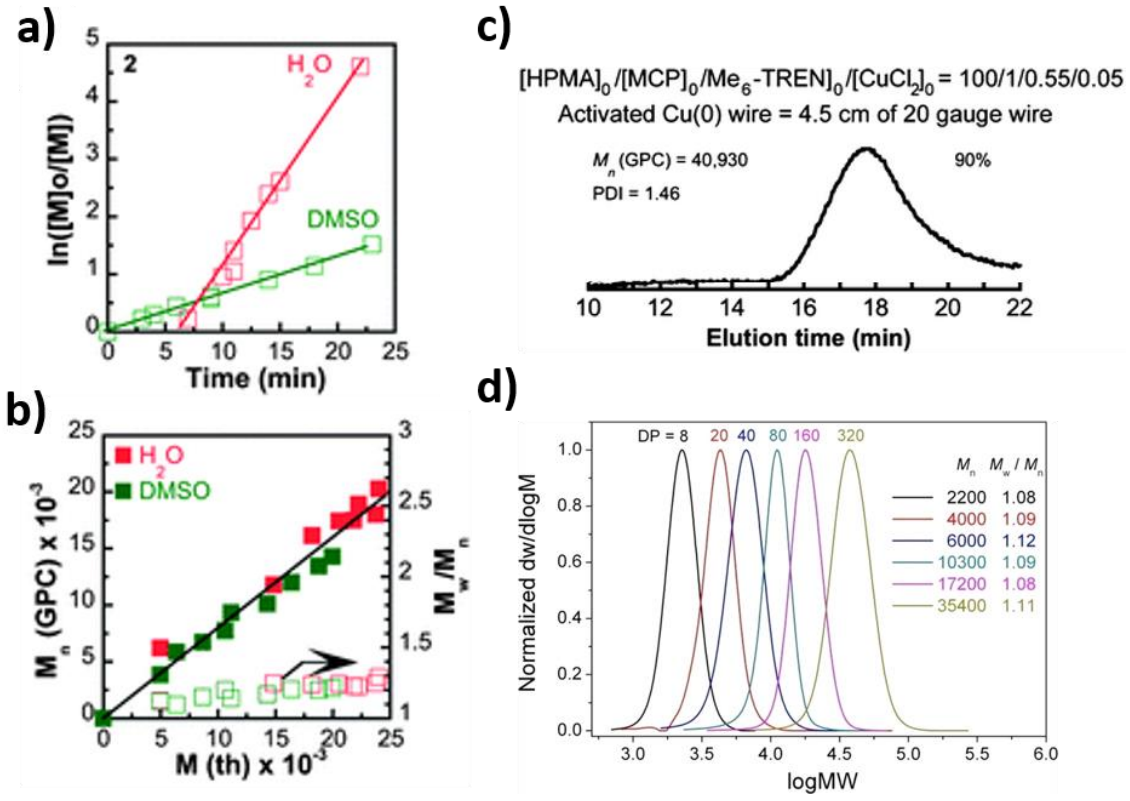

Figure I.17. Polymerization in water in the presence of Cu^0: kinetics and MW/MWD evolution for polymerization of OEOA (a,b); GPC trace for poly(HPMA) (c); GPC traces for poly(NIPAAm).Reprinted with the permission from the references.[45,124] Copyright © 2012 Royal Society of Chemistry and 2013 American Chemical Society.

Another interesting simultaneous activator and reducing agent relevant for aqueous polymerization is sodium dithionite $Na_2S_2O_4$.[126] This reagent is waters-soluble, inexpensive and eco-friendly, and can efficiently reduce a Cu^{II} complex. It was successfully used for polymerizations in mixtures of water and other polar solvents,[31,127] but reactions in pure water have not yet been investigated in detail.

I.4.3. Iron mediated ATRP.

Iron complexes are less studied and less utilized for ATRP than copper complexes, but they are still very promising catalysts. Iron itself is inexpensive and non-toxic, and diverse iron complexes were extensively studied in many other chemistry areas providing an array of various complexes for investigation as ATRP catalysis. It was shown that many iron complexes can successfully control an ATRP.[128-132] Due to iron coordination chemistry, in some cases simple ligands like halogens or solvents can form iron complexes that act as a catalyst, which significantly simplifies polymerization procedure.[133-135] However, there are still a number of limitations to iron mediated ATRP. Among them are the mediocre activity of the current catalyst complexes, complicated coordination chemistry, various spin and oxidation states of iron, unstable complexes and formation of multiple species in polar environments.[132] The stability of catalyst complexes is especially relevant for polymerization in aqueous media, and it was shown that traces of water interfere for polymerization conducted in organic media and slow down the rate of polymerization.[136] All these factors contribute to limited examination of iron catalyzed ATRP in water. Until recently there was only one report on aqueous Fe mediated ATRP of OEOMA which utilized TDA-1 as a ligand (**Figure I.7**).[82] The polymerization resulted in

linear kinetics and formed polymers with low MWD, but suffered from inefficient initiation. Nevertheless, this paper indicated that it was possible to use iron complexes catalyze ATRP in water. Chapter IV details an extension of this subject by investigating the utility of iron porphyrins as ATRP catalysts.

I.4.4. Enzymatic, biomimetic and bacterial ATRP.

Application of enzymes in polymerization was known for years and has been primarily applied to the polymerization of natural polysaccharides, polyesters, polyamides and many others.[137] Recently Bruns et al. and di Lena et al. reported application of proteins with metal centers to catalyze ATRP in water.[109,138-141] Proteins with both iron and copper in their active center were tested (**Figure I.18**). Iron containing proteins were represented by proteins with heme as their prosthetic group. including horseradish peroxidase, hemoglobin and catalase.[109,138-140] Heme is a type of iron porphyrin where the iron can undergo interactions requiring development of different oxidation states depending on the reaction.[142] It is most likely that for an ATRP reaction the Fe^{III} in the protein is reduced to Fe^{II} by reaction with ascorbic acid to start polymerization. When a copper containing protein laccase was used the copper is complexed by histidine and cysteine residues (**Figure I.18c**).[138,139] Polymerization of methacrylates, acrylates and acrylamides in the presence of these types of proteins were reported to produce polymers with relatively narrow MWDs at lower monomer conversions within several hours, but at higher conversions the polymers suffered from broader MWD (~1.5). Polymerization in the presence of iron porphyrins as catalysts was inspired by such enzymatic ATRP and are described in Chapter IV.

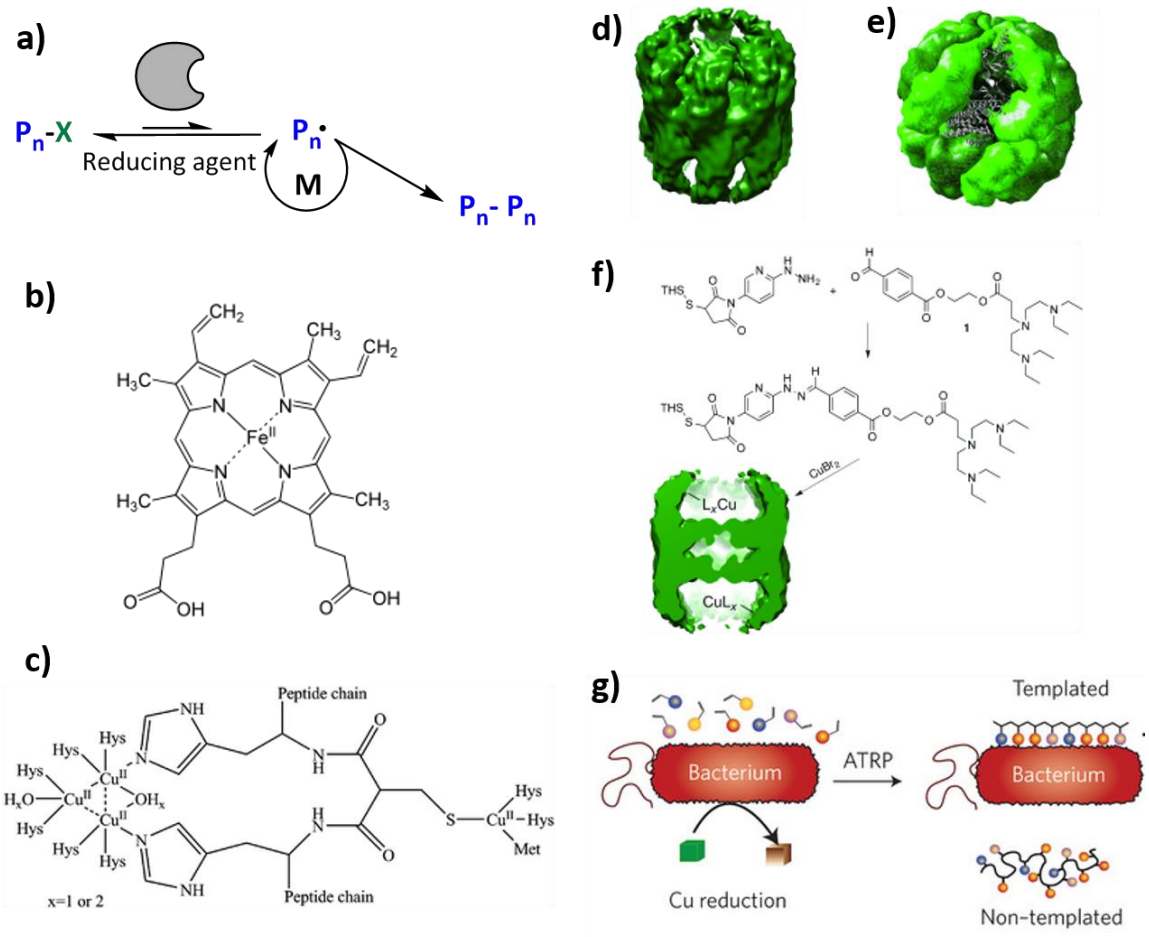

Figure I.18. Enzymatic, biomimetic and bacterial ATRP: (a) general scheme for ATRP catalyzed by a protein; (b) heme structure; (c) laccase metal center structure; (d, e, f) chaperonin frontal and top view, and with immobilized copper complex; (g) scheme of bacteria catalyzed ATRP. Reprinted with permission from the references.[138,143,144] Copyright © 2013 WILEY-VCH Verlag GmbH & Co and 2014 Nature Publishing Group.

In another study a copper complex was covalently entrapped within a hollow protein complex, or so-called protein cage (**Figure I.18d-e**).[143] Thermosome, a chaperonin from an archaea, was chosen as a nano-reactor and macromolecules could migrate in and out of the complex when it is in its open state. Such entrapment of polymerization resulted in formation of polymer with very low MWD (~1.11), which is especially interesting when compared to the results of polymerization catalyzed by globular proteins modified with

copper complexes which yielded final polymers of much higher MW and broader MWD (~2.0).

Another noticeable example of utilizing naturally available tools for polymerization is ATRP conducted due to the enzymatic apparatus of bacteria.[144] In a recent publication by C. Alexander et al. the reducing activity generated via respiratory chains of *E. coli* was used to form Cu^{I} species from added Cu^{II} complexes resulting in successful polymerization. An additional implication of this work is that copolymers produced within close proximity to the bacteria are templated by the cell membrane surface and drastically differ from copolymers produced further in solution. It was shown in that particular study that templated copolymers can be potentially utilized for recognition of cells based on copolymer adhesion behavior.

I.4.5. Polymerization in inverse mini- and microemulsion.

Aqueous ATRP can also be performed in inverse mini- or microemulsion, where water droplets containing all necessary polymerization components are dispersed in an oil phase stabilized with surfactant.[145-148] ATRP in inverse mini- and microemulsions was reported to be useful for production of water-soluble polymers and nanogels (nanosized hydrogels).[146-148] Inverse miniemulsion typically utilizes up to 5 wt. % of surfactant and requires homogenizing techniques like ultrasonication or high speed mechanical stirring.[149-152] Typical droplets formed using this method are in the range 150 – 200 nm.[149-152] With an increase of surfactant content up to 15 wt. % one can form thermodynamically stable microemulsion system with droplet sizes around 20 – 30 nm with simple stirring.[153-155] AGET ATRP is a convenient method to produce polymers under dispersed media conditions. Water-soluble reducing agents like ascorbic acid or hydrazine can be used to

reduce Cu^{II} in situ. In a photoinitated ATRP in inverse microemulsion a water-soluble photoinitiator can be used instead of a reducing agent.[147]

Among advantages of polymerization in mini- and microemulsion are the low viscosity of the reaction medium and high yields of polymers.[150,152,156] However purification from surfactant makes these methods less attractive for preparation of simple linear polymers. Nevertheless, such methods can be quite suitable for preparation of nanogels, or nanosized hydrogels.[145,146,157] Nanogels can be prepared in the presence of a crosslinker, and macroscopic gelation is avoided due to segregation of the reaction within individual monomer droplets. Depending on whether mini- or microemulsion was used, the average size of the final nanogels are in the range of 80 – 350 nm.[145-150,157,158]

Nevertheless, it can be challenging to prepare uniform nanogels by such methods due to the Ostwald ripening process.[149,150,158,159] Ostwald ripening is a thermodynamically driven spontaneous process of molecular diffusion which results in increased size of the final polymer droplets and even coalescence. Such effects can be limited by use of costabilizers or polymeric surfactants.[149,150,158,159] Typically a salt or a polymer with high water solubility can be used as a costabilizer. For instance, during polymerization of acrylamides the formed polymer acts as a costabilizer due to its high insolubility in organic media. But with some other less hydrophilic polymers addition of salts can limit Ostwald ripening and prevent phase separation. Another approach is use of polymeric surfactants (including reactive surfactants) due to their higher affinity to the interphase compared to conventional surfactants.[149,158,160] However, even with costabilizers and various surfactants an increase in size of the final polymer droplet (2-3 times) is often observed. Chapter VI addresses this issue by description of conditions for polymerization of hydrophilic inimer

under inverse microemulsion conditions, which results in efficient nucleation and subsequently preservation of size of the initial micelle in the final polymer droplet.

I.5. Summary

To summarize this Chapter, conducting ATRP in water can be difficult due to associated side reactions occurring in this media in addition to significantly higher ATRP equilibrium constant K_{ATRP}. Nevertheless, such method can be quite beneficial to generate various types of materials under environmentally friendly conditions, shorter polymerization times, and biologically friendly conditions. As evident from the literature, diverse catalytic systems, polymerization conditions and monomers were studied delivering functional materials. However, there were still certain limitations in this field and this Thesis had attempted to address the following aspects:

Chapter II describes generalized polymerization conditions to prepare protein-polymer hybrids with narrow MWD andhigh monomer conversions. Both normal and AGET ATRP were investigated, but slow feeding of reducing agent during AGET ATRP allowed well-defined protein-polymer hybrids utilizing active catalyst, like Cu/TPMA.

Chapter III takes developed AGET ATRP one step further and describes well-controlled polymerization at low ppm (<300) copper catalyst concentration.

Chapter IV focuses on the development of novel bio-inspired iron catalysts. Iron porphyrins stable and reducing structure was utilized to successfully catalyze ATRP in water.

Chapter V is more focused on material generation and describes copolymerization of vinyl monomers with cyclic ketene acetal monomer to generate uniformly degradable polymers by ATRP.

Chapter VI as was mentioned previously describes hydrophilic inimer polymerization in inverse microemulsion to generate cationic nanogels with size control throughout polymerization.

Chapter VII deviates from previous type of materials and focuses on preparation of macrogels and how hydrophilic and hydrophobic gels can be combined into one material.

I.6. References

(1) Odian, G. In *Principles of Polymerization*; John Wiley & Sons, Inc.: 2004, p 198.

(2) Matyjaszewski, K.; Tsarevsky, N. V. *J. Am. Chem. Soc.* **2014**, *136*, 6513.

(3) Wang, J.-S.; Matyjaszewski, K. *J. Am. Chem. Soc.* **1995**, *117*, 5614.

(4) Chiefari, J.; Chong, Y. K.; Ercole, F.; Krstina, J.; Jeffery, J.; Le, T. P. T.; Mayadunne, R. T. A.; Meijs, G. F.; Moad, C. L.; Moad, G.; Rizzardo, E.; Thang, S. H. *Macromolecules* **1998**, *31*, 5559.

(5) Kato, M.; Kamigaito, M.; Sawamoto, M.; Higashimura, T. *Macromolecules* **1995**, *28*, 1721.

(6) Hawker, C. J.; Bosman, A. W.; Harth, E. *Chem. Rev.* **2001**, *101*, 3661.

(7) Nicolas, J.; Guillaneuf, Y.; Lefay, C.; Bertin, D.; Gigmes, D.; Charleux, B. *Prog. Polym. Sci.* **2013**, *38*, 63.

(8) Braunecker, W. A.; Matyjaszewski, K. *Prog. Polym. Sci.* **2007**, *32*, 93.

(9) Matyjaszewski, K.; Xia, J. *Chem. Rev.* **2001**, *101*, 2921.

(10) Matyjaszewski, K. *Macromolecules* **2012**, *45*, 4015.

(11) Wang, Y.; Soerensen, N.; Zhong, M.; Schroeder, H.; Buback, M.; Matyjaszewski, K. *Macromolecules* **2013**, *46*, 683.

(12) Tang, W.; Kwak, Y.; Braunecker, W.; Tsarevsky, N. V.; Coote, M. L.; Matyjaszewski, K. *J. Am. Chem. Soc.* **2008**, *130*, 10702.

(13) Tang, W.; Matyjaszewski, K. *Macromolecules* **2006**, *39*, 4953.

(14) Matyjaszewski, K.; Jakubowski, W.; Min, K.; Tang, W.; Huang, J.; Braunecker, W. A.; Tsarevsky, N. V. *Proc. Natl. Acad. Sci. U. S. A.* **2006**, *103*, 15309.

(15) Tang, W.; Matyjaszewski, K. *Macromolecules* **2007**, *40*, 1858.

(16) Xia, J.; Paik, H.-j.; Matyjaszewski, K. *Macromolecules* **1999**, *32*, 8310.

(17) Debuigne, A.; Caille, J.-R.; Willet, N.; Jerome, R. *Macromolecules* **2005**, *38*, 9488.

(18) Lee, S. B.; Russell, A. J.; Matyjaszewski, K. *Biomacromolecules* **2003**, *4*, 1386.

(19) Senkal, B. F.; Yavuz, E. *Polym. Adv. Technol.* **2006**, *17*, 928.

(20) Rademacher, J. T.; Baum, M.; Pallack, M. E.; Brittain, W. J.; Simonsick, W. J., Jr. *Macromolecules* **2000**, *33*, 284.

(21) Wang, X. S.; Armes, S. P. *Macromolecules* **2000**, *33*, 6640.

(22) Zeng, F.; Shen, Y.; Zhu, S.; Pelton, R. *J. Polym. Sci. A: Polym. Chem.* **2000**, *38*, 3821.

(23) Perrier, S.; Armes, S. P.; Wang, X. S.; Malet, F.; Haddleton, D. M. *J. Polym. Sci., Part A: Polym. Chem.* **2001**, *39*, 1696.

(24) Tsarevsky, N. V.; Pintauer, T.; Matyjaszewski, K. *Macromolecules* **2004**, *37*, 9768.

(25) Heredia, K. L.; Bontempo, D.; Ly, T.; Byers, J. T.; Halstenberg, S.; Maynard, H. D. *J. Am. Chem. Soc.* **2005**, *127*, 16955.

(26) Gao, W.; Liu, W.; Mackay, J. A.; Zalutsky, M. R.; Toone, E. J.; Chilkoti, A. *Proc. Natl. Acad. Sci. U. S. A.* **2009**, *10*, 15231.

(27) Coca, S.; Jasieczek, C. B.; Beers, K. L.; Matyjaszewski, K. *J. Polym. Sci. A: Polym. Chem.* **1997**, *36*, 1417.

(28) Wang, X. S.; Jackson, R. A.; Armes, S. P. *Macromolecules* **1999**, *33*, 255.

(29) Wang, X. S.; Armes, S. P. *Polym. Prepr.* **2000**, *41*, 484.
(30) Oh, J. K.; Min, K.; Matyjaszewski, K. *Macromolecules* **2006**, *39*, 3161.
(31) Abreu, C. M. R.; Serra, A. C.; Popov, A. V.; Matyjaszewski, K.; Guliashvili, T.; Coelho, J. F. J. *Polym. Chem.* **2013**, *4*, 5629.
(32) Leng, X.; Nguyen, N. H.; van Beusekom, B.; Wilson, D. a.; Percec, V. *Polym. Chem.* **2013**, *4*, 2424.
(33) Nguyen, N. H.; Rodriguez-Emmenegger, C.; Brynda, E.; Sedlakova, Z.; Percec, V. *Polym. Chem.* **2013**, *4*, 2424.
(34) Wang, X. S.; Malet, F. L. G.; Armes, S. P.; Haddleton, D. M.; Perrier, S. *Macromolecules* **2000**, *34*, 162.
(35) Lobb, E. J.; Ma, I.; Billingham, N. C.; Armes, S. P.; Lewis, A. L. *J. Am. Chem. Soc.* **2001**, *123*, 7913.
(36) Robinson, K. L.; Khan, M. A.; de Paz Banez, M. V.; Wang, X. S.; Armes, S. P. *Macromolecules* **2001**, *34*, 3155.
(37) Li, Y.; Armes, S. P.; Jin, X.; Zhu, S. *Macromolecules* **2003**, *36*, 8268.
(38) Chung, I.-D.; Britt, P.; Xie, D.; Harth, E.; Mays, J. *Chem. Comm.* **2005**, 1046.
(39) Lele, B. S.; Murata, H.; Matyjaszewski, K.; Russell, A. J. *Biomacromolecules* **2005**, *6*, 3380.
(40) Masci, G.; Giacomelli, L.; Crescenzi, V. *J. Polym. Sci., Part A: Polym. Chem.* **2005**, *43*, 4446.
(41) Paneva, D.; Mespouille, L.; Manolova, N.; Degée, P.; Rashkov, I.; Dubois, P. *Macromol. Rapid Commun.* **2006**, *27*, 1489.
(42) Lutz, J.-F. *J. Polym. Sci., Part A: Polym. Chem.* **2008**, *46*, 3459.
(43) Lutz, J.-F.; Boerner, H. G. *Prog. Polym. Sci.* **2008**, *33*, 1.
(44) Tan, Y.; Yang, Q.; Sheng, D.; Su, X.; Xu, K.; Song, C.; Wang, P. *e-Polymers* **2008**, No pp. given.
(45) Nguyen, N. H.; Kulis, J.; Sun, H.-J.; Jia, Z.; van Beusekom, B.; Levere, M. E.; Wilson, D. a.; Monteiro, M. J.; Percec, V. *Polym. Chem.* **2013**, *4*, 144.
(46) Pelegri-O'Day, E. M.; Lin, E.-W.; Maynard, H. D. *J. Am. Chem. Soc.* **2014**, *136*, 14323.
(47) Sumerlin, B. S. *ACS Macro Letters* **2012**, *1*, 141.
(48) Velonia, K. *Polym. Chem.* **2010**, *1*, 944.
(49) Magnusson, J. P.; Bersani, S.; Salmaso, S.; Alexander, C.; Caliceti, P. *Bioconjugate Chem.* **2010**, *21*, 671.
(50) Gao, W.; Liu, W.; Christensen, T.; Zalutsky, M. R.; Chilkoti, A. *Proc. Natl. Acad. Sci. U. S. A.* **2010**, *107*, 16432.
(51) Hoffman, A. S. *Adv. Drug Delivery Rev.* **2002**, *54*, 3.
(52) Albertsson, A.-C.; Varma, I. K. *Biomacromolecules* **2003**, *4*, 1466.
(53) Duncan, R. *Nat. Rev. Drug Discovery* **2003**, *2*, 347.
(54) Smela, E. *Adv. Mater.* **2003**, *15*, 481.
(55) Gil, E. S.; Hudson, S. M. *Prog. Polym. Sci.* **2004**, *29*, 1173.
(56) Alarcon, C. d. l. H.; Pennadam, S.; Alexander, C. *Chem. Soc. Rev.* **2005**, *34*, 276.
(57) Nair, L. S.; Laurencin, C. T. *Prog. Polym. Sci.* **2007**, *32*, 762.
(58) Matyjaszewski, K.; Tsarevsky, N. V. *Nat. Chem.* **2009**, *1*, 276.

(59) Merdan, T.; Kopecek, J.; Kissel, T. *Adv. Drug Delivery Rev.* **2002**, *54*, 715.
(60) Brannon-Peppas, L.; Blanchette, J. O. *Adv. Drug Delivery Rev.* **2004**, *56*, 1649.
(61) Farokhzad, O. C.; Jon, S.; Khademhosseini, A.; Tran, T.-N. T.; LaVan, D. A.; Langer, R. *Cancer Res.* **2004**, *64*, 7668.
(62) Kukowska-Latallo, J. F.; Candido, K. A.; Cao, Z.; Nigavekar, S. S.; Majoros, I. J.; Thomas, T. P.; Balogh, L. P.; Khan, M. K.; Baker, J. R., Jr. *Cancer Res.* **2005**, *65*, 5317.
(63) Nasongkla, N.; Bey, E.; Ren, J.; Ai, H.; Khemtong, C.; Guthi, J. S.; Chin, S.-F.; Sherry, A. D.; Boothman, D. A.; Gao, J. *Nano Lett.* **2006**, *6*, 2427.
(64) Rapoport, N. *Prog. Polym. Sci.* **2007**, *32*, 962.
(65) Dhar, S.; Gu, F. X.; Langer, R.; Farokhzad, O. C.; Lippard, S. J. *Proc. Natl. Acad. Sci. U. S. A.* **2008**, *105*, 17356.
(66) Davis, M. E. *Mol. Pharmaceutics* **2009**, *6*, 659.
(67) Fox, M. E.; Szoka, F. C.; Frechet, J. M. J. *Acc. Chem. Res.* **2009**, *42*, 1141.
(68) Malam, Y.; Loizidou, M.; Seifalian, A. M. *Trends Pharmacol. Sci.* **2009**, *30*, 592.
(69) Deming, T. J. *Prog. Polym. Sci.* **2007**, *32*, 858.
(70) Owens, D. E.; Peppas, N. A. *Int. J. Pharm.* **2006**, *307*, 93.
(71) Haag, R.; Kratz, F. *Angew. Chem., Int. Ed.* **2006**, *45*, 1198.
(72) Perrier, S.; Haddleton, D. M. *Macromol. Symp.* **2002**, *182*, 261.
(73) Coullerez, G.; Carlmark, A.; Malmstroem, E.; Jonsson, M. *J. Phys. Chem. A* **2004**, *108*, 7129.
(74) Braunecker, W. A.; Tsarevsky, N. V.; Gennaro, A.; Matyjaszewski, K. *Macromolecules* **2009**, *42*, 6348.
(75) Horn, M.; Matyjaszewski, K. *Macromolecules* **2013**, *46*, 3350.
(76) Bortolamei, N.; Isse, A. a.; Magenau, A. J. D.; Gennaro, A.; Matyjaszewski, K. *Angew. Chem. Int. Ed.* **2011**, *50*, 1.
(77) Smolne, S.; Buback, M. *Macromol. Chem. Phys.* **2015**, *216*, 894.
(78) Chmielarz, P.; Park, S.; Simakova, A.; Matyjaszewski, K. *Polymer* **2015**, *60*, 302.
(79) Tsarevsky, N. V.; Braunecker, W. A.; Brooks, S. J.; Matyjaszewski, K. *Macromolecules* **2006**, *39*, 6817.
(80) Huang, W.; Kim, J.-B.; Bruening, M. L.; Baker, G. L. *Macromolecules* **2002**, *35*, 1175.
(81) Nguyen, N. H.; Rosen, B. M.; Jiang, X.; Fleischmann, S.; Percec, V. *J. Polym. Sci., Part A: Polym. Chem.* **2009**, *47*, 5577.
(82) He, W.; Zhang, L.; Miao, J.; Cheng, Z.; Zhu, X. *Macromol. Rapid Commun.* **2012**, *33*, 1067.
(83) Bontempo, D.; Maynard, H. D. *J. Am. Chem. Soc.* **2005**, *127*, 6508.
(84) Peeler, J. C.; Woodman, B. F.; Averick, S.; Miyake-Stoner, S. J.; Stokes, A. L.; Hess, K. R.; Matyjaszewski, K.; Mehl, R. A. *J. Am. Chem. Soc.* **2010**, *132*, 13575.
(85) Broyer, R. M.; Grover, G. N.; Maynard, H. D. *Chem. Comm.* **2011**, *47*, 2212.
(86) Finn, M. G.; Pokorski, J. K.; Breitenkamp, K.; Liepold, L. O.; Qazi, S. *J. Am. Chem. Soc.* **2011**, *133*, 9242.

(87) Wong, L. S.; Okrasa, K.; Micklefield, J. *Organic & Biomolecular Chemistry* **2010**, *8*, 782.

(88) Konno, T.; Watanabe, J.; Ishihara, K. *Biomacromolecules* **2004**, *5*, 342.

(89) Le Droumaguet, B.; Velonia, K. *Angew. Chem.* **2008**, *120*, 6359.

(90) Depp, V.; Alikhani, A.; Grammer, V.; Lele, B. S. *Acta Biomater.* **2009**, *5*, 560.

(91) Mougin, N. C.; van Rijn, P.; Park, H.; Müller, A. H. E.; Böker, A. *Adv. Func. Mat.* **2011**, *21*, 2470.

(92) Murata, H.; Cummings, C. S.; Koepsel, R. R.; Russell, A. J. *Biomacromolecules* **2013**, *14*, 1919.

(93) Cummings, C.; Murata, H.; Koepsel, R.; Russell, A. J. *Biomaterials* **2013**, *34*, 7437.

(94) von Werne, T.; Patten, T. E. *J. Am. Chem. Soc.* **2001**, *123*, 7497.

(95) Ohno, K.; Morinaga, T.; Koh, K.; Tsujii, Y.; Fukuda, T. *Macromolecules* **2005**, *38*, 2137.

(96) Matyjaszewski, K.; Dong, H.; Jakubowski, W.; Pietrasik, J.; Kusumo, A. *Langmuir* **2007**, *23*, 4528.

(97) Matyjaszewski, K.; Miller, P. J.; Shukla, N.; Immaraporn, B.; Gelman, A.; Luokala, B. B.; Siclovan, T. M.; Kickelbick, G.; Vallant, T.; Hoffmann, H.; Pakula, T. *Macromolecules* **1999**, *32*, 8716.

(98) Edmondson, S.; Osborne, V. L.; Huck, W. T. S. *Chem. Soc. Rev.* **2004**, *33*, 14.

(99) Wu, L.; Glebe, U.; Boeker, A. *Polym. Chem.* **2015**, *6*, 5143.

(100) Perruchot, C.; Khan, M. A.; Kamitsi, A.; Armes, S. P.; von Werne, T.; Patten, T. E. *Langmuir* **2001**, *17*, 4479.

(101) Jayachandran, K. N.; Takacs-Cox, A.; Brooks, D. E. *Macromolecules* **2002**, *35*, 4247.

(102) Lou, X.; Wang, C.; He, L. *Biomacromolecules* **2007**, *8*, 1385.

(103) Vo, C.-D.; Schmid, A.; Armes, S. P.; Sakai, K.; Biggs, S. *Langmuir* **2007**, *23*, 408.

(104) Xu, F. J.; Li, J.; Su, F.; Zhao, X. S.; Kang, E. T.; Neoh, K. G. *J. Nanosci. Nanotechnol.* **2008**, *8*, 5858.

(105) Dunderdale, G. J.; Urata, C.; Miranda, D. F.; Hozumi, A. *ACS Appl. Mater. Inter.* **2014**, *6*, 11864.

(106) Balamurugan, S. S.; Subramanian, B.; Bolivar, J. G.; McCarley, R. L. *Langmuir* **2012**, *28*, 14254.

(107) Jakubowski, W.; Matyjaszewski, K. *Macromolecules* **2005**, *38*, 4139.

(108) Zhu, W.-P.; Zhong, M.-J.; Li, W.-W.; Dong, H.-C.; Matyjaszewski, K. *Macromolecules* **2011**, *44*, 1920.

(109) Silva, T. B.; Spulber, M.; Kocik, M. K.; Seidi, F.; Charan, H.; Rother, M.; Sigg, S. J.; Renggli, K.; Kali, G.; Bruns, N. *Biomacromolecules* **2013**, *14*, 2703.

(110) Yasayan, G.; Saeed, A. O.; Fernandez-Trillo, F.; Allen, S.; Davies, M. C.; Jangher, A.; Paul, A.; Thurecht, K. J.; King, S. M.; Schweins, R.; Griffiths, P. C.; Magnusson, J. P.; Alexander, C. *Polym. Chem.* **2011**, *2*, 1567.

(111) Xie, L.; Lan, F.; Li, W.; Liu, Z.; Ma, S.; Yang, Q.; Wu, Y.; Gu, Z. *Colloids Surf., B* **2014**, *123*, 413.

(112) Li, B.; Yu, B.; Huck, W. T. S.; Liu, W.; Zhou, F. *J. Am. Chem. Soc.* **2013**, *135*, 1708.

(113) Park, S.; Chmielarz, P.; Gennaro, A.; Matyjaszewski, K. *Angew. Chem.* **2015**, *127*, 2418.

(114) Magenau, A. J. D.; Bortolamei, N.; Frick, E.; Park, S.; Gennaro, A.; Matyjaszewski, K. *Macromolecules* **2013**, *46*, 4346.

(115) Jackson, A.-M. S.; Sheiko, S. S.; Ashby, V. S. *Langmuir* **2015**, *31*, 5489.

(116) Konkolewicz, D.; Wang, Y.; Krys, P.; Zhong, M.; Isse, A. A.; Gennaro, A.; Matyjaszewski, K. *Polym. Chem.* **2014**, *5*, 4396.

(117) Percec, V.; Guliashvili, T.; Ladislaw, J. S.; Wistrand, A.; Stjerndahl, A.; Sienkowska, M. J.; Monteiro, M. J.; Sahoo, S. *J. Am. Chem. Soc.* **2006**, *128*, 14156.

(118) Lligadas, G.; Rosen, B. M.; Monteiro, M. J.; Percec, V. *Macromolecules* **2008**, *41*, 8360.

(119) Konkolewicz, D.; Wang, Y.; Zhong, M.; Krys, P.; Isse, A. A.; Gennaro, A.; Matyjaszewski, K. *Macromolecules* **2013**, *46*, 8749.

(120) Lin, C. Y.; Coote, M. L.; Gennaro, A.; Matyjaszewski, K. *J. Am. Chem. Soc.* **2008**, *130*, 12762.

(121) Lorandi, F.; Fantin, M.; Isse, A. A.; Gennaro, A. *Polymer* **2015**, *72*, 238.

(122) Visnevskij, C.; Makuska, R. *Macromolecules* **2013**, *46*, 4764.

(123) Zhang, Q.; Li, Z.; Wilson, P.; Haddleton, D. M. *Chem. Comm.* **2013**, *49*, 6608.

(124) Zhang, Q.; Wilson, P.; Li, Z.; McHale, R.; Godfrey, J.; Anastasaki, A.; Waldron, C.; Haddleton, D. M. *J. Am. Chem. Soc.* **2013**, *135*, 7355.

(125) Konkolewicz, D.; Krys, P.; Góis, J. R.; Mendonça, P. V.; Zhong, M.; Wang, Y.; Gennaro, A.; Isse, A. A.; Fantin, M.; Matyjaszewski, K. *Macromolecules* **2014**, *47*, 560.

(126) Abreu, C. M. R.; Mendonça, P. V.; Serra, A. C.; Popov, A. V.; Matyjaszewski, K.; Guliashvili, T.; Coelho, J. F. J. *ACS Macro Letters* **2012**, *1*, 1308.

(127) Gois, J. R.; Rocha, N.; Popov, A. V.; Guliashvili, T.; Matyjaszewski, K.; Serra, A. C.; Coelho, J. F. J. *Polym. Chem.* **2014**, *5*, 3919.

(128) Louie, J.; Grubbs, R. H. *Chem. Comm.* **2000**, 1479.

(129) Gibson, V. C.; O'Reilly, R. K.; Reed, W.; Wass, D. F.; White, A. J. P.; Williams, D. J. *Chem. Comm.* **2002**, 1850.

(130) Matyjaszewski, K.; Wei, M.; Xia, J.; McDermott, N. E. *Macromolecules* **1997**, *30*, 8161.

(131) Xue, Z.; He, D.; Xie, X. *Polym. Chem.* **2015**, *6*, 1660.

(132) Poli, R.; Allan, L. E. N.; Shaver, M. P. *Prog. Polym. Sci.* **2014**, *39*, 1827.

(133) Mukumoto, K.; Wang, Y.; Matyjaszewski, K. *ACS Macro Letters* **2012**, *1*, 599.

(134) Wang, Y.; Matyjaszewski, K. *Macromolecules* **2010**, *43*, 4003.

(135) Wang, Y.; Zhang, Y.; Parker, B.; Matyjaszewski, K. *Macromolecules* **2011**, *44*, 4022.

(136) Wang, Y.; Zhang, Y.; Parker, B.; Matyjaszewski, K. *Macromolecules* **2011**, *44*, 4022.

(137) Kobayashi, S.; Makino, A. *Chem. Rev.* **2009**, *109*, 5288.

(138) Ng, Y.-H.; di Lena, F.; Chai, C. L. L. *Polym. Chem.* **2011**, *2*, 589.

(139) Ng, Y.-H.; di Lena, F.; Chai, C. L. L. *Chem. Comm.* **2011**, *47*, 6464.

(140) Sigg, S. J.; Seidi, F.; Renggli, K.; Silva, T. B.; Kali, G.; Bruns, N. *Macromol. Rapid Commun.* **2011**, *32*, 1710.

(141) Kali, G.; Silva, T. B.; Sigg, S. J.; Seidi, F.; Renggli, K.; Bruns, N. In *Progress in Controlled Radical Polymerization: Mechanisms and Techniques.* 2012, p 171.

(142) Poulos, T. L. *Chem. Rev.* **2014**, *114*, 3919.

(143) Renggli, K.; Nussbaumer, M. G.; Urbani, R.; Pfohl, T.; Bruns, N. *Angew. Chem. Int. Ed.* **2013**, 1443.

(144) Magennis, E. P.; Fernandez-Trillo, F.; Sui, C.; Spain, S. G.; Bradshaw, D. J.; Churchley, D.; Mantovani, G.; Winzer, K.; Alexander, C. *Nat Mater* **2014**, *13*, 748.

(145) Matyjaszewski, K.; Oh, J. K.; Perineau, F.; Charleux, B. *J. Polym. Sci., Part A: Polym. Chem.* **2009**, *47*, 1771.

(146) Oh, J. K.; Tang, C.; Gao, H.; Tsarevsky, N. V.; Matyjaszewski, K. *J. Am. Chem. Soc.* **2006**, *128*, 5578.

(147) Ciftci, M.; Tasdelen, M. A.; Li, W.; Matyjaszewski, K.; Yagci, Y. *Macromolecules* **2013**, *46*, 9537.

(148) Li, W.; Matyjaszewski, K. *Polym. Chem.* **2012**, *3*, 1813.

(149) Durand, A.; Marie, E. *Adv. Colloid Interface Sci.* **2009**, *150*, 90.

(150) Solans, C.; Izquierdo, P.; Nolla, J.; Azemar, N.; Garcia-Celma, M. J. *Curr. Opin. Colloid Interface Sci.* **2005**, *10*, 102.

(151) Anton, N.; Benoit, J.-P.; Saulnier, P. *J. Controlled Release* **2008**, *128*, 185.

(152) Cunningham, M. F. *Prog. Polym. Sci.* **2008**, *33*, 365.

(153) Schwuger, M.-J.; Stickdorn, K.; Schomaecker, R. *Chem. Rev.* **1995**, *95*, 849.

(154) McAllister, K.; Sazani, P.; Adam, M.; Cho, M. J.; Rubinstein, M.; Samulski, R. J.; DeSimone, J. M. *J. Am. Chem. Soc.* **2002**, *124*, 15198.

(155) Candau, F.; Leong, Y. S.; Pouyet, G.; Candau, S. *J. Colloid Interface Sci.* **1984**, *101*, 167.

(156) Qiu, J.; Charleux, B.; Matyjaszewski, K. *Prog. Polym. Sci.* **2001**, *26*, 2083.

(157) Averick, S. E.; Magenau, A. J. D.; Simakova, A.; Woodman, B. F.; Seong, A.; Mehl, R. A.; Matyjaszewski, K. *Polym. Chem.* **2011**, *2*, 1476.

(158) Pham, B. T. T.; Zondanos, H.; Such, C. H.; Warr, G. G.; Hawkett, B. S. *Macromolecules* **2010**, *43*, 7950.

(159) Asua, J. M. *Prog. Polym. Sci.* **2002**, *27*, 1283.

(160) Raffa, P.; Wever, D. A. Z.; Picchioni, F.; Broekhuis, A. A. *Chem. Rev.* **2015**.

Chapter II. ATRP under Biologically Relevant Conditions: Grafting From a Protein*

II.1.Preface

The motivation for the project described in this Chapter was the lack of systematic investigations in the field of grafting from a protein by controlled radical polymerization process, and thus the goal was to study and determine the best conditions for grafting from a protein by ATRP in water. The results of this specific study could be further applied to various other systems with appropriate adjustments. This work was started by my former collaborator Dr Saadyah Averick and was carried out in collaboration with other Matyjaszewski group members: Sangwoo Park, Dr Andrew Magenau and Dr Dominik Konkolewicz.

Two ATRP methods were selected for study grafting from a protein: normal ATRP and AGET ATRP. Both methods were optimized for grafting well-controlled polymers from a protein, while preserving the tertiary structure of the biomolecule. In particular the influence of halide species, ligand, reducing agent and buffers on the polymerization of oligo(ethylene oxide) methyl ether methacrylate was investigated in aqueous media at ambient temperature.

I studied AGET ATRP in water using ascorbic acid as the reducing agent. During my research I discovered that one can utilize very active copper complex with ligands such

* Work described in this Chapter was partially published and was reformatted for this Thesis: **Simakova**, **A**., **Averick, S.,** Park, S., Konkolewicz, D., Magenau, A. J. D., Mehl, R. A., & Matyjaszewski, K. ATRP under Biologically Relevant Conditions: Grafting from a Protein. *ACS Macro Letters* 2011, 1, 6-10.

as TPMA, but it was essential that only very small amounts of Cu^{I} was generated. This was successfully achieved by slow feeding of ascorbic acid at such rate that only total of 1% of the Cu^{II} was reduced to Cu^{I} by adding 8 nmol/min of the solution. Using this method, polymerizations could reach high monomer conversions, and final polymers were characterized by symmetrical GPC curves and low M_w/M_n (~1.1). This approach was especially valuable for polymerization in buffered solution, where polymerization under normal ATRP conditions was characterized by decreased reaction rate after 1h, inefficient initiation, and higher M_w/M_n.

My role in this project was investigating AGET ATRP method for grafting from a protein, and I had performed, analyzed and summarized all reactions conducted by this method. I would like to acknowledge whole team who participated in this project: Dr Saadyah Averick, who prepared ATRP initiator functionalized protein and worked on development of normal ATRP for grafting from a protein, Sangwoo Park, who worked on development of normal ATRP in water, Dr Andrew Magenau and Dr Dominik Konkolewicz for their mentorship during this project. The fundamentals of conducting an ATRP in water, which were investigated in this work, served as a starting point for further projects related to low ppm method (Chapter III) and bioinspired iron catalysts (Chapter IV).

II.2.Introduction

Controlled/living radical polymerizations (CRPs) provide a methodology to create polymers with predefined molecular weights, compositions, architectures and narrow distributions.[1] Atom transfer radical polymerization (ATRP) is among the most well-studied and robust CRP techniques, since it is compatible with a variety of functional monomers, reaction conditions and gives high chain-end functionality, which can be used for post-polymerization modifications.[2,3] ATRP can create a diverse array of compositions, topologies, and materials exemplified by blocks and gradients, complex architectures such as stars, combs and brushes,[4] and inorganic-polymeric hybrid materials.[5] Furthermore, ATRP along with other CRP techniques are widely used to prepare bio-hybrids including conjugates between peptides, proteins, nucleic acids, and carbohydrates and synthetic polymers.[6]

Protein-polymer hybrids (PPH) are a rapidly developing field of bionconjuagtes typically finding application in the pharmaceutical industry.[7] Linking a protein with a polymer improves pharmacokinetics, physical and proteolytic stability of proteins.[8] Poly(ethylene oxide) (PEO or PEG) is the polymer which has been most commonly conjugated to a protein.[9] However, a new generation of "smart" PPHs can be created by conjugating well-defined responsive polymers (*e.g.* thermo-, photo-, pH-) to proteins. For instance, novel drug delivery systems with stimuli responsive activity can be produced by conjugating thermoresponsive polymers, such as poly(*N*-isopropylacrylamide) (PNIPAM) or poly(oligo(ethylene oxide) methacrylate) (POEOMA) to proteins.[10-14]

Preparation of well-defined PPHs can be achieved by two methods: "grafting to" (GT) and "grafting from" (GF).[10,15,16] The GT approach links a well-defined preformed polymer

with a reactive chain-end to a complimentary functionalized protein,[8,11,12,17,18] whereas the GF involves growing a polymer directly from an initiating site on the protein.[19,20] The GF method leads to high yields of PPH and simpler of purification of the resulting hybrid,[15,16] although it requires modification of a protein with initiating moieties.[10,15] ATRP is widely used for GF proteins. This technique was introduced by Maynard *et. al.*,[21] and subsequently applied to create a variety of PPHs.[22-24] Recently the GF approach was extended beyond traditional ATRP to include activators generated by electron transfer (AGET) ATRP, with ascorbic acid as reducing agent, was used to make well-defined PPHs.[19,25,26]

ATRP is traditionally conducted in bulk or in various organic solvents,[2] however, for preparation of bioconjugates, using the GF method, polymers must be grown in aqueous media. Although, there have been reports where ATRP has been used in the GF approach to grow OEOMA based polymers from several proteins, the control of these polymerizations has been difficult to achieve.[21,27,28] Among the major challenges of aqueous ATRP is high predicted equilibrium constant K_{eq}, which leads to high radical concentrations and termination rates.[29,30] Moreover, ATRP in aqueous media suffers from many additional complications, which include dissociation of copper(II) halide species, lability of the copper(I)/ligand complex, disproportionation of certain copper(I) species, and hydrolysis of the carbon – halogen bond[31]. These factors all contribute to poorly controlled polymerizations with broad distributions, as a result of low deactivator concentrations and loss of ATRP activity. Furthermore, when utilizing proteins, undesired binding of the protein to the ATRP catalyst can occur which may denature the protein[32] and cause inactivity of the copper complex when a sufficiently high binding constant ligand is not used. Last, many monomers and polymers of interest have limited solubility in pure

water. Due to the above listed challenges, it is important to develop general conditions for synthesis of well-defined PPHs by the GF approach using ATRP in aqueous media.

Herein is described an ATRP methodology to create PPHs using the GF approach in aqueous media under biologically relevant conditions. These conditions were designed to preserve the protein's tertiary structure and activity, while simultaneously offering control over polymerization. Preservation of a protein's native structure imposes several restrictions; specifically in regard to reaction temperatures, concentrations, and organic content. Thus, polymerizations should be performed at near ambient temperatures (30 °C in this work), to avoid thermal denaturation of the protein. Also, most proteins denature at high concentrations, and hence, must be kept in dilute conditions near 2 mg/ml; whereas, and the presence of a high concentration of organic media can destabilize proteins therefore limiting the total organic content to no greater than 20% (monomer and cosolvent).[33]

In this work an ATRP initiator was attached to bovine serum albumin (BSA) (**Scheme II.1**). This protein was selected because of its wide usage as a valid model protein, and due to its abundance and low cost.[14,34,35] Furthermore, the initiating moiety attached to BSA was designed to contain a base cleavable ester linkage to facilitate the direct analysis of the polymer GF the protein. This study investigates the influence of ligand, halide species and organic cosolvent on the ATRP process under biologically relevant conditions. In particular, conventional ATRP and AGET ATRP processes were studied and optimized. Finally, the conditions developed for ATRP under biologically relevant conditions were used to synthesize a well-defined smart polymer with LCST behavior, demonstrating the utility of these techniques.

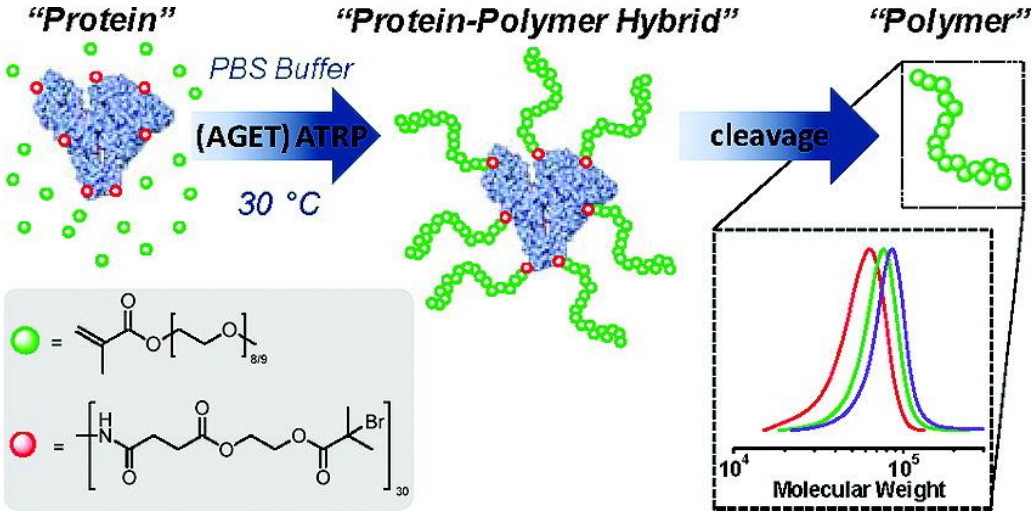

Scheme II.1. Grafting from a protein by ATRP and analysis of cleaved polymer chains.

II.3.Results and discussion

Successful ATRP from a protein requires the protein to be stable in the presence of copper halides. Therefore, the green fluorescent protein (GFP) was used as a model protein to test protein stability towards different pre-complexed Cu:ligand species, under typical reaction conditions (*i.e.* 1 mg/ml GFP, 10% monomer in 0.1 M PBS) (**Figure II.1**). Initially three ligands were selected ranging from very activating tris(2-pyridylmethyl)amine (TPMA), moderately activating 2,2'-bipyridine (Bpy), and highly deactivating N-(n-Propyl)pyridylmethanimine (PI).[36] GFP was selected for the stability studies because denaturation of its beta-barrel structure leads to a loss of its fluorescent properties[37]. Fluorescence measurements showed that TPMA and bpy copper complexes do not greatly influence on the GFP's tertiary structure as indicated by similar emission spectra for GFP and GFP in the presence of $CuCl_2$/TPMA and $CuCl_2$/bpy. In contrast, upon the addition of pre-complexed $CuCl_2$/PI the GFP denatured, demonstrated by a 100 fold decrease in fluorescence intensity of GFP, with comparable results seen upon the addition of copper halide to GFP. Based on these results, bpy and TPMA ligands were selected for the development of ATRP under biologically relevant conditions.

In addition to assessing protein stability, rigorous analysis of the synthetic polymer in a PPH is needed for the characterization of bioconjugates as it demonstrates control over polymerization. In order to facilitate direct analysis of the polymer grafted from BSA, the protein was modified with cleavable ester initiator (BSA-O-$[iBBr]_{30}$) (**Scheme II.2**). The ester bond linking the initiator to the protein can be selectively cleaved by 5% KOH (w/v) solution, without affecting the oligoethylene oxide methyl ether side chains[38]. This allows

real time monitoring of the GF reactions, since the synthetic polymers can be cleaved and directly analyzed using gel permeation chromatography.

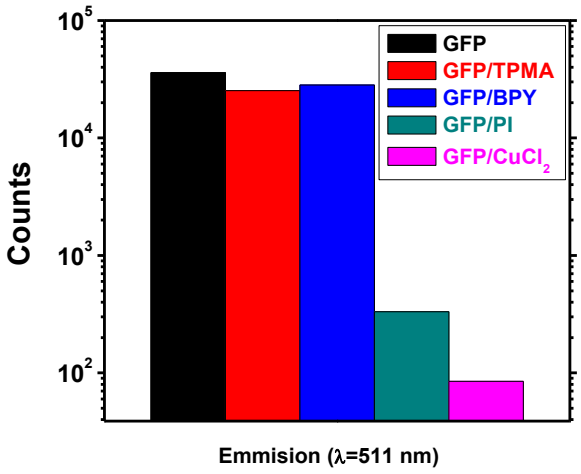

Figure II.1. Effect of $CuCl_2$:L on GFP (1 mg/ml) stability. $[CuCl_2]/[L]=1/[bpy]$,[PI] and [TPMA] = 2.2 and 1.1 $[CuCl_2]=19$ mM, $[OEOMA_{475}] = 0.23$ M

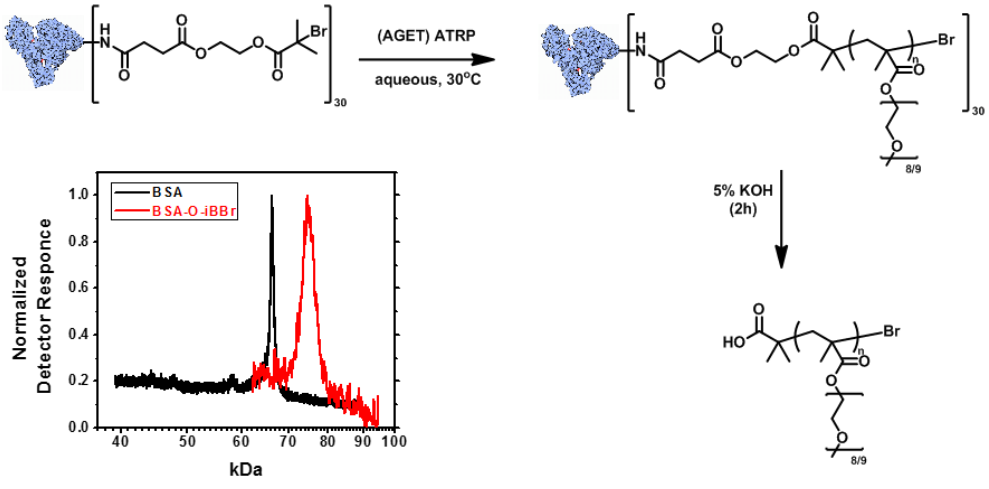

Scheme II.2. Scheme of polymerization from BSA-O-$[iBBr]_{30}$ and cleavage of grafted polymer. Insertion:MALDI-TOF spectra of BSA and BSA-O-$[iBBr]_{30}$.

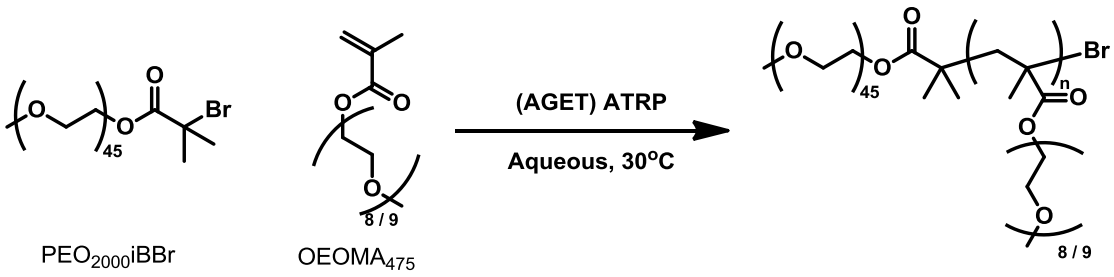

$PEO_{2000}iBBr$ $OEOMA_{475}$

Scheme II.3. (AGET) ATRP of $OEOMA_{475}$ under biologically relevant conditions.

Table II.1. Experimental conditions of normal ATRP from PEO-iBBr and BSA-O-$[iBBr]_{30}$

	M/I/CuX/CuX_2/L	I	L	X	Conv./%	$M_{n,theo}\times10^{-3}$	$M_{n,GPC}\times10^{-3}$	M_w/M_n
1	455/1/1/9/22	PEO	bpy	Br	45	94	108	1.54
2	455/1/1/9/22	PEO	bpy	Cl	27	55	58	1.16
3	455/1/1/9/11	PEO	TPMA	Br	2	40	12	1.27
4	455/1/1/9/11	PEO	TPMA	Cl	2	36	18	1.22
5	227/1/1/9/21	BSA	bpy	Br	66	71	100	1.16
6	227/1/1/9/11	BSA	bpy	Cl	58	63	97	1.18
7	227/1/1/9/21	BSA	TPMA	Br	5	5	40	1.10
8	227/1/1/9/11	BSA	TPMA	Cl	2	2	35	1.16

1mM initiator, 10 – 20% monomer (v/v), water, 30°C, 4h of polymerization

In order to investigate the feasibility of forming well-controlled PPHs using the GF approach, different ATRP methods were investigated. Initially, the traditional ATRP method was examined for the synthesis of PPHs based on BSA and OEOMA, since it is conceptually the simplest of all the ATRP methods. Previous work showed that successful ATRP in protic solvents required high concentrations of the Cu^{II} halide species (up to 80% of total copper concentration), due to a high equilibrium constant and partial dissociation of the deactivator.[31] Based on these results, 10% of the total copper used was Cu^{I} and the remaining was Cu^{II}, where the latter promotes a well-controlled polymerization. Initial experiments were performed with a PEO-macroinitiator (PEO-iBBr) (**Scheme II.3**), and then later translated to the BSA-O-$[iBBr]_{30}$ system (**Scheme II.2**). The model systems used PEO based initiators to facilitate rapid screening of polymerization conditions prior to

grafting from the protein tethered initiator. $OEOMA_{475}$ was polymerized by ATRP, targeting DP = 455 (20% of monomer) or 227 (10% monomer) using the following formulation of $[OEOMA_{475}]/[I]/CuX]/[CuX_2]$=455(227)/1/1/9 with a ratio of copper(I) to ligands of CuX/bpy = 1/22 and CuX/TPMA = 1/11. The effect of halide salt on the polymerization control was also investigated by using $CuBr/CuBr_2$ and $CuCl/CuCl_2$. Table 1 presents detailed experimental conditions, conversion and polymer characterization. **Figure II.2** and **Figure II.3** shows the first order kinetic plot for ATRP initiated by PEO-iBBr and BSA-O-iBBr, number average molecular weight (M_n) versus conversion and molecular weight distribution (M_w/M_n) versus conversion. Both figures show similar plots for ATRP with both initiators showing essentially the same behavior.

Interestingly, the CuX/bpy system provides better control and allowed significantly higher conversions than CuX/TPMA based system. The latter observation is surprising in light of the fact that TPMA is one of the most active ligands,[39] although close inspection of the kinetics showed that the CuX/TPMA reached 5% conversion in the initial stage of the polymerization, after which point the further monomer conversion stopped. These results indicate that the TPMA based catalyst is too active, leading to too many radicals and significant termination. This minimal polymerization due to termination was observed for both the chloride based and bromide based CuX/TPMA catalysts. In contrast, the effect of halide species is readily observed for CuX/bpy systems. The CuCl/bpy catalyzed polymerizations showed a more linear increase in the semilogarithmic plot (**Figure II.3**) compared to CuBr/bpy system. This effect can be attributed to higher activity of the bromine initiators than of corresponding chloride, leading to a larger number of terminated

chains[36]. Altogether for GF proteins by normal ATRP CuCl/bpy is the optimum catalytic system.

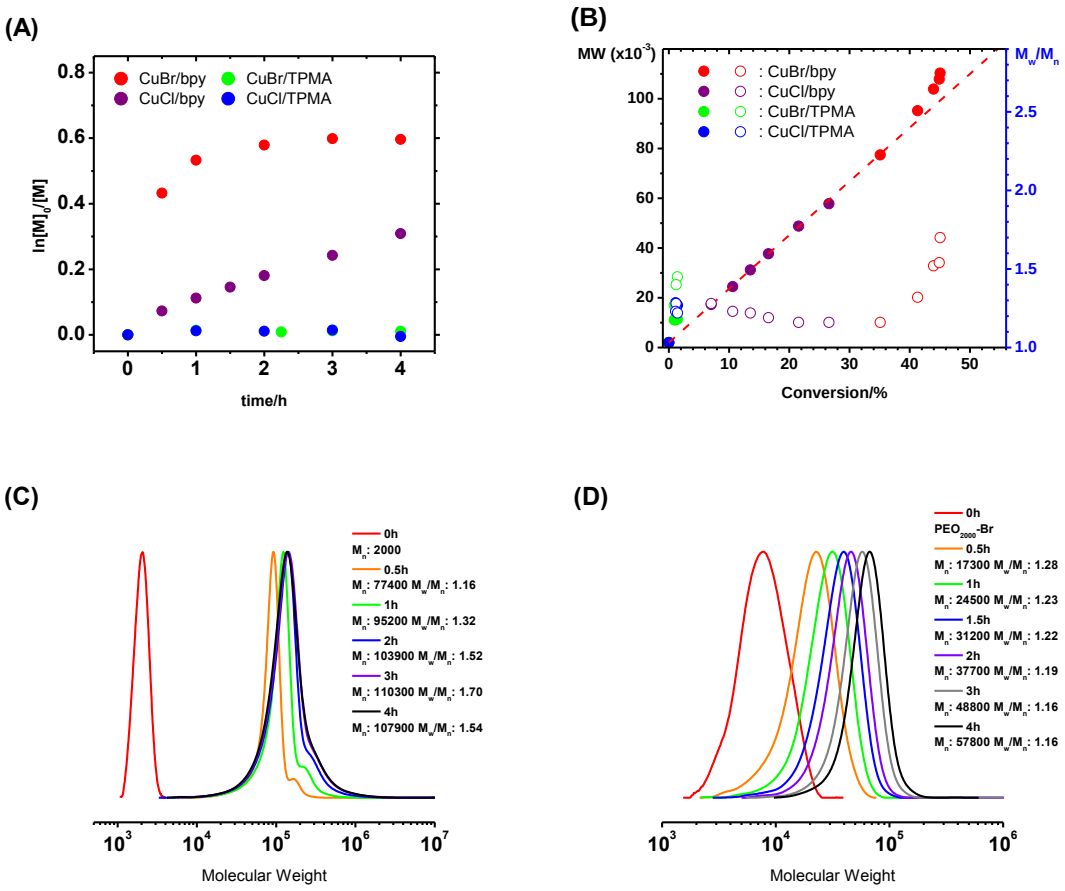

Figure II.2. Effect of copper halide (X=Br or Cl) on ATRP of $OEOMA_{475}$ under aqueous conditions at 30 °C. (A) First order kinetic plot and (B) M_n and M_w/M_n versus conversion plot; (C) GPC traces for $CuBr/CuBr_2$/bpy, (D) GPC traces for $CuCl/CuCl_2$/bpy. Polymerizations were conducted with $[OEOMA_{475}]_0$=0.45M and $[OEOMA_{475}]/[I]/[L]/[CuX]/[CuX_2]$ = 455/1/11/1/9 ([L]: [TPMA] = 2[Bpy]).

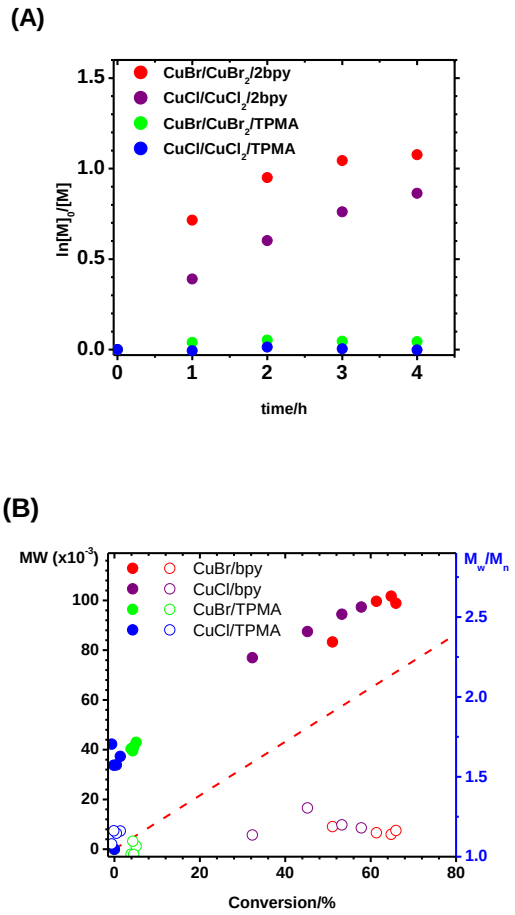

Figure II.3. Effect of ligand (L = bpy or TPMA) and halide (X = Br or Cl) on ATRP of $OEOMA_{475}$ GF BSA-O-$[iBBr]_{30}$ at 30 °C (reactions 5 - 8, Table 1). (A) First order kinetic plot and (B) M_n and M_w/M_n versus conversion plot. Polymerizations were conducted with $[OEOMA_{475}]_0$ = 0.21 M and $[OEOMA_{475}]/[PEO\text{-}iBBr]/[Cu(I)X]/[Cu(II)X_2]/[L]$ = 227/1/1/9/11 ([L]: [TPMA] = 2[Bpy]).

An alternative ATRP method that could be used to create well defined PPHs, is the activators generated by electron transfer (AGET) ATRP method, where an active CuX/L catalyst is formed by the reaction between a reducing agent and an oxidatevely stable CuX_2/L[40]. The reaction conditions for AGET ATRP in water from PEO-iBBr and BSA-O-$[iBBr]_{30}$ with ascorbic acid (AA) as reducing agent are presented at the **Table II.2**. Amount of AA used in this series of reactions was only 1% to $CuBr_2$ total concentration. As in previous case, for catalytic system with TPMA there was a rapid increase in the conversion

in the initial stages of the reaction, with no reaction after a relatively short period of time. This is in contrast to the linear semi-logarithmic plot observed in the bpy complex (**Figure II.4**). One interesting feature is that the polymer synthesized using the TPMA based complex had a very narrow molecular weight distribution (M_w/M_n=1.09). In traditional AGET ATRP, the reducing agent is injected into reaction mixture at the beginning of the reaction; however the results with PEO-iBBr (**Figure II.5**) and previous report[41] showed that feeding with AA for AGET ATRP in water solution can promote the continuous polymerization. **Figure II.6** illustrates that slow addition of the an identical amount of AA lead to 88% conversion in 4 h, compared to 5% conversion by conventional AGET ATRP is performed with the same amount of AA. The resulting polymer had a high molecular weight and very narrow molecular weight distribution – 1.08 (**Table II.2**). Every molecule of ascorbic acid during redox reactions provides two electrons.[42] In this reaction the rate of feeding of AA was 8 nmol/min, which implies that every minute only 0.008% of the total $CuBr_2$ is reduced, and after 4 hours to the total amount of AA added corresponds to 2% of the total amount of $CuBr_2$ reduced. Considering these results, preparation of well-defined PPHs with narrow molecular weight distributions by AGET ATRP with TPMA in water solution requires continual feeding with AA to ensure sustained and controlled polymerization.

Table II.2. Experimental conditions of AGET ATRP from PEO-iBBr and BSA-O-$[iBBr]_{30}$

	M/I/$CuBr_2$/L /AA	I	L	Time/h	Conv./%	$M_{n,theo}\times10^{-3}$	$M_{n,GPC}\times10^{-3}$	M_w/M_n
1	455/1/10/22/0.1	PEO	bpy	6	20	43	25	1.30
2	455/1/10/11/0.1	PEO	TPMA	6	15	32	30	1.09
3	455/1/10/11/0.01	PEO	TPMA	6	5	11	15	1.09
4	455/1/10/11/0.03[a]	PEO	TPMA	1	12	26	27	1.10
5	227/1/10/11/0.2[b]	PEO	TPMA	4	60	65	37	1.09
6	227/1/10/11/0.1	BSA	TPMA	4	5	5	30	1.10
7	227/1/10/11/0.1[c]	BSA	TPMA	4	88	95	82	1.08

1mM initiator, 10 – 20% monomer (v/v), water, 30°C; [a] charges of AA were 0.1 ml of a 0.5 mM solution, [b] AA was slowly fed to the reaction mixture at the rate 16 nmol/min, [c] AA was slowly fed to the reaction mixture at the rate 8 nmol/min

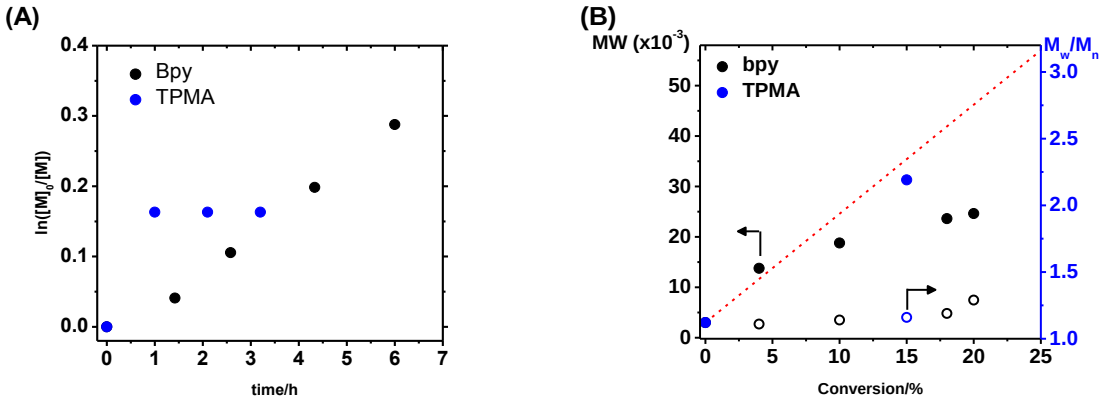

Figure II.4. Effect of ligand (L=Bpy or TPMA) on AGET ATRP of $OEOMA_{475}$ under aqueous conditions at 30 °C. (A) First order kinetic plot and (B) M_n and M_w/M_n versus conversion plot. Polymerizations were conducted with $[OEOMA_{475}]_0$=0.45M and $[OEOMA_{475}]/[I]/[CuX_2]/[AA]$ = 455/1/10/0.1. [Bpy] and [TPMA] = 21 and 11 mM, respectively.

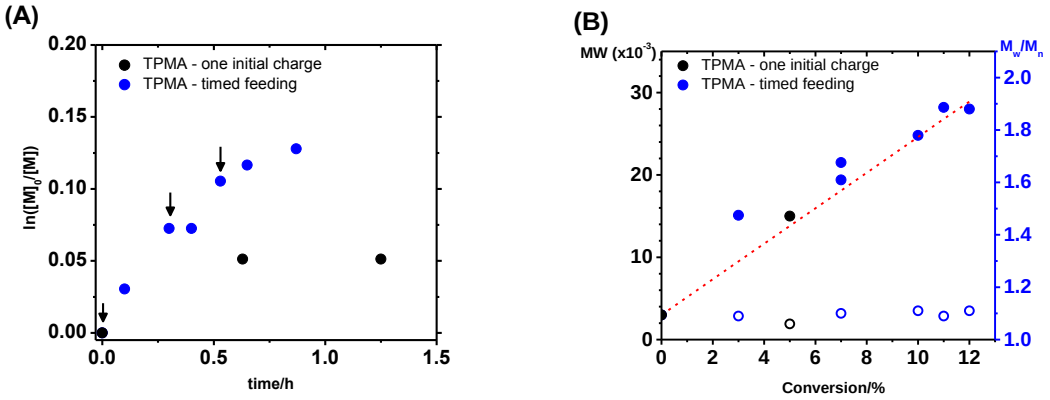

Figure II.5. Effect of reducing agent addition time on ATRP of $OEOMA_{475}$ under aqueous conditions at 30 °C (reactions 3-4, Table 2). (A) First order kinetic plot and (B) M_n and M_w/M_n versus conversion plot. Polymerizations were conducted with $[OEOMA_{475}]_0$=0.45M and $[OEOMA_{475}]/[I]/[TPMA]/[CuX_2]$ = 455/1/11/10. Charges of reducing agent were 0.1 ml of a 0.5 mM ascorbic acid. Black arrows indicate addition times of ascorbic acid.

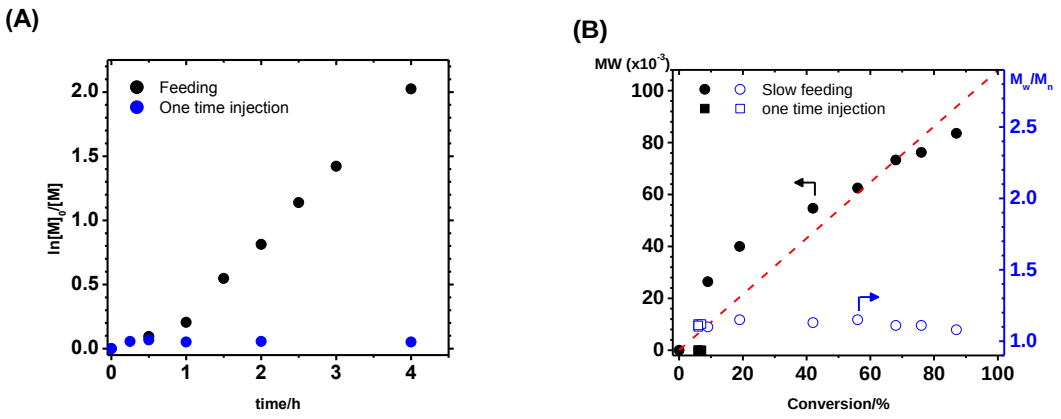

Figure II.6. Effect of reducing agent feeding on AGET ATRP of $OEOMA_{475}$ GF BSA-O-$[iBBr]_{30}$ at 30 °C (reactions 6 – 7, Table 2). (A) First order kinetic plot and (B) M_n and M_w/M_n versus conversion plot. Polymerizations were conducted with $[OEOMA_{475}]_0$ = 0.21M and $[OEOMA_{475}]/[I]/[TPMA]/[Cu(II)Br_2]$ = 227/1/11/10. Reducing agent's rate of feeding was 8 nmol/min.

Table II.3. Experimental conditions of (AGET) ATRP from PEO-iBBr and BSA-O-$[iBBr]_{30}$

	M/I/ CuX/CuX_2/L/AA	X Species[d]	Time/h	Conv./%	$M_{n,theo}\times10^{-3}$	$M_{n,GPC}\times10^{-3}$	M_w/M_n
1	227/1/1/9/22/-	Cl	3	6	6	10	1.19
2	227/1/1/9/22/-	Br	3	33	36	28	1.19
3	227/1/1/9/22/-	Br	3	40	43	50	1.26
4	227/1/-/10/11/0.2[a]	Br	4	60	65	37	1.09
5	227/1/-/10/11/0.1[b]	Br	4	75	81	83	1.19

1 mM initiator, 10% monomer (v/v), PBS, 30°C; [a] AA was fed to the reaction mixture at the rate 16 nmol/min; [b] AA was fed to the reaction mixture at the rate 8 nmol/min; entries 1-3: L = bpy; entries 4-5: L = TPMA; entry 1: X = Cl; entries 2 – 5: X = Br.

The final set of conditions studied was the optimization of the GF reaction under buffered conditions. Phosphate buffer saline (PBS) (pH = 7.4) is a widely utilized protein buffer[33] and was chosen as reaction media for the GF reactions. ATRP in PBS can be challenging for several reasons. Firstly, the copper and phosphate ions can form insoluble Cu_3PO_4 causing loss of active species and consequently retardation of polymerization. Secondly, chloride ions from the buffer can displace ligands from copper, and produce an inactive catalyst. However, under appropriate conditions these two effects can be minimized, and a well-controlled polymerization can be performed in PBS. To determine

these optimized conditions, $OEOMA_{475}$ was polymerized in PBS using both normal ATRP and AGET ATRP processes. Experimental conditions and polymer characteristics are presented in **Table II.3**. The PEO-iBBr model system showed that the $CuCl/CuCl_2$ catalyzed polymerization reached only 6% monomer conversion after four hours and was therefore not extended to GF BSA-O-$[iBBr]_{30}$. The $CuBr/CuBr_2$ catalyzed polymerization in PBS was approximately 3 times slower than the reaction in a purely aqueous system, although the PBS still allowed good control over the polymerization (**Figure II.7**). Therefore, the CuBr/bpy system was used for the traditional ATRP in buffered media from a protein. The polymers grown from BSA-O-$[iBBr]_{30}$ had relatively narrow molecular weight distributions, but as seen in the PEO-iBBr reaction the semilogarithmic plot became noticeably curved after the first hour.

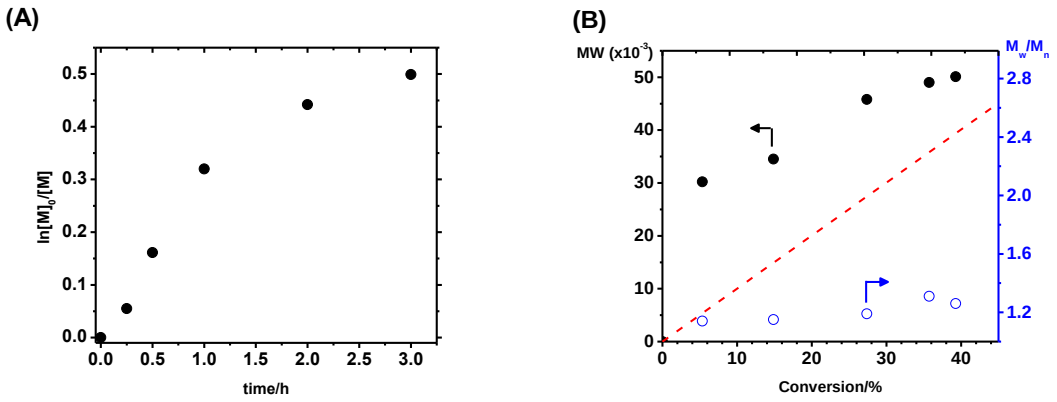

Figure II.7. Normal ATRP of $OEOMA_{475}$ GF BSA-O-$[iBBr]_{30}$ at 30 °C in PBS. (A) First order kinetic plot and (B) M_n and M_w/M_n versus conversion plot. Polymerizations were conducted with $[OEOMA_{475}]_0$ = 0.21 M and $[OEOMA_{475}]/[I]/[Cu(I)X]/[Cu(II)X_2]/[L]$ = 227/1/1/9/ 21.

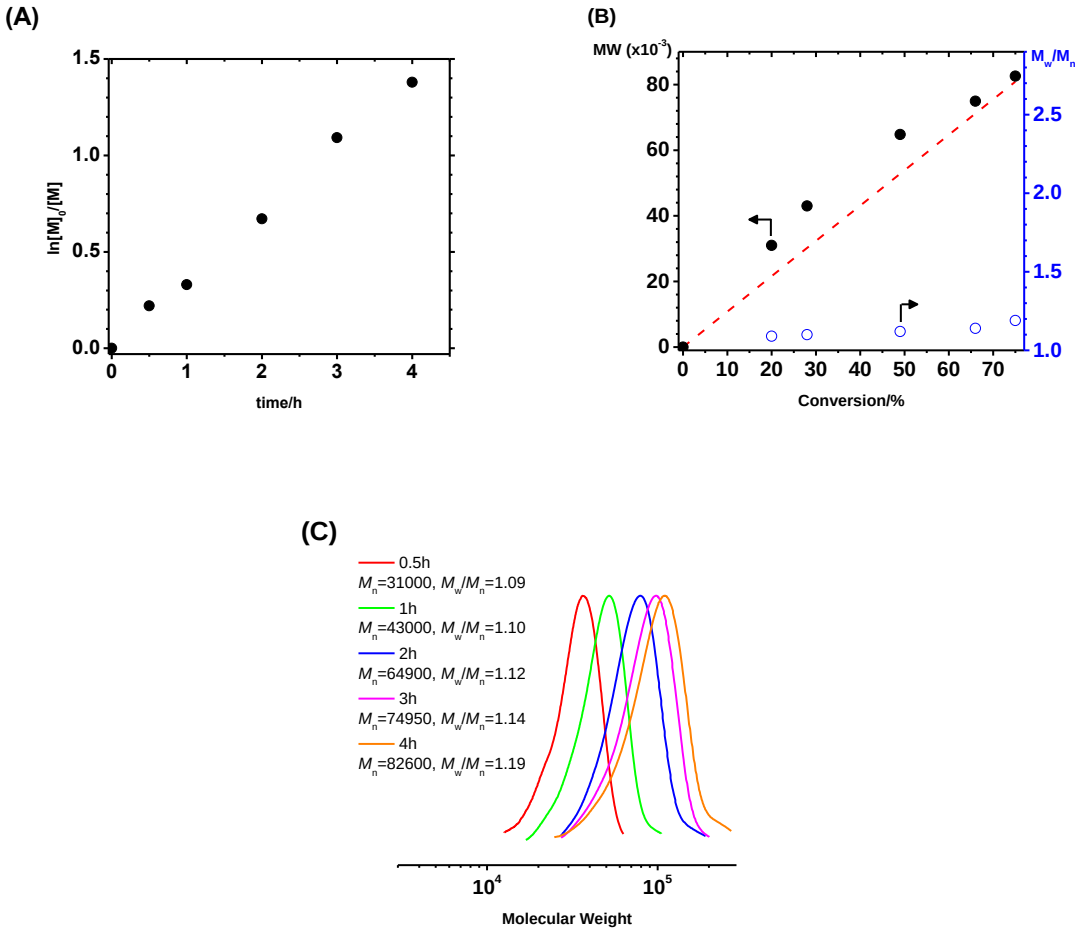

Figure II.8. AGET ATRP of $OEOMA_{475}$ GF BSA-O-$[iBBr]_{30}$ at 30 °C in PBS. (A) First order kinetic plot and (B) M_n and M_w/M_n versus conversion plot, and (C) GPC traces. Polymerizations were conducted with $[OEOMA_{475}]_0$ = 0.21 M and $[OEOMA_{475}]/[I]/[Cu(II)Br_2]/[TPMA]$ = 227/1/10/11. Reducing agent's rate of feeding was 8 nmol/min.

When AGET ATRP used with slow feeding of AA there is linear increase in the first-order kinetic plot (**Figure II.8A**) up to moderately high monomer conversion. **Figure II.8**B illustrates that the AGET ATRP gives a nearly linear increase in molecular weight with conversion and narrow molecular weight distribution, M_w/M_n<1.2. These results demonstrate that well-defined PPHs can be synthesized in PBS by using traditional or AGET ATRP, however, at the expense of slower polymerization rates as compared to a purely aqueous media.

II.4.Conclusions

In conclusion, this Chapter demonstrates how well-defined polymers can be grafted from proteins by ATRP under biologically relevant conditions. These conditions were designed both to maintain protein stability thought the polymerization and grow well-defined polymers with narrow molecular weight distributions. Biologically relevant conditions have been defined as a polymerization conducted at near ambient temperatures (30 °C) with a low initiator concentration (1 mM), low monomer and cosolvent concentrations (total organic content should not exceed 20% of the total reaction volume). Furthermore, the catalyst selected must bind the copper sufficiently strongly to prevent protein denaturation. When conducting traditional ATRP the optimal catalyst was found to be CuX/CuX_2/bpy (1/9/22), where X is either Cl or Br. The optimal halide depends upon the reaction media selected: in pure water the chloride species are preferred while in PBS the bromide species are needed to maintain an acceptable polymerization rate. AGET ATRP with slow feeding of reducing agent (AA) allows the strongly activating TPMA based catalysts to be used, giving polymerization, even with a very low ratio of copper(I) to copper(II) species. Moreover, AGET ATRP with slow feeding of AA gives a rapid reaction and well-controlled polymers in both pure water and PBS. These results show that under the specified conditions, uniform well-defined PPH can be prepared by ATRP in aqueous media under biologically relevant conditions.

II.5.Experimental section

II.5.1. Materials.

Oligo(ethylene oxide) monomethyl ether methacrylate (average molecular weight ~475g/mol, $OEOMA_{475}$), BSA, mono-*tert*-butyl succinate, N-hydroxysuccinimide (NHS), trifluoroacetic acid, bromoisobutyryl bromide, 2,2'-bipyridine (Bpy) , N-(n-propyl)pyridylmethanimine (PI), ascorbic acid (AA), CuCl, $CuCl_2$, CuBr, and $CuBr_2$ were purchased from Aldrich in the highest available purity. Tris(2-pyridylmethyl)amine (TPMA) was purchased from ATRP Solutions. Monomers were passed over a column of basic alumina prior to use. Poly(ethylene oxide) isobutyryl bromide (PEO-iBBr M_n = 2000) was prepared, as previously described[43]. GFP was prepared as previously described.[24]

II.5.2. Instrumentation and characterization.

Molecular weight and molecular weight distribution (M_w/M_n) were determined by GPC. The GPC system used a Waters 515 HPLC Pump and Waters 2414 Refractive Index Detector using PSS columns (Styrogel 10^2, 10^3, 10^5 Å) in dimethylformamide (DMF) as an eluent at a flow rate of 1 ml/min at 50 °C and in tetrahydrofuran (THF) as an eluent at a flow rate of 1 mL/min at 35 °C. All samples were filtered over anhydrous magnesium sulfate and neutral alumina prior to analysis. The column system was calibrated with 12 linear polystyrene (M_n = 376 ~ 2,570,000). Monomer conversion was measured using ^1H NMR spectroscopy in D_2O, using a Bruker Avance 300 MHz spectrometer at 27 °C. Thermoresponsivity was measured by dynamic light scattering (DLS) on a Zetasizer from Malvern Instruments, Ltd. The temperature ramp used in this study was from 15 °C to 64 °C at 1 °C intervals. Samples were equilibrated for 2 minutes before measuring particle size. Tangential flow filtration was conducted on a Labscale TFF system from Millipore.

Zebra Spin desalting columns were purchased from Fisher and used according to the manufactures instructions.. The fluorecence spectra for GFP stability testing were obtained on a Tecan Safire2 using a 384 well plate.

II.5.3. Stability of GFP under polymerization conditions.

The following amounts of ligand were complexed with $CuCl_2$ (5 mg, 0.037 mmol) respectively: PI(12.2 mg, 0.082 mmol), Bpy(12.8 mg, 0.082 mmol) and TPMA (11.9 mg, 0.041 mmol). The $CuCl_2$:L were precomplexed in 200 μL of water and an additional solution of $CuCl_2$ was prepared in 200 μL of water. Once clear solutions of $CuCl_2$:L and $CuCl_2$ were obtained they were added to 2 ml of GFP solution (1 mg/ml) in PBS with 10% $OEOMA_{475}$. The solutions were centrifuged at 4000 r.p.m. to remove any particulates formed (only observed for free $CuCl_2$ and $CuCl_2$:PI). 100 μL of each solution was removed for analysis using a Tecan Safire2 plate reader with a 384 well plate.

II.5.4. Preparation of NHS ester initiator.

Mono-*tert*-butyl succinate-EBiB :Mono-*tert*-butyl succinate (1.0 g, $5.74*10^{-3}$ mol), hydroxyl-EBiB (1.33 g, $6.31*10^{-3}$ mol), EDC-HCl (1.43 g, $7.46*10^{-3}$ mol) and DMAP (0.07 g, $5.74*10^{-4}$ mol) were added to a 100 ml round bottom flask. The reaction mixture was dissolved in 50 ml of dichloromethane and stirred overnight. The reaction mixture was extracted once with 20 ml of water, twice with 1N HCl, once with 1N NaOH, once with water and brine. The organic layer was dried over anhydrous sodium sulfate and solvent was removed under reduced pressure. ^{1}H NMR: 1.44 ppm (s, 9H), 1.93 ppm (d, 6H), 2.56 ppm (m, 4H) 4.36 ppm (s, 4H).

COOH- *tert*-butyl succinate-EBiB: Mono-*tert*-butyl succinate-EBiB (1 g, $2.72*10^{-3}$ mol) was dissolved in 50 ml of dichloromethane and trifloroacidic acid (2.09 ml, $2.72*10^{-2}$ mol)

was added dropwise to the reaction mixture. The reaction was stirred for 36 hours, and subsequently extracted 3 times with 30 ml of water and once with brine. The organic phase was dried over anhydrous sodium sulfate, filtered and the solvent was removed under reduced pressure. ^{1}H NMR: 1.94 ppm (d, 6H), 2.68 ppm (m, 4H) 4.38 ppm (s, 4H).

NHS-*tert*-butyl succinate-EBiB: Mono-*tert*-butyl succinate-EBiB (0.83 g, $2.69*10^{-3}$ mol), EDC-HCl (0.77 g, $4.04*10^{-3}$ mol) and NHS (0.46 g, $4.04*10^{-3}$ mol) were dissolved in 10 ml of $CHCl_3$ and stirred for 16 hours. 40 ml of ethyl acetate and 30 ml of water were then added to the reaction mixture and stirred for 10 minuets. The organic phase was separated and the aqueous phase was washed 3 times with 20 ml of ethyl acetate. The combined organic phases were washed with brine, dried over anhydrous sodium sulfate, filtered and the solvent was removed under reduced pressure. The NHS activated initiator was directly used to modify BSA.

II.5.5. Synthesis of BSA-O-[iBBr]$_{30}$.

NHS-ester-initiator (**1**) (1 g, 2.45 mmol) was dissolved in 2 ml of DMSO. BSA (1 g, 0.53 mmol Lys) was dissolved in 500 ml of 0.1 M PBS (pH 7.4) and **1** was added dropwise. The reaction was stirred overnight and purified using tangential flow filtration with a 30-kDa molecular weight cut off membrane. 15 dia-volumes of water were used to purify BSA-O-iBBr.

II.5.6. Polymer cleavage from protein.

Polymers were cleved from proteins was by adding 200 μL of reaction mixture to 200 μL of 5% KOH solution and left at room temperature for 2 hours.

II.5.7. Synthesis of POEOMA by ATRP from PEO2000iBBr/BSA-O-[iBBr]$_{30}$.

PEO_{2000}iBBr (10.0 mg 0.005 mmol) or BSA-O-[iBBr]$_{30}$ (12.5 mg, 0.01 mmol) was dissolved in 3.5 ml of Millipore water and placed in a 10 ml Schlenk flask. $OEOMA_{475}$ (476.2 mg, 1.14mmol) and 50 μL of DMF (internal standard for NMR) were added dropwise to the initiator solution. The flask was sealed and bubbled for 20 min, while stirring, with nitrogen to deoxygenate the reaction mixture. After the solution was deoxygenated 1 ml of catalyst stock solution was added via gastight syringe to the reaction mixture to initiate polymerization. The polymerization was carried out at 30 °C. Samples were taken at allotted times throughout the reaction for GPC and NMR analysis. Stock solutions of CuX:L were prepared in 10 ml of deoxygenated ultra pure water as follows: ***X=Br, L=bpy***: Cu(I)Br (7.2 mg, 0.05 mmol), Cu(II)Br_2 (101.0 mg, 0.45 mmol), and bpy (164.3 mg, 1.053 mmol). ***X=Cl, L=bpy***: CuCl (4.96 mg, 0.050 mmol), $CuCl_2$(60.5 mg, 0.25 mmol) and bpy(164.3 mg, 1.05 mmol). ***X=Br, L=TPMA***: Cu(I)Br (7.2 mg, 0.05 mmol), Cu(II)Br_2 (101.0 mg, 0.45 mmol), and TPMA (160.0 mg, 5.50 mmol). ***X=Cl, L=TPMA***: CuCl (4.96 mg, 0.050 mmol), $CuCl_2$(60.5 mg, 0.25 mmol) and TPMA (160.0 mg, 5.50 mmol).

II.5.8. AGET ATRP from PEO-iBBr/BSA-O-[iBBr]$_{30}$.

PEO_{2000}iBBr (40.0 mg 0.02 mmol) or BSA-O-[iBBr]$_{30}$ (50 mg, 0.02 mmol), $OEOMA_{475}$ (2 ml, 4.54 mmol), $CuBr_2$ (44.6 mg, 0.22 mmol), and TPMA (63.8 mg, 0.22 mmol) were dissolved in 18.4 ml of pure water and charged into a 25 ml Schlenk flask. 0.4 ml of DMF was added as internal standard. Next, the reaction mixture was purged with N_2 for 20 minutes then placed in an oil bath at 30 °C. Then AA was added either at the beginning of the reaction, or slowly fed in via a syringe pump.

II.6.References

(1) Matyjaszewski, K.; Braunecker, W. A. *Prog. Polym. Sci.* **2007**, *32*, 93.

(2) Matyjaszewski, K.; Xia, J. *Chem. Rev.* **2001**, *101*, 2921.

(3) Coessens, V.; Pintauer, T.; Matyjaszewski, K. *Prog. Polym. Sci.* **2001**, *26*, 337.

(4) Davis, K. A.; Matyjaszewski, K. *Adv. Polym. Sci.* **2002**, *159*, 1.

(5) Pyun, J.; Jia, S.; Kowalewski, T.; Patterson, G. D.; Matyjaszewski, K. *Macromolecules* **2003**, *36*, 6952.

(6) Le Droumaguet, B.; Nicolas, J. *Polym. Chem.* **2010**, *1*, 563.

(7) Duncan, R. *Nat. Rev. Drug Discov.* **2003**, *2*, 347.

(8) Veronese, F. M. *Biomaterials* **2001**, *22*, 405.

(9) Harris, J. M.; Chess, R. B. *Nat. Rev. Drug Discovery* **2003**, *2*, 214.

(10) Lutz, J. F.; Borner, H. G. *Prog. Polym. Sci.* **2008**, *33*, 1.

(11) Li, H.; Bapat, A. P.; Li, M.; Sumerlin, B. S. *Polym. Chem.* **2011**.

(12) Zarafshani, Z.; Obata, T.; Lutz, J.-F. *Biomacromolecules* **2010**, *11*, 2130.

(13) Boyer, C.; Bulmus, V.; Davis, T. P.; Ladmiral, V.; Liu, J.; Perrier, S. *Chem. Rev.* **2009**, *109*, 5402.

(14) Heredia, K. L.; Bontempo, D.; Ly, T.; Byers, J. T.; Halstenberg, S.; Maynard, H. D. *J. Am. Chem. Soc.* **2005**, *127*, 16955.

(15) Broyer, R. M.; Grover, G. N.; Maynard, H. D. *Chem. Commun.* **2011**, *47*, 2212.

(16) Bulmus, V.; Boyer, C.; Huang, X.; Whittaker, M. R.; Davis, T. P. *Soft Matter* **2011**, *7*, 1599.

(17) Nicolas, J.; Mantovani, G.; Haddleton, D. M. *Macromol. Rapid Commun.* **2007**, *28*, 1083.

(18) Shi, W.; Dolai, S.; Averick, S.; Fernando, S. S.; Saltos, J. A.; L'Amoreaux, W.; Banerjee, P.; Raja, K. *Bioconjugate Chem.* **2009**, *20*, 1595.

(19) Magnusson, J. P.; Bersani, S.; Salmaso, S.; Alexander, C.; Caliceti, P. *Bioconjugate Chem.* **2010**, *21*, 671.

(20) Lele, B. S.; Murata, H.; Matyjaszewski, K.; Russell, A. J. *Biomacromolecules* **2005**, *6*, 3380.

(21) Bontempo, D.; Maynard, H. D. *J. Am. Chem. Soc.* **2005**, *127*, 6508.

(22) Peeler, J. C.; Woodman, B. F.; Averick, S.; Miyake-Stoner, S. J.; Stokes, A. L.; Hess, K. R.; Matyjaszewski, K.; Mehl, R. A. *J. Am. Chem. Soc.* **2010**, *132*, 13575.

(23) Finn, M. G.; Pokorski, J. K.; Breitenkamp, K.; Liepold, L. O.; Qazi, S. *J. Am. Chem. Soc.* **2011**, *133*, 9242.

(24) Averick, S. E.; Magenau, A. J. D.; Simakova, A.; Woodman, B. F.; Seong, A.; Mehl, R. A.; Matyjaszewski, K. *Polym. Chem.* **2011**, *2*, 1476.

(25) Zhu, B. B.; Lu, D. N.; Ge, J.; Liu, Z. *Acta Biomaterialia* **2011**, *7*, 2131.

(26) Yasayan, G.; Saeed, A. O.; Fernandez-Trillo, F.; Allen, S.; Davies, M. C.; Jangher, A.; Paul, A.; Thurecht, K. J.; King, S. M.; Schweins, R.; Griffiths, P. C.; Magnusson, J. P.; Alexander, C. *Polym. Chem.* **2011**, *2*, 1567.

(27) Gao, W.; Liu, W.; Christensen, T.; Zalutsky, M. R.; Chilkoti, A. *Proc. Natl. Acad. Sci. U.S.A.* **2010**, *107*, 16432.

(28) Gao, W. P.; Liu, W. G.; Mackay, J. A.; Zalutsky, M. R.; Toone, E. J.; Chilkoti, A. *Proc. Natl. Acad. Sci. U.S.A.* **2009**, *106*, 15231.

(29) Braunecker, W. A.; Tsarevsky, N. V.; Gennaro, A.; Matyjaszewski, K. *Macromolecules* **2009**, *42*, 6348.

(30) Perrier, S.; Haddleton, D. M. *Macromolecular Symposia* **2002**, *182*, 261.

(31) Tsarevsky, N. V.; Pintauer, T.; Matyjaszewski, K. *Macromolecules* **2004**, *37*, 9768.

(32) Velonia, K. *Polym. Chem.* **2010**, *1*, 944.

(33) Hermanson, G. T. *Bioconjugate techniques*; Academic Press: San Diego, 1996.

(34) Bulmus, V.; Liu, J. Q.; Herlambang, D. L.; Barner-Kowollik, C.; Stenzel, M. H.; Davis, T. R. *Angew. Chem. Int. Ed.* **2007**, *46*, 3099.

(35) Le Droumaguet, B.; Velonia, K. *Angew. Chem. Int. Ed.* **2008**, *47*, 6263.

(36) Tang, W.; Kwak, Y.; Braunecker, W.; Tsarevsky, N. V.; Coote, M. L.; Matyjaszewski, K. *J. Am. Chem. Soc.* **2008**, *130*, 10702.

(37) Enoki, S.; Saeki, K.; Maki, K.; Kuwajima, K. *Biochemistry* **2004**, *43*, 14238.

(38) Lutz, J. F.; Andrieu, J.; Uzgun, S.; Rudolph, C.; Agarwal, S. *Macromolecules* **2007**, *40*, 8540.

(39) Matyjaszewski, K.; Tang, W. *Macromolecules* **2006**, *39*, 4953.

(40) Jakubowski, W.; Matyjaszewski, K. *Macromolecules* **2005**, *38*, 4139.

(41) Matyjaszewski, K.; Oh, J. K.; Perineau, F.; Charleux, B. *J. Polym. Sci., Part A: Polym. Chem.* **2009**, *47*, 1771.

(42) Davey, M. W.; Van Montagu, M.; Inze, D.; Sanmartin, M.; Kanellis, A.; Smirnoff, N.; Benzie, I. J. J.; Strain, J. J.; Favell, D.; Fletcher, J. *J. Sci. Food Agric.* **2000**, *80*, 825.

(43) Matyjaszewski, K.; Bencherif, S. A.; Siegwart, D. J.; Srinivasan, A.; Horkay, F.; Hollinger, J. O.; Washburn, N. R. *Biomaterials* **2009**, *30*, 5270.

Chapter III. Aqueous ARGET ATRP[†]

III.1. Preface

In the previous chapter the development of conditions for conducting ATRP in water, initially utilizing higher catalyst concentration (several thousand ppm), was discussed. This work then led to significant advantages through development of ARGET ATRP with slow feeding of reducing agent allowing polymerization at low ppm (≤ 300 ppm) concentrations of copper catalyst. Aqueous ARGET ATRP is more complicated due to prevalence of side reactions discussed in the Chapter I, particularly, halide dissociation from deactivator and copper complex dissociation at low catalyst concentrations. In parallel with my colleague Dr Dominik Konkolewicz, we developed first aqueous ATRP methods, which used only ppm amounts of copper. He was working on ICAR ATRP of a water soluble acrylate, where decomposition of a standard free radical initiator slowly reduced Cu^{II} complex. I was working on ARGET ATRP of water soluble methacrylate, where ascorbic acid was continuously fed into the reaction mixture to regenerate the activator complex. A well-controlled polymerization of oligo(ethylene oxide) methyl ether methacrylate (OEOMA) was developed which required 300 ppm or less of a copper/tris(2-pyridylmethyl)amine (TPMA) complex in the presence of an excess of halide salts. This polymerization method produced well-defined polymers and the procedure can be applied to synthesis of block copolymers and bioconjugates.

I would like to acknowledge Dr Saadyah Averick and Dr Dominik Konkolewicz for collaborating with me on this project. I was leading this project by planning required

[†] This Chapter includes work, which was published and reformatted: **Simakova, A**.; Averick, S. E.; Konkolewicz, D.; Matyjaszewski, K. Aqueous ARGET ATRP. *Macromolecules* 2012, *45*, 6371–6379

experimentation, performing the majority of reactions and analysis, and summarizing final results in the manuscript. Dr Saadyah Averick applied this method to grafting from a protein, and analyzed resulting protein-polymer hybrid. Dr Dominik Konkolewicz conducted few polymerizations and mentored this project.

III.2. Introduction

Atom transfer radical polymerization (ATRP) is robust and versatile reversible deactivation radical polymerization (RDRP) method, which has been used to prepare well-defined polymers and materials with complex architectures.[1,2] ATRP is a catalytic process where an alkyl halide is activated by a transition metal catalyst in a lower oxidation state, to generate the corresponding alkyl radical and the transition metal complex in a higher oxidation state. The alkyl radical can propagate by adding monomer for a short time before being deactivated to the corresponding dormant alkyl halide by the higher oxidation state metal complex. These repeated activation/deactivation cycles in ATRP ensure that the majority of the polymer chains grow at the same rate, which provides access to various copolymers, nanocomposites, bioconjugates, networks, and supramolecular structures.[1,3]

Well controlled polymers can be created by ATRP under various polymerization conditions including bulk, homogeneous and heterogeneous systems.[4] Typically, organic solvents are used for homogeneous ATRP, however, it is desirable to replace these volatile and potentially hazardous organic solvents with "green" solvents[5,6] like supercritical carbon dioxide,[7,8] ionic liquids[9,10] or water.[11-13] Water is a safe, inexpensive, environmentally benign solvent that can be used for direct synthesis of hydrophilic polymers. These advantages have stimulated efforts to conduct ATRP in aqueous media[12,14,15] resulting in several well-defined synthetic polymers, as well as well-defined protein-polymer hybrids using the "grafting from" method.[16-20] The resulting protein-polymer hybrids had improved stability and pharmokinetics, and thermoresponsive bioactivity compared to non-modified proteins. However, in many cases, the control over the polymerization and resulting polymer structure was limited, leading to formation of

materials with broad molecular weight distributions, significant tailing to low molecular weights and inefficient initiation. These complications are due to the highly polar nature of water, which has made the implementation of ATRP in aqueous media challenging.[21]

There are several factors associated with ATRP in water that result in the observed poor levels of control. One factor is the large ATRP equilibrium constant in aqueous media, which generates high radical concentrations and consequently an increased rate of termination.[21] Another factor that complicates conducting an ATRP in water is the partial dissociation of the halide ion from deactivator complex, leading to inefficient deactivation of the propagating radicals.[22] Furthermore, certain Cu(I)/L complexes can disproportionate, or undergo partial dissociation.[22] Lastly, hydrolysis of the carbon-halogen bond can diminish chain-end functionality.[22] To overcome these issues, ATRP in water was traditionally performed with a low ratio of Cu(I):Cu(II) to reduce the radical concentration, and a high overall concentration of copper to minimize the deactivator dissociation.[12,16,22-25]

Recently, our group prepared protein-polymer hybrids by "grafting from" using normal and activators generated by electron transfer (AGET) ATRP under biologically relevant conditions.[26] In order to prepare the protein-polymer hybrid strongly binding ligands 2,2'-bipyridine (bpy) or TPMA are required to avoid protein denaturation that was observed for N-(n-propyl)pyridylmethanimine (PI) ligand. Another important conclusion of this earlier work is that when the very active ligand TPMA was used, the reducing agent, ascorbic acid, must be fed into the reaction mixture slowly to minimize termination, allowing the reaction to be driven to high monomer conversion. In these reactions, catalyst concentrations of 20,000 – 45,000 parts per million were used while targeting very low

ratios of Cu(I):Cu(II) to minimize termination. Due to the high catalyst loadings required, the polymer must be extensively purified after the reaction generating both economic and environmental costs. Thus, development of procedures for aqueous ATRP that permit the use of low concentrations of catalyst is desirable.

In the past decade, ATRP methods have been developed for organic media that allow the catalyst concentration to be reduced to parts per million (ppm) concentrations.[27,28] In these procedures, the activator is regenerated *in situ* from the deactivator complex that builds up due to termination reactions. This reduction can be achieved by introducing either a reducing agent, as in activators regenerated by electron transfer (ARGET) ATRP,[29] or a thermal free radical initiator, as in initiators for continuous activator regeneration (ICAR) ATRP[28], or a cathodic current as in electrochemically mediated ATRP.[15,30] However, in aqueous media the addition of such low concentrations of catalyst resulted in almost complete dissociation of the deactivator complex, leading to poorly controlled polymerizations. To overcome this problem, an excess of a halide salt can be added, to promote the reformation of the deactivator complex.[15,22,31]

Very recently, conditions for an aqueous ICAR ATRP were developed that resulted in formation of well-controlled polymers of oligo(ethylene oxide) methyl ether (meth)acrylate (OEO(M)A) with 100 parts per million (ppm) or lower catalyst concentration in the presence of a large excess of bromide salts.[31] Under optimal conditions, the ICAR ATRP proceeded with linear first-order kinetics, progressive molecular weight evolution with conversion and dispersities that remained below 1.3. The aqueous ICAR method was also used to create a thermoresponsive block copolymer and a protein-polymer hybrid. However, the limitation of ICAR ATRP is that the process

generates new chains due to the use of a thermal free radical initiator, which broadens the molecular weight distribution and introduces homopolymers during block copolymer preparation.

This Chapter systematically investigates the variables associated with ARGET ATRP of oligo(ethylene oxide) methyl ether (meth)acrylate (OEO(M)A) in aqueous media at ambient temperature (30°C) with slow feeding of ascorbic acid (**Scheme III.1**). In all cases a Cu/TPMA catalyst was used, since this complex shows significant stability at high dilutions in aqueous media with minimal disproportionation,[32] and catalyst concentrations as low as 100 ppm were examined. This study optimizes reaction conditions for preparation of well-defined water soluble polymers in aqueous media at low copper concentrations, and subsequently extends the technique to prepare block copolymers and a protein-polymer hybrid.

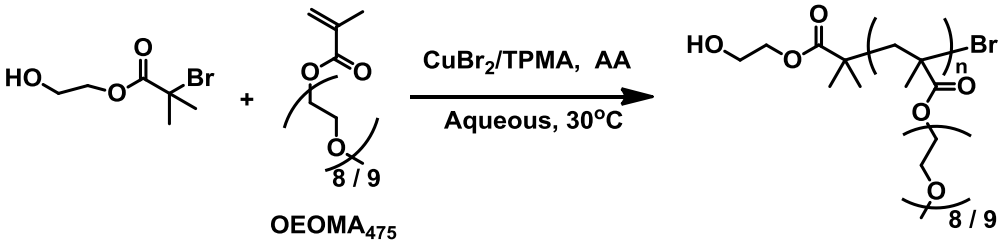

Scheme III.1. ARGET ATRP of $OEOMA_{475}$ in aqueous media with feeding ascorbic acid (AA).

III.3. Results and discussion

One of the major challenges associated with aqueous ATRP is the dissociation of the halide anion from the Cu(II) deactivator complex, which both reduces the deactivator concentration and affects the dispersity of the final product (**Scheme III.2**).[22]

A

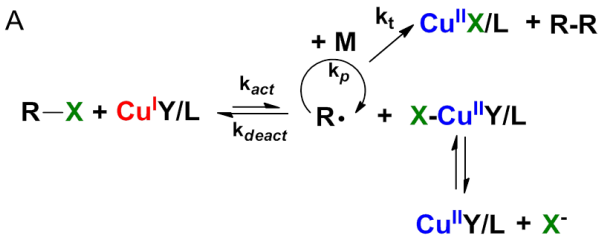

B

$$\frac{M_w}{M_n} = 1 + \frac{1}{DP_n} + \left(\frac{k_p[RX]_0}{k_{deact}[XCu^{II}/L]}\right)\left(\frac{2}{conv.} - 1\right)$$

Scheme III.2. ATRP with dissociation of the halide anion from deactivating complex (A), and equation for calculating the dispersity of the polymer (B).

Previously, it was shown that the addition of a halide salt increases the concentration of the XCu^{II}/L species and promotes efficient deactivation.[15,22,31,33] Therefore, initial experiments were designed to confirm that the addition of an excess of halide salt improves the control over the polymerization. Polymerizations without and with 100 mM tetraethylammonium bromide (TEABr) were performed. Kinetic plots, molecular weight, dispersity, and GPC traces are presented in **Figure III.1**. In the absence of the added salt, the rate of the reaction was significantly higher than with the salt, but the system without additional halide ions did not follow linear first-order kinetics. The dispersities of the final polymer were higher than 1.5, whereas with the addition of extra bromide ions they were lower than 1.4. In addition, the GPC traces showed that polymers synthesized without added TEABr displayed a high molecular weight shoulder, which could be due to termination reactions caused by the higher concentration of radicals. In contrast, when the

salt was added, the distributions were monomodal and shifted cleanly towards higher molecular weight. These results confirm that addition of extra halide species promotes efficient deactivation.

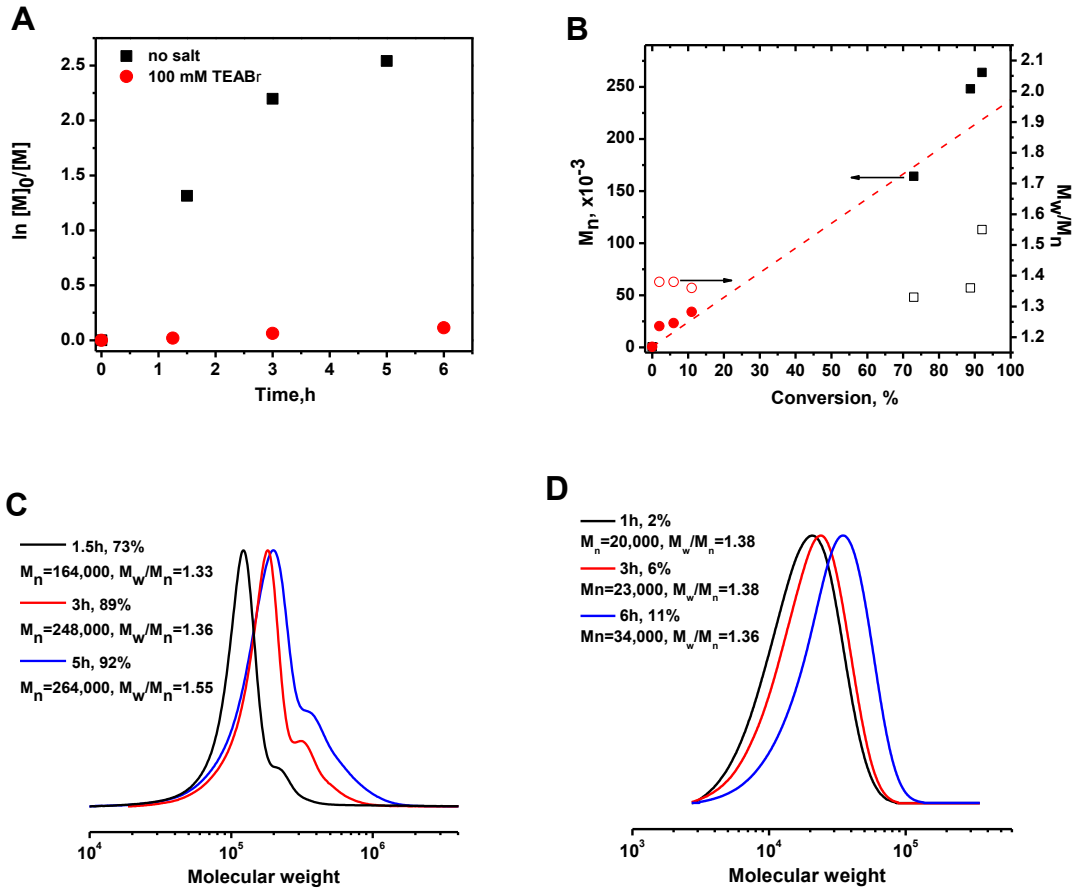

Figure III.1. Effect of the extra TEABr on the ARGET ATRP of $OEOMA_{475}$ in water at 30 °C. (A) First-order kinetic plot, (B) evolution of molecular weight and molecular weight distribution with conversion (the dash line represents theoretical molecular weight at a given conversion), (C) GPC traces with conversion for reaction without extra salt, and (D) with 100 mM TEABr. $[OEOMA_{475}]_0$ = 0.5 M; $[OEOMA_{475}]_0/[I]_0/[TPMA]_0/[CuBr_2]_0$ = 500/1/0.1/0.05; FR_{AA} = 2 nmol/min.

Effect of the feeding rate of ascorbic acid (FR_{AA}). Although the preliminary results showed that an ARGET ATRP can proceed in a controlled manner, the rate of the reaction was quite slow under conditions that provided good control. As discussed above, the addition of a halide salt significantly reduced rate of the reaction and reached only 11%

conversion in 6 h compared to 92% in 5h for a reaction without added TEABr. Therefore, the feeding rate of the ascorbic acid (FR_{AA}) was varied from 8 to 32 nmol/min to determine if higher amounts of ascorbic acid would increase the rate of a controlled polymerization (**Table III.1**). As expected, higher FR_{AA} led to higher rates of polymerization. However, feeding rates of 16 and 32 nmol/min resulted in a significant increase in M_w/M_n at conversions above 50%. This broadening of the dispersity could be due to either a high termination rate or to a poor deactivation rate. The first order kinetic plot, molecular weight evolution, and M_w/M_n values can be found in the **Figure III.2.**

Table III.1. ARGET ATRP of $OEOMA_{475}$ with varied feeding rate of ascorbic acid (FR_{AA}).

Entry	M/I/TPMA/$CuBr_2$	FR_{AA}, nmol/ min	Cu[a], ppm	Time, h	Conv., %	$M_{n\ th}$[b] ×10^{-3}	$M_{n\ GPC}$[c] ×10^{-3}	M_w/M_n
1	500/1/0.1/0.05	8	100	23	41	98	72	1.35
2	500/1/0.1/0.05	16	100	23	68	161	104	1.66
3	500/1/0.1/0.05	32	100	23	67	159	122	1.85

All polymerizations were conducted with $[M]_0$ = 0.5 M, $[I]_0$ = 1 mM, $[TEABr]_0$ = 100 mM; [a] Calculated by the initial molar ration of $CuBr_2$ to the monomer; [b] $M_{n\ th} = ([M]_0/[I]_0) \times conversion \times M_{monomer}$; [c] universal calibration (SI).

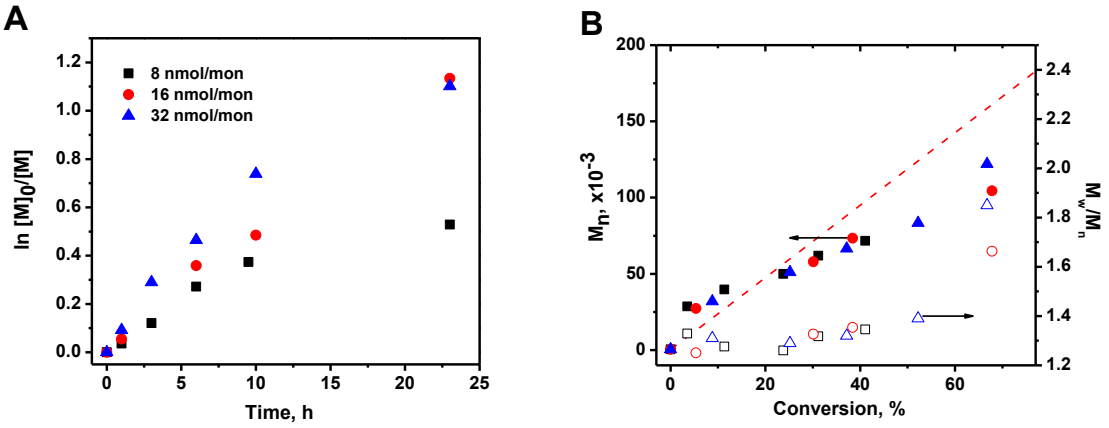

Figure III.2. Influence of the rate of addition of ascorbic acid on the ARGET ATRP of $OEOMA_{475}$ in water at 30°C. First-order kinetic plot (A), evolution of molecular weight and molecular weight distribution with conversion (B). $[OEOMA_{475}]_0$ = 0.5 M; $[OEOMA_{475}]/[I]/[TPMA]/[CuBr_2]$ = 500/1/0.1/0.05.

Table III.2. ARGET ATRP of $OEOMA_{475}$ with varied Cu/L ratio at 100 ppm Cu.

Entry	M/I/TPMA/$CuBr_2$	L/Cu	Time, h	Conv., %	$M_{n\ th}$[b] $\times 10^{-3}$	$M_{n\ GPC}$[c] $\times 10^{-3}$	M_w/M_n
1	500/1/0.1/0.05	2/1	23	68	161	104	1.66
2	500/1/0.2/0.05	4/1	6	30	71	93	1.29
3	500/1/0.4/0.05	8/1	10	90	212	147	1.27

All polymerizations were conducted with $[M]_0$ = 0.5 M, $[I]_0$ = 1 mM, $[TEABr]_0$ = 100 mM, FR_{AA} = 16 nmol/min; [a] Calculated by the initial molar ration of $CuBr_2$ to the monomer; [b] $M_{n\ th} = ([M]_0/[I]_0)\times conversion\times M_{monomer}$; [c] universal calibration (SI).

Effect of the ligand concentration. It has been reported that the presence of an excess of ligand compared to copper can increase rate of polymerization in an ARGET ATRP.[27] Since ARGET ATRP uses low concentrations of catalyst, partial dissociation of the ligand from the metal in the presence of an excess of other reagents can occur and influence the rate of polymerization. Therefore, the addition of an excess of the ligand can increase the concentration of activator and consequently the rate of polymerization. This was confirmed in the next set of experiments which were performed using the ligand to copper ratios of 2/1, 4/1 and 8/1, and showed that a higher ligand to copper ratio accelerates the polymerization rate (

Table III.2). The kinetic plots showed that there is no difference in the polymerization rates between the ratios 2/1 and 4/1 (**Figure III.3A**), but with an 8-fold excess of ligand the reaction was approximately 5 times faster. Furthermore, there was no broadening of molecular weight distributions at higher conversions ($M_w/M_n \leq 1.40$). The polymerizations results suggest that despite the relatively high stability of TPMA complex, at the low catalyst concentrations used in ARGET ATRP system, L/Cu ratios of 2/1 and 4/1 provided insufficient stabilization of the copper complexes, and a larger excess of ligand was needed to shift equilibrium towards the Cu(I)/L species. Thus, a L/Cu ratio of 8/1 was used for all subsequent experiments targeting a well-controlled aqueous ARGET

ATRP. Other parameters were examined since while the reaction was faster with more ligand, the molecular weights slightly deviated from the theoretical values at higher conversions, which could be due to transfer reactions (**Figure III.3B**).

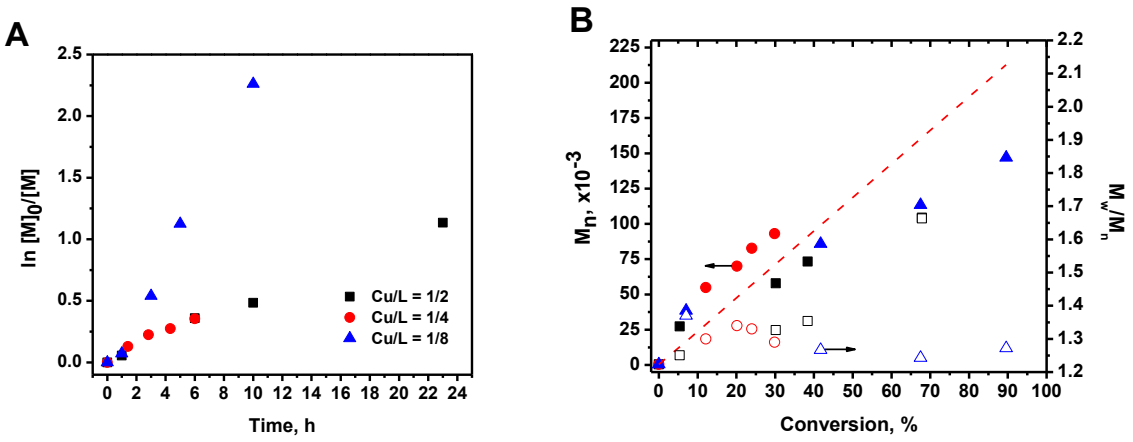

Figure III.3. Effect of the Cu/L ratio on the ARGET ATRP of $OEOMA_{475}$ in water at 30 °C. (A) First-order kinetic plot, (B) evolution of molecular weight and molecular weight distribution with conversion (the dash line represents theoretical molecular weight at a given conversion). $[OEOMA_{475}]_0$ = 0.5 M; $[OEOMA_{475}]_0/[I]_0/[TPMA]_0/[CuBr_2]_0$ = 500/1/0.05n/0.05 (where n is 2, 4, 8); FR_{AA} = 16 nmol/min.

Influence of an added salt. The next parameter examined was the nature of the halogen species which can influence the polymerization. A chlorine capped chain is typically 10 – 100 times less active than bromine capped chain[34] but the carbon-chlorine bond is more hydrolytically stable. **Table III.3** (entries 1 – 3) and **Figure III.4** illustrate polymerization results for polymerizations conducted in the presence of different salts: TEABr, TEACl, and NaCl. When chloride salts were used the reaction proceeded slower but in more controlled manner. Linear first-order kinetics and linear evolution of molecular weight with conversion was observed for polymerizations in the presence of TEACl and NaCl. As expected, polymerization with TEACl is similar to the polymerization with NaCl, indicating that only the anion, not the cation, affects the polymerization. Furthermore,

experimental molecular weight values correlated well with theoretical and polymers dispersities remained below 1.3 up to high monomer conversions.

Table III.3. ARGET ATRP of $OEOMA_{475}$ with varied salt and salt concentration.

Entry	M/I/TPMA/$CuBr_2$	Salt, mM	Cu[a], ppm	Time, h	Conv., %	$M_{n\ th}$[b] $\times 10^{-3}$	$M_{n\ GPC}$[c] $\times 10^{-3}$	M_w/M_n
1	500/1/0.4/0.05	TEABr, 100	100	10	90	212	147	1.27
2	500/1/0.4/0.05	TEACl, 100	100	8	43	102	102	1.40
3	500/1/0.4/0.05	NaCl, 100	100	15	72	170	192	1.28
4	500/1/0.4/0.05	NaCl, 300	100	8	27	64	59	1.33
5	500/1/0.4/0.05	NaCl, 30	100	6.75	71	169	145	1.29
6	500/1/0.4/0.05	NaCl, 10	100	6	98	233	292	1.48

All polymerizations were conducted with $[M]_0$ = 0.5 M, $[I]_0$ = 1 mM, $[TEABr]_0$ = 100 mM, FR_{AA} = 16 nmol/min; [a] Calculated by the initial molar ration of $CuBr_2$ to the monomer; [b] $M_{n\ th} = ([M]_0/[I]_0) \times conversion \times M_{monomer}$; [c] universal calibration (SI).

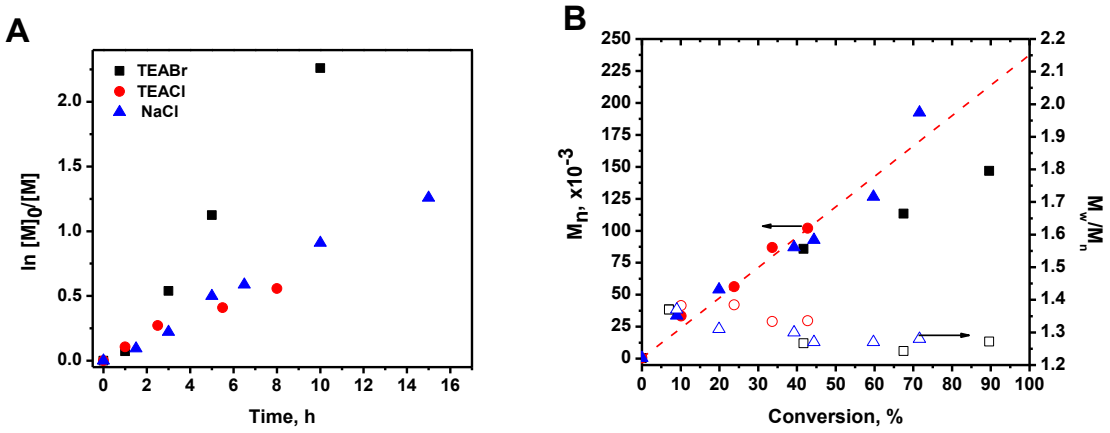

Figure III.4. Effect of the halide type on the ARGET ATRP of $OEOMA_{475}$ in water at 30 °C. (A) First-order kinetic plot, (B) evolution of molecular weight and molecular weight distribution with conversion (the dash line represents theoretical molecular weight at a given conversion). $[OEOMA_{475}]_0$ = 0.5 M; $[OEOMA_{475}]_0/[I]_0/[TPMA]_0/[CuBr_2]_0$ = 500/1/0.4/0.05, FR_{AA} = 16 nmol/min.

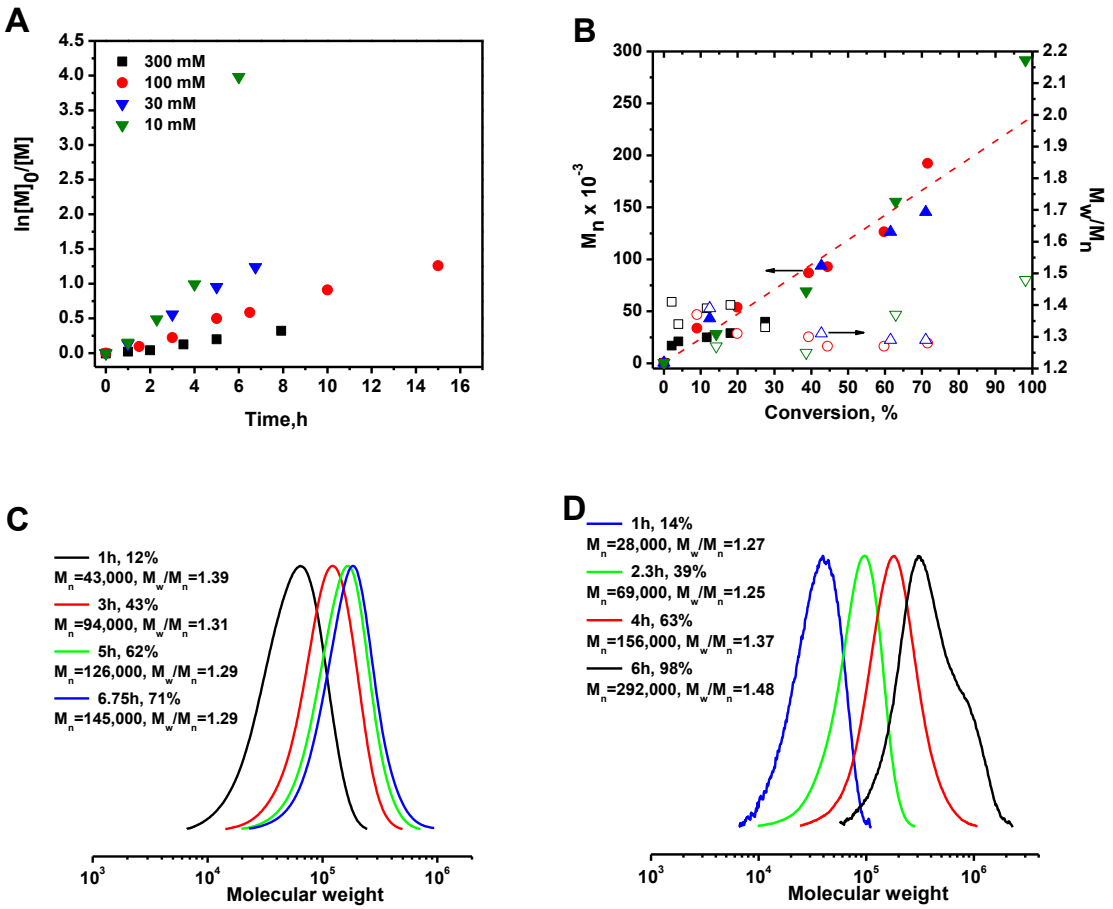

Figure III.5. Effect of the NaCl concentration on the ARGET ATRP of $OEOMA_{475}$ in water at 30 °C. (A) First-order kinetic plot, (B) evolution of molecular weight and molecular weight distribution with conversion (the dash line represents theoretical molecular weight at a given conversion), (C) GPC traces with conversion with 30 mM and (D) 10 mM NaCl. $[OEOMA_{475}]_0$ = 0.5 M; $[OEOMA_{475}]_0/[I]_0/[TPMA]_0/[CuBr_2]_0$ = 500/1/0.4/0.05, FR_{AA} = 16 nmol/min.

While addition of a halide salt shifts the equilibrium toward formation of a stable deactivator and improves control over polymerization it is also important to determine the effect of the concentration of the salt on the polymerization. Entries 3 – 6 of **Table III.1** show the influence of varying the concentration NaCl starting from 10 mM to 300 mM. **Figure III.5A** shows that the rate of polymerization decreases in the presence of higher concentrations of NaCl. The reaction with 300 mM NaCl reached less than 30% conversion in 8h, while with 10 mM it reached almost 100% in 6h. The slower rate of polymerization

in the presence of higher salt concentration could be caused by presence of a higher concentration XCu^{II}/L, or by the formation of inactive XCu^{I}/L species, or substitution of TPMA ligand by halide anions. The results suggest that a concentration of 300 mM NaCl was too high, as it significantly decreased the rate of polymerization without a significant improvement in the M_w/M_n values. Lower salt concentrations of 30 and 100 mM provided linear evolution of the molecular weight with conversion and good correlation between the experimental and theoretical values (**Figure III.5B**). Furthermore, there was a minimal change in the dispersity of polymers synthesized with 30 and 100 mM NaCl, while polymerization with 30 mM NaCl was 2 times faster. When a lower concentration of salt, 10 mM, was used, the first-order kinetic plot deviated from linearity and M_w/M_n values increased to approximately 1.5 (**Figure III.5**) which suggests that a NaCl concentration of 10 mM was too low to prevent deactivator dissociation.

Variation of Cu concentration and targeted DP. In ATRP the ratio of Cu^{I} to Cu^{II} determines rate of polymerization, while absolute Cu^{II} concentration influences the molecular weight dispersity.[4] Therefore, it is important to determine the minimal amount of Cu needed to gain control over the polymerization and still achieve an acceptable rate of reaction. The copper concentration was varied from 30 to 300 ppm (**Table III.1**, entries 1 – 4). In general, the rate of polymerization was faster and control was better with higher concentrations of copper. **Figure III.6A** shows that the reaction rate decreased approximately 5 fold, and **Figure III.6B** showed that dispersities increased from 1.2 to 1.5, as the copper concentration was progressively decreased from 300 to 30 ppm. The results suggest that both 100 and 300 ppm provided acceptable rates of reaction and control over the polymerization, whereas 30 ppm was too low to control the reaction. The dispersity in

ATRP is a function of the ratio of the concentration of the ATRP initiator and the concentration of XCu(II)/L in solution. Therefore when a polymerization is poorly controlled, such as the reaction with 30 ppm catalyst, increasing the targeted degree of polymerization (DP) from 500 to 1000 could improve the level of control over the structure of the final polymer. Although, there was some improvement in the dispersity when the targeted DP was increased from 500 to 1000, both polymers had high dispersities, nonlinear evolution of molecular weight, and poor correlation between theoretical and experimental molecular weights which could be due to transfer reactions.

Table III.4. ARGET ATRP of $OEOMA_{475}$ with varied copper concentration and DP.

Entry	M/I/TPMA/$CuBr_2$	DP	Cu[a], ppm	Time, h	Conv., %	$M_{n\ th}$[b] $\times 10^{-3}$	$M_{n\ GPC}$[c] $\times 10^{-3}$	M_w/M_n
1	500/1/0.4/0.05	500	100	15	72	170	192	1.28
2	500/1/1.2 /0.15	500	300	5	79	189	226	1.23
3	500/1/0.12/0.015	500	30	15	69	164	113	1.51
4	500/0.5/0.12/0.015	1000	30	13	20	47	103	1.46
5	500/0.5/0.4 /0.05	1000	100	10	36	200	198	1.33
6	500/2/0.4/0.05	250	100	10	62	74	91	1.28

All polymerizations were conducted with $[M]_0$ = 0.5 M, $[NaCl]_0$ = 100 mM, FR_{AA} = 16 nmol/min; $[I]_0$ = 1 mM, except for entry 4 - 5: $[I]_0$ = 0.5 mM, and for entry 6: $[I]_0$ = 2 mM; [a] Calculated by the initial molar ration of $CuBr_2$ to the monomer; [b] $M_{n\ th} = ([M]_0/[I]_0) \times \text{conversion} \times M_{monomer}$; [c] universal calibration (SI).

Finally, while retaining the concentration of catalyst at 100 ppm, the targeted DP was varied. In these reactions the concentration of initiator was varied in the presence of constant concentrations of copper and monomer (**Table III.4**, entries 1, 5 – 6). The rate of reaction was faster at higher initiator concentrations, which was expected because of the dependency between rate of reaction and initiator concentration. In all cases the reactions showed linear first-order kinetics, linear evolution of molecular weight with conversion,

good correlation between experimental and theoretical molecular weights and generated polymers with narrow dispersity <1.3 (**Figure III.7**).

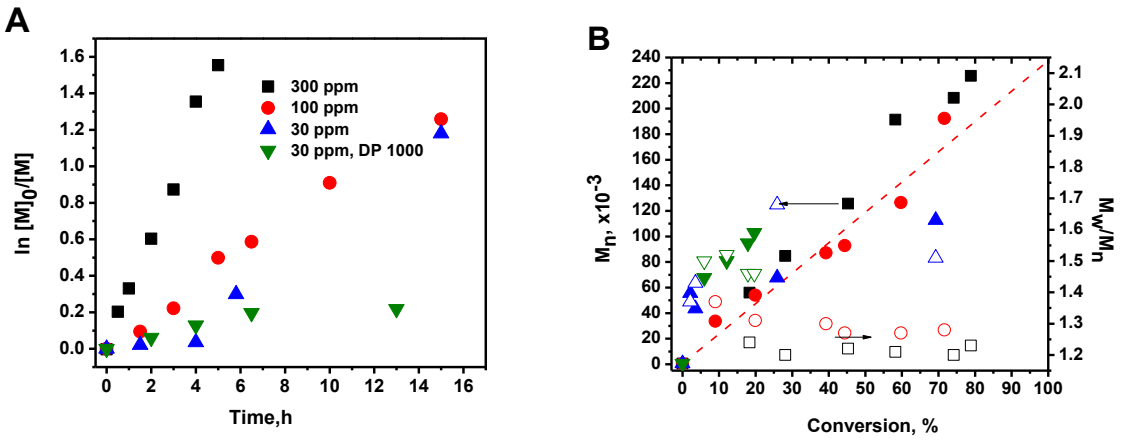

Figure III.6. Effect of the copper concentration on the ARGET ATRP of $OEOMA_{475}$ in water at 30 °C. (A) First-order kinetic plot, and (B) evolution of molecular weight and molecular weight distribution with conversion (the dash line represents theoretical molecular weight at a given conversion). $[OEOMA_{475}]_0$ = 0.5 M; FR_{AA} = 16 nmol/min.

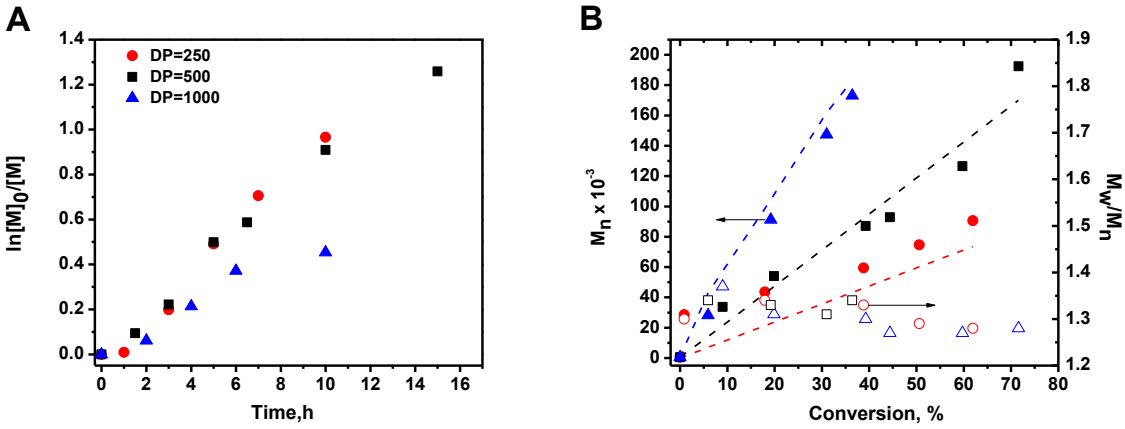

Figure III.7. Influence of the different target DP on the ARGET ATRP of $OEOMA_{475}$ in water at 30°C. First-order kinetic plot (A), evolution of molecular weight and molecular weight distribution with conversion (B). $[OEOMA_{475}]_0$ = 0.5 M; $[OEOMA_{475}]/[I]/[TPMA]/[CuBr_2]$ = 500/1/0.4/0.05; RA_{AA} = 16 nmol/min.

Chain extension. Living chain-end functionality was confirmed by chain extension of a poly($OEOMA_{475}$) macroinitiator with $OEOA_{480}$. The macroinitiator was synthesized using aqueous ARGET ATRP with 100 ppm of copper, Cu/L=1/8, 100 mM NaCl and RA_{AA} = 16 nmol/min, and then the poly($OEOA_{480}$) block was prepared using similar

conditions, except that the ascorbic acid was fed at a higher rate; RA_{AA} = 50 nmol/min. The higher feeding rate was chosen since acrylates have lower ATRP equilibrium constant than methacrylates, implying that a larger fraction of the copper must be reduced for the reaction to commence. The formation of the block copolymer was confirmed by a clear shift in the molecular weight distribution after chain extension (**Figure III.8**). The resulting block copolymer had a low dispersity of 1.32, and its molecular weight was close the theoretically expected value.

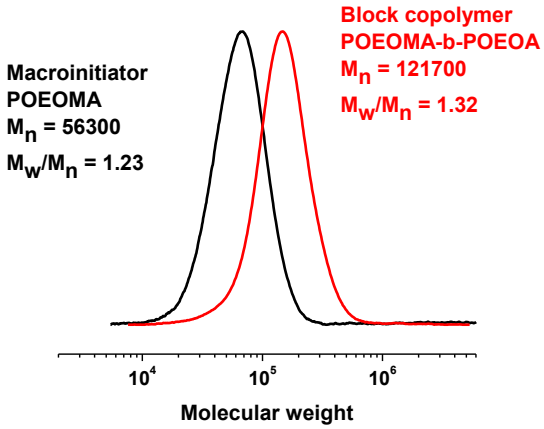

Figure III.8. GPC chromatographs of the poly($OEOMA_{475}$)-Cl macroinitiator and poly($OEOMA_{475}$)-*b*-poly($OEOA_{480}$) block copolymer. Polymerization of $OEOMA_{475}$ conducted in water (~80%) at 30 °C with $[M]_0$ = 0.5 M, $[I]_0$ = 2 mM, $[NaCl]_0$ = 100 mM, FR_{AA} = 16 nmol/min; polymerization of $OEOA_{480}$ conducted in water (~80%) at 30°C with $[M]_0$ = 0.5 M, $[I]_0$ = 1 mM, $[NaCl]_0$ = 30 mM, FR_{AA} = 50 nmol/min.

Start/Stop polymerization. In the aqueous ARGET ATRP method developed and discussed in this article, ascorbic acid is continuously added to the reaction in order to regenerate Cu^I species in solution and promote a controlled polymerization. Therefore, if the reducing agent is not added, a small amount of unavoidable termination will lead to a significant buildup of the deactivator, and shift the ATRP equilibrium toward the dormant species. The following experiment demonstrated that the reaction can be

started or stopped on demand by turning on or off the feeding of ascorbic acid, as demonstrated previously in electrochemically mediated ATRP[30] or photoinduced ATRP.[35] The start/stop reaction was performed using a catalyst loading of 300 ppm with FR_{AA} = 16 nmol/min (**Figure III.9**). The ascorbic acid was fed to the reaction for 1h, during which time the polymerization proceeded at a relatively fast rate. After 1h the feeding of the ascorbic acid was turned off, and the polymerization rate decreased. This cycle was repeated two more times, resulting in step-wise conversion up to 60%. Throughout the whole experiment the dispersities were low and the molecular weights agreed with the theoretical values. The clustering of the points during non-feeding regimes shows that slow feeding is required to continue the polymerization. Furthermore, the efficient reinitiation of polymers in solution confirms retention of high end group functionality throughout the polymerization.

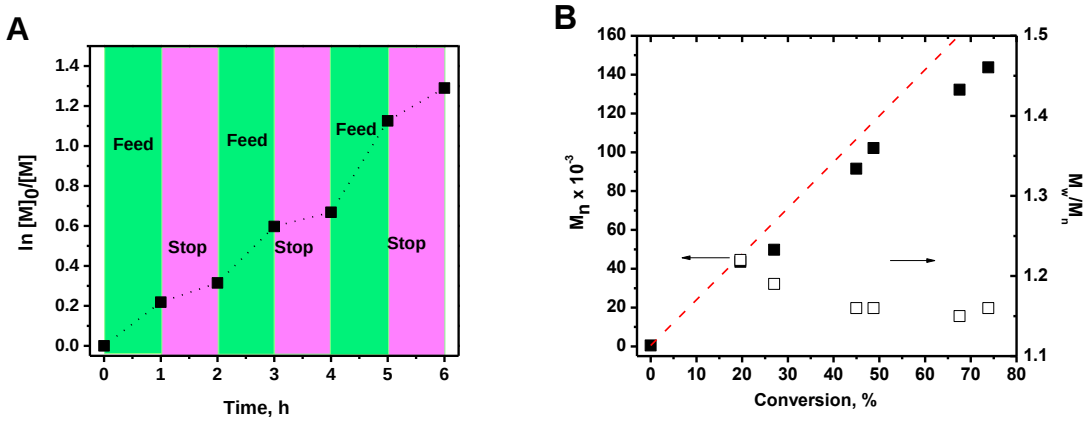

Figure III.9. Effect of the feeding of AA on the ARGET ATRP of $OEOMA_{475}$ in water at 30 °C. (A) First-order kinetic plot, and (B) evolution of molecular weight and molecular weight distribution with conversion (the dash line represents theoretical molecular weight at a given conversion). $[OEOMA_{475}]_0$ = 0.5 M; $[OEOMA_{475}]_0/[I]_0/[TPMA]_0/[CuBr_2]_0$ = 500/1/1.2 /0.15.

Table III.5. ARGET ATRP of $OEOMA_{475}$ in PBS initiated by HOEBiB and BSA-O-$[iBBr]_{30}$.

Entry	M/I/TPMA/$CuBr_2$	FR_{AA}, nmol/min	Cu[a], ppm	Time, h	Conv., %	$M_{n\ th}$[b] $\times 10^{-3}$	$M_{n\ GPC}$[c] $\times 10^{-3}$	M_w/M_n
1	500/1/0.4/0.05	16	100	10	76	180	226	1.38
2	500/1/0.4/0.05	16	100	10	84	199	405	1.9
3	250/1/0.6/0.075	8	300	10	79	99	109	1.35

Entry 1: HOEBiB; entries 2 – 3: BSA-O-$[iBBr]_{30}$. All polymerizations were conducted with $[M]_0$ = 0.5 M, $[I]_0$ = 1 mM, except for entry 3: $[M]_0$ = 0.25 mM; [a] Calculated by the initial molar ration of $CuBr_2$ to the monomer; [b] $M_{n\ th} = ([M]_0/[I]_0) \times conversion \times M_{monomer}$; [c] universal calibration (SI).

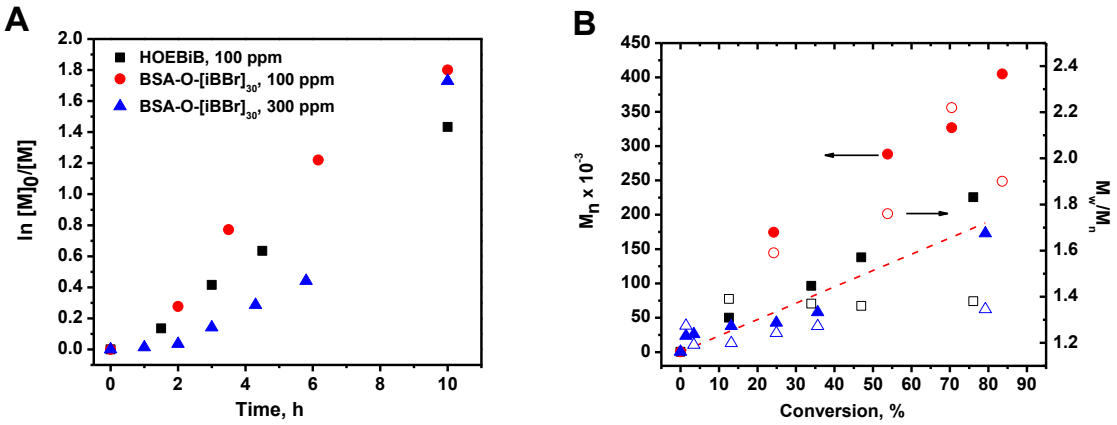

Figure III.10. ARGET ATRP of $OEOMA_{475}$ from HOEBiB/BSA-iBBr in PBS at 30 °C. (A) First-order kinetic plot, and (B) evolution of molecular weight and molecular weight distribution with conversion (the dash line represents theoretical molecular weight at a given conversion). $[OEOMA_{475}]_0$ = 0.5 M, $[OEOMA_{475}]_0/[I]_0/[TPMA]_0/[CuBr_2]_0$ = 500/1/0.4/0.05 (black/red aquare), FR_{AA} = 16 nmol/min; $[OEOMA_{475}]_0$ = 0.25 M, $[OEOMA_{475}]_0/[I]_0/[TPMA]_0/[CuBr_2]_0$ = 250/1/0.6/0.075 (blue circle), FR_{AA} = 8 nmol/min.

Preparation of a protein-polymer hybrid. One motivation for the development of this aqueous ARGET ATRP method that uses low copper concentrations and a biologically friendly reducing agent was design of biologically compatible reaction conditions. Therefore, the aqueous ARGET method is an excellent candidate for the preparation of protein-polymer hybrids by the "grafting from" approach. Bovine serum albumin (BSA) with 30 ATRP initiating sites was used as a model protein. Initially, a reaction with a small molecule initiator was performed in phosphate buffered saline (PBS).

PBS is used for protein stabilization, and it consists of NaCl and NaH_2PO_4 salts. **Table III.5** summarizes the polymerization conditions using both a water-soluble initiator and the protein. When the small molecule initiator was used, the polymerization in PBS showed a linear first-order kinetic plot, linear evolution of molecular weight with conversion and good correlation between experimental and theoretical molecular weight values, indicating well-controlled polymerization (**Figure III.10**). The dispersities were slightly higher than for polymerization carried out with only NaCl, but remained below 1.4 until *ca.* 80% conversion. These reaction conditions were subsequently used for the grafting of poly($OEOMA_{475}$) from BSA-O-$[iBBr]_{30}$. The system showed almost linear first order kinetics, however the evolution of the average molecular weight was above the theoretical values, and the M_w/M_n values were close to 2. To improve the degree of control over the system monomer concentration was reduced from 22 vol. % to 11 vol. %, copper concentration was increased from 100 ppm to 300 ppm, and the rate of addition of ascorbic acid, RA_{AA}, was reduced from 16 nmol/min to 8 nmol/min. The kinetics show an induction period of approximately 2 hours, which could be caused by steric hindrance of the initiating sites on the protein. But after 2h the polymerization proceeded at an almost linear rate in semilogarithmic coordinates. The molecular weight evolution correlated well with the theoretical values, and the dispersity of the resulting polymers remained below 1.35. TEM showed that protein-polymer hybrids synthesized under these optimized conditions formed nanoparticles without aggregation (**Figure III.11**).

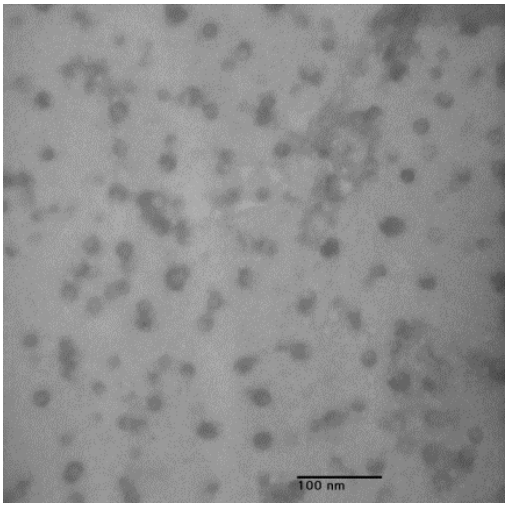

Figure III.11. Transition electron microscopy image of BSA – $[poly(OEOMA_{475})]_{30}$ nanoparticles obtained by ARGET ATRP of $OEOMA_{475}$ from BSA-$[iBBr]_{30}$ in PBS (**Table III.5**, entry 3).

III.4. Conclusions

Conditions were developed for the aqueous ARGET ATRP of $OEOMA_{475}$ to prepare well defined polymers at ambient temperature (30 °C) using catalyst concentrations between 100 – 300 ppm. Critical parameters for preparation of well-controlled polymers were that the ascorbic acid should be slowly fed to the reaction medium and that a large excess of halide salt should be added to ensure the presence of a sufficiently high concentration of the deactivator complex. Polymerizations with chloride ions showed a slower reaction with slightly improved control compared to bromide ions, with the optimal concentration of the halide salt being between 30 and 100 mM. Furthermore an excess of the ligand over copper is essential to provide conditions for improved control and faster kinetics. Whereas a faster feeding rate of the reducing agent only gave a minimal improvement in the kinetics and leads to a decrease in the level of control over the final polymer. Since the ascorbic acid reducing agent should be slowly and continuously fed into the aqueous ARGET ATRP system, this generates an additional handle for controlling the reaction, allowing the reaction to be stopped or restarted at any point simply by ceasing or recommencing the feeding of the reducing agent. The low catalyst concentration employed in this aqueous ARGET ATRP make the procedure biologically friendly and hence an excellent technique for creating bioconjugates, as demonstrated by the synthesis of a BSA based protein-polymer hybrid.

III.5. Experimental section

III.5.1. Materials.

Oligo(ethylene oxide) methyl ether methacrylate ($OEOMA_{475}$, 99%, average molecular weight 475, Aldrich) and oligo(ethylene oxide) methyl ether acrylate ($OEOA_{480}$, 99%, average molecular weight 480, Aldrich) were passed over a column of basic alumina (Fisher Scientific) prior to use. Copper (II) bromide (99.999%, Aldrich), tetraethylammonium bromide (TEABr, 98%, Aldrich), tetraethylammonium chloride (TEACl, 98%, Aldrich), sodium chloride (Fisher Scientific), ascorbic acid (AA, Sigma Aldrich), water (HPLC grade, Fisher Scientific), tetrahydrofuran (THF, ACS grade, Fisher Scientific), N,N-dimethylformamide (DMF, ACS grade, Fisher Scientific), dichloromethane (DCM, HPLC grade, Fisher Scientific), ethyl ether (ACS grade, Fisher Scientific), deuterium oxide (99.9%, Cambridge Isotope Laboratories), anhydrous magnesium sulfate (99%, Aldrich) were used as received. Tris(pyridin-2-ylmethyl)amine (TPMA),[36] 2-hydroxyethyl 2-bromo-*iso*-butyrate (HEBiB),[37] and bovine serum albumin (BSA) protein initiator (BSA-O-$[iBBr]_{30}$)[26] were prepared as previously reported in literature.

III.5.2. Instrumentation and characterization.

A syringe pump (KDS Scientific, Legato 101) was used for continuous feeding of the reducing agent at the rate of 0.5 – 1 μl/min. Monomer conversion was measured using ^{1}H NMR spectroscopy in D_2O using a Bruker Avance 500 MHz spectrometer at 27 °C. Molecular weight and dispersities (M_w/M_n) were determined by GPC. The GPC system was equipped with a Waters 515 HPLC Pump and Waters 2414 Refractive Index Detector using PSS columns (SDV 10^2, 10^3, 10^5 Å) in tetrahydrofuran (THF) as an eluent at a flow

rate of 1 mL/min at 35 °C. The apparent molecular weights (M_n) and dispersities (M_w/M_n) were determined using linear poly(methyl methacrylate) (M_n = 800 ~ 1,820,000) standards using WinGPC 7.0 software from PSS. A triple detector system containing RI detector (Wyatt Technology, Optilab REX), viscometer detector (Wyatt Technology, ViscoStar), and a multiangle laser light scattering (MALLS) detector (Wyatt Technology, DAWN EOS) with the light wavelength at 690 nm were used to determine dn/dc value and Mark-Houwink parameters (a, K) using Astra software from Wyatt Technology. The determined Mark-Houwink parameters were used for universal calibration using WinGPC 7.0 software from PSS. Transmission electron microscopy (TEM) was conducted on a Hitachi H-7100 TEM. Samples were drop-coated onto TEM carbon coated grids and negatively stained with phosphotungstic acid.

III.5.3. dn/dc value and Mark-Houwink parameters.

Universal calibration was used to determine molecular weight of the synthesized polymers. The dn/dc value of the poly($OEOMA_{475}$) was 0.07 mL/g in THF at 35°C. Mark-Houwink parameters for poly(methyl methacrylate) poly(MMA) and poly($OEOMA_{475}$) were used for universal calibration. Mark-Houwink parameters for poly(MMA) were taken from literature: a = 0.731, K = 0.00756 mL/g.[38] Mark-Houwink parameters for poly($OEOMA_{475}$) were calculated using measurements performed on the MALLS GPC and viscometer in THF at 35 °C: a = 0.62, K = 0.013 mL/g.

III.5.4. General procedure for ARGET ATRP of OEOMA.

A series of aqueous ARGET ATRP reactions were carried out under systematically varied conditions to determine optimal conditions for ARGET ATRP of OEOMA. Conditions developed for polymerization of $OEOMA_{475}$ generally followed this procedure: NaCl (19

mg, 0.33 mmol), $OEOMA_{475}$ (2.375 g, 5 mmol), 100 mM stock solution HOEBiB (0.1 ml, 0.01 mmol), 25 mM stock solution $CuBr_2$ and 200 mM stock solution TPMA (20 µl, 0.5µmol $CuBr_2$ and 4µmol TPMA) were dissolved in H_2O (7.6 ml). DMF (0.1 ml) was added as internal standard for ^1H NMR analysis. The mixture was added to a 10 ml Schlenk flask and purged with nitrogen for 30 min, then the flask was placed in an oil bath at 30 °C. An ascorbic acid solution (16 mM) was purged with nitrogen, and the solution continuously injected into the reaction medium using a syringe pump at the rate 1 µl/min. Samples were taken throughout the reaction for GPC and NMR analysis.

III.5.5. Synthesis of a POEOMA-b-POEOA block copolymer.

NaCl (58 mg, 1 mmol), $OEOMA_{475}$ (2.375 g, 5 mmol), 100 mM stock solution HOEBiB (0.2 ml, 0.02 mmol), 25 mM stock solution $CuBr_2$ and 200 mM stock solution TPMA (20 µl, 0.5µmol $CuBr_2$ and 4µmol TPMA), DMF (0.1 ml) were dissolved in H_2O (7.5 ml). The mixture was added to a 10 ml Schlenk flask and purged with nitrogen for 30 min before being placed in an oil bath at 30 °C. An ascorbic acid solution (16 mM) was purged with nitrogen, and then injected into the flask via syringe pump at the rate 1 µl/min. After 10 h the reaction was stopped by exposure to air and dilution with water. The polymer was extracted from the reaction mixture with 4 × 50 mL DCM. The organic phases were combined and the solvent removed under reduced pressure. The residue was dissolved in THF and passed over neutral alumina to remove the copper catalyst. The polymer was precipitated into diethyl ether, and then the mixture was centrifuged at 4000 rpm for 5 min. The supernatant was decanted and the procedure repeated 2 more times. The poly(OEOMA) was dried under vacuum overnight, and characterized by GPC. A polymer with M_n = 56,000, and M_w/M_n = 1.23 was obtained. The procedure for chain extension

with OEOA follows: the POEOMA macroinitiator (0.3 g, 0.005 mmol), $OEOA_{480}$ (1.2 g, 2.5 mmol), NaCl (19 mg, 0.33 mmol), 25 mM of a stock solution $CuBr_2$ and 200 mM of a stock solution of TPMA (20 µl, 0.25µmol $CuBr_2$ and 2µmol TPMA), and DMF (0.1 ml) were dissolved in H_2O (3 ml). The mixture was added to a 10 ml Schlenk flask and purged with nitrogen for 30 min then placed in an oil bath at 30 °C. An ascorbic acid solution (50 mM) was purged with nitrogen, and then fed into the reaction mixture using a syringe pump at the rate 1 µl/min. The reaction was stopped after 15h and analyzed by GPC.

III.5.6. Grafting from the protein initiator BSA-O-[iBBr]$_{30}$.

BSA-O-$[iBBr]_{30}$ (25.0 mg (protein), 0.01 mmol (initiator)), $OEOMA_{475}$ (1.188 g, 2.5 mmol), 25 mM stock solution $CuBr_2$ and 200 mM stock solution TPMA (30 µl, 0.75µmol $CuBr_2$ and 6µmol TPMA) were dissolved in 0.1 M PBS (7.6 ml). DMF (0.1 ml) was added as internal standard for ^1H NMR analysis. The mixture was added to a 10 ml Schlenk flask and purged with nitrogen for 30 min then placed in an oil bath at 30°C. An ascorbic acid solution (8 mM) was purged with nitrogen prior to injecting the solution into the reaction using a syringe pump at a rate 1 µl/min. Samples were taken throughout the reaction for GPC and NMR analysis. The grafted polymers were cleaved from the protein by adding 200 µl of the reaction mixture to 200 µl of 5% KOH solution. The resulting solution was allowed to react for 2 h at room temperature, followed by GPC analysis, as described in the literature.[26]

III.6. References

(1) Matyjaszewski, K.; Xia, J. *Chem. Rev.* **2001**, *101*, 2921.

(2) Kamigaito, M.; Ando, T.; Sawamoto, M. *Chem. Rev.* **2001**, *101*, 3689.

(3) Matyjaszewski, K.; Tsarevsky, N. V. *Nat. Chem.* **2009**, *1*, 276.

(4) Braunecker, W. A.; Matyjaszewski, K. *Prog. Polym. Sci.* **2007**, *32*, 93.

(5) Tsarevsky, N. V.; Matyjaszewski, K. *Chem. Rev.* **2007**, *107*, 2270.

(6) Ouchi, M.; Terashima, T.; Sawamoto, M. *Chem. Rev.* **2009**, *109*, 4963.

(7) Duxbury, C. J.; Wang, W.; de Geus, M.; Heise, A.; Howdle, S. M. *J. Am. Chem. Soc.* **2005**, *127*, 2384.

(8) Xia, J.; Johnson, T.; Gaynor, S. G.; Matyjaszewski, K.; DeSimone, J. *Macromolecules* **1999**, *32*, 4802.

(9) Kubisa, P. *Progr. in Polym. Sci.* **2004**, *29*, 3.

(10) Sarbu, T.; Matyjaszewski, K. *Macromol. Chem. Phys.* **2001**, *202*, 3379.

(11) Coca, S.; Jasieczek, C. B.; Beers, K. L.; Matyjaszewski, K. *J. Polym. Sci. A Polym. Chem.* **1998**, *36*, 1417.

(12) Wang, X. S.; Armes, S. P. *Macromolecules* **2000**, *33*, 6640.

(13) Min, K.; Matyjaszewski, K. *Cent. Eur. J. Chem.* **2009**, *7*, 657.

(14) Chung, I.-D.; Britt, P.; Xie, D.; Harth, E.; Mays, J. *Chem. Comm.* **2005**, *8*, 1046.

(15) Bortolamei, N.; Isse, A. A.; Magenau, A. J. D.; Gennaro, A.; Matyjaszewski, K. *Angew. Chem. Int. Ed.* **2011**, *50*, 11391.

(16) Heredia, K. L.; Bontempo, D.; Ly, T.; Byers, J. T.; Halstenberg, S.; Maynard, H. D. *J. Am. Chem. Soc.* **2005**, *127*, 16955.

(17) Gao, W.; Liu, W.; Mackay, J. A.; Zalutsky, M. R.; Toone, E. J.; Chilkoti, A. *Proc. Natl. Acad. Sci. USA* **2009**, *106*, 15231.

(18) Strozyk, M. S.; Chanana, M.; Pastoriza-Santos, I.; Pérez-Juste, J.; Liz-Marzán, L. M. *Adv. Func. Mater.* **2012**, *22*, 1436.

(19) Peeler, J. C.; Woodman, B. F.; Averick, S.; Miyake-Stoner, S. J.; Stokes, A. L.; Hess, K. R.; Matyjaszewski, K.; Mehl, R. A. *J. Am. Chem. Soc.* **2010**, *132*, 13575.

(20) Lele, B. S.; Murata, H.; Matyjaszewski, K.; Russell, A. J. *Biomacromolecules* **2005**, *6*, 3380.

(21) Braunecker, W. A.; Tsarevsky, N. V.; Gennaro, A.; Matyjaszewski, K. *Macromolecules* **2009**, *42*, 6348.

(22) Tsarevsky, N. V.; Pintauer, T.; Matyjaszewski, K. *Macromolecules* **2004**, *37*, 9768.

(23) Robinson, K. L.; Khan, M. A.; de Paz Báñez, M. V.; Wang, X. S.; Armes, S. P. *Macromolecules* **2001**, *34*, 3155.

(24) Oh, J. K.; Perineau, F.; Charleux, B.; Matyjaszewski, K. *J. Polym. Sci. A Polym. Chem.* **2009**, *47*, 1771.

(25) Magnusson, J. P.; Bersani, S.; Salmaso, S.; Alexander, C.; Caliceti, P. *Bioconjugate Chem.* **2010**, *21*, 671.

(26) Averick, S.; Simakova, A.; Park, S.; Konkolewicz, D.; Magenau, A. J. D.; Mehl, R. A.; Matyjaszewski, K. *ACS Macro Letters* **2012**, *1*, 6.

(27) Pintauer, T.; Matyjaszewski, K. *Chem. Soc. Rev.* **2008**, *37*, 1087.

(28) Matyjaszewski, K.; Jakubowski, W.; Min, K.; Tang, W.; Huang, J.; Braunecker, W. A.; Tsarevsky, N. V. *Proc. Natl. Acad. Sci. USA* **2006**, *103*, 15309.

(29) Jakubowski, W.; Matyjaszewski, K. *Angew. Chem. Int. Ed.* **2006**, *118*, 4594.

(30) Magenau, A. J. D.; Strandwitz, N. C.; Gennaro, A.; Matyjaszewski, K. *Science* **2011**, *332*, 81.

(31) Konkolewicz, D.; Magenau, A. J. D.; Averick, S. E.; Simakova, A.; He, H.; Matyjaszewski, K. *Macromolecules* **2012**, *45*, 4461.

(32) Tsarevsky, N. V.; Braunecker, W. A.; Matyjaszewski, K. *J. Organomet. Chem.* **2007**, *692*, 3212.

(33) Paneva, D.; Mespouille, L.; Manolova, N.; Degée, P.; Rashkov, I.; Dubois, P. *Macromol. Rapid Commun.* **2006**, *27*, 1489.

(34) Tang, W.; Kwak, Y.; Braunecker, W.; Tsarevsky, N. V.; Coote, M. L.; Matyjaszewski, K. *J. Am. Chem. Soc.* **2008**, *130*, 10702.

(35) Kwak, Y.; Matyjaszewski, K. *Macromolecules* **2010**, *43*, 5180.

(36) Tyeklar, Z.; Jacobson, R. R.; Wei, N.; Murthy, N. N.; Zubieta, J.; Karlin, K. D. *J. Am. Chem. Soc.* **1993**, *115*, 2677.

(37) Jayachandran, K. N.; Takacs-Cox, A.; Brooks, D. E. *Macromolecules* **2002**, *35*, 4247.

(38) Gruendling, T.; Junkers, T.; Guilhaus, M.; Barner-Kowollik, C. *Macromol. Chem. Phys.* **2010**, *211*, 520.

Chapter IV. Bioinspired Fe-Based Catalyst for Atom Transfer Radical Polymerization[‡]

IV.1. Preface

This project was inspired by several papers published in parallel by F. di Lena and N. Bruns on the role of metal containing proteins as catalysts for ATRP. This topic was described in Chapter I and, according to the polymerization results described there, heme-containing proteins were promising catalysts for ATRP. However, catalysis was likely dominated by the metal center within the proteins and, to a lesser extent, the surrounding amino acid residues within the active center of the protein. This motivated the use of heme itself as a catalyst, without a protein shell. Before starting experimentation I had thoroughly researched this topic, because this project was significantly different from my previous expertise. A review of iron porphyrins showed that this class of iron compounds are quite complex and they participate in many reactions, however, their high stability and relatively negative redox potential suggested that they might be able to catalyze ATRP reactions.

In this Chapter, hemin was modified to improve water solubility and introduce axial ligation to imitate the complexation present in protein. Polymerization studies revealed that all of the synthesized complexes were capable of ATRP catalysis, and additionally possessed activity comparable to active copper complexes such as Cu/TPMA.

[‡]Part of this Chapter includes work, which was published and reformatted: **Simakova, A**., Mackenzie, M., Averick, S. E., Park, S. and Matyjaszewski, K. Bioinspired Iron-Based Catalyst for Atom Transfer Radical Polymerization. *Angew. Chem. Int. Ed*. 2013, 52, 12148–12151

I would like to acknowledge Matthew Mackenzie for assistance in several reactions, Sangwoo Park for electrochemical characterizations of catalysts, and Dr. Saadyah Averick for valuable discussions.

IV.2. Introduction

Atom Transfer Radical Polymerization (ATRP) provides well-defined polymers with predetermined molecular weight, narrow molecular weight distributions, and precisely controlled architecture.[1-4] Copper based ATRP catalysts are the most efficient for the preparation of a broad range of well-defined polymers.[5] However, the development of new transition metal-based catalysts remains of great interest to extend the range of polymers that could be prepared by ATRP.[6] Consequently, iron-mediated ATRP has been widely investigated due to its low toxicity and biocompatibility, which is particularly advantageous when targeting biological applications.[7-15] Despite these potential benefits of iron-based catalysts, their application in ATRP is quite limited due to their lower activity and selectivity. Therefore, the design and development of new iron-based catalysts, with activity comparable to traditional catalysts and the ability to polymerize a broader range of monomers, is critical for progress in this field.

ATRP is typically carried out in organic solvents, but performing ATRP in aqueous media provides several advantages. Water is an environmentally benign solvent that enables direct polymerization of water-soluble monomers, faster reactions, and polymerization in the presence of biomolecules.[16-21] Several methods for well-controlled Cu-based ATRP in water have been developed, but most reports utilize a limited number of catalytic systems and a narrow range of monomers.[22-25] Difficulty in control of ATRP in aqueous media is often attributed to side reactions, including catalyst and chain end instabilities, as well as a large equilibrium constant (K_{ATRP}) responsible for significantly increased rate of reactions.[26-28] Our group has recently reported the synthesis of protein-polymer hybrids by ATRP under biologically relevant conditions. Conditions were

designed to maintain the structure of the protein during polymerization, as well as provide good control.[23] In this system a protein served as an initiator, but recent publications by Bruns[29,30] and diLena[31,32] showed that certain proteins/enzymes could also act as catalysts for ATRP. They reported that protein based catalysts, so called ATRPases, with iron heme centers such as horseradish peroxidase (HRP), catalase, or hemoglobin (Hb), could catalyze ATRP and produce high molecular weight (MW) polymers with polydispesities close to 1.5, indicative of limited control. These catalytic systems could potentially expand the range of polymerizable monomers due to different catalyst structure and higher tolerance to pH variation. However, two major drawbacks of utilizing proteins for catalysis are their sensitivity to reaction conditions and high molecular weight.[33] Therefore, the development of synthetic analogues that can reproduce or even enhance the properties of native catalytic proteins, without the need for such stringent conditions and high mass-loading of catalyst, would allow for broader application of these bio-inspired catalytic systems (**Scheme IV.1**).[34,35]

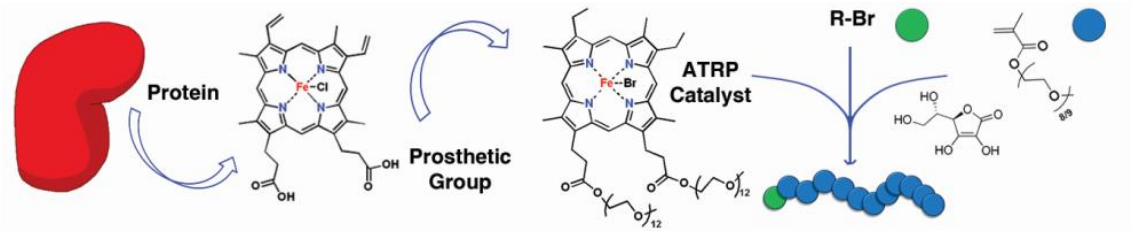

Scheme IV.1. Bio-inspired Fe-based catalyst for ATRP.

Application of the naturally occurring iron porphyrin hematin, whose structure is similar to the prosthetic group of HRP, Hb, or catalase, in catalysis of radical polymerization of vinyl monomers showed that hematin can successfully replace HRP in this reactions.[36,37] Indeed, it was shown that some iron porphyrins can induce an atom transfer process, as in ATRP, and could even provide a certain level of control as indicated

by linear increase of molecular weight with conversion and moderate dispersity values ($M_w/M_n < 2$).[38,39] PolyNIPAAm prepared in the presence of alkyl halide initiator and hematin had relatively high M_w/M_n values, 1.8-2.1. These results indicated that iron porphyrins could act as catalysts for ATRP, but significant improvements are needed to prepare well-defined materials. A recent publication reported ATRP catalysis by a heme-containing peroxidase mimic, which consisted of deuterohemin with an attached sequence of 6 amino acids.[40] The ATRP of water-soluble $OEOMA_{500}$ monomer performed in the presence of this catalyst resulted in formation of low MW polymers with polydispersity $M_w/M_n < 1.2$.

Hemin was initially chosen as an iron based catalyst for ATRP because hemin is a commercially available another ferric variation of heme, with a chloride ligand instead of a hydroxyl (**Figure IV.1a**).[41] However, this complex is characterized by low halidophilicity,[42] low solubility in water, and can self (co)polymerize due to the presence of vinyl moieties.[43] Therefore, we developed second generation hemin-inspired catalysts that addressed these issues and provided significantly improved performance in the preparation of well-defined polymers (**Figure IV.1**).

The first second-generation catalyst is a hemin derivative, which was PEGylated to improve its water-solubility (mesohemin-$(MPEG_{550})_2$) (**Figure IV.1b**). Two additional modified catalysts were prepared with differnt ligands, which were selected to imitate axial ligation from amino acids residues present in proteins (**Figure IV.1c, d**). The iron center in heme, present in proteins, is often additionally complexed by residues of amino acids such as histidine, cysteine, methionine, or tyrosine.[44,45] Therefore we chose two types of modification: one with an imidazole moiety to mimic complexation by histidine

(Mesohemin-MPEG$_{550}$-N), and the other with a thioether moiety to mimic complexation by methionine (Mesohemin-MPEG$_{550}$-S). Imidazole has very high complexation affinity towards iron, and thus forms a well-defined iron porphyrin complex.[41,46-48] The iron porphyrin complex with thiol has been extensively studied,[41,49] but we chose to incorporate a thioether to prevent the radical transfer characteristic of thiols.[50]

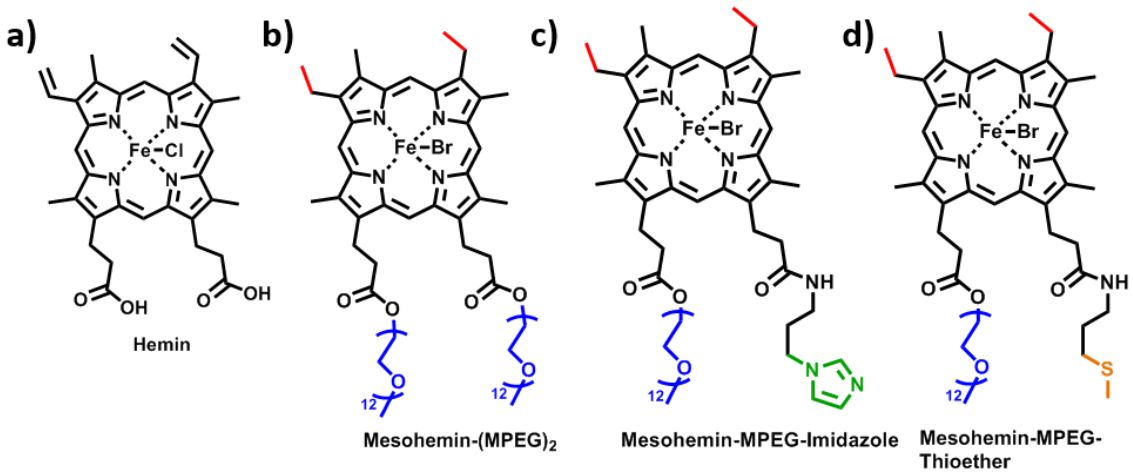

Figure IV.1. Iron porphyrin derivatives used for catalysis of ATRP.

IV.3. Results and discussion

IV.3.1. PEGylated Iron Mesohemin as a Catalyst for ATRP in Water.

Hemin was used to catalyze Activators Generated by Electron Transfer (AGET) ATRP of oligo(ethylene oxide) methyl ether methacrylate[51] in aqueous media with ascorbic acid as a reducing agent (**Scheme IV.4**). This method allows *in situ* generation of Fe^{II} species, thereby preventing the irreversible formation of μ-oxo bisiron(III) complexes that could occur between two iron (II) porphyrins in the presence of oxygen.[41,52] A set of polymerizations were conducted to determine if the prosthetic group, hemin, could be used alone to catalyze ATRP without a protein support. Initial results demonstrated that hemin could be reduced in-situ by ascorbic acid and could catalyze ATRP; however, the deactivation rate was slow, resulting in rapid but poorly controlled polymerization (**Table IV.1**, entry 2). Polymerization reached 60% monomer conversion in 1 h and stopped after that time, forming a polymer with a high M_w/M_n=1.65. The presence of a macroinitiator residue in the gel permeation chromatography (GPC) traces indicated low initiation efficiency (**Figure IV.2a).** To determine if the low halidophilicity of hemin caused the poor control over the polymerization, reactions were conducted in the presence of excess of halide salts (**Table IV.1**, entries 3-4). Addition of KBr resulted in more linear kinetic plots and improved initiation efficiency (**Figure IV.2b, Figure IV.3**). Addition of NaCl led to slower polymerization and higher M_w/M_n (**Figure IV.2c, Figure IV.3**), indicating that the presence of extra halide ions shifted equilibrium towards the stable Fe(III)-X species, increasing deactivation efficiency. The presence of a chloride salt reduced both the polymerization rate and initiation efficiency compared to a bromide salt. Therefore,

further polymerizations were conducted in the presence of excess bromide salt to enhance deactivation and initiation efficiency.

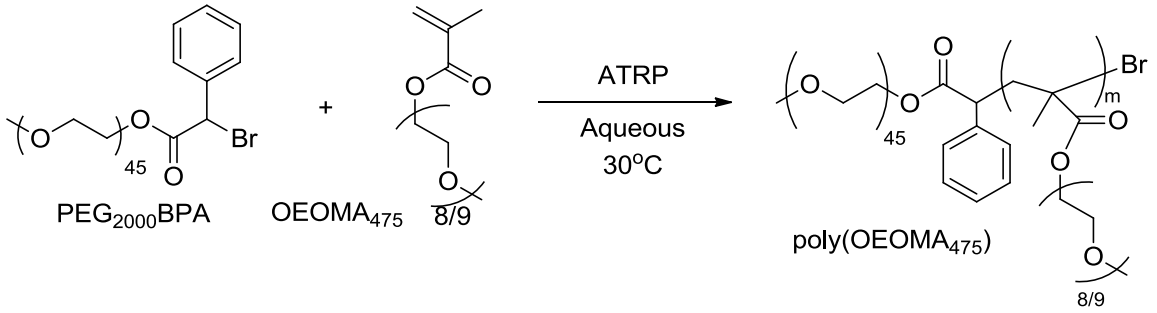

Scheme IV.2. AGET ATRP of $OEOMA_{475}$.

Table IV.1. Experimental conditions and results of ATRP of $OEOMA_{475}$.[a]

	M/I/RA/Cat	Catalyst	Salt	Conv./%, (time,h)	$M_{n,th}\times10^{-3}$ [f]	$M_{n,GPC}\times10^{-3}$ [g]	M_w/M_n
1	227/1/10/1[c,d]	Hemin	-	60 (1)	67	178	1.65
2	227/1/10/1[c,d]	Hemin	KBr	50 (18)	56	60	1.32
3	227/1/10/1[c,d]	Hemin	NaCl	14 (20)	17	27	3.26
4	227/1/10/1[c,e]	Hemin-$(PEG_{1000})_2$	KBr	78 (5)	86	116	1.32
5	227/1/1/1[c,e]	Hemin-$(PEG_{1000})_2$	KBr	47 (6)	53	103	1.72
6	227/1/10/1[c,e]	Mesohemin-$(MPEG_{550})_2$	KBr	75 (5.5)	83	101	1.30
7	227/1/5/1[c,e]	Mesohemin-$(MPEG_{550})_2$	KBr	65 (6)	72	86	1.28
8	227/1/1/1[c,e]	Mesohemin-$(MPEG_{550})_2$	KBr	60 (6)	66	63	1.19
9	227/1/1/1[c]	Mesohemin-$(MPEG_{550})_2$	TBABr	54 (6)	61	94	1.22

[a] 30 °C, 20% [M] (v/v), [b] [I] = $[PEG_{2000}BBr]$ = 5 mM, M = $OEOA_{480}$, [c] [I] = $[PEG_{2000}BPA]$ = 2 mM, M = $OEOMA_{475}$, [d] 20% DMF (v/v), [e] 6% DMF (v/v); [f] $M_{n\,th} = ([M]_0/[I]_0)\times\text{conversion}\times M_{monomer}$; [g] universal calibration.

Although initiation efficiency was improved by addition of extra halide salt, complete consumption of the macroinitiator required more than 1 h, according to the GPC traces (**Figure IV.2b**). The slow initiation led to higher than predicted MW and broader MWD. This is likely due to limited solubility of the hemin catalyst in the aqueous media. It was reported that hematin with pendent poly(ethylene glycol) (PEG) chains could be

used in aqueous media without cosolvents or pH adjustments.[37] Therefore, to determine if modification of hemin with water-soluble moieties could improve catalytic performance, the hemin carboxyl groups were esterified with PEG_{1000} (**Scheme IV.3**).

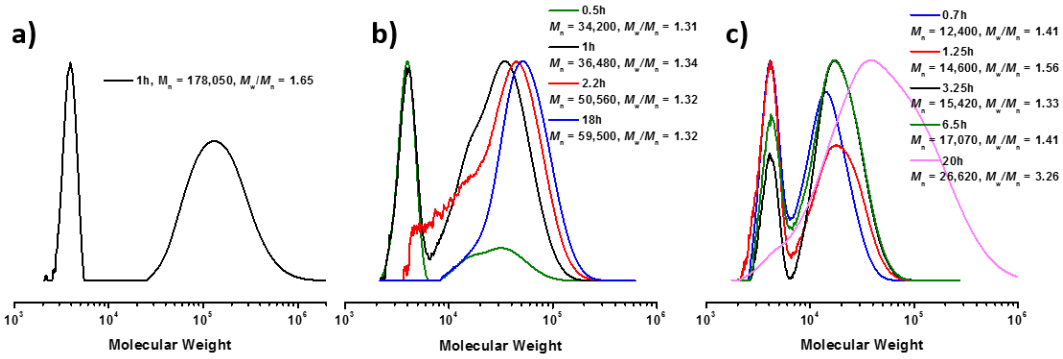

Figure IV.2. GPC traces for ATRP reaction catalazed by hemin: no extra salt (a), or 100 mM KBr (b) and NaCl (c). $[OEOMA_{475}]_0$ = 0.45 M; $[OEOMA_{475}]/[I]/[Asc.\ A]/[Hemin]$ = 227/1/10/1, water/DMF (3/1), 30 °C.

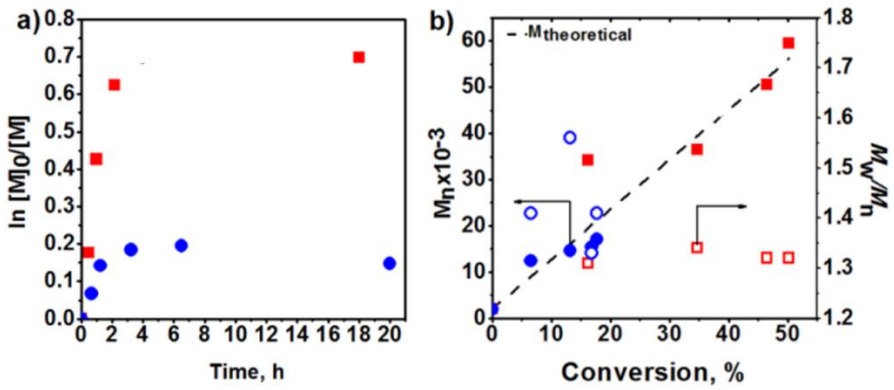

Figure IV.3. First-order kinetic plots (a), evolution of M_n and M_w/M_n with conversion (b). Entry 2(■) and 3 (●), Table IV.1. $[OEOMA_{475}]_0$ = 0.45 M; $[OEOMA_{475}]/[I]/[Asc.\ A]/[Hemin]$ = 227/1/10/1, 100 mM NaCl/KBr, water, 30 °C.

Initial experiments using hemin-PEG instead of unmodified hemin resulted in a well-controlled polymerization (Table IV.1**, entry 5), as evidenced by linear semilogarithmic kinetic plots up to high conversion, linear increase of MW with**

conversion, and narrow MWD, with M_w/M_n ~1.3 (Figure IV.4

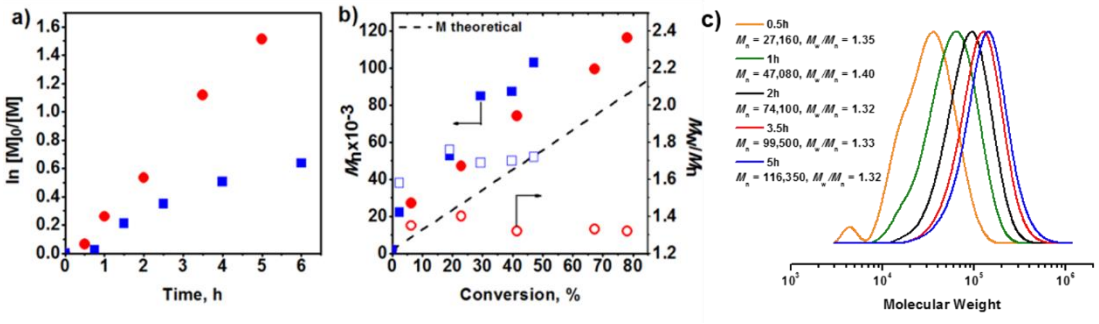

Figure IV.4). Another indication of enhanced control was a significant reduction of macroinitiator residues in the GPC traces, which was already unobservable after 30 min (**Figure IV.4c**). These results suggested that in addition to excess bromide salt, PEG tails improve catalyst performance due to better solubility and stability of the catalyst.[13] However, a 10 fold excess of ascorbic acid was required for successful polymerization. With only 1 equivalent of reducing agent, poor control was observed and MWD broadened to M_w/M_n ~1.7 (**Table IV.1**, entry 6). This limited control could have been due to a possible copolymerization of hemin through its vinyl bonds. Indeed, precipitated polymers had a brown color characteristic of hemin, and UV-Visible spectroscopy revealed spectra typical for metal porphyrins (**Figure IV.5**).[53]

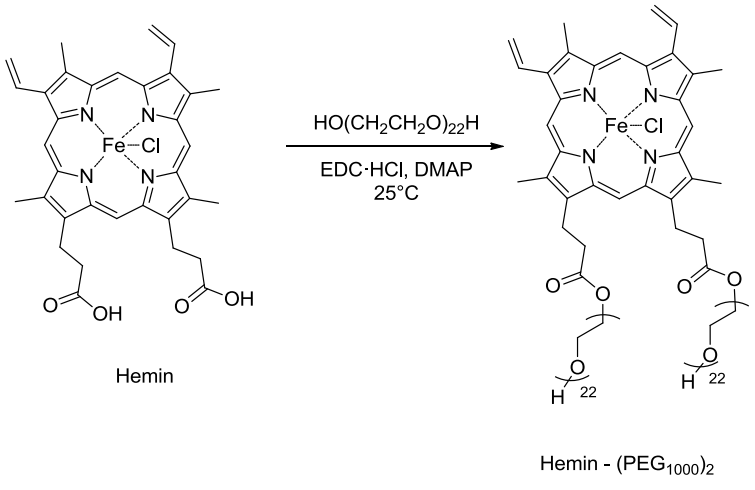

Scheme IV.3. Hemin modification scheme with PEG.

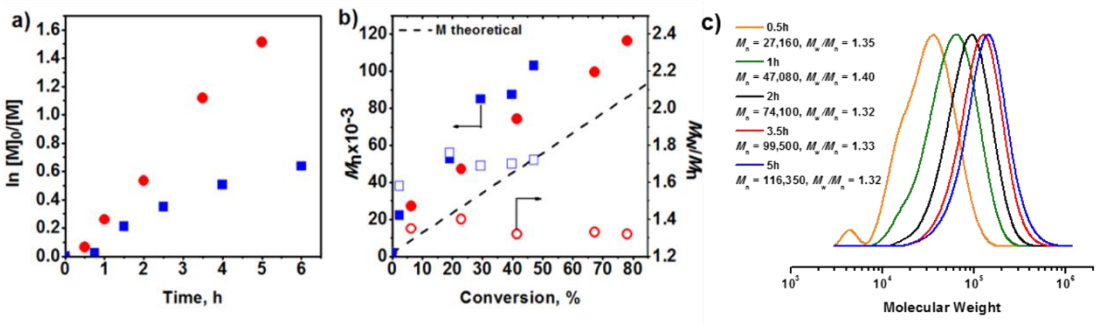

Figure IV.4. First-order kinetic plots (a), evolution of M_n and M_w/M_n with conversion (b), GPC traces. Entry 4(●) and 5 (■), Table IV.1. $[OEOMA_{475}]_0$ = 0.45 M; $[OEOMA_{475}]/[I]/[Asc.\ A]/[Hemin\text{-}(PEG_{1000})_2]$ = 227/1/n/1, n = 1, 10, water, 30 °C, 100 mM KBr.

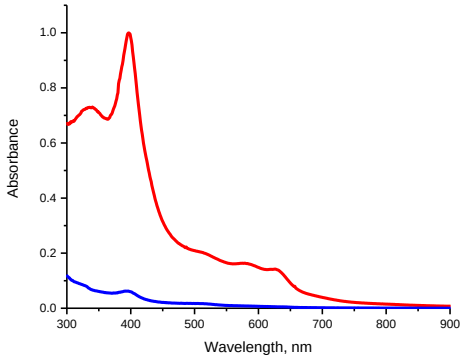

Figure IV.5. UV-Vis spectra of the purified polymer after AGET ATRP catalyzed by hemin-$(PEG_{1000})_2$ (red trace) and mesohemin-$(MPEG_{550})_2$ (blue trace) (1 wt. %).

To exclude the possibility of copolymerization of the catalyst, hemin was converted to mesohemin by hydrogenation, and then esterified with methoxy PEG_{550} (**Scheme IV.4**). The resulting modified iron porphyrin had a preserved its structure, as confirmed by the presence of a characteristic Soret band at 437 nm and Q bands in the visible region as seen by UV-Vis spectra in $CHCl_3$ (**Figure IV.13**). The structure of the complex was characterized by electrospray mass spectrometry (ESI-MS) with a [mesohemin-$(MPEG_{550})_2]^+$ species at m/z ranging from 1266.1 to 1927 with interval of 44 due to the

distribution present in $MPEG^{54}$ and [mesohemin-$(MPEG_{550})_2$]$^{2+}$ species at m/z ranging from 584.8 to 1064 with interval of 22 (**Figure IV.15**).

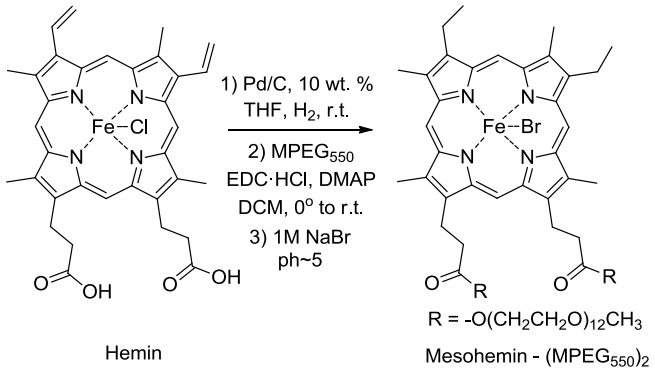

Scheme IV.4. Synthesis of mesohemin-$(MPEG_{550})_2$.

Cyclic voltammetry (CV) analysis of mesohemin-$(PEG_{550})_2$ showed two reduced states, E_{pc}=-0.73 and -0.94 V versus $F^{c0/+}$, **Figure IV.6**, likely due to interaction of iron with side PEG groups. However, upon addition of 10 equivalent of NaBr, only one cathodic peak was observed with E_{pc}=-0.89 V versus $Fc^{0/+}$, suggesting formation of a mesohemin-$(MPEG_{550})_2$Br species. The CV indicated a quasi-reversible reaction. The half-wave potential ($E_{1/2}$) was slightly more negative for mesohemin-$(PEG_{550})_2$Br than for hemin-Br, -0.78 and -0.75 V vs. $Fc^{0/+}$, respectively. Upon addition of an initiator, ethyl α-bromophenylacetate, the cyclic voltammogram showed an increase of the cathodic current and a decrease of the anodic current, due to a reaction of electrochemically produced Fe^{II} species with the alkyl halide, i.e., a regeneration of Fe^{III} species (**Scheme IV.5**).

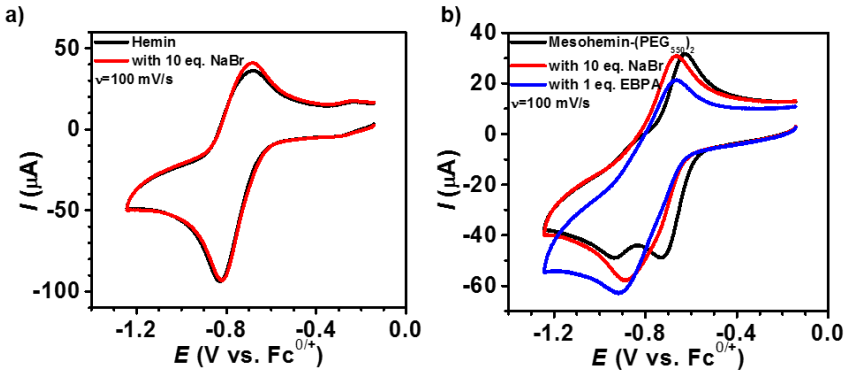

Figure IV.6. Cyclic voltammogram of (A) Hemin and (B) Mesohemin-(MPEG$_{550}$)$_2$, scan rate=100 mV/s, supporting electrolyte=TBAPF$_6$ (0.1 M in DMF).

$$[\text{X-Fe}^{\text{III}}/\text{L}]^+ + e^- \rightleftharpoons [\text{X-Fe}^{\text{II}}/\text{L}]$$

$$[\text{X-Fe}^{\text{II}}/\text{L}] \rightleftharpoons [\text{Fe}^{\text{II}}/\text{L}]^+ + \text{X}^-$$

$$[\text{Fe}^{\text{II}}/\text{L}]^+ + \text{R-X} \rightarrow [\text{X-Fe}^{\text{III}}/\text{L}]^+ + \text{R}^\bullet$$

(X = halogen, and R-X = alkyl halide (Initiator), L = hemin or mesohemin-(MPEG$_{550}$)$_2$)

Scheme IV.5. Catalytic electrochemical-chemical reaction.

This optimized second-generation catalyst, consisting of hydrogenated hemin (mesohemin) with MPEG$_{550}$ tails, performed significantly better than the original hemin or hemin-(PEG$_{1000}$)$_2$ catalyst systems (**Table IV.1**, entries 7-10). Polymerizations carried out using mesohemin-(MPEG$_{550}$)$_2$ as a catalyst were fast, providing initially linear first order kinetic plots, linear evolution of MW with conversion, and M_w/M_n values close to 1.2 (**Figure IV.7**). However, after approximately 60% conversion, the rate of polymerization decreased, likely due to the presence of an excessive amount of ascorbic acid. A decrease of the molar ratio of ascorbic acid to mesohemin-(MPEG$_{550}$)$_2$ from 10/1 to 5/1 to 1/1 resulted in more linear kinetic plots, linear increase of MW with conversion, and narrower MWD. When the ratio of ascorbic acid to mesohemin was 1/1, the experimental MW correlated well with theoretical values. Mesohemin cannot copolymerize with monomers

and become incorporated into the polymer chain. Thus, it has enhanced catalytic performance because a catalyst incorporated into polymer chain cannot efficiently participate in atom transfer reactions. Indeed, essentially colorless polymers were prepared with mesohemin (**Figure IV.5**).

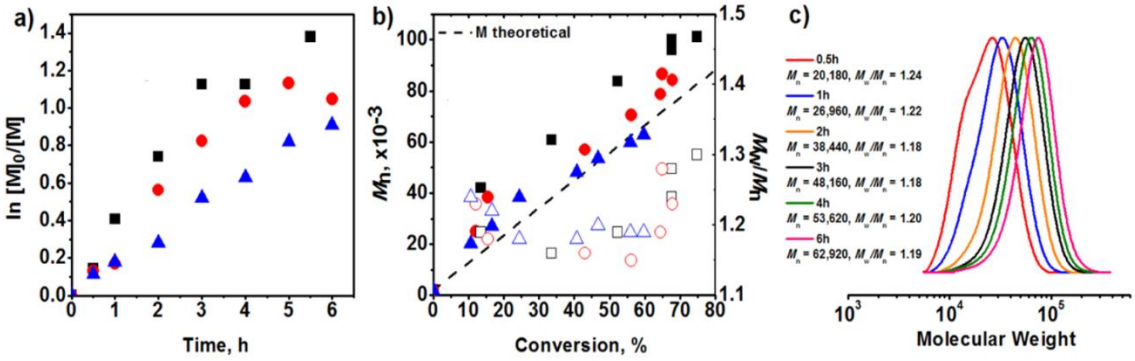

Figure IV.7. First-order kinetic plots (a), evolution of MW and MWD with conversion (b), GPC traces with conversion for entry 8 (c). Entry 6(■), 7 (●), and 8 (▲), Table IV.1. $[OEOMA_{475}]_0$ = 0.45 M; $[OEOMA_{475}]/[I]/[Asc.\ A]/[Mesohemin\text{-}(MPEG_{550})_2]$ = 227/1/1n/1, n = 1, 5, 10, water, 30 °C, 100 mM KBr.

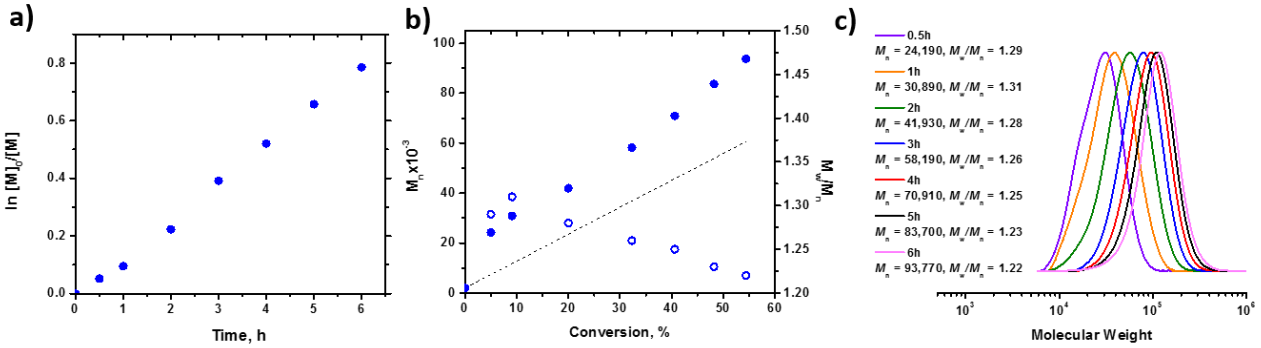

Figure IV.8. First-order kinetic plot (a), evolution of molecular weight and molecular weight distribution with conversion (b), GPC traces with conversion (c). $[OEOMA_{475}]_0$ = 0.45 M; $[OEOMA_{475}]/[I]/[Sn(EH)_2]/[Mesohemin\text{-}(MPEG_{550})_2]$ = 227/1/1/1, anisole, 60°C.

To show the versatility of the mesohemin based catalyst for ATRP, a polymerization was performed in organic media, Table 1, entry 10. An AGET ATRP of $OEOMA_{475}$ in anisole was activated by addition of tim 2-ethylhexanoate ($Sn(EH)_2$) as a reducing agent and displayed close to linear first order kinetic plots and linear MW

evolution with conversion (**Figure IV.8**). Slow initiation was indicated by slight curvature during initial stage of polymerization in the semilogarithmic kinetic plot and experimental MW higher than theoretically predicted. Nevertheless, dispersities remained low throughout the course of polymerization.

IV.3.2. Axially Ligated Mesohemins as Catalysts for Water ATRP

To expand the scope of heme-based catalysts, a series of axially ligated mesohemin complexes were synthesized (**Scheme IV.6**). In this series, only one carboxyl group was modified with a PEG tail and the second carboxyl group was modified with either imidazole or thioether via an amidation reaction. Using hemin as starting material was a convenient way to synthesize modified iron porphyrins because hemin is less photosensitive than protoporphyrin IX (hemin without iron) and this strategy didn't require additional step of metal insertion.[55] However, protoporphyrin IX could be used as well for synthesis of modified heme complexes, and typically provided easier purification and analysis.

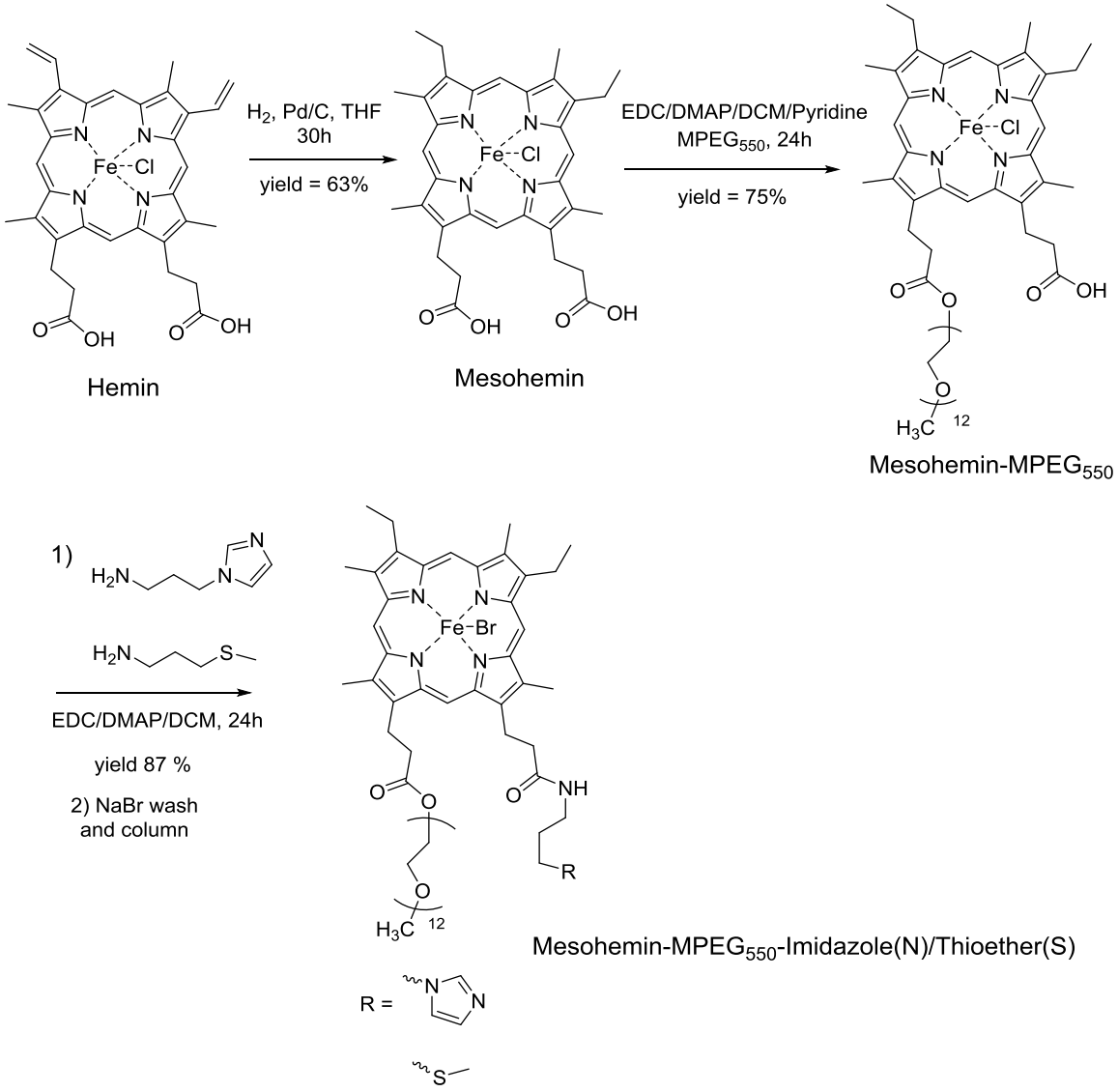

Scheme IV.6. Preparation of the axially ligated mesohemins.

The modified mesohemin complexes were characterized by mass spectroscopy, UV-Vis (Experimental section) and CV (**Figure IV.9**, **Table IV.2**). According to CV measurements, the iron porphyrins formed cleanly with varied redox potential $E_{1/2}$ (**Figure IV.6, Figure IV.**9**, Table IV.2**). The two new complexes were characterized by less negative $E_{1/2}$values, when compared to fully PEGylated mesohemin, but formed only a single catalytic species, even in the absence of excess bromide. Imidazole modified

mesohemin was not significantly affected by addition of excess bromide ions, but the thioether-modified mesohemin showed a shift towards a more negative potential by CV.

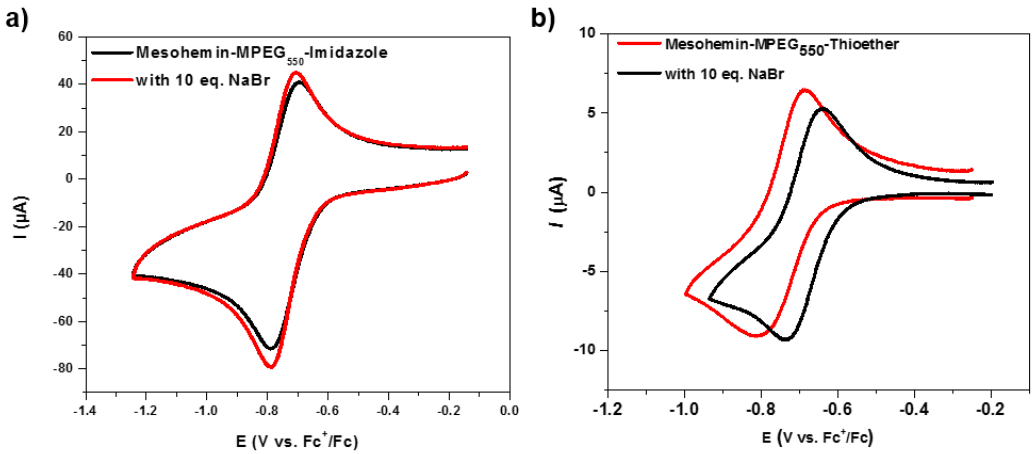

Figure IV.9. Cyclic voltammogram of (a) Mesohemin-MPEG$_{550}$-N and (b) Mesohemin-MPEG$_{550}$-S, scan rate=100 mV/s, supporting electrolyte=TBAPF$_6$ (0.1 M in DMF).

Table IV.2. Redox potentials for catalysts in DMF

Catalyst	**$E_{1/2}$ (V vs. Fc^+/Fc) with 10 mM NaBr**
Hemin	-0.750
Mesohemin-$(MPEG)_2$	-0.777
Mesohemin-MPEG-Imidazole	-0.735
Mesohemin-MPEG-Thioether	-0.725

Scan rate = 100 mV/s, supporting electrolyte = TBAPF$_6$ (0.1 M in DMF), 1 mM of iron porphyrin complex.

Table IV.3. Experimental conditions and results of ATRP catalyzed by axially ligated mesohemins[a]

	M/I/RA/Cat	Catalyst	Conv./%, (time, h)	$M_{n,th}\times10^{-3}$ [f]	$M_{n,GPC}\times10^{-3}$ [g]	M_w/M_n
1	227/1/1/1 [b]	Mesohemin-$MPEG_{550}$-N	76 (2.5)	84	76	1.27
2	200/1/1/1 [b]	Mesohemin-$MPEG_{550}$-S	25 (3.5)	27	40	1.28
3	216:1:0.3x2:1[b]	Mesohemin-$MPEG_{550}$-N	75 (5)	83	108	1.15
4	227/1/1/1[b]	Mesohemin-$(MPEG_{550})_2$/Imidazole	33 (2)	37	78	1.91
5	227:1:10:0.1[b]	Hemin-$(PEG_{1000})_2$	- (7.5)	-	96	1.57
6	216:1:0.6:0.1[b]	Mesohemin-$MPEG_{550}$-N	60 (5)	69	190	1.42
7	200/1/0.5/0.1[b]	Mesohemin-$MPEG_{550}$-S	61 (8.7)	61	57	1.18
8	581:1:1:1[c]	Mesohemin-$MPEG_{550}$-N	- (4)	-	9	1.37
9	200/1/1/0.1[d]	Mesohemin-$MPEG_{550}$-S	- (20)	-	10	2.1
10	200/1/1/0.1[d,e]	Mesohemin-$MPEG_{550}$-S	24 (20)	4	77	1.36

[a] 30 °C; H_2O/DMF = 9/1; entries 1 – 8: 100mM NaBr, RA – ascorbic acid; entries 9 – 10: 100 mM NaCl, sodium dithionite; I - PEG_{2000}BPA; [b] [I] = 2 mM, M – $OEOMA_{500}$; [c] [I] = 4 mM, M - MAA; [d] [I] = 10 mM, M - MAA; [e] HCl was added in the solution until pH = 0.9; [f] $M_{n\,th} = ([M]_0/[I]_0)\times\text{conversion}\times M_{monomer}$; [g] universal calibration.

The initial polymerization of $OEOMA_{500}$ was performed in the presence of mesohemin-$MPEG_{550}$-N/S under conditions identical to those previously used (**Table IV.3**, entry 1-2). Polymerization with mesohemin-$MPEG_{550}$-N was over two times faster than that with mesohemin-$(MPEG_{550})_2$, monomer conversion reaching 76% in only 2h. The final polymer showed relatively low M_w/M_n ~ 1.27, but higher than that obtained with mesohemin-$(MPEG_{550})_2$. Polymerization in the presence of thioether-ligated mesohemin (mesohemin-

$MPEG_{550}$-S) did not proceed to high conversion (**Table IV.3**, entry 2), and the final polymer also displayed a M_w/M_n < 1.3. These reactions suggested that the modifications of mesohemin with axial ligands, did provide complexes that could catalyze ATRP, but additional optimization of reaction conditions needed to be addressed. In one such optimization, the addition of less reducing agent in a polymerization catalyzed by mesohemin-$MPEG_{550}$-N resulted in a linear first-order kinetics and linear increase of MW with conversion, with values of MW close to theoretical values (**Table IV.3**, entry 3, **Figure IV.10**). This polymerization resulted in formation of polymers with polydispersity values lower than previously obtained for mesohemin-$(MPEG_{550})_2$ indicating better controlled polymerization (**Table IV.1**, entry 8). Additionally, the reaction was faster despite of decreased amounts of reducing agent.

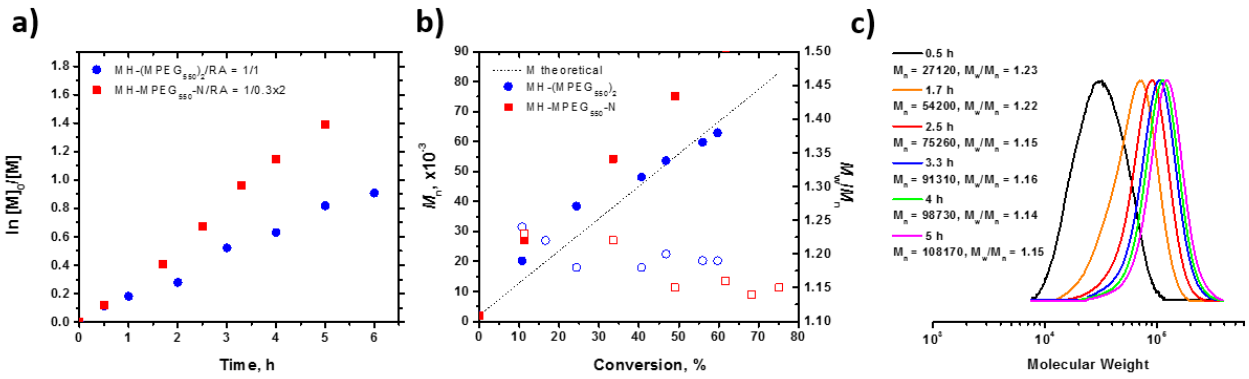

Figure IV.10. First-order kinetic plots (a), evolution of MW and MWD with conversion (b), GPC traces with conversion for entry 3, **Table IV.3** (c). Entry 9(●), **Table IV.1**, 3 (■), **Table IV.3**. $[OEOMA_{475/500}]_0$ = 0.45 M; $[OEOMA_{475/500}]/[I]/[Asc.\ A]/[Mesohemin\text{-}(MPEG_{550})_x\text{-}N_y]$ = 227/1/1 or 0.3x2/1, where x = 2, y = 0 or x = 1 and y = 1;water, 30 °C, 100 mM KBr or NaBr.

To verify that covalent attachment of the imidazole moiety was necessary for the formation of a 1/1 iron porphyrin/imidazole complex, an ATRP with fully PEGylated mesohemin was performed in the presence of free imidazole in a ratio of 1:1 to the iron porphyrin (**Table IV.3**, entry 4). This reaction resulted in slow and poorly controlled

polymerization. The final MW of the polymer formed under these conditions was double the theoretically predicted value, indicating inefficient initiation, and M_w/M_n was as high as 1.91. This poor polymerization could be explained by the fact that imidazole preferentially complexes to the formed pentacoordinated iron porphyrin complex creating a situation in which half of the catalyst is the hexacoordinated mesohemin with two imidazole ligands and half of the catalyst has no imidazole ligands.[41,56] Deactivation of a propagating radical cannot occur without a Fe-Br species, and consequently the loss of deactivation efficiency results in a poorly controlled polymerization. Thus, covalent attachment of an imidazole moiety forces formation of a clean 1/1 complex of iron porphyrin and imidazole with a remaining Fe-Br bond, necessary for performing well-controlled ATRP.

In the next set of experiments (**Table IV.3**, entries 5 – 7), polymerizations were performed with 10-fold lower concentration of catalyst. Because iron porphyrins are highly colored compounds, reaction with a lower concentration of the catalyst would be beneficial for purification. PEGylated hemin did not provide well-defined polymers when concentration was reduced by a factor of 10 (**Table IV.3**, entries 5). This could be explained by copolymerization of the catalyst and the subsequent inability of the incorporated complex to participate in efficient catalysis. However, both axially ligated mesohemins efficiently catalyzed ATRP when their concentrations were decreased 10-fold (**Figure IV.11**). The reaction catalyzed by imidazole-modified mesohemin resulted in formation of a polymer with higher MW than theoretically predicted, and relatively high M_w/M_n, reaching highest a value of ~ 1.5 (**Table IV.3**, entry 6). Nevertheless, the uniform shift in GPC traces toward higher MW indicated that a certain level of control over

polymerization was attained (**Figure IV.11c**). Polymerization in the presence of thioether ligated mesohemin reached higher monomer conversions, > 60% (**Table IV.3**, entry 7), which was significantly higher than when used at higher concentration (**Table IV.3**, entry 2). MWs were in good agreement with theoretically predicted values, and the final polymer M_w/M_n was < 1.2 (**Figure IV.11**). These results demonstrated that it is possible to use modified hemin complexes as ATRP catalysts at lower concentrations, but further optimization of the amount of reducing agent is required.

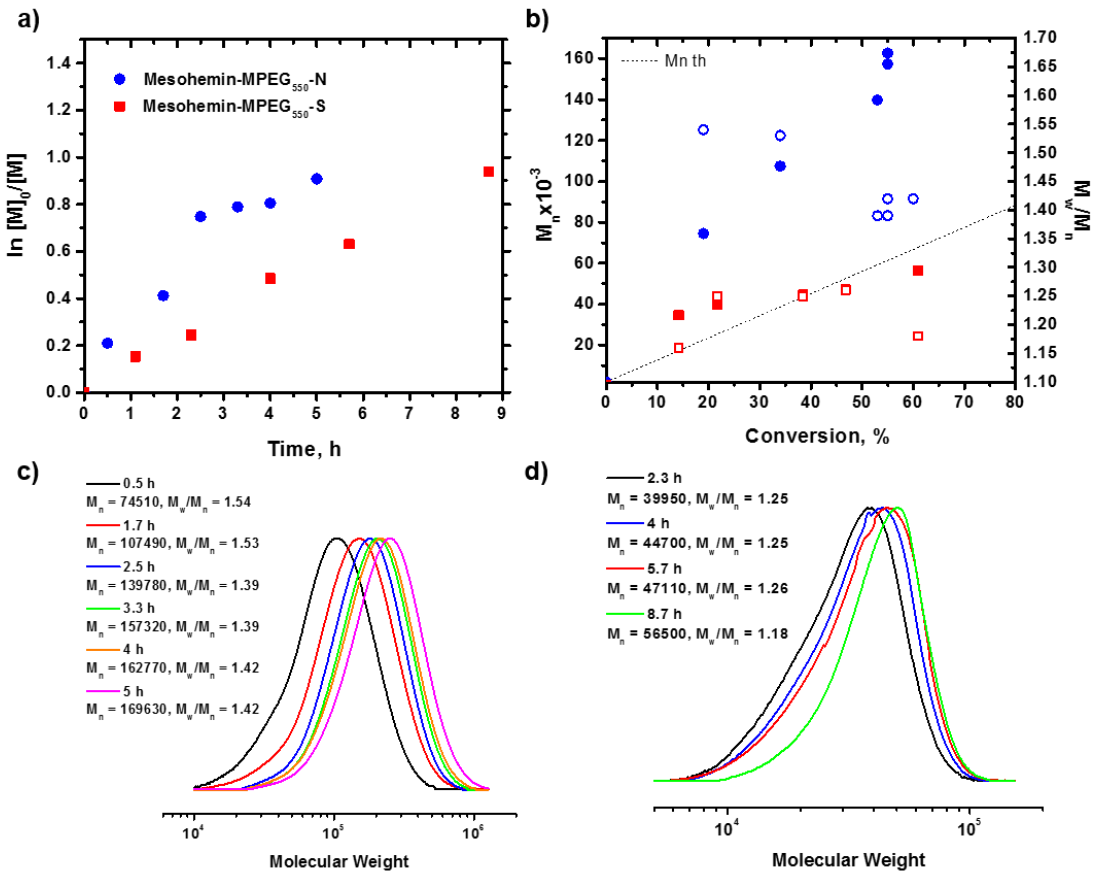

Figure IV.11. First-order kinetic plots (a), evolution of MW and MWD with conversion (b), GPC traces with conversion for entry 6 and 7, **Table IV.3** (c, d). Entry 6(●), 7 (■). $[OEOMA_{500}]_0$ = 0.45 M; $[OEOMA_{500}]/[I]/[Asc.\ A]/[Mesohemin\text{-}MPEG_{550}\text{-}N/S]$ = 216 or 200/1/0.5 or 0.6/0.1, water, 30 °C, 100 mM NaBr.

Finally, axially ligated mesohemins were evaluated as catalysts for polymerization of methacrylic acid (MAA) (**Table IV.3**, entries 8 – 10). MAA is difficult to polymerize by ATRP due to potential protonation and displacement of ligands.[57] However, iron porphyrin complexes have high stability, even at acidic pH values, and should not be affected in the presence of MAA. However, iron porphyrins are still capable of forming a complex with carboxylates through ligation at their axial positions.[58] Indeed, a recent publication on a polymerization with heme-containing peroxidase mimic demonstrated that polymerization could be performed at the same rate over a range of pH (3 – 11), but monomer conversion remained low at pH = 2.[40] Both versions of the axially ligated mesohemins prepared in this work were able to catalyze ATRP of MAA (**Table IV.3**, entries 8 – 9; **Figure IV.12**). Polymerization with mesohemin-MPEG$_{550}$-S was tested under two different conditions: with and without addition of extra HCl to reduce the pH of the solution to 0.9 and fully protonate MAA. Interestingly, the polymerization carried out at lower pH resulted in formation of a polymer with lower dispersity, $M_w/M_n < 1.4$, while polymerization without addition of HCl produced polymer with $M_w/M_n > 2$.

These experiments demonstrate that functionalized mesohemins can be used to catalyze the ATRP of MAA; however, a more detailed study should be conducted to investigate the influence of MAA concentration on polymerization and the effect of acid addition on polymerizaiton with all types of mesohemin complexes presented here.

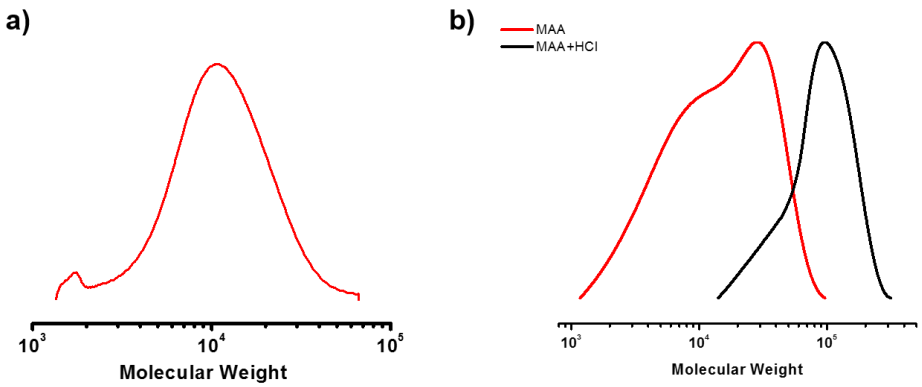

Figure IV.12. GPC traces of pMAA prepared by ATRP catalyzed by mesohemin-MPEG-N (a) (**Table IV.3**, entry 8), [MAA]/[I]/[RA]/[Mesohemin] = 518/1/1/1, [I] = 4 mM, RA – ascorbic acid, water, 30 °C, 100 mM NaBr; and by mesohemin-MPEG-S (b) (**Table IV.3**, entry 9 (red curve), and 10 (black curve)). [MAA]/[I]/[RA]/[Mesohemin] = 200/1/1/0.1, [I] = 10 mM, RA – sodium dithionite, water, 30 °C, 100 mM NaBr.

IV.4. Conclusions

In conclusion, a series of bioinspired iron porphyrin-based complexes were designed and successfully utilized as new ATRP catalysts. Mesohemin-$(MPEG_{550})_2$, prepared from naturally occurring hemin, performs significantly better that hemin itself or previously-reported hematin. This can be attributed to the increased solubility of the catalysts in the reaction medium due to the presence of PEG tails, as well as hydrogenated vinyl bonds, preventing copolymerization and allowing for faster deactivation in the presence of excess bromide salt. Mesohemin-$(MPEG_{550})_2$can be used for the ATRP of methacrylates in both organic and aqueous media. This new, environmentally benign class of ATRP catalysts showed promise, so further modification of mesohemin based catalysts with different axial ligands were synthesized and studied. Mesohemin-$MPEG_{550}$, additionally modified with imidazole and thioether units, efficiently catalyzed polymerizations in water at low catalyst concentration, and showed promising results in polymerization of MAA.

IV.5. Experimental section

IV.5.1. Materials.

All chemicals were purchased from commercial sources, *e.g.*, Aldrich, TCI, and used as received if not stated otherwise. Oligo(ethylene oxide) methyl ether methacrylate ($OEOMA_{475}$, 99%, average molecular weight 475, Aldrich) and oligo(ethylene oxide) methyl ether acrylate ($OEOA_{480}$, 99%, average molecular weight 480, Aldrich) were passed over a column of basic alumina (Fisher Scientific) prior to use to remove inhibitor. Poly(ethylene glycol) bromophenyl acetate ($PEG_{2000}BPA$), poly(ethylene oxide) isobutyryl bromide ($PEO_{2000}iBBr$)[59] and mesohemin[60] were prepared as previously reported in literature.

IV.5.2. Instrumentation and characterization.

Gel permeation chromatography (GPC): GPC was used to determine number average molecular weight (M_n) and M_w/M_n values. The GPC was conducted with a Waters 515 HPLC Pump and Waters 2414 Refractive Index Detector using PSS columns (SDV 10^2, 10^3, 10^5 Å) in tetrahydrofuran (THF) as an eluent at a flow rate of 1 mL/min at 35 °C. The apparent molecular weights (M_n) and polydispersities (M_w/M_n) were determined using linear poly(methyl methacrylate) (M_n = 800 ~ 1,820,000) standards using WinGPC 7.0 software from PSS. The previously reported Mark-Houwink parameters[24] were used for universal calibration using WinGPC 7.0 software from PSS. Conversion was determined using GPC by following the decrease of monomer peak area relative the increase of polymer peak area as previously reported. **Mass spectroscopy:** Mass spectra were recorded on a mass spectrometer with a *Varian* Saturn 2100T *MS* with *3900* GC using an EI source. In each case, characteristic fragments with their relative intensities in percentages are shown. Electrospray mass spectra were measured on a Thermo-Fisher LCQ

ESI/APCI Ion Trap containing a quadrupole field ion trap mass spectrometer with electrospray ionization (ESI). **Electrochemical Analysis**: All of the cyclic voltammograms (CV) were recorded at 25 °C with a Gamry Reference 600 potentiostat using a standard three-electrode system consisting of a glassy carbon (GC) working electrode, platinum mesh counter electrode, and $Ag/AgI/I^-$ reference electrode. A solution of 0.1 M $TBAPF_6$ supporting electrolyte in 20 mL of DMF was prepared using previously dried reagents. To prepare 1 mM solutions this mixture were added either to 13 mg hemin or 34 mg of mesohemin-$(MPEG_{550})_2$. CV measurements were carried out under a nitrogen atmosphere at a scan rate of 100 mV/s. Potentials were recorded versus a $Ag/AgI/I^-$ reference electrode and the recorded voltammograms were externally referenced to ferrocene/ferrocenium ($Fc^{0/+}$).

IV.5.3. Hemin-$(PEG_{1000})_2$ synthesis.

Hemin (200 mg, 0.307 mmol), poly(ethylene glycol) (PEG_{1000}, $MW_{avg.}$=1000) (1227 mg, 1.227 mmol) and N-(3-dimethylaminopropyl)-N (ethylcarbodiimide hydrochloride (EDC·HCl) (259 mg, 1.350 mmol) were mixed in 8 mL of dry dichloromethane (DCM) in a flask. The mixture was cooled by immersion in ice and DMAP (8 mg, 0.067 mmol) was added. The reaction mixture was brought to room temperature and stirred for 24h. After completion of reaction the solution was washed with 0.1 M HCl (2x10 ml), and with saturated $NaHCO_3$ (2x10 ml). After that mixture was dried over $MgSO_4$ and solvent was removed under reduced pressure. The product was tested without further purification.

IV.5.4. Mesohemin synthesis.

Mesohemin was synthesized according to the previously reported method for hydrogenation of Hemin (1.1 mmol, 700 mg), Pd/C (15 wt. % to hemin, 105 mg) were mixed in 25 ml Schlenk flask, which was sealed, equipped with balloon and purged with

nitrogen. Dry THF (15 ml), obtained from solvent purification system, was added to the dry components through syringe. Balloon was filled with hydrogen, and refilled every 12 h. Reaction was kept for 30 h, then reaction mixture was diluted with 100 ml of methanol, and filtered through layer of celite. Solvent was evaporated under reduced pressure yielding 441 mg (yield = 63%) of mesohemin, which was used for further reaction. Obtained compound was analyzed by ESI-MS. m/z $[M\text{-}Fe+H]^+$ = 567.5, $[M]^+$ = 620.4, $[M+MeOH]^+$ = 651.3, $[2M-H]^+$ = 1239.4 (**Figure IV.14**).

IV.5.5. Mesohemin-$(MPEG_{550})_2$ synthesis.

Mesohemin (400 mg, 0.610 mmol), poly(ethylene glycol) methyl ether ($MPEG_{550}$, MW_{avg}.=550) (1341 mg, 2.440 mmol) and N-(3-dimethylaminopropyl)-N (ethylcarbodiimide hydrochloride (EDC·HCl) (515 mg, 2.680 mmol) were mixed in 8 mL of dry dichloromethane (DCM) in a small flask. Mixture was cooled by immersion in ice and DMAP (16 mg, 0.130 mmol) was added. The reaction mixture was brought to room temperature and stirred for 24h. After completion of reaction the solution was washed with 0.1 M HCl (2x10 ml), and with saturated $NaHCO_3$ (2x10 ml). After that mixture was dried with $MgSO_4$ and solvent was removed under reduced pressure. The residue was purified by column chromatography on alumina with chloroform/methanol (9/1) mixture. Fractions were collected, solvent was removed, the residue was dissolved in 1M HCl in DCM, washed with saturated $NaHCO_3$, and washed with slightly acidic 1M NaBr, and passed through short NaBr column. The solution of the product was dried over $MgSO_4$ and solvent was removed under reduced pressure yielding 418 mg of mesohemin-$(MPEG_{550})_2$ (45 % yield). The final compound was analyzed by ESI-MS and UV-Vis. λmax: 402, 494, 530 and 617 nm. m/z $[M]^+$: 1266.1-1927 with interval of 44, $[M]^{2+}$: 584.8-1086 with interval 22 (**Figure IV.13, Figure IV.**15).

IV.5.6. Mesohemin-MPEG$_{550}$ synthesis.

Mesohemin (550 mg, 0.838 mmol) was dissolved in 5 ml of pyridine. Poly(ethylene glycol) methyl ether (MPEG$_{550}$, MW$_{avg.}$=550) (461 mg, 0.838 mmol) and N-(3-dimethylaminopropyl)-N (ethylcarbodiimide hydrochloride (EDC·HCl) (177 mg, 0.922 mmol) and DMAP (6 mg, 0.046 mmol) were mixed in 40 mL of DCM in a small flask. Solution with mesohemin was immersed in ice bath, and second mixture was added slowly. The reaction mixture was brought to room temperature and stirred for 24h. After completion of reaction the solution was washed with 0.1 M HCl (2x50 ml), and with saturated $NaHCO_3$ (2x50 ml). After that mixture was dried with $MgSO_4$ and solvent was removed under reduced pressure. The residue was purified by column chromatography on alumina with chloroform/methanol (9/1) mixture. Fractions were collected, solvent was removed, the residue was dissolved in 1M HCl in DCM, and washed with saturated $NaHCO_3$. The solution of the product was dried over $MgSO_4$ and solvent was removed under reduced pressure yielding 750 mg of mesohemin-(MPEG$_{550}$)$_2$ (75 % yield). The final compound was analyzed by ESI-MS. m/z $[M]^+$: 853.6 – 1470.7 with interval of 44 (**Figure IV.16**).

IV.5.7. Mesohemin-MPEG$_{550}$-N-[3-(1-imidazoyl)propyl]amide synthesis.

This mesohemin derivative was synthesized in similar manner to the previously published method.[61] Mesohemin-MPEG$_{550}$ (550 mg, 0.630 mmol), 1-(3-aminopropyl)imidazole (158 mg, 1.260 mmol), and N-(3-dimethylaminopropyl)-N(ethylcarbodiimide hydrochloride (EDC·HCl) (266 mg, 1.390 mmol) and DMAP (8 mg, 0.070 mmol) were mixed in 10 mL of DCM in a small flask while on ice bath. The reaction mixture was brought to room temperature and stirred for 24h. After completion of reaction the solution was washed with 0.1 M HCl (3x10 ml), with saturated $NaHCO_3$ (2x10 ml), and washed with slightly acidic

1M NaBr, and passed through short NaBr column. After that mixture was dried with $MgSO_4$ and solvent was removed under reduced pressure yielding 707 mg of mesohemin-$(MPEG_{550})_2$ (87 % yield). The final compound was analyzed by ESI-MS and UV-Vis. λmax: 401, 496, 518, 567 and 621 nm. m/z $[M+Na]^+$: 981.6 – 1605.4 with interval of 44 (**Figure IV.13, Figure IV.**17).

IV.5.8. Mesohemin-MPEG$_{550}$-N-[3-(1-methylthio)propyl]amide synthesis.

This derivative was synthesized in a similar manner as imidazole modified version, but reaction mesohemin-$MPEG_{550}$ with 3-(methylthio)propylamine. The final compound was analyzed by ESI-MS and UV-Vis. λmax: 402, 494, and 620 nm. m/z $[M-CH_3+CH_3OH]^+$: 956.6 – 1485.9 with interval of 44 (**Figure IV.13Figure IV.18**).

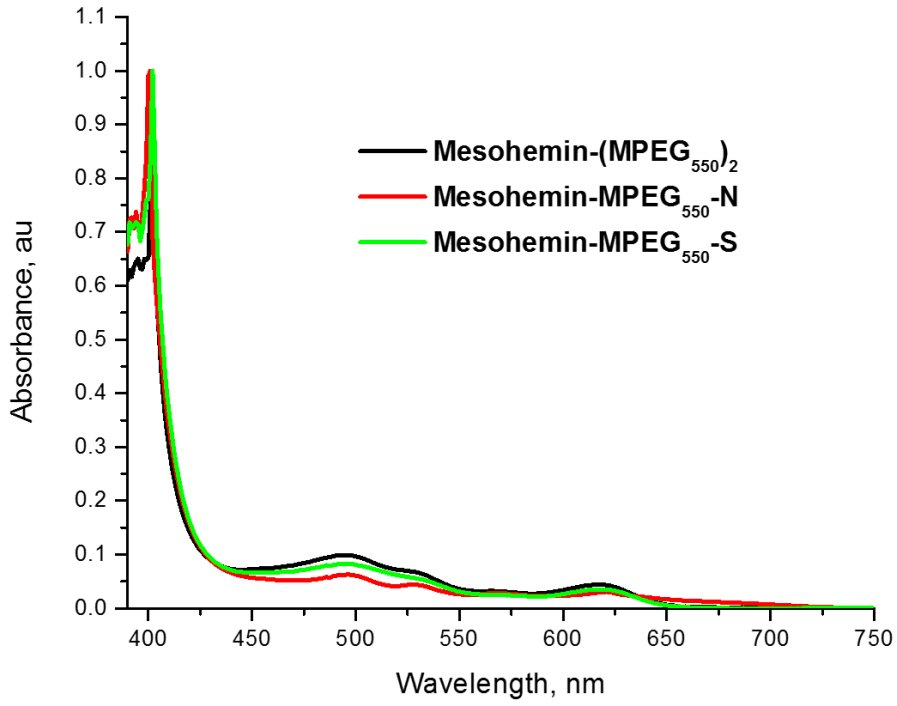

Figure IV.13. UV-Vis spectra of mesohemin derivatives in methanol (100 µM).

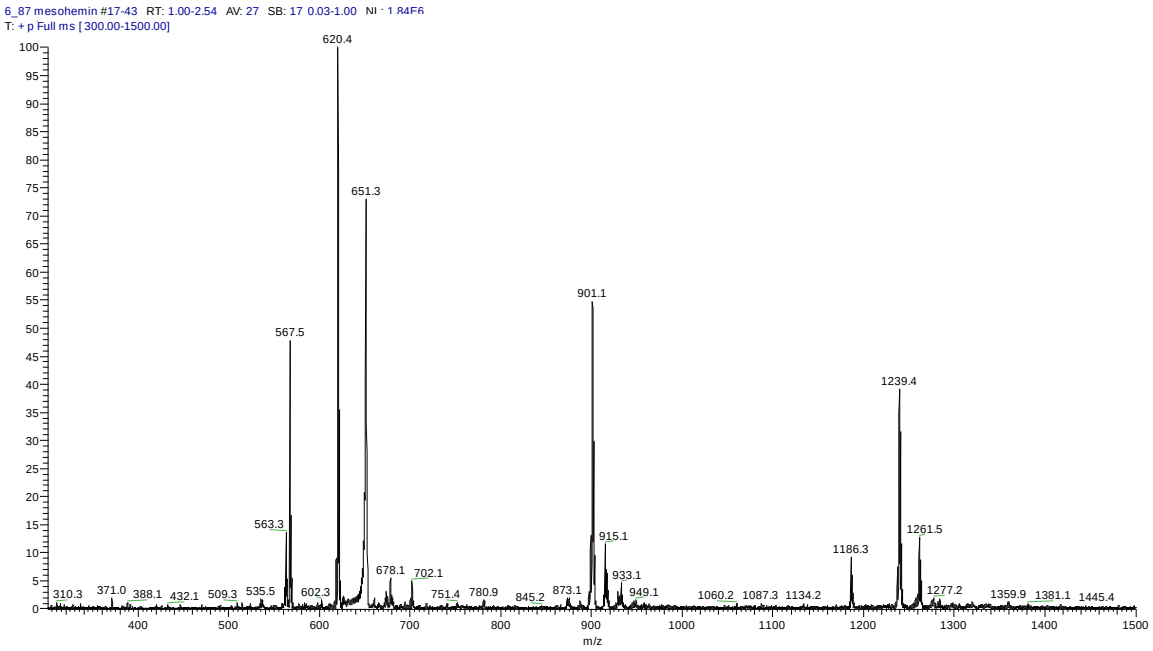

Figure IV.14. ESI of mesohemin: 250µM in water:methanol = 1:3

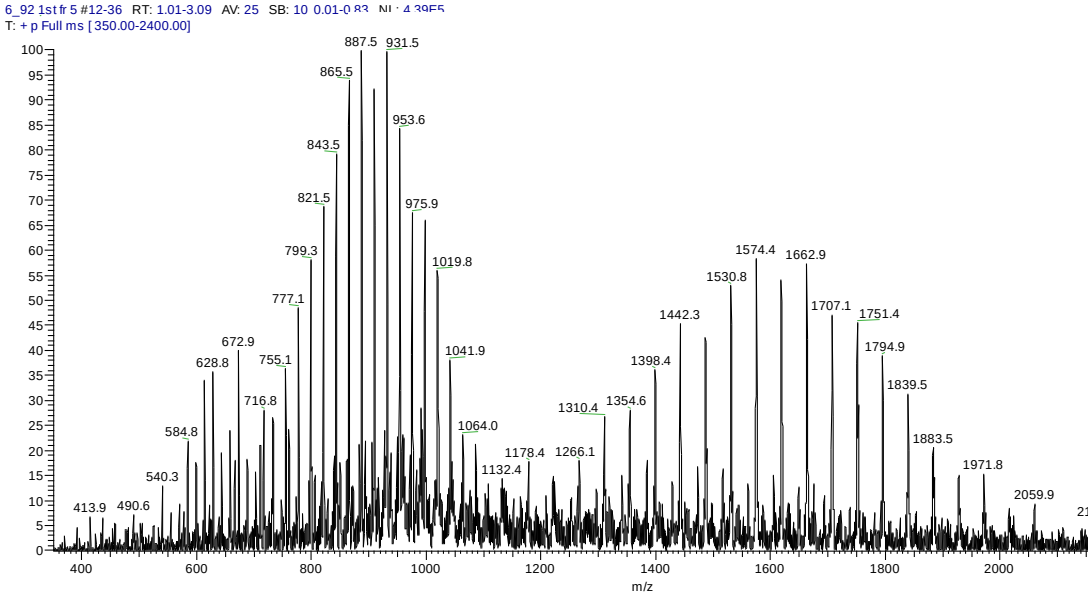

Figure IV.15. ESI of mesohemin-$(MPEG_{550})_2$: 250µM in water:methanol = 1:3

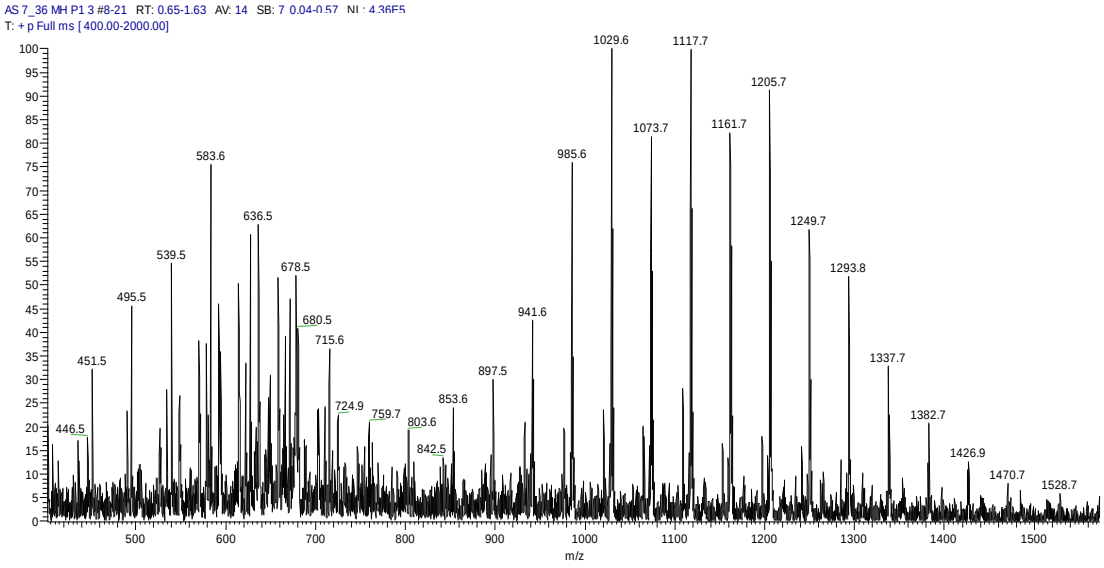

Figure IV.16. ESI of mesohemin-MPEG$_{550}$: 250µM in water:methanol = 1:3

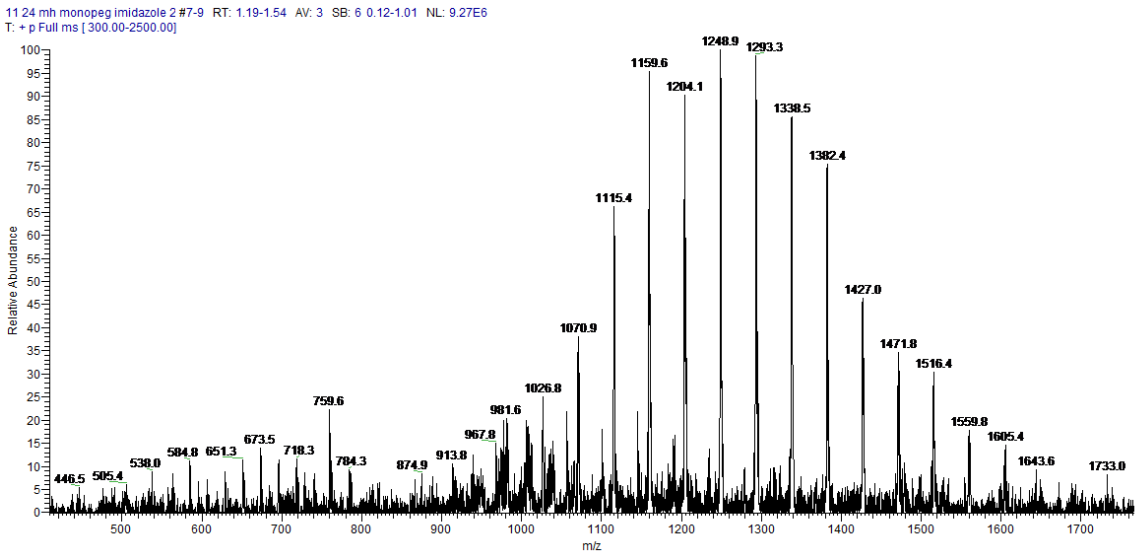

Figure IV.17. ESI of mesohemin-MPEG$_{550}$-N: 250µM in water:methanol = 1:3

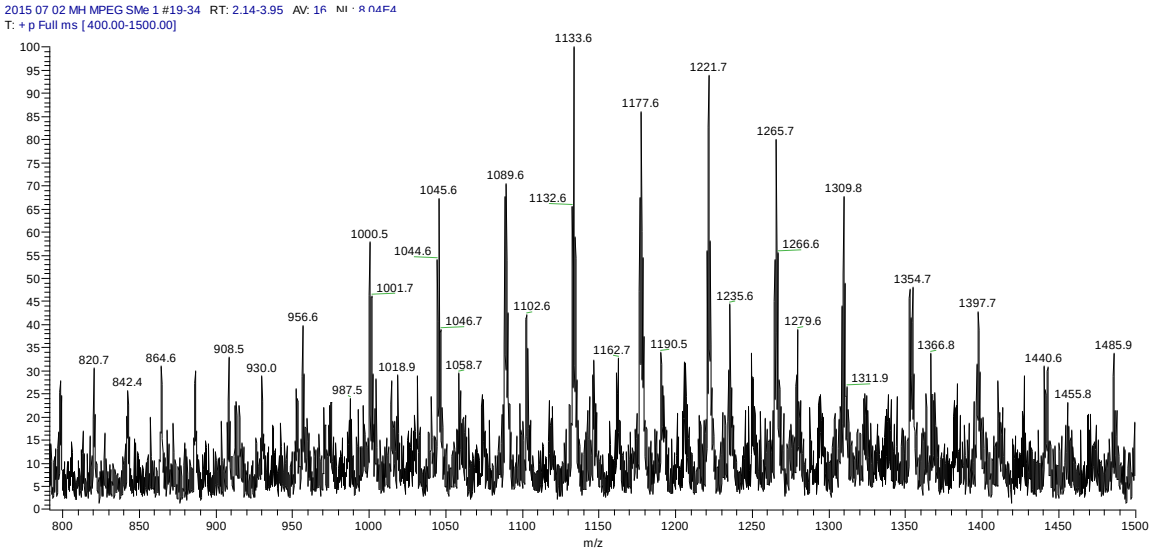

Figure IV.18. ESI of mesohemin-MPEG$_{550}$-S: 250µM in water:methanol = 1:3

IV.5.9. General procedure for synthesis of poly(OEOMA$_{475/500}$) by A(R)GET ATRP.

A series of aqueous AGET ATRP reactions were carried out and the following procedure describes the conditions selected for a typical polymerization of OEOMA$_{475}$ catalyzed by mesohemin-(MPEG$_{550}$)$_2$. KBr (60 mg, 0.5 mmol), OEOMA$_{475}$ (1.08 g, 2.27 mmol), mesohemin-(MPEG$_{550}$)$_2$ (17.9 mg, 0.01 mmol) were dissolved in H_2O (3.6 ml) then the mixture was added to a 10 ml Schlenk flask and purged with nitrogen for 1h, then placed in an oil bath at 30 °C. An ascorbic acid solution (100 mM) was purged with nitrogen, and then added to the reaction mixture (0.1 ml). 33 mM stock solution of PEG$_{2000}$BPA in DMF was purged with nitrogen, and then added into reaction mixture (0.3 ml). Samples were taken throughout the reaction for GPC analysis.

IV.6. References

(1) Matyjaszewski, K.; Xia, J. *Chem. Rev.* **2001**, *101*, 2921.

(2) Matyjaszewski, K.; Tsarevsky, N. V. *Nat. Chem.* **2009**, *1*, 276.

(3) Matyjaszewski, K. *Macromolecules* **2012**, *45*, 4015.

(4) Kamigaito, M.; Ando, T.; Sawamoto, M. *Chem. Rev.* **2001**, *101*, 3689.

(5) Braunecker, W. A.; Matyjaszewski, K. *Prog. Polym.Sci.* **2007**, *32*, 93.

(6) di Lena, F.; Matyjaszewski, K. *Prog. Polym. Sci.* **2010**, *35*, 959.

(7) O'Reilly, R. K.; Gibson, V. C.; White, A. J. P.; Williams, D. J. *J. Am. Chem. Soc.* **2003**, *125*, 8450.

(8) Tsarevsky, N. V.; Matyjaszewski, K. *Chem. Rev.* **2007**, *107*, 2270.

(9) Wang, Y.; Zhang, Y.; Parker, B.; Matyjaszewski, K. *Macromolecules* **2011**, *44*, 4022.

(10) He, W.; Zhang, L.; Miao, J.; Cheng, Z.; Zhu, X. *Macromol. Rapid Commun.* **2012**, *33*, 1067.

(11) Mukumoto, K.; Wang, Y.; Matyjaszewski, K. *ACS Macro Lett.* **2012**, *1*, 599.

(12) Schroeder, H.; Yalalov, D.; Buback, M.; Matyjaszewski, K. *Macromol. Chem. Phys.* **2012**, *213*, 2019.

(13) Nishizawa, K.; Ouchi, M.; Sawamoto, M. *Macromolecules* **2013**, *46*, 3342.

(14) Eckenhoff, W. T.; Biernesser, A. B.; Pintauer, T. *Inorg. Chim. Acta* **2012**, *382*, 84.

(15) Aoshima, H.; Satoh, K.; Umemura, T.; Kamigaito, M. *Polym. Chem.* **2013**, *4*, 3554.

(16) Wang, X. S.; Armes, S. P. *Macromolecules* **2000**, *33*, 6640.

(17) Heredia, K. L.; Bontempo, D.; Ly, T.; Byers, J. T.; Halstenberg, S.; Maynard, H. D. *J. Am. Chem. Soc.* **2005**, *127*, 16955.

(18) Gauthier, M. A.; Klok, H.-A. *Chem. Comm.* **2008**, *0*, 2591.

(19) Lutz, J.-F.; Börner, H. G. *Prog. Polym. Sci.* **2008**, *33*, 1.

(20) Peeler, J. C.; Woodman, B. F.; Averick, S.; Miyake-Stoner, S. J.; Stokes, A. L.; Hess, K. R.; Matyjaszewski, K.; Mehl, R. A. *J. Am. Chem. Soc.* **2010**, *132*, 13575.

(21) Finn, M. G.; Pokorski, J. K.; Breitenkamp, K.; Liepold, L. O.; Qazi, S. *J. Am. Chem. Soc.* **2011**, *133*, 9242.

(22) Mougin, N. C.; van Rijn, P.; Park, H.; Müller, A. H. E.; Böker, A. *Adv. Func. Mat.* **2011**, *21*, 2470.

(23) Konkolewicz, D.; Magenau, A. J. D.; Averick, S. E.; Simakova, A.; He, H.; Matyjaszewski, K. *Macromolecules* **2012**, *45*, 4461.

(24) Simakova, A.; Averick, S. E.; Konkolewicz, D.; Matyjaszewski, K. *Macromolecules* **2012**, *45*, 6371.

(25) Nguyen, N. H.; Kulis, J.; Sun, H.-J.; Jia, Z.; van Beusekom, B.; Levere, M. E.; Wilson, D. a.; Monteiro, M. J.; Percec, V. *Polym. Chem.* **2013**, *4*, 144.

(26) Tsarevsky, N. V.; Pintauer, T.; Matyjaszewski, K. *Macromolecules* **2004**, *37*, 9768.

(27) Bortolamei, N.; Isse, A. a.; Magenau, A. J. D.; Gennaro, A.; Matyjaszewski, K. *Angew. Chem. Int. Ed.* **2011**, *50*, 1.

(28) Zhang, Q.; Wilson, P.; Li, Z.; McHale, R.; Godfrey, J.; Anastasaki, A.; Waldron, C.; Haddleton, D. M. *J. Am. Chem. Soc.* **2013**, *135*, 7355.

(29) Sigg, S. J.; Seidi, F.; Renggli, K.; Silva, T. B.; Kali, G.; Bruns, N. *Macromol. Rapid Commun.* **2011**, *32*, 1710.

(30) Silva, T. B.; Spulber, M.; Kocik, M. K.; Seidi, F.; Charan, H.; Rother, M.; Sigg, S. J.; Renggli, K.; Kali, G.; Bruns, N. *Biomacromolecules* **2013**.

(31) Ng, Y.-H.; di Lena, F.; Chai, C. L. L. *Polym. Chem.* **2011**, *2*, 589.

(32) Ng, Y.-H.; di Lena, F.; Chai, C. L. L. *Chem. Comm.* **2011**, *47*, 6464.

(33) Polizzi, K. M.; Bommarius, A. S.; Broering, J. M.; Chaparro-Riggers, J. F. *Curr. Opin. Chem. Biol.* **2007**, *11*, 220.

(34) Guin, J.; De Sarkar, S.; Grimme, S.; Studer, A. *Angew. Chem. Int. Ed.* **2008**, *47*, 8727.

(35) Shu, J. Y.; Tan, C.; DeGrado, W. F.; Xu, T. *Biomacromolecules* **2008**, *9*, 2111.

(36) Akkara, J. A.; Wang, J.; Yang, D.-P.; Gonsalves, K. E. *Macromolecules* **2000**, *33*, 2377.

(37) Singh, A.; Roy, S.; Samuelson, L. *J. Macromol. Sci. Pure Appl. Chem.* **2001**, *A38*, 37.

(38) Islamova, R. M.; Nazarova, S. V.; Koifman, O. I. *Macroheterocycles* **2011**, *4*, 97.

(39) Yamashita, K.; Yamamoto, K.; Kadokawa, J. *Polymer* **2013**, *54*, 1775.

(40) Zhou, H.; Jiang, W.; An, N.; Zhang, Q.; Xiang, S.; Wang, L.; Tang, J. *RSC Advances* **2015**, *5*, 42728.

(41) Morgan, B.; Dolphin, D. In *Metal Complexes with Tetrapyrrole Ligand I*; Buchler, J., Ed.; Springer Berlin Heidelberg: 1987; Vol. 64, p 115.

(42) Wade, R. S.; Castro, C. E. *J. Am. Chem. Soc.* **1973**, *95*, 226.

(43) Nishide, H. *J. Polym. Sci., Part A: Polym. Chem.* **1981**, *19*, 1109.

(44) Ryabova, E. S.; Rydberg, P.; Kolberg, M.; Harbitz, E.; Barra, A.-L.; Ryde, U.; Andersson, K. K.; Nordlander, E. *J. Inorg. Biochem.* **2005**, *99*, 852.

(45) Poulos, T. L. *Chem. Rev.* **2014**, *114*, 3919.

(46) Weyermann, P.; Gisselbrecht, J.-P.; Boudon, C.; Diederich, F.; Gross, M. *Angew. Chem., Int. Ed.* **1999**, *38*, 3215.

(47) Traylor, T. G.; Lee, W. A.; Stynes, D. V. *J. Am. Chem. Soc.* **1984**, *106*, 755.

(48) Casella, L.; Monzani, E.; Fantucci, P.; Gullotti, M.; De Gioia, L.; Strini, A.; Chillemi, F. *Inorg. Chem.* **1996**, *35*, 439.

(49) Traylor, T. G.; Mincey, T. C.; Berzinis, A. P. *J. Am. Chem. Soc.* **1981**, *103*, 7084.

(50) Odian, G. In *Principles of Polymerization*; John Wiley & Sons, Inc.: 2004, p 198.

(51) Lutz, J.-F. *J. Polym. Sci., Part A: Polym. Chem.* **2008**, *46*, 3459.

(52) Zhang, L.; Cheng, Z.; Tang, F.; Li, Q.; Zhu, X. *Macromol. Chem. Phys.* **2008**, *209*, 1705.

(53) Mamardashvili, N. Z.; Golubchikov, O. A. *Russ. Chem. Rev.* **2001**, *70*, 577.

(54) Varray, S.; Aubagnac, J. L.; Lamaty, F.; Lazaro, R.; Martinez, J.; Enjalbal, C. *Analusis* **2000**, *28*, 263.

(55) Chang, C. K.; Dinello, R. K.; Dolphin, D.; Lever, A. B. P.; Ramaswamy, B. S. In *Inorg. Synth.*; John Wiley & Sons, Inc.: 1980, p 147.

(56) Wang, J.-T.; Yeh, H. J. C.; Johnson, D. F. *J. Am. Chem. Soc.* **1978**, *100*, 2400.
(57) Matyjaszewski, K.; Xia, J. *Chem. Rev.* **2001**, *101*, 2921.
(58) Fidalgo-Marijuan, A.; Barandika, G.; Bazán, B.; Urtiaga, M.-K.; Arriortua, M.-I. *Polyhedron* **2011**, *30*, 2711.
(59) Lee, S. B.; Russell, A. J.; Matyjaszewski, K. *Biomacromolecules* **2003**, *4*, 1386.
(60) Burns, D. H.; Lai, J.-j.; Smith, K. M. *J.Chem.Soc. Perkin Trans I* **1988**, 3119.
(61) Chang, C. K.; Traylor, T. G. *Proc. Natl. Acad. Sci. U.S.A.* **1973**, *70*, 2647.

Chapter V. Degradable Copolymers with Incorporated Ester Groups by ATRP

V.1. Preface

Radical ring-opening polymerization (RROP) was first reported in the 1980s, but has only recently received adequate attention in the RDRP community. A limited number of papers were published during the first decade of RDRP on RROP and related copolymerization. However, during the last decade several groups have explored the synthesis of functional copolymers through a combination of RDRP and RROP. Of particular interest is the preparation of degradable copolymers. Degradable materials can be synthesized by combining RROP of cyclic ketene acetals (CKAs), and other compounds with an exocyclic vinyl group, with polymerization of other radically copolymerizable vinyl monomers ((meth)acrylates and other vinyl monomers), yielding copolymers with degradable ester moieties distributed along the backbone.

There are literature examples of such materials synthesized by ATRP, however, preparation of well-defined polymers by ATRcoP of CKAs can be challenging. Previous reports showed that (co)polymers prepared by ATRP of CKA were characterized by formation of copolymers with broad MWDs and only partial ring-opening of the CKA. This motivated me to conduct a systematic study of conditions for ATRcoP of CKAs and prepare copolymers for degradation studies in addition to identifying the reasons for the limitations and providing information to resolve the problems.

ICAR ATRP was selected as suitable method for preparation of such copolymers because of the desire to use low concentrations of copper, while still taking into consideration CKAs intolerance towards acids which would limit applications of such

methods as A(R)GET ATRP. Polymerization results indicated that one can prepare degradable copolymers by ATRcoP of CKA and (meth)acrylates. However while the basic concept has been confirmed, a more detailed investigation of polymerization is required to establish how to optimize the radical ring-opening of the CKA and related monomers, and identify side reactions that are contributing towards generation of broader MWDs and lower chain-end functionality in the copolymers than expected for a well-controlled ATRP.

V.2. Introduction

Degradability is one of the most important requirements for materials targeting biomedical applications,[1-4] including degradable sutures, drug delivery systems, hydrogels, wound dressings and cell growing platforms.[1-3,5-8] Indeed, designed degradable polymers have become the material of choice for drug/biomolecule delivery due to their initially large hydrodynamic size, solubility, stealth properties, and stimuli responsiveness.[9-12] These degradable materials can be applied for delivery of hydrophobic drugs, which have very limited solubility in aqueous environment,[13-16] or biomolecules which would degrade or cause an immune response if added to a living entity on their own.[10,17-20] A larger hydrodynamic radius provides longer circulation time, and also helps targeting cancer cells due to enhanced permeability and retention effect.[17,18,20,21]

Robust drug delivery systems can accumulate in organs, such as liver and kidneys, during their circulation and without timely excretion can cause immune response and inflammation.[1,22,23] Thus for the drug delivery applications, where the delivery material is targeted to circulate inside a human body, polymer degradability is especially important. This is why degradable synthetic polymers such as polycaprolactone, poly(lactic acid) or natural polymers such as chitosan are often utilized in this field.[3,6,23,24]

Reversible deactivation radical polymerization (RDRP) methods allow incorporation of various functionalities during the synthesis of polymers with diverse compositions and architectures.[25] However, if only vinyl monomers are incorporated into the polymers, the resulting materials consist solely of carbon-carbon bonds that have very limited degradability under physiological conditions.[23] Consequently, generating polymers by RDRP methods with appropriate degradation profiles remains a subject of high interest.

There are several degradable linkages that are commonly utilized in synthetic delivery systems such as esters, acetals and disulfide bonds.[2,7,23,26,27] Acetals and esters can be hydrolytically degraded, while disulfide bonds are redox sensitive.[2,23,26] There are several approaches to incorporate degradable functionalities into copolymers synthesized by atom transfer radical polymerization (ATRP). Linear polymers can be grown from a degradable dual functional initiator, which would allow splitting polymer in half upon degradation.[28-30] For a star polymer synthesis one can either use multifunctional degradable initiators, or star cores prepared with a degradable crosslinker to dissociate the star copolymer into its arms.[31-33] Degradable crosslinkers or inimers can also be utilized in the synthesis of degradable hydrogels and nanogels.[7,34] However these approaches can result in preparation of materials, which degrade into chains with broad MWDs, and one has to consider the upper limits for the MW of the degraded components.

In order to incorporate several degradable groups along a polymer chains made from (meth)acrylates or (meth)acrylamides (comprised of only C-C bonds in a homopolymer) one can use cyclic monomers with double bonds and incorporated degradable units, which will undergo ring opening once reacted with a radical, and the degradable moiety will be subsequently incorporated into the backbone of the copolymer.[35-39] Cyclic ketene acetals (CKAs) are such monomers, capable of copolymerization with vinyl monomers via both free radical polymerization (FRP) and RDRP systems (**Figure V.1**).[37-46] Once such monomeric units are incorporated into the main C-C chain, the final product would include ester bonds distributed along the backbone, which would provide desirable degradable properties under physiological conditions.

Several CKAs have been examined as comonomers for RDRP procedures (**Figure V.1**). Copolymers with both water-soluble and hydrophobic monomers and CKA monomers, such as 5,6-benzo-2-methylene-1,3-dioxepane (BMDO), were synthesized by RAFT, ATRP, and NMP.[39,42-51] Polymerizations were characterized by "living" behavior yielding degradable copolymers. Among other CKAs polymerizable by RDRP were 5-methylene-2-phenyl-1,3-dioxolan-4-one (MPDO),[52,53] 2-methylene-1,3-dioxepane (MDO), and 2-methylene-4-phenyl-1,3-dioxolane (MPDL).[45,49,51,54] Recently it was reported that NMP copolymerization of MPDL and a water-soluble methacrylate yielded polymers with the highest incorporation efficiency of the CKA comonomer, compared to other tested CKAs like MDO and BMDO.[45,49,51] There is only one report on homopolymerization of MPDL by ATRP,[55] and copolymerization was not investigated. Therefore, it would be of interest to investigate copolymerization of MPDL with various types of monomers typically polymerizable by ATRP (**Scheme V.1b**) for potential biomedical applications.

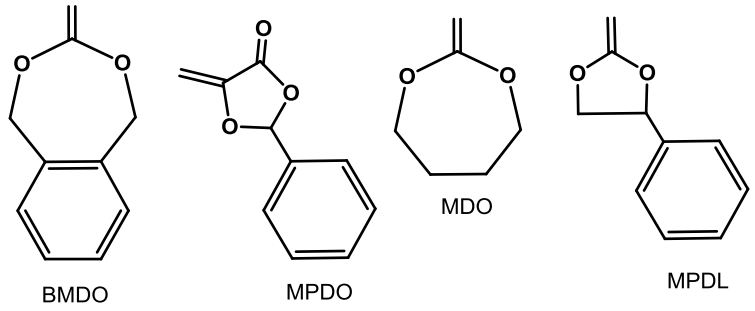

Figure V.1. Structures of various CKA

This Chapter reports the results of a series of studies conducted on the preparation of copolymers of MPDL with hydrophobic and hydrophilic monomers. *n*-Butyl acrylate was chosen as a hydrophobic monomer. (Meth)acrylates with either oligo(ethylene oxide) (8-9 units) or poly(ethylene oxide) (45 units) as a side chain were chosen as hydrophilic

monomers. This type of water-soluble monomers form biocompatible polymers with comb structures due to their longer side chains. They are commonly used in biomaterials preparation, and it would be beneficial to develop their hydrolytically degradable equivalents. The level of MPDL incorporation, ring-opening efficiency and degradation behavior of the synthesized copolymers were studied.

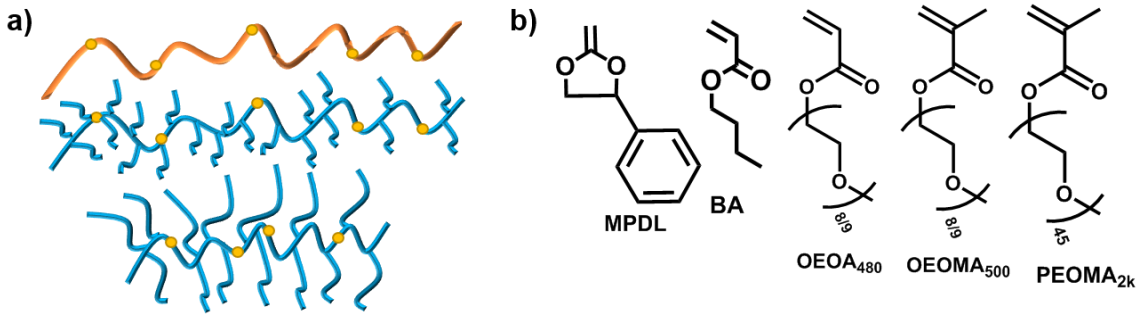

Scheme V.1. (a) Architecture of copolymers prepared via copolymerization of (b) MPDL and several (meth)acrylates.

V.3. Results and discussion

There are several factors, which influence ring-opening efficiency during RROP. It has been reported that the presence of high ring strain in the monomer, the formation of a thermodynamically stable functional group, presence of a radical stabilizing group, and elevated temperatures, all favor a ring-opening reaction during a radical polymerization.[38] It was also reported that MPDL can be (co)polymerized by FRP with 100% ring-opening at temperatures between 60°C - 120°C (**Scheme V.2, reaction A)**.[36,37] However, the homopolymerization of MPDL by ATRP showed a strong temperature dependency of the efficiency of the ring-opening reaction. The ring-opening became prevalent over vinyl-addition (**Scheme V.2, reaction B)** only at higher temperatures, 120°C.[55]

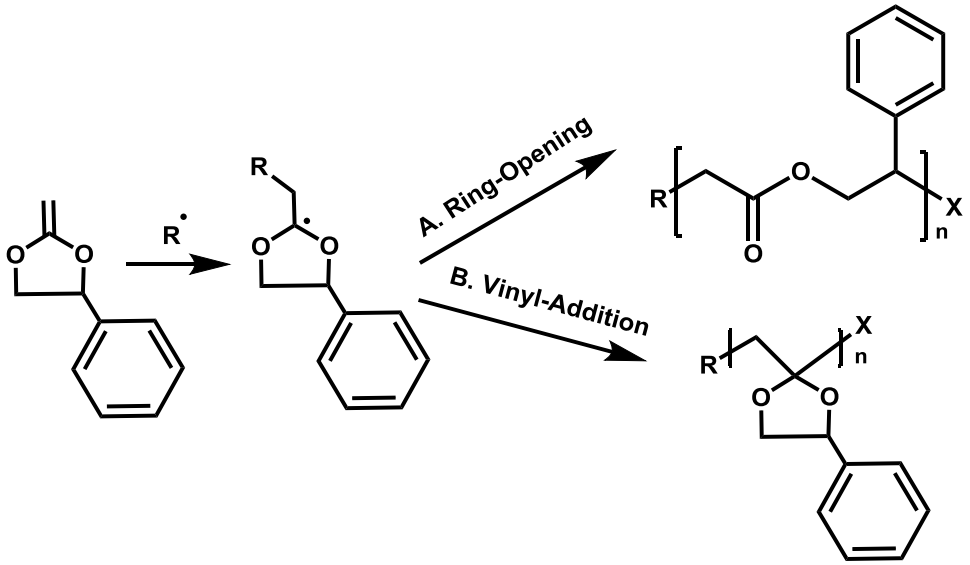

Scheme V.2. Possible modes of incorporation of MPDL monomer into a polymer backbone: ring-opening vs. vinyl addition reaction.

Therefore, the first set of experiments was designed to investigate ring-opening efficiency during copolymerization of MPDL with BA at different temperatures (**Scheme V.3, and Table V.1)**. Monomer conversion during copolymerization of BA with MPDL can be conveniently calculated from the ^{1}H NMR for both comonomers in the formed

copolymers (**Figure V.2**). The initial reaction was conducted at 65°C (**Table V.1, entry 1)**, and kinetic analysis indicated a well-controlled polymerization (**Figure V.3a**). Linear first-order kinetics plots were obtained for both comonomers, with MPDL being incorporated into the copolymer at a rate slower than BA at the given monomer feed ratio, BA/MPDL = 2/1. At low monomer conversions, MW increased linearly with conversion, but started to deviate toward lower MW when conversion increased to >20% (**Figure V.3b**). M_w/M_n values also increased with conversion. According to GPC traces, last two samples were characterized by shift towards higher MW, but low MW tailing was detected (**Figure V.3c**). Such results suggested that some loss of chain-end functionality occurred. Nevertheless, the final copolymer still had a relatively low M_w/M_n, and thus it was isolated and further characterized to determine its composition.

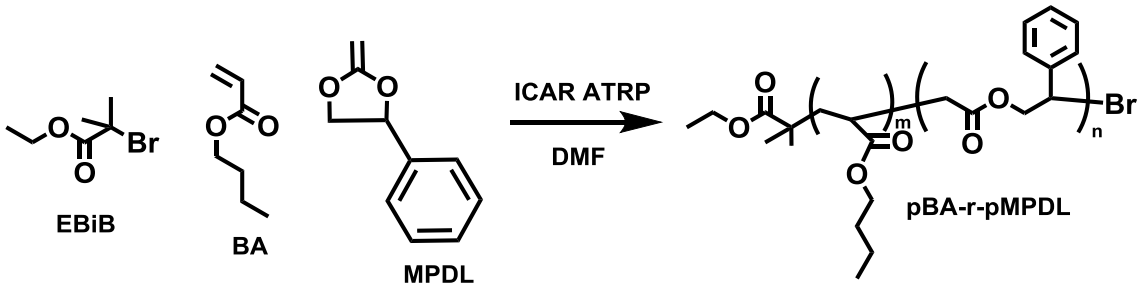

Scheme V.3. Copolymerization of BA and MPDL by ICAR ATRP.

Table V.1. Copolymerization of BA with MPDL by ICAR ATRP.

	BA/MPDL/EBiB/$CuBr_2$/Me_6TREN/RI	T, °C	Time, h	Conv. M_1/M_2, %	M_n	M_w/M_n	f_{MPDL}, %	RO, %
1	200/100/1/0.03/0.06/0.1	65	10.7	54/48	8050	1.37	24.2	16
2	200/100/1/0.03/0.06/0.1	90	5	87/78	8380	1.49	27.0	48
3	200/100/1/0.03/0.06/0.1	120	5	98/93	7090	1.59	28.3	56

[EBiB] = 17 mM, 5.5 ml total, [BA] = 3.4 M, [MPDL] = 1.7 M; reaction solvent – DMF; RI – radical initiator: entry 1 – AIBN ($T_{t1/2=10h}$ = 65°C), entry 2 – V40 ($T_{t1/2=10h}$ = 88°C), entry 3 – Vam110 ($T_{t1/2=10h}$ = 110°C); RO – % of MPDL monomer in ring-opened form to ring-closed form; monomer conversion was measured by ^{1}H NMR; MW was obtained by THF GPC with PMMA calibration standards.

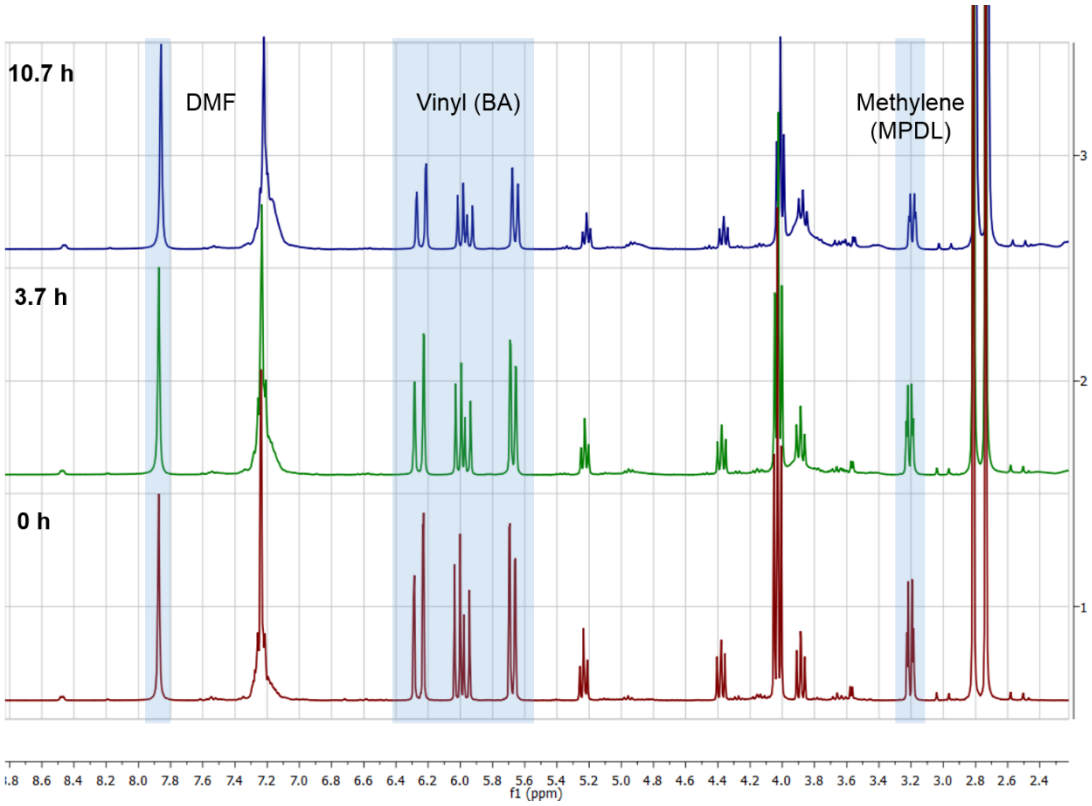

Figure V.2. ^{1}H NMR of polymerization mixture at different time intervals. All spectra were normalized to DMF signal at 7.9 ppm (300 MHz, $CDCl_3$).

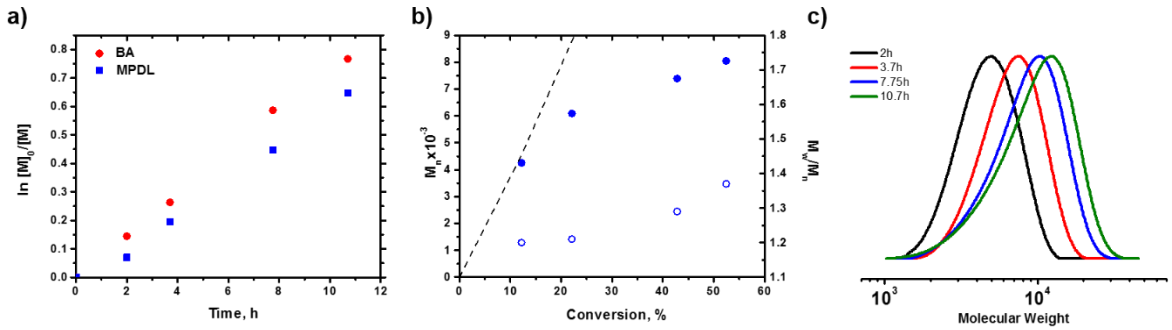

Figure V.3. First-order kinetic plots (a), evolution of M_n and M_w/M_n with conversion (b), and GPC traces for ATRP of BA/MPDL. [BA]:[MPDL]:[EBiB]:[$CuBr_2$]:[Me_6TREN]:[AIBN] = 200:100:1:0.03:0.06:0.1, DMF, 65°C, [BA] = 3.4 M, [MPDL] = 1.7 M. MW and GPC traces were obtained by THF GPC with PMMA calibration standards.

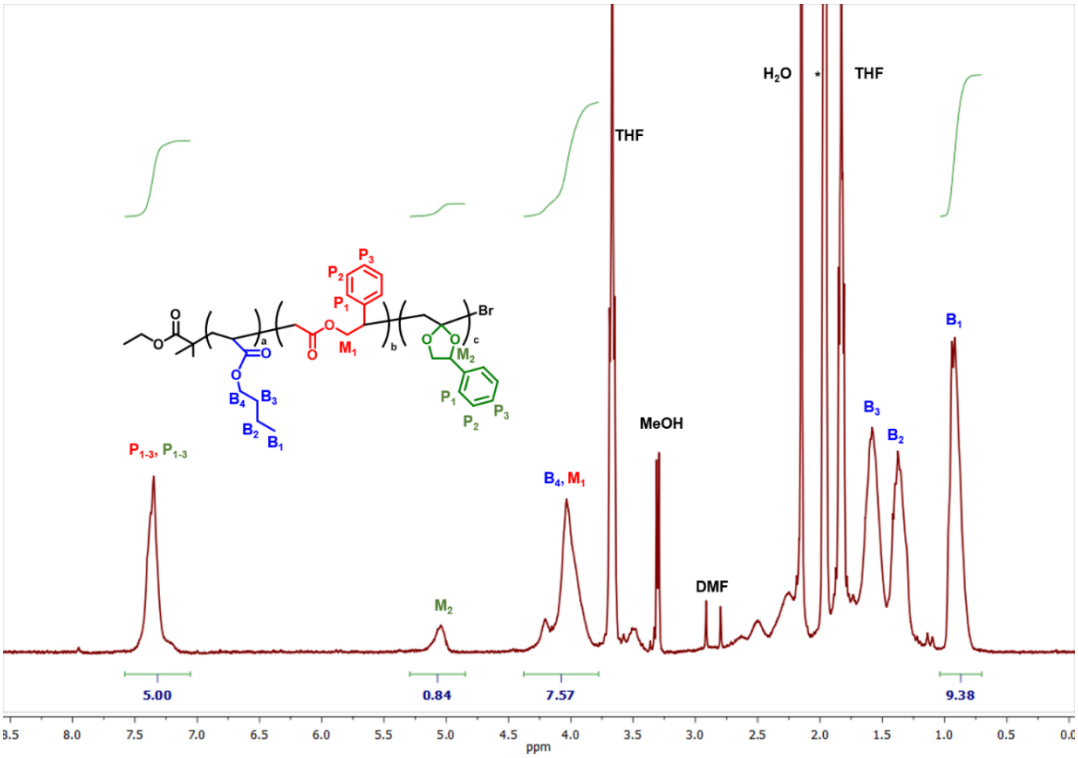

Figure V.4. ^{1}H NMR of purified copolymer pBA-r-pMPDL synthesized at 65°C (300 MHz, CD_3CN).

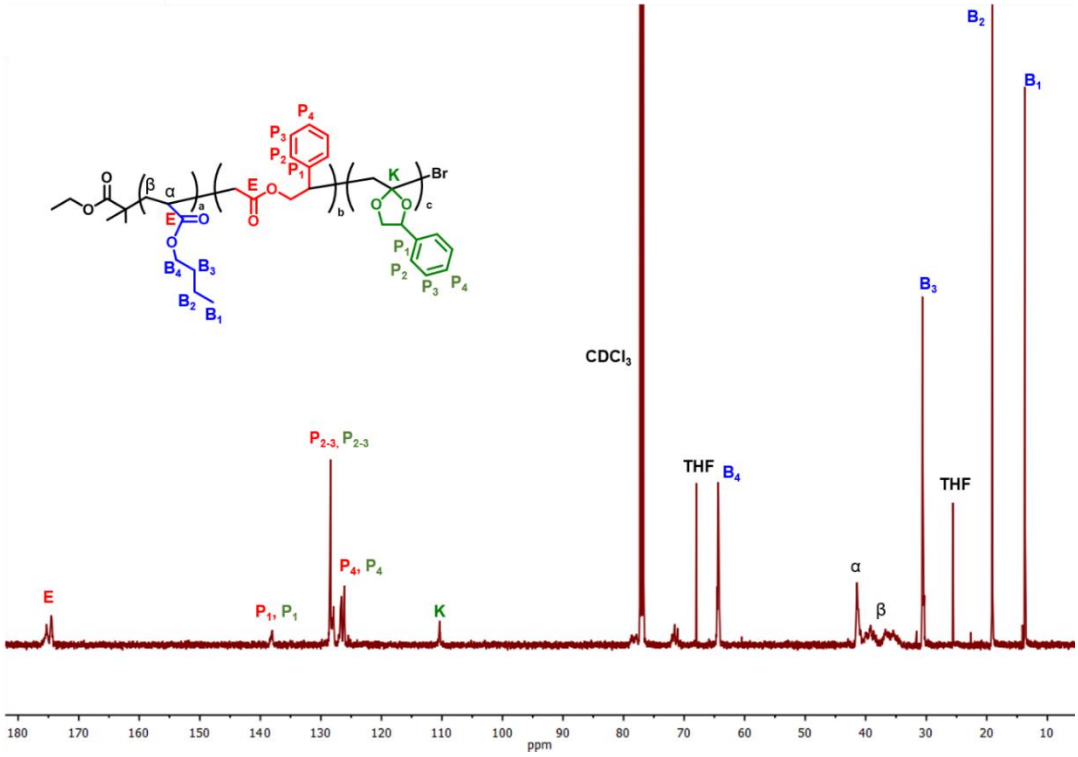

Figure V.5. ^{13}C NMR spectra of purified copolymer pBA-rpMPDL synthesized at 65°C (500 MHz, $CDCl_3$).

The purified copolymer was further characterized by ^{1}H NMR to determine the mode of incorporation of MPDL, i.e. determine what fraction of incorporated monomer exhibited ring-opening versus vinyl addition. The composition of the pBA-*r*-pMPDL copolymer could be determined from the ratio of aromatic protons (P_{1-3}) present in MPDL to the protons from butyl acrylate side chain (B_1) (**Figure V.4).** According to this calculation, MPDL incorporation was 24.2 %, which is lower than the value calculated from monomer conversion, ~30.7%. It is likely that during the purification process a fraction of the copolymer was lost resulting in difference in composition. The ring-opening efficiency was calculated from ^{1}H NMR spectra, where the signal at ~5.05 ppm corresponds to the methine proton (M_2) on the carbon between the acetal oxygen and the phenyl group (**Figure V.4)**. The difference between the integration of methine proton and phenyl proton would provide a value for the percentage of MPDL, which underwent the ring-opening reaction. According to the values calculated for copolymerization of BA with MPDL at 65°C only 16% of incorporated MPDL was in its ring-opened form. ^{13}C NMR was also used to confirm the presence of an acetal carbon (**Figure V.5)** detected at 110 ppm.

The next two copolymerizations of BA with MPDL were performed at higher temperatures (**Table V.1, entries 2-3)**. Different free radical initiators were selected for each reaction; the initial radical initiator (RI) AIBN was replaced by RIs with higher decomposition temperatures, V40 with $T_{t1/2=10h}$ = 88°C, and Vam110 with $T_{t1/2=10h}$ = 110°C for the highest temperature reaction. Polymerizations at 90°C and 120°C were characterized by faster rate, but were also less controlled yielding polymers with higher M_w/M_n. However, the final copolymers were characterized by higher percentage of

incorporated MPDL, which underwent ring-opening instead of vinyl addition. According to ^{1}H NMR analysis the peak due to the methine proton present in MPDL (M_2), which represents incorporated MPDL that underwent vinyl addition, decreased for the polymers synthesized at the elevated temperatures (**Figure V.6**). ^{1}H NMR spectra obtained for the polymers synthesized at different temperatures were normalized to aromatic protons, and their compositions were calculated based on integration values presented in the **Table V.2**. Increasing the temperature from 65°C to 90°C resulted in a 3-fold increase in MPDL incorporation via ring-opening process. A further increase from 90°C to 120°C resulted in an additional 20% increase in the fraction of ring-opened MPDL in the copolymer. Therefore, while it was demonstrated that ring-opening efficiency could be improved by increase in temperature, the most significant improvement was detected for the first increase from 65°C to 90°C. A further 30°C increase in temperature resulted in marginally higher ring-opening occurrence which, unfortunately, was accompanied by a decrease in control over the polymerization reaction, M_w/M_n increased from 1.49 to 1.59.

Table V.2. Calculations of pBA-r-pMPDL compositions during copolymerization at different temperatures

Entry	T, °C	Integration values for the following protons in pBA-r-pMPDL			Composition a:b:c (mol. %)*
		B_1	$P_{1\text{-}3}$	M_2	
1	65	9.38	5	0.84	76:4:20
2	90	8.15	5	0.52	73:13:14
3	120	7.68	5	0.44	72:16:12

*composition a:b:c is for the copolymer structure depicted in Figure V.6a

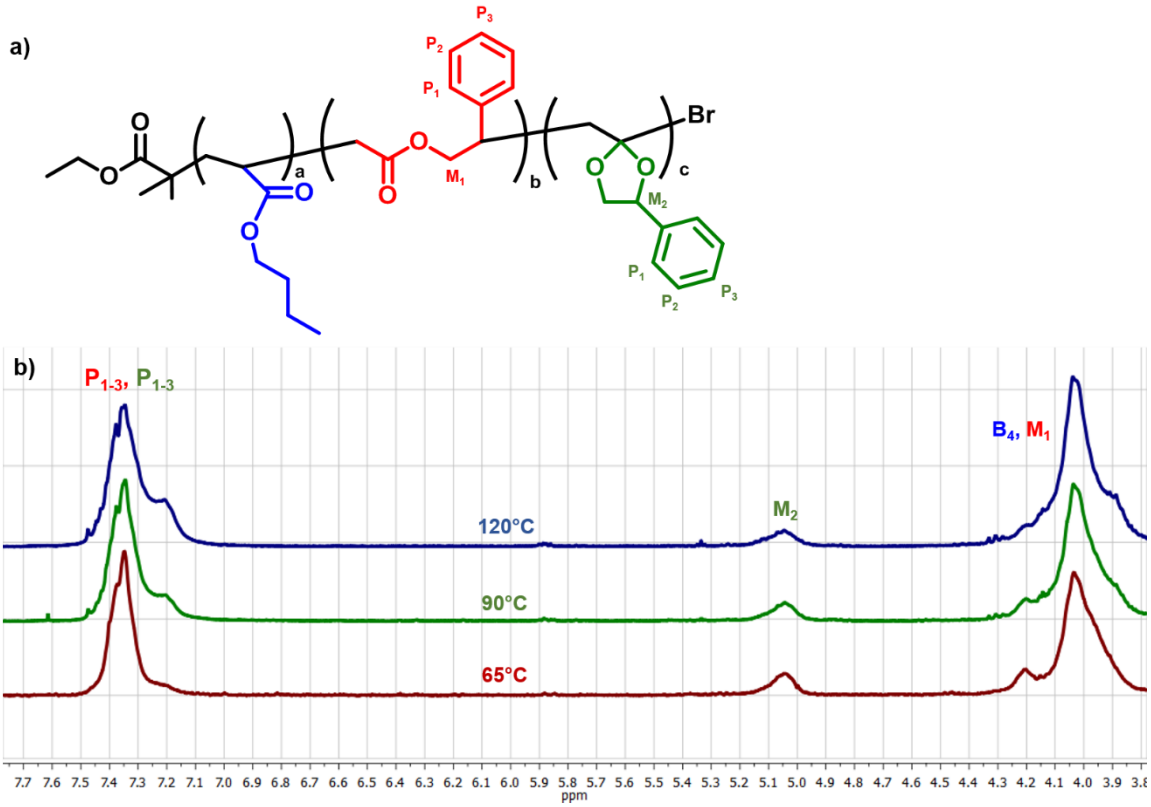

Figure V.6. ^{1}H NMR of purified copolymers pBA-r-pMPDL synthesized at different temperatures (300 MHz, CD_3CN). Spectra were normalized to phenyl protons in each sample. Signal at 5.05 ppm corresponds to methine proton depicted in red color in the polymer unit structure.

The pBA-*r*-pMPDL copolymers synthesized at varied temperatures were incubated under basic conditions to determine their degradation properties and GPC was used to determine decrease in MW resulting from the degradation reactions (**Figure V.7)**. As expected, according to this analysis, the pBA-*r*-pMPDL copolymer with highest MPDL content in the ring-opened form was characterized by the largest decrease in MW. Since the total incorporation of MPDL in these copolymers varied insignificantly, it is likely that drastic difference in the amount of ring-opened MPDL versus MPDL incorporated via vinyl addition is responsible for more efficient degradation of copolymers prepared at 90°C and 120°C.

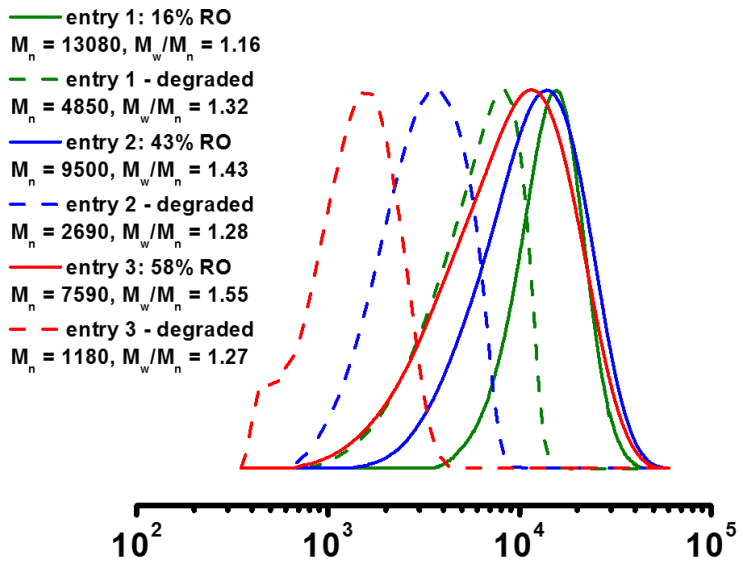

Figure V.7. GPC traces of copolymers pBA-r-pMPDL prepared at different temperatures before and after degradation (**Table V.1**). Each sample was incubated for 45 h in 5% KOH in THF/MeOH (1/1), and the polymer was precipitated after acidification with 1M HCl, dissolved in THF and analyzed by THF GPC. MW values for purified polymers differed from values obtained during reaction.

In the next set of experiments, MPDL was copolymerized with a selection of water-soluble monomers, such as $OEOA_{480}$, $OEOMA_{500}$ and $PEOMA_{2k}$ (**Scheme V.1, and Scheme V.4).** The initial polymerization reaction was conducted at 65°C with the ratio of reagents identical to BA/MPDL copolymerization (**Table V.3**, entry 1). ^{1}H NMR could only be used for OEO_{A480} conversion analysis, but it was not possible to calculate MPDL conversion due to an overlap of peaks. Therefore only the final polymer sample was analyzed for MPDL incorporation. Additionally all final polymer samples from **Table V.3 were purified and analyzed on GPC with DMF as eluent and MALLS detector to obtain absolute MW, due to inability of standard calibration to provide adequate MW values.**[56]

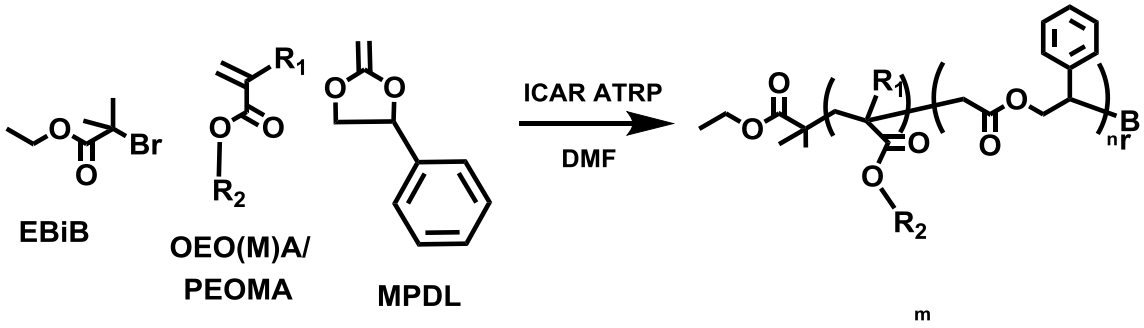

Scheme V.4. Copolymerization of MPDL with hydrophilic monomers.

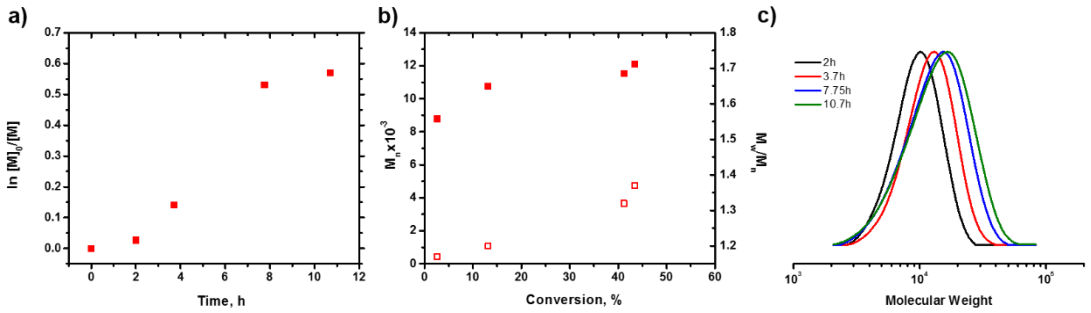

Figure V.8. First-order kinetic plots (a), evolution of M_n (●) and M_w/M_n (○) with conversion (b), and GPC traces for ATRP of $OEOA_{480}$/MPDL (Table V.3, entry 1). [$OEOA_{480}$]:[MPDL]:[EBiB]:[$CuBr_2$]:[Me_6TREN]:[AIBN] = 200:100:1:0.03:0.06:0.1, DMF, 65°C, [$OEOA_{480}$] = 1.0 M, [MPDL] = 0.5 M. MW and GPC traces were obtained by THF GPC with PMMA calibration standards.

The first-order kinetics plots of the copolymerization of $OEOA_{480}$ with MPDL were characterized by ~2 h induction period (**Figure V.8**). The final point on the first-order kinetic plot deviated from linearity, which could be due to oxygen contamination during sample removal. GPC traces showed similar results to the copolymerization of MPDL with BA: namely a shift towards higher MW occurred, but low MW tailing was also detected. The MW provided by GPC for the copolymer was quite low but similar types of polymers with OEO/PEO in their side-chain cannot be adequately characterized by GPC with standard calibration due to their comb-like structure causing delayed elution.[56-58] Thus we used a GPC equipped with MALLS detector to analyze purified p$OEOA_{480}$-*r*-pMPDL

copolymer to obtain absolute MW values. The final copolymer was also analyzed by ^{1}H NMR to estimate MPDL incorporation into the pOEOA$_{480}$ backbone and determine the percentage of MPDL, which underwent ring-opening copolymerization (**Figure V.9**).

Table V.3. Copolymerization of MPDL with hydrophilic monomers by ICAR/SARA ATRP.

	M_1/MPDL/EBiB/CuX_2/ Me_6TREN/RI	**M_1/X**	**Conv. M_1, % (time, h)**	**$M_{n\ th}$**	**M_n**	**M_w/ M_n**	**f_{MPDL}, %**	**RO, %**
1	200/100/1/0.03/0.06/0.1	$OEOA_{480}$ /Br	43 (10.7)	45	31	1.07	20.5	32
2	1000/500/1/0.15/0.3/0.5	$OEOA_{480}$ /Br	64 (10)	316	50	1.37	9.2	62
3	1000/500/1/0.15/0.3/0.5	$OEOA_{480}$ /Cl	69 (0)	366	83	1.54	23.8	52
4	1000/500/1/0.75/1.5/0.5	$OEOA_{480}$ /Br	36 (6)	183	18	1.40	14.7	78
5	1000/500/1/0.15/0.3/0.25	$OEOMA_{500}$ /Br	76 (10)	388	147	1.73	6.1	82
6	1000/500/1/0.15/0.3/0.25	$OEOMA_{500}$ /Cl	77 (5)	397	135	1.74	8.6	67
7	1000/500/1/0.75/1.5/0.25	$OEOMA_{500}$ /Br	64 (6)	327	125	1.49	5.9	74
8	150/150/1/0.03/0.06/0.1	$PEOMA_{2k}$ /Br	30 (13)	91	52	1.08	6.0	96

5 ml total; reaction solvent – DMF; entry 1: 65°C, entries 2-8: 90°C; RI – radical initiator: entry 1 – AIBN ($T_{t1/2=10h}$ = 65°C, entries 2 – 8: V40 ($T_{t1/2=10h}$ = 88°C); entries 1 – 7: [M_1] = 1 M, [M_2] = 0.5 M; entry 8: [M_1] = 0.3 M, [M_2] = 0.3 M; RO – % of MPDL monomer in ring-opened form to ring-closed form; only conversion of M_1 was measured by ^{1}H NMR; final M_n was measured by DMF GPC with MALLS detector based on dn/dc value of a copolymer.

According to the analysis the final copolymer contained around 20% of MPDL, and 32% of this MPDL underwent ring-opening. This is 2 times higher level of ring-opened MPDL than that obtained for BA/MPDL copolymerization. Although BA and OEOA$_{480}$ are both acrylates, the reaction conditions were different: monomer concentrations were lower for copolymerization with OEOA$_{480}$ and the rate of the reaction was slower. This means that there are several factors, which possibly could influence the ratio of ring-opening incorporation and radical propagation without ring-opening.

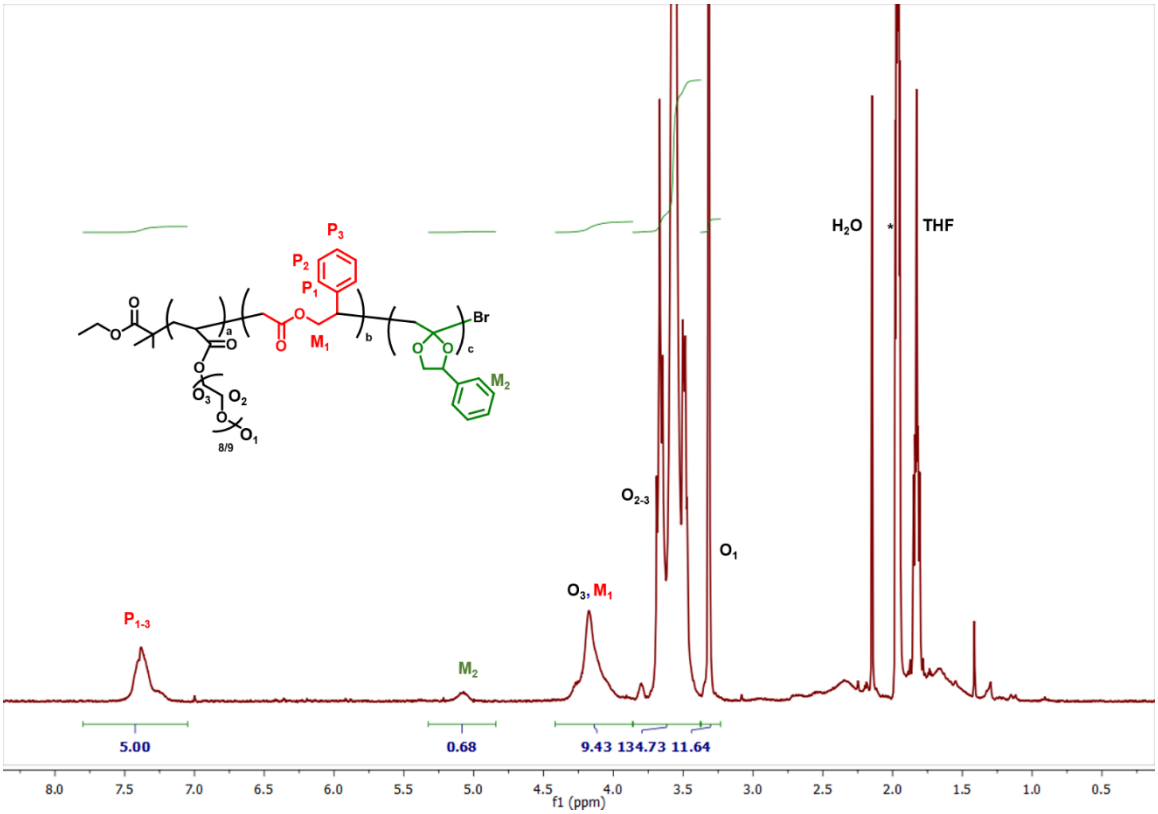

Figure V.9. ^{1}H NMR of purified copolymer pOEOA$_{480}$-*r*-pMPDL synthesized at 65°C (300 MHz, CD_3CN).

In the next set of experiments, polymerizations were conducted at 90°C to improve percentage of MPDL incorporated into the copolymer in its ring-opened form. Additionally, the targeted DP was increased to 1500 (**Table V.3**, entry 2 – 4). To date, most of synthesized copolymers with CKA were characterized by rather low MW (10,000 – 20,000), with some systems reaching ~50,000.[47] However for certain biological application the preparation of degradable high MW polymers would be especially beneficial for the reasons stated earlier and because lower MW polymers could be removed from a physiological circulation without need for their degradation. In a similar manner to copolymerization with BA, copolymerization of OEOA$_{480}$ with MPDL at 90°C resulted in the formation of a copolymer with a higher percentage of MPDL with ring-opened structure (**Table V.3**, entry 2). The percentage of incorporated MPDL which underwent ring-

opening during this copolymerization reached 62%. However, the fraction of MPDL incorporated into the $pOEOA_{480}$ backbone was less than 10%. Therefore, catalyst type and its concentration were varied to investigate how changes in the catalytic system could influence copolymerization. When $CuCl_2$ was used instead of $CuBr_2$, the amount of MPDL incorporated into the copolymer increased to >20%, but the M_w/M_n of the final copolymer was higher and ring-opening efficiency decreased from 62% to 52% (**Table V.3**, entry 3). When the catalyst concentration was increased 5 fold, then MPDL incorporation increased to ~15% and ring-opening efficiency was as high as 78% (**Table V.3**, entry 4). However, with higher catalyst concentration, MW of the copolymer was significantly lower than the theoretically predicted value. Currently the best polymerization control was attained when $CuBr_2$ was used at low catalyst concentrations, 100 ppm.

When MPDL was copolymerized with OEOA methacrylate analogue, $OEOMA_{500}$, the overall incorporation of MPDL was lower (**Table V.3**, entry 5 – 7). Polymerization in the presence of $CuCl_2$ instead of $CuBr_2$ resulted in marginally higher incorporation of MPDL, but there was no improvement in M_w/M_n. In the presence of a higher concentration of catalyst, control over polymerization improved and resulted in formation of copolymers with lower M_w/M_n, 1.49 vs. 1.73, but incorporation of MPDL remained constant. Even though copolymers of MPDL with $OEOMA_{500}$ were characterized by higher M_w/M_n compared to copolymerization with acrylate $OEOA_{480}$, it was possible to obtain polymers with measured MW > 120,000 with M_w/M_n ~ 1.5 (**Table V.3**, entry 7).

The degradability of both $pOEOA_{480}$-*r*-pMPDL and $pOEOMA_{500}$-*r*-pMPDL was evaluated by incubating the copolymers in 5% aqueous KOH. Hydrolytic degradation results were analyzed by aqueous GPC to determine the decrease in MW with time (**Figure**

V.10). After 20 h, the molecular weight of both the water-soluble polyacrylate and polymethacrylate copolymers decreased by a factor of 3 – 4, and did not change over the next 28 h indicating a full degradation had occurred. Final degradation products were characterized by M_n < 10,000 according to calibration with PEO standards. However it is important to point out that even though apparent M_n (based on linear PEO standards) of degradable copolymers were only 15,500 for pOEOA-r-pMPDL and 35,200 for pOEOMA-r-pMPDL, a fraction of copolymers of MW ≥ 100,000 were also present. Degradation of this higher MW fraction of copolymers resulted in formation of degraded products with MW significantly below 100,000.

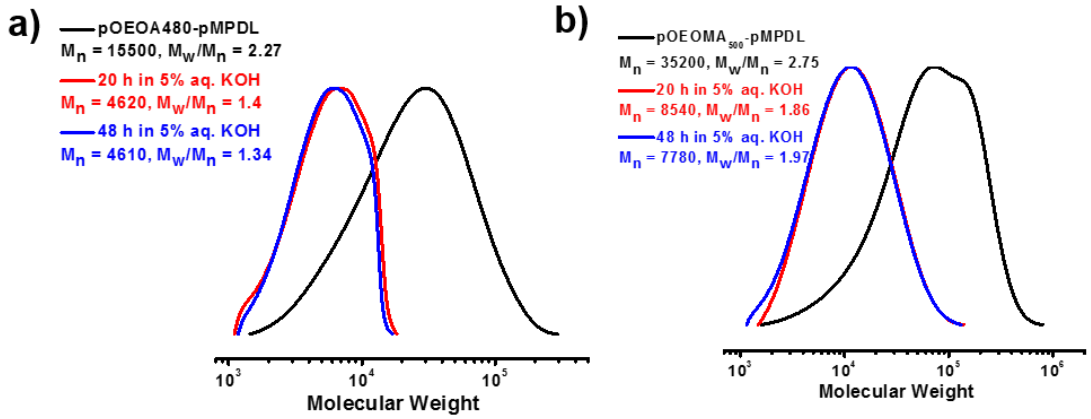

Figure V.10. Degradation studies of hydrophilic polymers. All samples were neutralized by 1M HCl and analyzed by water GPC in PBS at pH = 7 calibrated with linear PEO standards.

The final copolymerization in this series of experiments was the copolymerization of MPDL with a $PEOMA_{2k}$ macromonomer. This was evaluated to determine if this procedure would form a degradable brush copolymer by the "grafting through" method (**Table V.3**, entry 8). The synthesized polymer was characterized by incorporation of a similar fraction of MPDL (~6%) as the lower MW $OEOMA_{500}$ monomer, however, according to proton NMR analysis, 96% of the MPDL units had undergone ring-opening

during the copolymerization (**Figure V.11).** Besides structural difference of this type of macromonomer from other utilized monomers, the copolymerization was performed at very low comonomers concentrations (0.3 M) resulting in a relatively slow rate of polymerization (30% monomer conversion in 13 h). This result indicated that it would be important to investigate further if copolymerization under dilute conditions and at a slower rate of polymerization could increase the prevalence of ring-opening of MPDL over vinyl-addition.

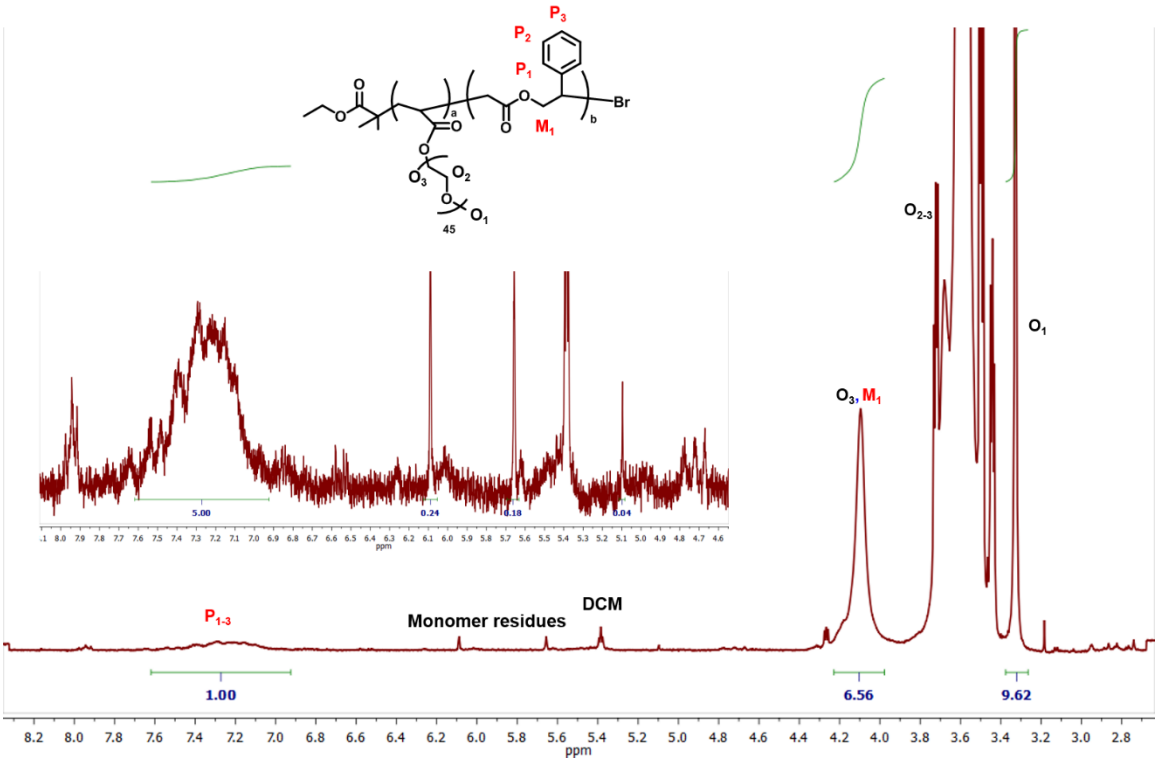

Figure V.11. ^{1}H NMR of purified copolymers pPEOMA$_{2k}$-*r*-pMPDL (500 MHz, CD_3CN) with insert with zoomed in region 4.8 – 8 ppm.

V.4. Conclusions

Degradable functional copolymers were synthesized by ATRP via copolymerization of (meth)acrylates with MPDL as an exemplary CKA monomer. The efficiency of ring-opening of MPDL during copolymerization, which is required for formation of the degradable units in the backbone of the copolymer, increased at higher temperatures. MPDL was successfully copolymerized with both acrylates and methacrylates, and copolymers with acrylates were characterized by higher levels of incorporation of MPDL into the copolymers (~2 to 3 times), compared to copolymers with methacrylates. High MW copolymers, MW >50,000, could be synthesized and successfully degraded forming fragmented chains below the renal threshold limit.

The final copolymers were characterized by relatively high dispersities, and the measured MWs were lower than theoretically predicted. The ring-opening efficiency of MPDL incorporation varied with different comonomers, which could be explained by several differences in reaction conditions including monomer concentration, deactivation efficiency, or (cross)propagation rate coefficients. Thus, additional detailed studies have to be performed to identify all side reactions and establish conditions for more effective ring-opening with specific comonomers despite temperature effects, and also to determine how to control MW, M_w/M_n, and produce well-defined copolymers of complex architectures.

V.5. Experimental Details

V.5.1. Materials.

Butyl acrylate (BA, 99%, Sigma Aldrich), oligo(ethylene oxide) methyl ether acrylate ($OEOA_{480}$, 99%, average molecular weight 480, Sigma Aldrich), oligo(ethylene oxide) methyl ether methacrylate ($OEOMA_{500}$, 99%, average molecular weight 475, Aldrich) and were passed over a column of basic alumina (Fisher Scientific) prior to use. Poly(ethylene oxide) methyl ether acrylate ($PEOMA_{2k}$, 50% aqueous solution, average molecular weight 2000, Sigma Aldrich) was extracted by dichloromethane and precipitated into hexane prior to use. Copper (II) bromide (99.999%, Sigma Aldrich), N,N-dimethylformamide (DMF, ACS grade, Fisher Scientific), dichloromethane (DCM, HPLC grade, Fisher Scientific), ethyl ether (ACS grade, Fisher Scientific), chloroform-d (Cambridge Isotope Laboratories), acetonitrile-d3 (Cambridge Isotope Laboratories), tris[2-(dimethylamino)ethyl]amine (Me_6TREN, 97%, Sigma Aldrich), ethyl-2-bromo-2-methylpropionate (EBiB, 98%, Sigma Aldrich), were used as received. Radical initiators 2,2'-azobis((2-methylpropionitrile) (AIBN, Sigma Aldrich), 1,1'-azobis(cyclohexanecarbonitrile) (V40, Sigma Aldrich), 2,2'-azobis(N-butyl-2-methylpropionamide) (Vam110, Wako) were used as received. Chloroacetaldehyde dimethyl acetal (97%), styrene glycol (97%), Dowex 50WX8 hydrogen form and potassium tert-butoxide (KO-tert-Bu,98%) were purchased from Acros. 2-Methylene-4-phenyl-1,3-dioxolane (MPDL) was synthesized according to previous procedure.[36]

V.5.2. Instrumentation and characterization.

^{1}H NMR (300 and 500 MHz) spectra were recorded on a Bruker Avance 300/500 spectrometer. The conversion of acrylates and methacrylates were determined by relative

integration of the vinyl protons and the protons of the solvent of reaction. Molecular weights and distributions were determined by THF, DMF and aqueous GPC. The THF GPC system was based on Polymer Standards Services (PSS) columns (Styrogel 102, 103, 105 Å) with, respectively, tetrahydrofuran (THF) as the eluent at a flow rate of 1 mL/min at 35 ^{0}C. DMF GPC utilized dimethylformamide (DMF) containing 50 mM LiBr as the eluent at a flow rate of 1 mL/min at 50 ^{0}C and differential refractive index (RI) detector (Waters, 2414) and multi-angle laser light scattering detector (MALLS) (Wyatt TREOS). The apparent molecular weights and dispersity (M_w/M_n) were determined with a calibration based on linear poly(methyl methacrylate) standards using for THF GPC. The aqueous GPC system (model Alliance 2695) was based on an Ultrahydrogel linear column (7.8 - 300 mm, Waters) with phosphate buffered saline (PBS) as the eluent at a flow rate of 1 mL/min at room temperature and differential RI detector (Waters, 2414). The apparent molecular weights and dispersity (M_w/M_n) were determined with a calibration based on linear PEG standards.

V.5.3. ICAR ATRcoP of BA with MPDL.

BA (2.4 g, 18.7 mmol), MPDL (1.5 g, 9.4 mmol) were mixed with 0.375 ml of radical initiator stock solution (25 mM), 0.375 ml of $CuBr_2/Me_6TREN$ stock solution (1/2, 7.5 mM of $CuBr_2$), 0.375 ml of EBiB stock solution (250 mM). Reaction mixture was placed in Schlenk flask, sealed and purged with nitrogen for 30 min. Polymerization was started by immersing reaction mixture in a heated oil bath set at either 65°C, 90°C, or 120°C.

V.5.4. ICAR ATRcoP of $OEOA_{480}$ with MPDL.

$OEOA_{480}$ (2.4 g, 5 mmol), MPDL (0.4 g, 2.5 mmol) were mixed with 0.1 ml of radical initiator stock solution (25 mM), 0.1 ml of $CuBr_2/Me_6TREN$ stock solution (1/2, 7.5 mM

of $CuBr_2$), 0.1 ml of EBiB stock solution (250 mM), and 2.2ml of DMF. Reaction mixture was placed in Schlenk flask, sealed and purged with nitrogen for 30 min. Polymerization was started by immersing reaction mixture in a heated oil bath set at either 65°C, or 90°C.

V.5.5. ICAR ATRcoP of $OEOMA_{500}$ with MPDL.

$OEOMA_{500}$ (2.5 g, 5 mmol), MPDL (0.4 g, 2.5 mmol) were mixed with 0.05 ml of radical initiator V40 stock solution (25 mM), 0.1 ml of $CuBr_2/Me_6TREN$ stock solution (1/2, 7.5 mM of $CuBr_2$), 0.1 ml of EBiB stock solution (50 mM), and 2.2ml of DMF. Reaction mixture was placed in Schlenk flask, sealed and purged with nitrogen for 30 min. Polymerization was started by immersing reaction mixture in a heated oil bath set at 90°C.

V.5.6. ICAR ATRcoP of $PEOMA_{2k}$ with MPDL.

$PEOMA_{2k}$ (3 g, 1.5 mmol) was dissolved in 4.5 ml of DMF. After that MPDL (0.4 g, 2.5 mmol) were mixed with 0.04 ml of radical initiator V40 stock solution (25 mM), 0.04 ml of $CuBr_2/Me_6TREN$ stock solution (1/2, 7.5 mM of $CuBr_2$), 0.1 ml of EBiB stock solution (50 mM) and added to the dissolved $PEOMA_{2k}$. Reaction mixture was placed in Schlenk flask, sealed and purged with nitrogen for 30 min. Polymerization was started by immersing reaction mixture in a heated oil bath set at 90°C.

V.5.7. Hydrolytic Degradation.

pBA-*r*-pMPDL copolymers were degraded in 5% KOH solution in mixture of THF/MeOH with a ratio 1/1. Degradation products were neutralized with HCl and precipitated into hexane prior to analysis. Water soluble polymers were degraded in aqueous 5% KOH. Samples were dissolved in PBS prior to analysis. Polymers were typically dissolved at 10 mg/ml concentration.

V.6. References

(1) Nair, L. S.; Laurencin, C. T. *Prog. Polym. Sci.* **2007**, *32*, 762.

(2) Meng, F.; Hennink, W. E.; Zhong, Z. *Biomaterials* **2009**, *30*, 2180.

(3) Pillai, C. K. S.; Paul, W.; Sharma, C. P. *Prog. Polym. Sci.* **2009**, *34*, 641.

(4) Li, Y.; Rodrigues, J.; Tomas, H. *Chem. Soc. Rev.* **2012**, *41*, 2193.

(5) Ulery, B. D.; Nair, L. S.; Laurencin, C. T. *J. Polym. Sci., Part B: Polym. Phys.* **2011**, *49*, 832.

(6) Malafaya, P. B.; Silva, G. A.; Reis, R. L. *Adv. Drug Delivery Rev.* **2007**, *59*, 207.

(7) Oh, J. K.; Siegwart, D. J.; Lee, H.-i.; Sherwood, G.; Peteanu, L.; Hollinger, J. O.; Kataoka, K.; Matyjaszewski, K. *J. Am. Chem. Soc.* **2007**, *129*, 5939.

(8) Kabanov, A. V.; Vinogradov, S. V. *Angew. Chem., Int. Ed.* **2009**, *48*, 5418.

(9) Knop, K.; Hoogenboom, R.; Fischer, D.; Schubert, U. S. *Angew. Chem. Int. Ed.* **2010**, *49*, 6288.

(10) Pack, D. W.; Hoffman, A. S.; Pun, S.; Stayton, P. S. *Nat. Rev. Drug Discovery* **2005**, *4*, 581.

(11) Schmaljohann, D. *Adv. Drug Delivery Rev.* **2006**, *58*, 1655.

(12) Lee, K. Y.; Yuk, S. H. *Prog. Polym. Sci.* **2007**, *32*, 669.

(13) Galaev, I. Y.; Mattiasson, B. *Trends Biotechnol.* **1999**, *17*, 335.

(14) Savic, R.; Eisenberg, A.; Maysinger, D. *J. Drug Targeting* **2006**, *14*, 343.

(15) He, C.; Kim, S. W.; Lee, D. S. *J. Controlled Release* **2008**, *127*, 189.

(16) Liechty, W. B.; Kryscio, D. R.; Slaughter, B. V.; Peppas, N. A. *Annu. Rev. Chem. Biomol. Eng.* **2010**, *1*, 149.

(17) Duncan, R. *Nat. Rev. Drug Discovery* **2003**, *2*, 347.

(18) Langer, R.; Peppas, N. A. *AIChE J.* **2003**, *49*, 2990.

(19) George, M.; Abraham, T. E. *J. Controlled Release* **2006**, *114*, 1.

(20) Haag, R.; Kratz, F. *Angew. Chem., Int. Ed.* **2006**, *45*, 1198.

(21) Maeda, H.; Wu, J.; Sawa, T.; Matsumura, Y.; Hori, K. *J. Control. Release* **2000**, *65*, 271.

(22) Vert, M. *Prog. Polym. Sci.* **2007**, *32*, 755.

(23) Tian, H.; Tang, Z.; Zhuang, X.; Chen, X.; Jing, X. *Prog. Polym. Sci.* **2012**, *37*, 237.

(24) Danhier, F.; Ansorena, E.; Silva, J. M.; Coco, R.; Le Breton, A.; Preat, V. *J. Controlled Release* **2012**, *161*, 505.

(25) Matyjaszewski, K.; Tsarevsky, N. V. *JACS* **2014**, *136*, 6513.

(26) Gillies, E. R.; Goodwin, A. P.; Frechet, J. M. J. *Bioconjugate Chem.* **2004**, *15*, 1254.

(27) Gu, Y.; Zhong, Y.; Meng, F.; Cheng, R.; Deng, C.; Zhong, Z. *Biomacromolecules* **2013**, *14*, 2772.

(28) Tsarevsky, N. V.; Matyjaszewski, K. *Macromolecules* **2005**, *38*, 3087.

(29) Johnson, J. A.; Lewis, D. R.; Díaz, D. D.; Finn, M. G.; Koberstein, J. T.; Turro, N. J. *JACS* **2006**, *128*, 6564.

(30) de Graaf, A. J.; Mastrobattista, E.; Vermonden, T.; van Nostrum, C. F.; Rijkers, D. T. S.; Liskamp, R. M. J.; Hennink, W. E. *Macromolecules* **2012**, *45*, 842.

(31) Gao, H.; Tsarevsky, N. V.; Matyjaszewski, K. *Macromolecules* **2005**, *38*, 5995.

(32) Johnson, J. A.; Finn, M. G.; Koberstein, J. T.; Turro, N. J. *Macromolecules (Washington, DC, U. S.)* **2007**, *40*, 3589.

(33) Cho, H. Y.; Srinivasan, A.; Hong, J.; Hsu, E.; Liu, S.; Shrivats, A.; Kwak, D.; Bohaty, A. K.; Paik, H.-j.; Hollinger, J. O.; Matyjaszewski, K. *Biomacromolecules* **2011**, *12*, 3478.

(34) Tsarevsky, N. V.; Huang, J.; Matyjaszewski, K. *J. Polym. Sci., Part A: Polym. Chem.* **2009**, *47*, 6839.

(35) Bailey, W. J.; Ni, Z. *J. Polym. Sci. Poly. Che. Ed.* **1982**, *20*, 3021.

(36) Bailey, W. J.; Wu, S.-r.; Nib, Z. *Makromol. Chem.* **1982**, *183*, 1913.

(37) Bailey, W. J. *Polym. J.* **1985**, *17*, 85.

(38) Sanda, F.; Endo, T. *J. Polym. Sci., Part A: Polym. Chem.* **2001**, *39*, 265.

(39) Agarwal, S. *Polymer Chemistry* **2010**, *1*, 953.

(40) Yuan, J.-Y.; Pan, C.-Y.; Tang, B. Z. *Macromolecules* **2001**, *34*, 211.

(41) He, T.; Zou, Y. F.; Pan, C. Y. *Polym. J.* **2002**, *34*, 1.

(42) Huang, J.; Gil, R.; Matyjaszewski, K. *Polymer* **2005**, *46*, 11698.

(43) Lutz, J.-F.; Andrieu, J.; Üzgün, S.; Rudolph, C.; Agarwal, S. *Macromolecules* **2007**, *40*, 8540.

(44) Riachi, C.; Schüwer, N.; Klok, H.-A. *Macromolecules* **2009**, *42*, 8076.

(45) Delplace, V.; Tardy, A.; Harrisson, S.; Mura, S.; Gigmes, D.; Guillaneuf, Y.; Nicolas, J. *Biomacromolecules* **2013**, *14*, 3769.

(46) Decker, C. G.; Maynard, H. D. *Eur. Polym. J.* **2015**, *65*, 305.

(47) Siegwart, D. J.; Bencherif, S. A.; Srinivasan, A.; Hollinger, J. O.; Matyjaszewski, K. *Journal of Biomedical Materials Research Part A* **2008**, *87A*, 345.

(48) Zhang, Y.; Chu, D.; Zheng, M.; Kissel, T.; Agarwal, S. *Polymer Chemistry* **2012**, *3*, 2752.

(49) Tardy, A.; Delplace, V.; Siri, D.; Lefay, C.; Harrisson, S.; de Fatima Albergaria Pereira, B.; Charles, L.; Gigmes, D.; Nicolas, J.; Guillaneuf, Y. *Polymer Chemistry* **2013**, *4*, 4776.

(50) d'Ayala, G. G.; Malinconico, M.; Laurienzo, P.; Tardy, A.; Guillaneuf, Y.; Lansalot, M.; D'Agosto, F.; Charleux, B. *J. Polym. Sci., Part A: Polym. Chem.* **2014**, *52*, 104.

(51) Delplace, V.; Harrisson, S.; Tardy, A.; Gigmes, D.; Guillaneuf, Y.; Nicolas, J. *Macromol. Rapid Commun.* **2014**, *35*, 484.

(52) Chung, I. S.; Matyjaszewski, K. *Macromolecules* **2003**, *36*, 2995.

(53) Smith, Q.; Huang, J.; Matyjaszewski, K.; Loo, Y.-L. *Macromolecules* **2005**, *38*, 5581.

(54) Delplace, V.; Guegain, E.; Harrisson, S.; Gigmes, D.; Guillaneuf, Y.; Nicolas, J. *Chem. Commun.* **2015**, *51*, 12847.

(55) Pan, C.-Y.; Lou, X.-D. *Macromol. Chem. Phys.* **2000**, *201*, 1115.

(56) Simakova, A.; Averick, S. E.; Konkolewicz, D.; Matyjaszewski, K. *Macromolecules* **2012**, *45*, 6371.

(57) Gaborieau, M.; Castignolles, P. *Anal. Bioanal. Chem.* **2011**, *399*, 1413.

(58) Sun, W.; Yu, F.; He, J.; Zhang, C.; Yang, Y. *J. Polym. Sci., Part A: Polym. Chem.* **2008**, *46*, 5518.

Chapter VI. Controlling Size and Surface Chemistry of Cationic Nanogels by Inverse Microemulsion ATRP

VI.1. Preface

This project was conducted in collaboration between our group and Prof. Jeffrey Hollinger's Group from the Biomedical Engineering Department at CMU. The project was started in order to develop novel materials to prevent heterotopic ossification (HO) by stopping the BMP-2 (bone morphogenetic protein 2) signaling cascade using siRNA. Our contribution was the development of novel siRNA delivery agents that were both biodegradable and biocompatible, and could effectively complex and deliver the siRNA cargo. Prof. Hollinger group's role was to evaluate and study effect of our materials in biological systems. Two types of polymeric materials were evaluated: cationic star copolymers, which were developed by Dr Hong Cho, and nanogels, developed by Dr Saadyah Averick. Both materials could deliver siRNA *in vitro* experiments. Furthermore, it was shown that nanogels complexed with siRNA could knockdown the expression of a protein in several *in vivo* mouse models including 1) expression of the green fluorescent protein and 2) the prevent formation of bone in a model of HO. Thus we were motivated to expand the chemistry of such types of materials.

Our initial results pointed to the superiority of the nanogels as the preferred polymeric architectures for siRNA delivery. We therefore sought to undertake a structure/function optimization providing enhancement of the nanogel siRNA delivery platform. Hydrophilic nanogels can be efficiently synthesized by ATRP in inverse

miniemulsion. However, often during such polymerization process, size of the nanogel would increase from an initial size of 100 – 150 nm to 250 - 400 nm due to the Ostwald ripening process. A review of the literature indicated that differences in the size of particles can dramatically alter the cellular delivery performance. Most literature reports demonstrated that particles of size below 200 nm had markedly better cellular internalization properties as well as more efficient endosomal escape. Therefore, our first aim was to develop a polymerization technique where we could efficiently control the size of the synthesized nanogels. Second, we sought to design nanogel particles that would have a core-shell polymer architecture. In these structures the core functionality is shielded by a functionalized shell. This architecture can be advantageous for preparing materials with exact control over core function, for drug loading and degradation, and shell properties, for surface charge, hydrophilicity, biocompatibility, and cell targeting via incorporation of targeting ligands into the shell.

This Chapter details how our stated aims were achieved through the preparation of cationic nanogels by ATRP of an inimer in an inverse microemulsion. This procedure allowed for preparation of nanogels with arrested Ostwald ripening resulting in preservation of the final nanogel particle size close to the initially formed monomer micelle. Additionally, such nanogels were capable of being modified with an amphiphilic shell through use of a reactive surfactant allowing a hydrophilic polymer to be introduced by "grafting from" the surface of the nanogel. Such core/shell materials can be conveniently synthesized by a "one-pot" method.

I designed, synthesized and performed all chemical characterization of all materials discussed in this Chapter. A former undergraduate student, Ernesto Acosta, helped to

generate and analyze some of the nanogels. TEM analysis was carried out by Dr Joseph Suhan from the Department of Biology at CMU. AFM analysis was performed by Jacob Mohin from Prof. Tomasz Kowalewski Group. All biological tests were performed by Dr Saadyah Averick and Dr Laura Beringer from the Laboratory for Biomolecular Medicine in the Allegheny Health Network Research Institute.

VI.2. Introduction

Polymer-based nucleic acid delivery systems are a powerful tool for the delivery of genes and have been used to treat a wide range of diseases including genetic disorders, various cancers and viral infections.[1-5] Polymer delivery platforms have come to the forefront of delivery systems due to the ability to tailor their composition and chemical functionality, while controlling polymer size, architecture and topology, using scalable synthetic procedures with retained biocompatibility of the conjugated active biological agent.[1,2,6] A plethora of nanosized delivery systems have been generated including micelles, hyperbranched polymers, random, block and star copolymers, and inorganic-polymer hybrids.[7-11] Among them it has been determined that nanogels, nanosized crosslinked polymer networks, are efficient delivery systems for both drugs and biomolecules.[6,12-19]

Various methods can be applied to the synthesis of nanogels including formation of chemically or physically crosslinked self-assembled amphiphilic copolymers.[16,18,20,21] Pre-assembly provides good control over composition due to use of preformed well-defined polymers. Mold-templated synthesis, like PRINT® technology, ensures uniformity and homogeneity of the nanogels.[22] The most prevalent nanogel preparation method is radical polymerization in dispersed media, which provides a simple one-step setup followed by polymerization of a wide spectrum of functional monomers in high yield.[23-27] Both free radical polymerization (FRP) and reversible deactivation radical polymerization (RDRP) methods, such as reversible addition-fragmentation chain transfer (RAFT)[23,28] and atom transfer radical polymerizations (ATRP)[22,26] were successfully applied to polymerizations in dispersed media, providing uniform crosslinked nanogels with control over internal and peripheral structure and reactive functionalities. Previously, we reported the preparation of

cationic nanogels by ATRP in inverse miniemulsion and their use in siRNA and plasmid DNA (pDNA) delivery.[26,29,30] These cationic nanogels had a diameter of 200 – 300 nm. However, some published data suggests that smaller particles of a size below 100 nm are more advantageous for the delivery of nucleic acids, due to formation of polyplexes that undergo endosomal escape more efficiently.[31,32] Therefore, we sought to prepare cationic nanogels under inverse microemulsion conditions where monomer micelles, with a diameter less than 100 nm, are spontaneously formed in the presence of two phases and a surfactant.[22,30,33]

Microemulsion polymerization utilizes high concentrations of surfactant; therefore it is thermodynamically stable and does not require additional homogenizing techniques beyond stirring.[22,30,33,34] Nevertheless, ATRP in inverse microemulsion has been rarely studied, possibly because significant optimization is required for each new comonomer system in order to form a stable microemulsion.[34-37] One of the main challenges for mini- and microemulsion polymerization is Ostwald ripening which occurs when monomer from smaller droplets diffuses into bigger ones.[34-37] This results in formation of larger particles and can lead to coalescence. A common approach to prevent Ostwald ripening is to add a co-stabilizer.[34-36] In the case of water in oil (w/o) mini- or microemulsion, these are typically salts or very lipophobic water soluble polymers, which can be formed *in situ* during polymerization.[34-37] However, the final polymer particles can still experience a 2-3 times increase in diameter compared to the initial micelles. Another approach to limit the Ostwald ripening process includes use of either a polymeric or reactive surfactant which can strongly adsorb on the w/o interface.[32,35,36] This approach requires synthesis of amphiphilic block copolymers as surfactants.

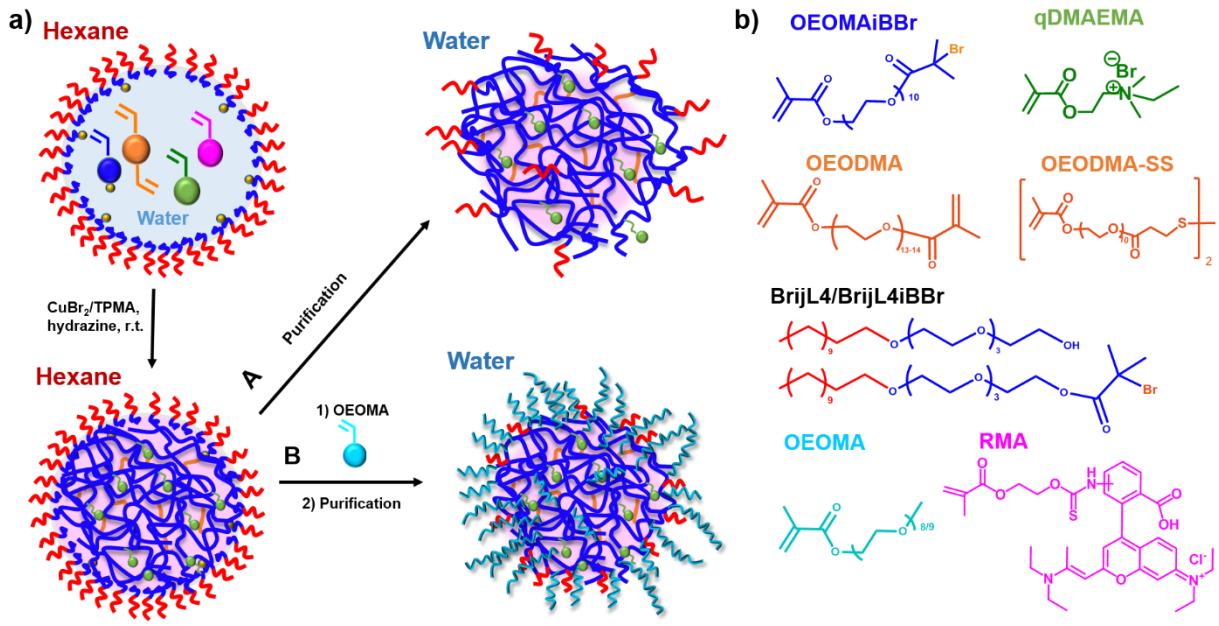

Scheme VI.1. Cationic nanogels synthesized by ATRP of a OEOMAiBBr inimer under inverse microemulsion conditions: a) synthesis of two types of nanogels with varied surface functionality; b) components utilized for nanogels synthesis

It was determined that the polymerization of a hydrophilic inimer, a monomer with an initiating group, by ATRP under inverse microemulsion conditions results in fast and efficient nucleation and polymerization, yielding final nanogel particles with a size similar to the initially formed micelle. A hydrophilic inimer, based on oligo(ethylene oxide) methacrylate (OEOMAiBBr), was copolymerized with a cationic monomer (qDMAEMA) and a crosslinker (OEODMA/OEODMA-SS) to form a cationic nanogel (**Scheme VI.1, route A**). Brij L4 was used as the surfactant because it had been successfully used previously for preparation of cationic nanogels by FRP.[25] An additional step forward was the use of a Brij L4-derived reactive surfactant (BrijL4iBBr), which was formed by esterification of Brij L4 with an ATRP initiator. Brij L4was selected to introduce hydrophobic functionality into the surface of the nanogel to improve delivery performance. In order to visualize internalization of nanogels into cells, a fluorescent dye monomer such as rhodamine methacrylate was incorporated into nanogels. Finally, water-soluble and

biocompatible polymer pOEOMA$_{500}$ was grafted from these cationic nanogels to improve their stability in water and potentially biocompatibility (**Scheme VI.1, route B**).[38-42]

VI.3. Results and discussion

VI.3.1. Cationic core synthesis and characterization.

The initial hydrophilic nanogels were synthesized via polymerization of a water-soluble monomer, OEOMA. Cationic nanogels were prepared by copolymerizing OEOMA with either DMAEMA or its quaternized derivative qDMAEMA, **Table VI.1**, entries 1-3. These initial results indicated that the original micelle size of 35 – 40 nm increased to 65 – 80 nm during these polymerizations, **Figure VI.1a**. One should note that although the diameter of the nanogels were only two times larger than the initially formed micelles, the volume of the polymer particles increased by a factor of 8, indicating inefficient (<15%) nucleation in the initial micelles. In ATRP, this can be caused by slow initiation. One way to ensure simultaneous initiation in all micelles is to increase the concentration of the ATRP initiator. However, this solution is thwarted by the use of a water soluble macroinitiator PEG_{2k}iBBr with a relatively high molecular weight (M_n= 2000), which would result in increased solids content. This, consequently, could lead to destabilization of the microemulsion. To preserve the ability to control composition and conditions of the formation of a stable microemulsion, a water soluble inimer OEOMAiBBr was prepared, **Scheme VI.2, Figure VI.13**. Previous studies on polymerization of inimers under microemulsion conditions indicated that the resulting increased initiator concentration resulted in a more efficient nucleation, providing smaller polymer particles upon completion of the polymerization.[43] Therefore, we investigated preparation of cationic nanogels from the designed hydrophilic inimer and a cationic monomer, qDMAEMA.

Table VI.1. Cationic nanogels synthesized by inverse microemulsion AGET ATRP.[a]

	$M_1/M_2/I/X/CuBr_2/L$[b]	$N_{SBr}/N_{\Sigma S}$[i]	Conv.,% (time, h)	D_0[j], nm	D[k], nm		ζ[l], mV
					In hexane	In water	
1	205/0/1/20/1/1.1[c,d]	0	73.3 (15)	39.7±1.0	66.3±0.1	-	-
2	205/40/1/20/1/1.1[c,e]	0	63.8 (15)	36.2±0.3	79.5±0.3	-	-
3	205/40/1/20/1/1.1[c,f]	0	55.7 (15)	35.3±0.5	68.4±0.7	-	-
4	88/12/0/20/1/1.1[g, h]	0	98.7 (3)	42.3±0.4	26.9±0.4	31.9±o.4	+15.9±1.5
5	88/12/0/20/1/1.1[g,h]	2	>99 (3)	36.6±0.5	35.8±0.4	30.0±3.4	+20.7±1.7
6	88/12/0/20/1/1.1[g,h]	4	>99 (3)	34.7±0.2	25.6±3.2	32.5±0.1	+20.3±3.6

[a] Polymerization conditions: M_1+X/H_2O/Surfactants/C_6H_6 = 0.5/0.55/1.4/7.5 (g) by weight, conducted at 25°C, reducing agent – hydrazine hydrate solution; [b] I – PEG_{2k}iBBr, X – OEODMA, L – TPMA; [c] $[M_1]$ = 1.3 M; [d] M_1/M_2 = $OEOMA_{300}$/-; [e] M_1/M_2 = $OEOMA_{300}$/DMAEMA; [f] M_1/M_2 = $OEOMA_{300}$/qDMAEMA; [g] $[M_1]$ = 0.6 M; [h] M_1/M_2 = OEOMAiBBr/qDMAEMA; [i] molar ratio of reactive surfactant BrijL4iBBr (SBr) to total amount of surfactant used (S); [j] D_0 – Z-average diameter of initial micelle; [k] D_f – Z-average diameter of nanogels after polymerization in hexane and in water (after purification); [l] ζ – zeta potential.

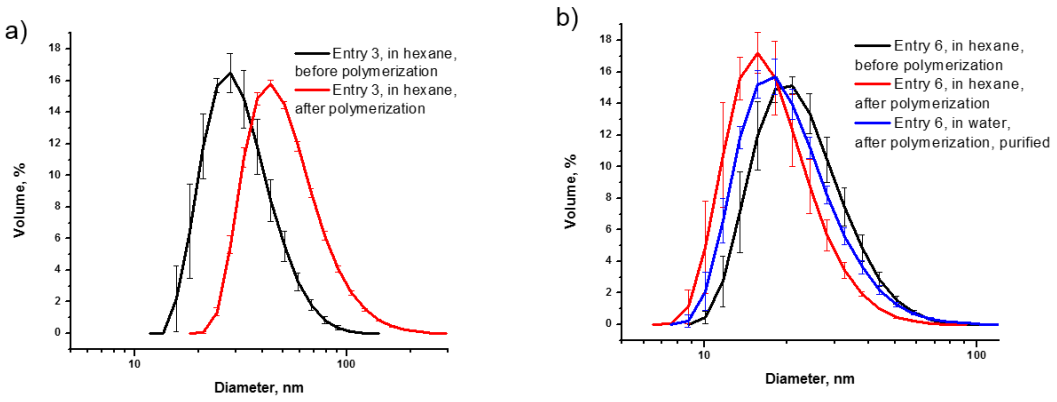

Figure VI.1. Size distribution by volume determined by DLS of initially formed micelles and formed nanogels after completed polymerization for a) monomer OEOMA and b) inimer OEOMAiBBr based nanogels.

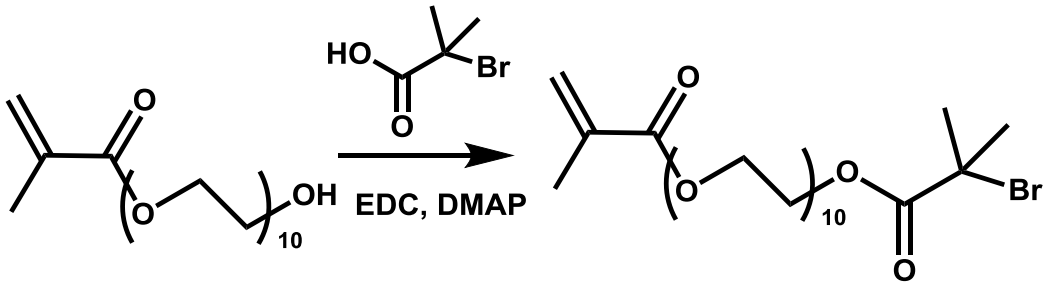

Scheme VI.2. OEOMAiBBr inimer synthesis.

Increased amounts of inimer should influence both polymerization rate and nucleation efficiency. Nanogels prepared by copolymerization of OEOMAiBBr and qDMAEMA had markedly faster rate of polymerization and good preservation of initial micelle size. After 3 h, the polymerization reached >99 % monomer conversion and no residual vinyl peaks could be detected by ^{1}H NMR (**Figure VI.2**). **Table VI.1**, entries 4 – 6, show that upon completion of the polymerization the size of the final nanogels were very similar to the size of the initially formed micelles, in the range of 25 – 40 nm. **Figure VI.1b** shows volume distribution by DLS for inimer copolymerization. It demonstrates that the micelle size did not increase during the polymerization and the final nanogels did not experience any significant swelling. This could be due to the relatively high content of the crosslinker in the final nanogel particle. Additional characterization by transmission electron microscopy confirmed the size of the formed nanogels and revealed their uniform spherical shape (**Figure VI.3**). TEM images of the negatively stained nanogels showed that they mainly consisted of particles in the range of 20 nm in diameter, but smaller and larger particles were also present.

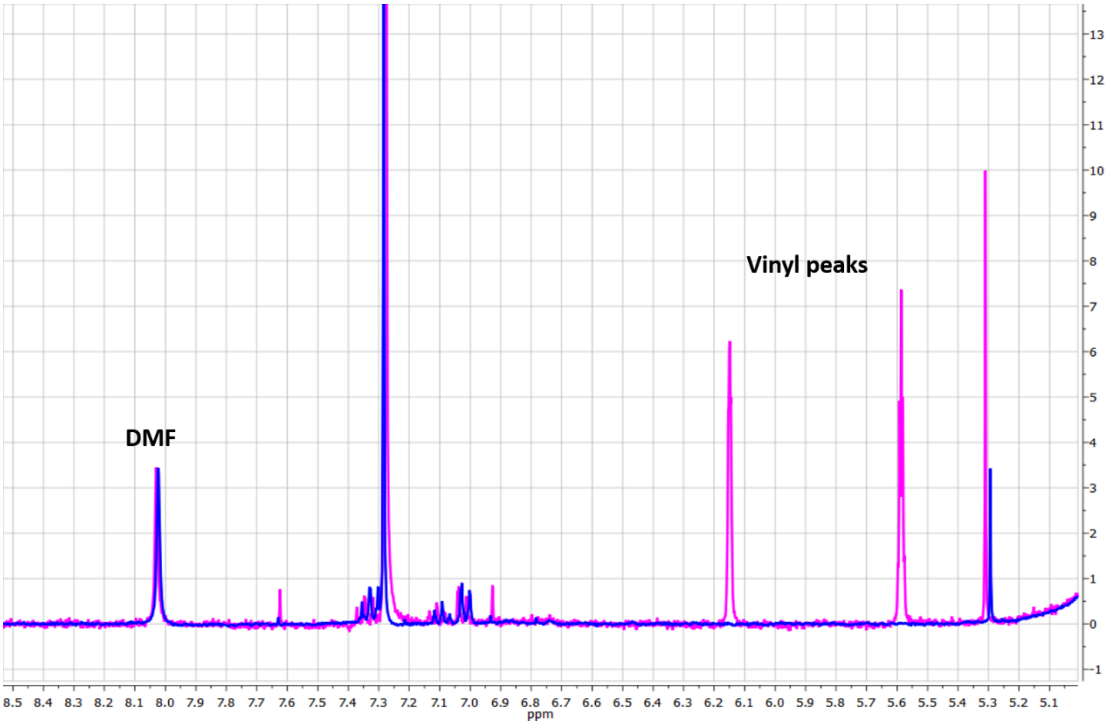

Figure VI.2. Proton NMR of polymerization mixture at t = 0 h (pink curve) and t = 3 h (blue curve) for polymerization conditions at entry 6, Table 1.

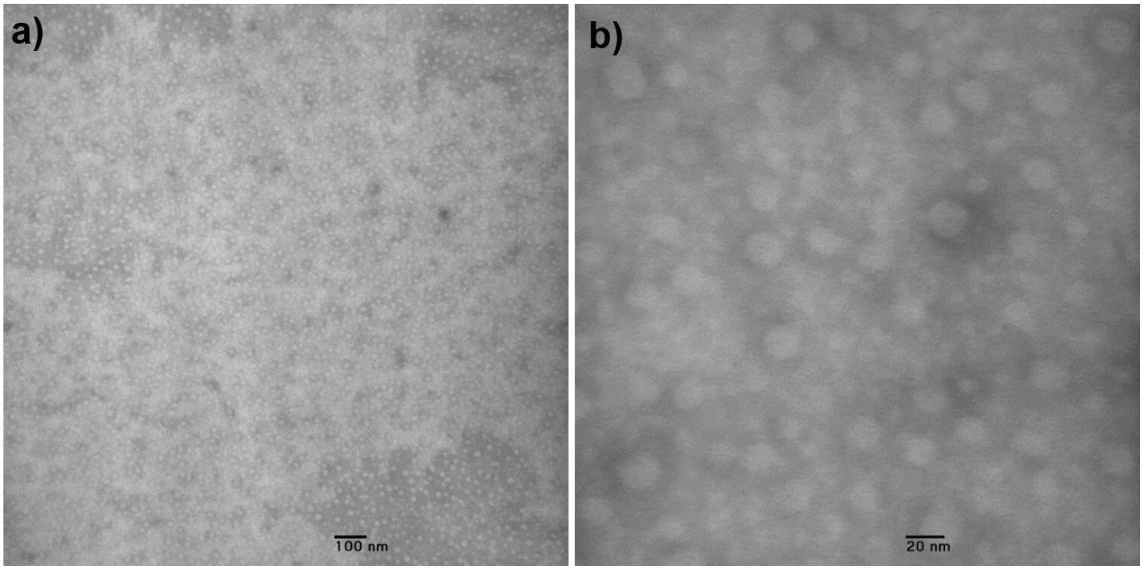

Figure VI.3. TEM images of inimer-based cationic nanogels at different magnifications (a, b) (sample from **Table VI.1**, entry 6): 50 µg/ml solution in water was negatively stained with phosphotungstic acid before analysis.

Incorporation of hydrophobic groups into nanomaterials enhances their cell internalization.[44] A convenient way to introduce hydrophobic moieties into such nanogels is via a reactive surfactant. Brij L4 surfactant was transformed into reactive surfactant by esterifying its hydroxyl chain end with an ATRP initiator moiety (

Scheme VI.3**, Figure VI.14**). Addition of a modified reactive surfactant results in covalent incorporation of hydrophobic moieties onto the surface of the nanogel.[45,46] The pristine Brij L4 surfactant was mixed with 2 and 4 mol. % of reactive BrijL4iBBr surfactant as reported in entries 5 and 6 in **Table VI.1**. Successful incorporation of the reactive surfactant was confirmed by an increase in contact angle of the films formed from corresponding nanogel solutions (**Table VI.2, Figure VI.4**). Incorporation of 2-4% of reactive surfactant did not lead to any aggregation of the nanogels in aqueous media as evidenced by DLS (**Figure VI.1b**).

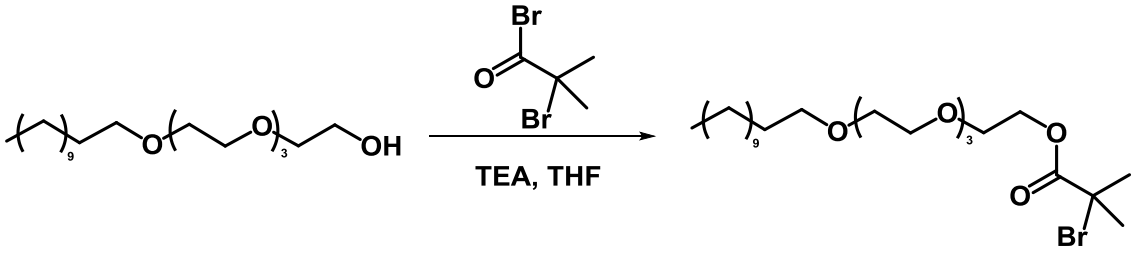

Scheme VI.3. BrijL4iBBr reactive surfactant synthesis.

Table VI.2. Contact angle measurements results for nanogels formed from micelles prepared with unmodified surfactants and nanogels prepared from micelles formed with surfactants including a fraction of BrijL4iBBr reactive surfactant.

Entry from Table 1	Contact Angle
4	31.3±3.2
5	46.7±3.9
6	55.8±2.2

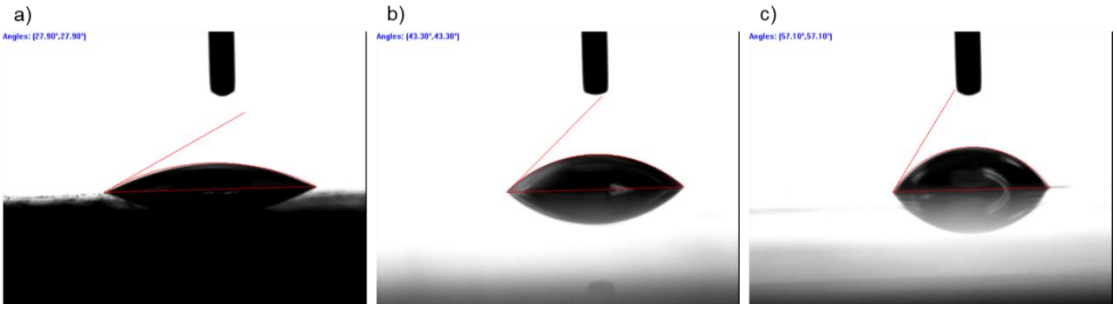

Figure VI.4. Change in contact angle upon incorporation of reactive surfactant BrijL4iBBr: a) no reactive surfactant used; b) 2 mol. % and c) 4 mol. % of reactive surfactant added to the unmodified surfactant.

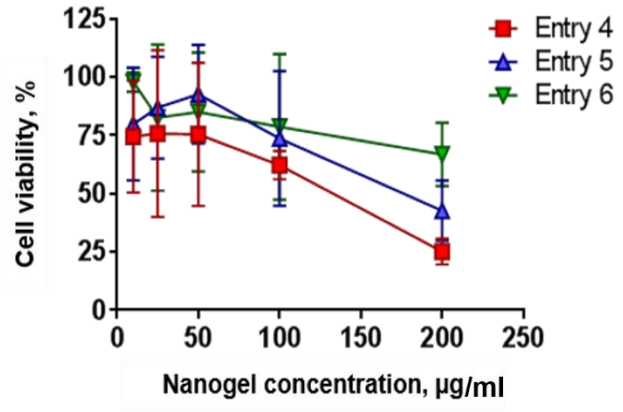

Figure VI.5. Cytotoxicity of cationic inimer-based nanogels for polymers in **Table VI.1**, entry 4, 5, and 6 after incubation at 72 h.

The cationic nanogels prepared from the inimer were further evaluated for biocompatibility and polyplex formation with plasmid DNA (pDNA). The biocompatibility of the cationic nanogels prepared by inverse microemulsion was tested using human embryonic kidney cells (HEK 293). Cell viability was measured after 72 h using a luminescent ATP viability assay and the results indicated that the cationic nanogels were biocompatible up to a concentration of 0.2 mg/ml (**Figure VI.5**). Interestingly, among the tested set, the nanogels with higher content of hydrophobic groups on the surface showed the highest biocompatibility. The cellular internalization of rhodamine tagged

nanogels, at a concentration of 50 µg/ml nanogels, was measured 24 hours after exposure to HEK293 cells. The localized rhodamine fluorescence indicates that the nanogels can successfully self-transfect into the cells (**Figure VI.6**).

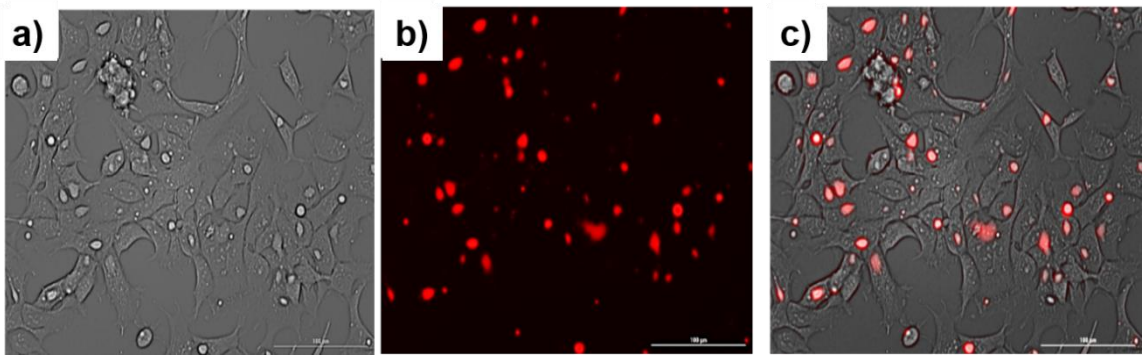

Figure VI.6. HEK cells incubated 24 h with 50 µg/ml of rhodamine tagged nanogels prepared with 4. mol. % of BrijL4iBBr (entry 6, Table 1). Scale bar = 100 µm.

Finally, the ability of the cationic nanogels to form polyplexes with pDNA was measured, **Figure VI.7**. All tested cationic nanogels were capable of complexing pDNA, but nanogels with introduced surface hydrophobicity (**Table VI.1**, entries 5-6) showed better complexation ability than the nanogel synthesized without any reactive surfactant (**Table VI.1**, entry 4). From **Figure VI.7**, it is evident that the nanogel without any hydrophobic patches on its surface could complex pDNA only at a weight ratio 3 of nanogel particles to one pDNA, while both samples with introduced surface hydrophobicity could form a complex with pDNA at 0.1 ratio of nanogel to pDNA. Even though most contribution to polyplex formation comes from the electrostatic interactions, hydrophobic interactions with nucleic acid bases could also improve binding and affinity.[47]

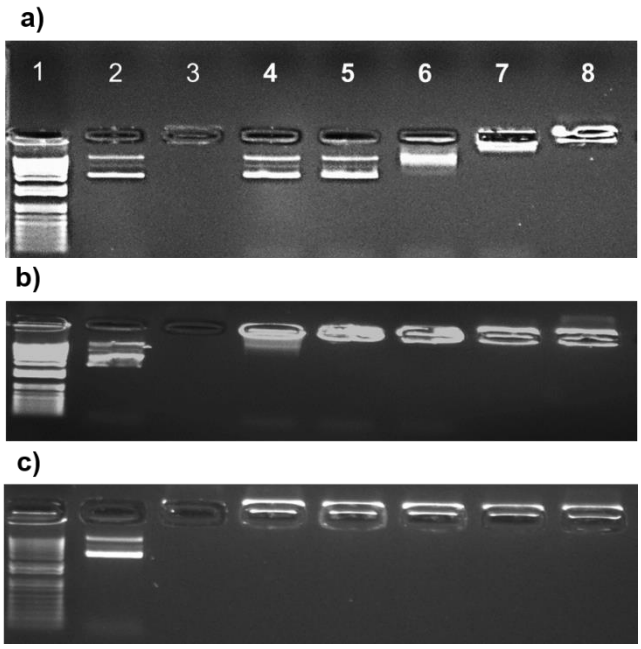

Figure VI.7. Agarose gel electrophoresis of incubated cationic inimer-based nanogels with pDNA: a) entry 4, Table 1; b) entry 5, Table 1; c) entry 6, Table 1. Lanes: 1 – 1 kb DNA ladder; 2 –pDNA control; 3 – cationic nanogel control; lanes 4-8 are correspond to the following nanogel:pDNA weight ratios : 0.1; 0.7; 1; 3; 10.

VI.3.2. Core-shell nanogels synthesis and characterization.

Based upon literature reports,[44,48-50] we designed nanogels with increased hydrophobicity to improve the cellular delivery efficiency of the polymer carrier. Therefore, the second part of this Chapter, reports the development of the next generation cationic nanogels with varied amounts of reactive surfactant. However, the enhanced delivery potential must be balanced with the increased probability of particle aggregation due to increased amount of hydrophobic groups on the surface of the nanogel. Furthermore, increased nanogel hydrophobicity may induce plasma protein surface adsorption and increased uptake by macrophages during in vivo application.[51,52] Thus, these new nanogels have an additional feature of a grafted $pOEOMA_{500}$ shell for enhanced hydrophilicity and biocompatibility (**Scheme VI.1**, route B). In addition, biodegradability of the nanogels was ensured via incorporation of a disulfide group in the cross-linker.

Table VI.3. Cationic core-shell nanogels synthesized by inverse microemulsion AGET ATRP.[a]

	$M_1/M_2/M_3/X/CuBr_2/L/BrijL4iBBr$	$R_{S/P}$	Nanogel Architecture	D^e, nm PBS	ζ^f, mV
1	88/12/0/12/1/1.1/56	0.56	Core	41.3±1.3	+21.3±0.5
2	88/12/0/12/1/1.1/108	1.08	Core	31.3±0.8	+33.5±0.6
3	88/12/0/12/1/1.1/242	2.42	Core	28.6±0.5	+27.0±0.6
4	88/12/144/12/1/1.1/0	0	Core-Shell	50.0±1.3	+28.4±2.5
5	88/12/144/12/1/1.1/56	0.56	Core-Shell	50.8±2.0	+21.6±2.5
6	88/12/144/12/1/1.1/108	1.08	Core-Shell	58.7±1.1	+24.0±1.7
7	88/12/144/12/1/1.1/242	2.42	Core-Shell	62.0±0.5	+27.0±0.9

[a] Polymerization conditions: $M_{1,3}+X/H_2O/Surfactants/C_6H_6$ = 0.5/0.55/1.4/7.5 (g) by weight, conducted at 25°C, reducing agent – hydrazine hydrate solution; M_1 – OEOMAiBBr; M_2 – qDMAEMA; M_3 – $OEOMA_{500}$; X – OEODMA-SS, L – TPMA; [c] $[M_1]$ = 0.6 M; $R_{S/P}$ – molar ration of BrijL4iBBr to PEG-containing components (M_1, X) in the core of nanogel; [e] D_f – Z-average diameter of nanogels in PBS; [f] ζ – zeta potential.

The functional nanogels with a core-shell structure were synthesized by first preparing a cationic core, comprised of inimer OEOMAiBBr, qDMAEMA and a disulfide-containing crosslinker OEOMA-SS. The composition of the core was varied by changing the amount of the reactive surfactant BrijL4iBBr from $R_{S/P}$ = 0.56 to 1.08 to 2.42 molar ratio to the PEG-based components of the core, the inimer and crosslinker (**Table VI.3**, entries 1 – 3). Due to the relatively large amounts of alkyl bromides in the core, imparted by the use of the inimer, the hydrophilic shell could be grafted from the particle in a "one-pot" method, i.e. without purification of the core. In order to graft the shell, $OEOMA_{500}$ monomer was mixed with the copper complex and water (50/50 v/v), added to the microemulsion, and stabilized with additional surfactant and continuous phase. The microemulsion was degassed, and additional reducing agent was added to generate the active catalyst species, **Table VI.3**, entries 5 – 7. A control nanogel was prepared without

addition of a reactive surfactant to evaluate the effects of differences in hydrophobicity on degradation and biological performance, **Table VI.3,** entry 4.

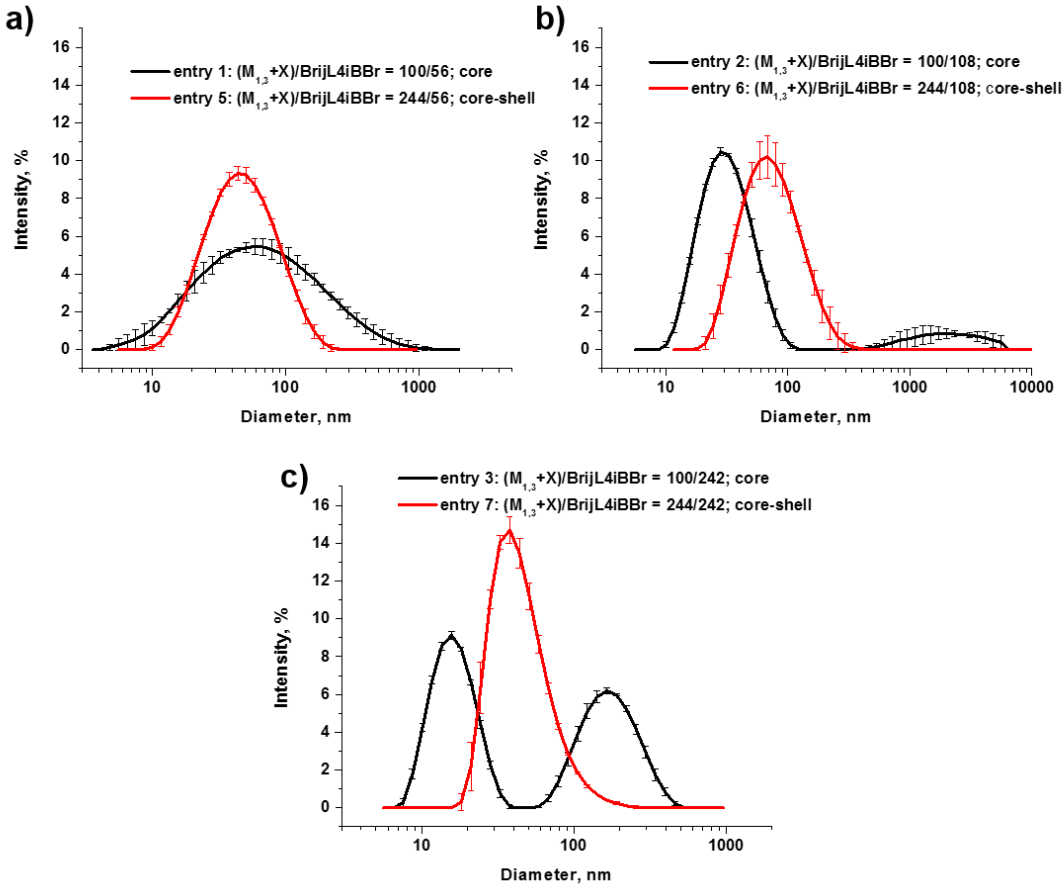

Figure VI.8. Aggregation behavior of cationic core versus core-shell nanogel in PBS: 1 mg/ml of nanogel in PBS was filtered through 0.45 µm PTFE filter prior to measurement.

After polymerization was complete, the nanogels were purified and their Zeta potential and size were characterized by DLS (**Table VI.3**). Both core and core-shell nanogels had similar positive zeta potential values, while the size measurements showed a 1.2-2.2 times increase in volume as one transitioned from core to core-shell particles. Aggregation of the cores was a function of the ratio of hydrophobicity/hydrophilicity in the core, i.e. the ratio of BrijL4iBBr to PEG-based components (OEOMAiBBr, OEODMA-SS, $OEOMA_{500}$) (**Figure VI.8**). The largest aggregation was observed in the

sample with a $R_{S/P}$ = 2.42. In all cases the aggregation was remediated by the grafting of a hydrophilic shell from the nanogel particle. Such shell effect demonstrated the advantages of a controlled surface functionality to influence particle dynamics and behavior.

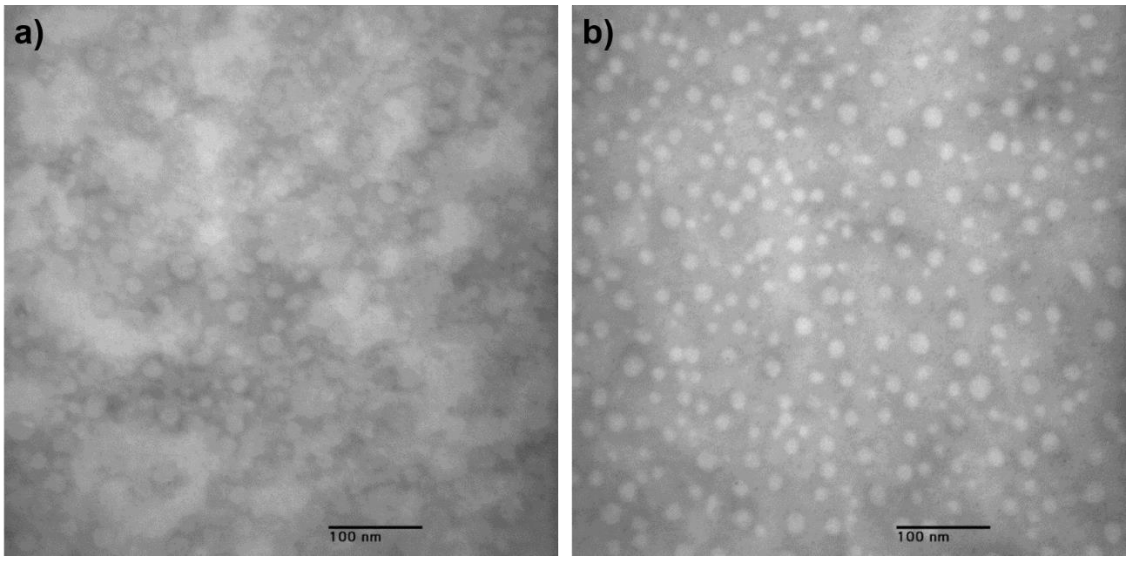

Figure VI.9. TEM images of inimer-based cationic core (a) and core-shell nanogel (b) (samples from **Table VI.1**, entry 1, 5): a 50 µg/ml solution in water was negatively stained with phosphotungstic acid before analysis.

Both TEM and AFM were used to directly characterize the core and core-shell nanogels. TEM of the negatively stained core and core-shell nanogels revealed particles with a circular shape without demonstrating any detectable difference in size, presumably due to a dehydrated state of the nanogel particles (**Figure VI.9**). AFM, however, was able to ascertain a difference of the core and core-shell particles (**Figure VI.10**). The phase image of the core structure showed uniform mechanical properties throughout the particle. The phase image of the core-shell nanogels revealed a clear demarcation of the core and shell regions of the particles: darker core was surrounded by lighter shell halo.

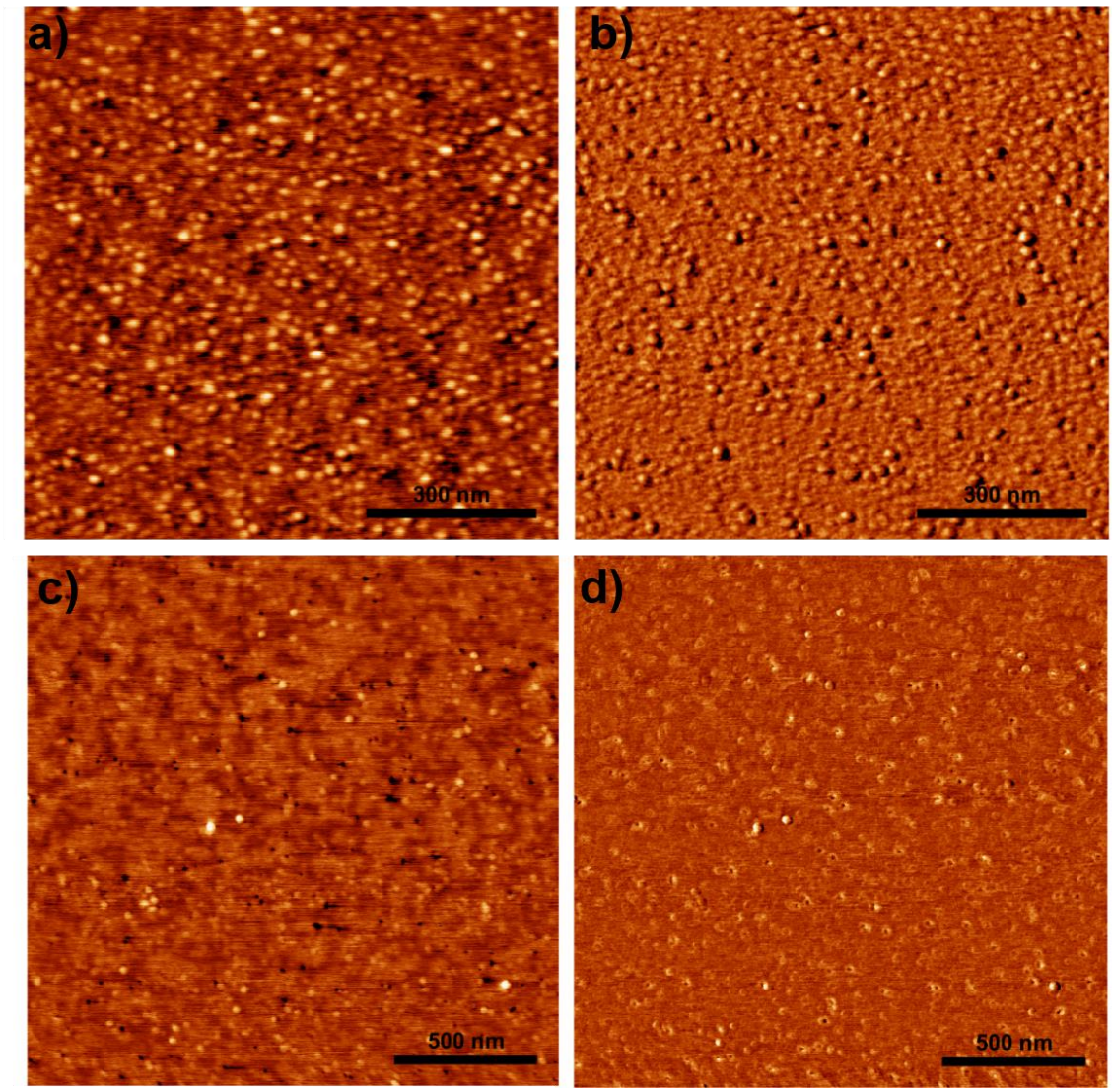

Figure VI.10. Height (left) and phase (right) AFM image for cationic core nanogel (a, b) and core-shell nanogel (c, d) (samples from **Table VI.1**, entry 1, 5): 50 µg/ml solution in water was drop casted on mica and dried under nitrogen flow before imaging.

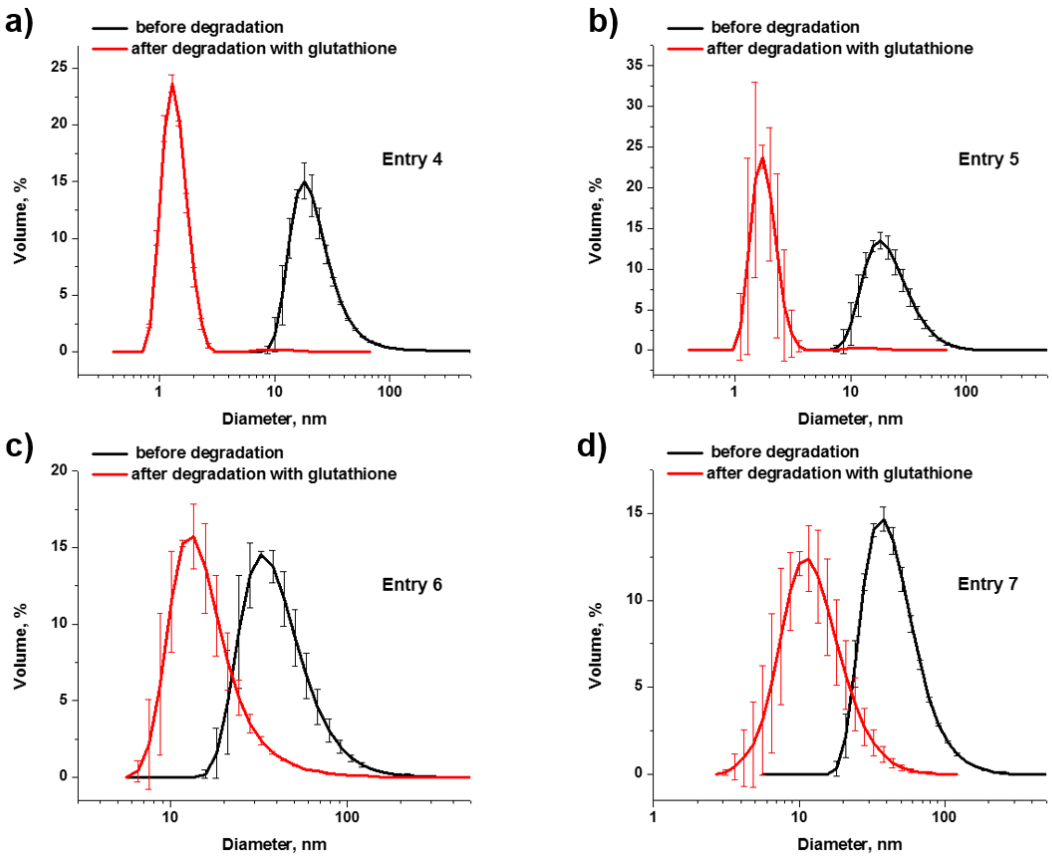

Figure VI.11. Core-shell nanogels degradation after incubation in the presence of glutathione for 3 days. 2 mg/ml of nanogel was dispersed in 100 mM glutathione solution in PBS.

Degradation of the core-shell nanogels can take place by the hydrolysis of either or both ester bonds and disulfide bonds present in the material. Reduction induced degradation was studied by incubating the core-shell nanogels with 100 mM of glutathione at 37°C. After 3 days, the solutions were analyzed by DLS to detect any decrease in the diameter of the nanogels (**Figure VI.11**). Full degradation, resulting in formation of a peak < 10 nm, was detected for the samples prepared either without any reactive surfactant RS/P = 0 or the lowest amount out of the array $R_{S/P}$ = 0.56 (**Figure VI.11a, b**). However, for samples with increased hydrophobicity ratios $R_{S/P}$ = 1.08 or 2.42, total degradation was not achieved resulting in degradation products of a size of approximately 10 nm. Such an effect

is likely due to the presence of a barrier to water and water-soluble molecules created by increased content of hydrophobic moieties present on the reactive surfactant. The rate of glutathione diffusion into the core of the nanogel could be slower as a consequence of the higher surface content of hydrophobic residues from the presence of the reactive surfactant. However, no difference was detected in the rate of hydrolytic degradation of the particles (**Figure VI.12**). The core-shell nanogels were incubated in 5% NaOH solution to degrade ester bonds present in the inimer and the crosslinker. Hydrolysis of all tested nanogels resulted in formation of degradation products of similar size suggesting that varied hydrophobicity didn't influence degradation under these conditions.

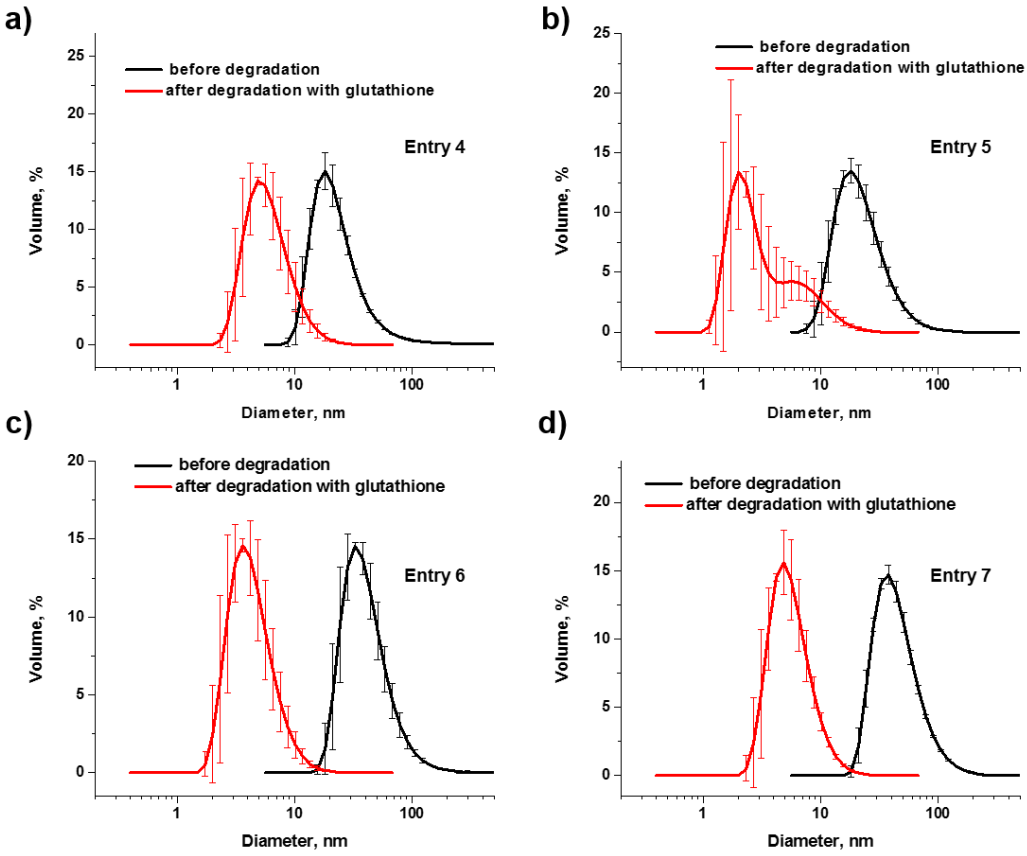

Figure VI.12. Core-shell nanogels hydrolytic degradation: 2 mg/ml of nanogel was dispersed in 5% NaOH. Measurements were taken after 24 h.

VI.4. Conclusions

This chapter reports the successful synthesis of cationic nanogels by ATRP using a hydrophilic inimer under inverse microemulsion conditions. The selection of the hydrophilic inimer instead of a regular monomer/initiator mixture ensures quick initiation providing efficient nucleation, resulting in formation of nanogels without any increase in size, compared to initially formed micelles. Surface functionality of such nanogels can be tuned by incorporation of a reactive hydrophobic surfactant into the initial micelle. The resulting cationic nanogels were biocompatible over a range of concentrations and capable of internalization into mammalian cells. They formed stable complexes with pDNA at a ratio as low as 0.1 of nanogel to nucleic acid.

Variable degrees of hydrophobicity were successfully introduced onto the surface of the nanogels through the use of reactive surfactants. However, one negative effect of increased reactive surfactant ratios was aggregation of the nanogels. Therefore, we devised a method to graft a hydrophilic shell from the core of the nanogel to stabilize the individual particles. The stabilized core-shell nanogels could be degraded either in the presence of biologically relevant reducing agents such as glutathione or under hydrolytic basic conditions. Our results demonstrated that through the use of an ATRP inimer under inverse microemulsion conditions well-defined nanogels with complex core chemistry can be prepared and stabilized through the use of a grafted hydrophilic shell. The work in this chapter opens up new avenues for advanced drug delivery systems.

VI.5. Experimental section

VI.5.1. Materials.

Cu(II)Br_2 (99%, Sigma Aldrich), hydrazine hydrate (reagent grade, N_2H_4 50-60 % , Sigma Aldrich), oligo(ethylene glycol) methyl ether methacrylate (average molecular weight ~300 g/mol, $OEOMA_{300}$, Sigma Aldrich), oligo(ethylene glycol) dimethacrylate (average molecular weight ~750 g/mol, OEODMA, Sigma Aldrich), oligo(ethylene glycol) methacrylate (average molecular weight ~500 g/mol, $OEOMA_{500\text{-}OH}$, Sigma Aldrich), hexane (Laboratory Reagent, ≥95%, Sigma Aldrich), Brij L4 (Sigma Aldrich), 4-(dimethylamino)pyridine (≥99%, Sigma Aldrich), N-(3-dimethylaminopropyl)-N'-ethylcarbodiimide hydrochloride (Carbosynth), methacryloxyethyl thiocarbamoyl rhodamine B (Polysciences, Inc), hydroquinone (≥99.5%, Sigma Aldrich), 2-bromo-2-methylpropionic acid (98%, Sigma Aldrich), 4-(dimethylamino)pyridine (99%, Sigma Aldrich), 2-bromo-2-methylpropionyl bromide (98%, Sigma Aldrich), were used without further purification. 2-(dimethylamino)ethyl methacrylate (DMAEMA, Sigma Aldrich) was quaternized with bromoethane as described previously to obtain qDMAEMA.[53] Tris(2-pyridilmethyl)amine (TPMA) was synthesized according to previously reported procedure.[54]

VI.5.2. Instrumentaion and characterization.

Nanogel particle size and zeta potential were measured using a Zetasizer Nano from Malvern Instruments. All samples were filtered through 0.45 micron PVDF filter prior to measurements. Monomer conversion, BrijL4iBBr and PEGMAiBBr were characterized via ^1H NMR in $CDCl_3$ using a Bruker Avance 300MHz instrument. TEM images were taken on Hitachi H-7100. Nanogels samples were diluted to concentration of 50μg/ml, and

negatively stained by phosphotungstic acid prior to imaging. Tapping mode-atomic force microscopy (TM-AFM) measurements were taken using a Veeco Metrology Group Digital Instruments Dimension V with NanoScope V controller and NanoScope 7 software. NT-MDT/K-Tek Nano NSG30 cantilevers with a spring constant of 22–100 N/m and resonance frequency of 240–440 kHz we used. Cantilevers were operated between 0-15% away from their resonant frequency, with varying amplitude setpoints and integral gain near 0.5. Imaging was performed with scan rates about 0.3-0.8 Hz, depending on image size, to insure low tip velocity and thus good tracking of both nano- and micro- sized features. Nanogels samples were diluted to concentration of 50µg/ml, drop casted onto mica substrate (New York Mica Company), and dried under nitrogen flow.

VI.5.3. OEOMAiBBr inimer synthesis.

The OEOMAiBBr inimer was synthesized via esterification. $OEOMA_{500\text{-}OH}$ and was purified prior to use to remove PEGDMA.[55] 2-Bromo-2-methylpropionic acid (0.10 mol, 22.10 g), and N-(3-dimethylaminopropyl)-N'-ethylcarbodiimide hydrochloride (0.15 mol, 27.90 g) were dissolved in 100 ml of DCM in a round bottom flask and cooled in an ice bath. $OEOMA_{500\text{-}OH}$ (0.06 mol, 30 mL) and 4-(dimethylamino)pyridine (0.008 mol, 1.02 g) were dissolved in 100 ml of DCM and added dropwise into the solution in the reaction flask. The reaction flask was sealed, the solution was removed from the ice bath and allowed to react overnight at room temperature. The inimer was purified by washing the solution with dilute HCl (0.1 M) three times, once with water, then three times with saturated $NaHCO_3$, followed by a final water wash. The final organic solution was then dried over magnesium sulfate, filtered and concentrated in a rotary evaporator. To prevent

degradation and crosslinking inhibitor (hydroquinone) was added to the inimer solution prior to solvent removal. Final product was characterized by ^{1}H NMR (**Figure VI.13**).

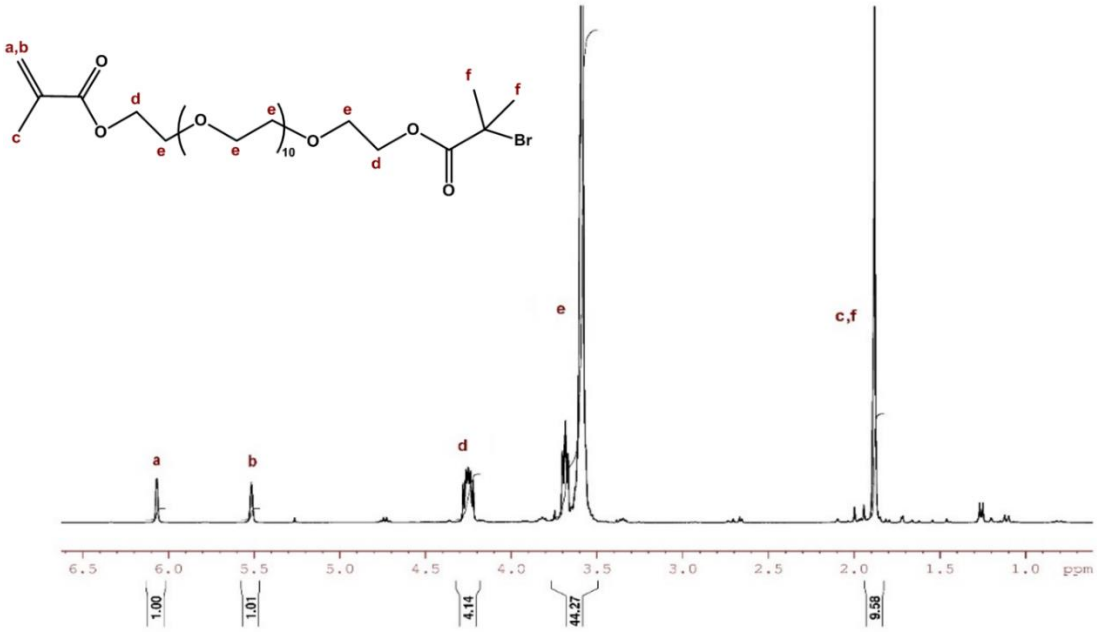

Figure VI.13. ^{1}H NMR of inimer OEOMAiBBr in $CDCl_3$.

VI.5.4. BrijL4iBBr reactive surfactant synthesis.

2-Bromo-2-methylpropionyl bromide (0.03moles, 6.99 g) and triethylamine (0.07 moles, 3.35 g) were dissolved in 40mL of THF in a round bottom flask that was then immersed in an ice bath. A solution of Brij L4 dissolved in 10 ml of THF (0.028 moles, 10.00 g) was added dropwise to the solution and allowed to react overnight at room temperature. The product was filtered and the solvent was removed by rotary evaporation. The product was then added to a cooled 5% Na_2CO_3 solution and extracted three times with 100mL DCM. The solution was then washed with water, dried over magnesium sulfate and the solvent removed by rotary evaporation. Final product was characterized by ^{1}H NMR (**Figure VI.14**).

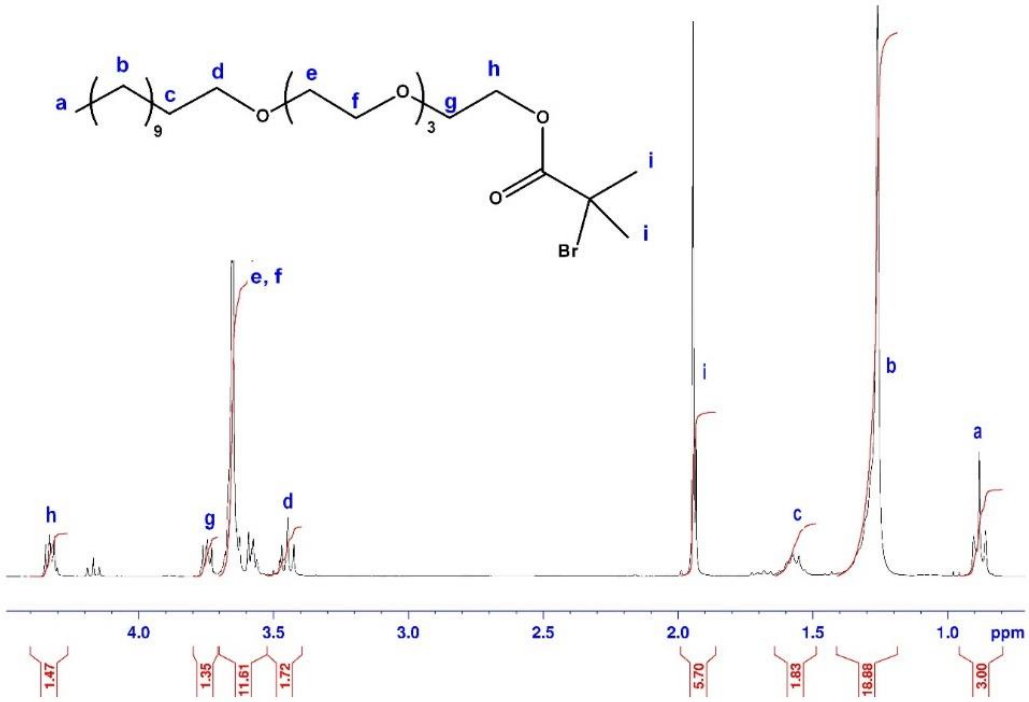

Figure VI.14. ^{1}H NMR of reactive surfactant BrijL4iBBr $CDCl_3$.

VI.5.5. Synthesis of cationic nanogels via AGET ATRP in an inverse microemulsion.

The nanogels were synthesized by inverse microemulsion AGET ATRP. The aqueous phase consisted of a solution of OEODMA (0.133 mmol, 100.0 mg), OEOMAiBBr (0.6 mmol, 400 mg), qDMAEMA (0.08 mmol, 20 mg) in in 275 mg of Cu(II)Br_2/TPMA stock solution in water (1/1.1, 5.5 mg/ml of $CuBr_2$), 275 mg of ultrapure water and 0.1mg of methacryloxyethyl thiocarbamoyl rhodamine B. The aqueous phase and 1.5 g of surfactant were added to 11.5 ml of hexane. The solution was vigorously shaken to form a stable microemulsion. The solution was degassed by bubbling with nitrogen for 15 minutes, and 4 µl of hydrazine hydrate was injected to the reaction under nitrogen to initiate polymerization, which was stopped after 3 hours reaction at room temperature by exposing the microemulsion to air. The nanogels solution was diluted with 10 ml of water, and the

mixture was poured in 300 ml of a 3:1 hexane/1-butanol solution and stirred for 2 h. After that aqueous layer was dialyzed in the sequence of solvents THF-water-acetone-water-acetone-water 10 h each, and then 2 more times against water to obtain the final solution, which was stored in the fridge.

VI.5.6. Synthesis of cationic core-shell nanogels via AGET ATRP in an inverse microemulsion.

The nanogels were synthesized by inverse microemulsion AGET ATRP. The aqueous phase consisted of a solution of OEODMA (0.133 mmol, 100.0 mg), OEOMAiBBr (0.6 mmol, 400 mg), qDMAEMA (0.08 mmol, 20 mg) in 275 mg of Cu(II)Br_2/TPMA stock solution in water (1/1.1, 5.5 mg/ml of $CuBr_2$), 275 mg of ultrapure water and 0.1mg of methacryloxyethyl thiocarbamoyl rhodamine B. The aqueous phase and 1.5 g of surfactant were added to 11.5 ml of hexane. The solution was vigorously shaken to form a stable microemulsion. The solution was degassed by bubbling with nitrogen for 15 minutes, and 4 µl of hydrazine hydrate was injected to the reaction under nitrogen to initiate the polymerization. After 3 hours more 11.5 ml of hexane was added. Then solution of 500 mg of $OEOMA_{500}$ in 275 mg of Cu(II)Br_2/TPMA stock solution in water (1/1.1, 5.5 mg/ml of $CuBr_2$) and 275 mg of ultrapure water was added. Mixture was stabilized by addition of 1 ml of surfactant. The solution was degassed by bubbling with nitrogen for 15 minutes, and 8 µl of hydrazine hydrate was injected to the reaction under nitrogen to initiate the polymerization. Reaction was allowed to run overnight and was stopped by exposing the microemulsion to air. The nanogels solution was diluted with 10 ml of water, and the mixture was poured in 300 ml of a solution containing a 3:1 ratio of hexane/1-butanol and stirred for 2 h. After that aqueous layer was dialyzed in the sequence of solvents THF-

water-acetone-water-acetone-water 10 h each, and then 2 more times against water to obtain a final solution, which was stored in the fridge.

VI.5.7. Degradation conditions.

Degradation via disulfide bonds: 2 mg/ml of core-shell nanogels were dissolved in 100 mM of glutathione. Solution was purged with nitrogen and stirred at 37°C for 3 days. *Hydrolytic degradation:* 2 mg/ml of core-shell nanogels were incubated in 5 wt. % NaOH for 48 h. Final samples were filtered through 0.22 μm PTFE filter, and analyzed by DLS. The reported value is the average of 3 measurements.

VI.5.8. Biology materials and methods

Agarose gel preparation. Agarose gels were created using a 1% agarose in 1x TAE buffer and allowed to set for approximately 30 min after addition of EtBr to the solution prior to the gel run. Samples were prepared by mixing nuclease free water, 10 % glycerol, and polymers (concentration varied depending upon the type) before addition of a constant amount of DNA and allowed to react for 30 min. Gels were run at 100 kV for approximately 30 min before being photographed with a gel doc machine in order to determine polymer-DNA binding efficiency.

Promega Cell Titer Glo Assay to assess viability. A luminescent ATP assay was performed in order to assess the biocompatibility of the newly synthesized rhodamine polymers used for DNA complexation. All cells were seeded into a 96-well TCP plate at approximately 40k cells/ well and allowed to grow overnight prior to addition of polymers. Concentrations tested included 10, 25, 50, 100, and 200 μg. The Cell Titer Glo assay was performed according to the manufacturer's protocol. Briefly, cells were incubated for a specific amount of time (72 h) then incubated with an equal volume of cell titer glo reagent

for 10 min, with one min. of vigorous shaking to induce cell lysis. Luminescence was measured using the area scan function on the Biotek spectrophotometer with an average RLU being calculated within a 4 x 4 grid for each well.

Internalization assay of Entry 4,5, and 6 within HEK 293 cells. An internalization assay was conducted in order to determine how efficiently the rhodamine modified cationic polymers were transported across the cell membrane. Cells were seeded into a 12-well plate at a density of approximately 500k cells/well and allowed to grow overnight. Polymers were added to each cell well at 25 or 50 μg. Only polymers from entries 5 and 6 were used in the internalization assay due to preliminary research indicating entry 4 was a poor transfection candidate.

VI.6. References

(1) Pack, D. W.; Hoffman, A. S.; Pun, S.; Stayton, P. S. *Nat. Rev. Drug. Discov.* **2005**, *4*, 581.

(2) Wong, S. Y.; Pelet, J. M.; Putnam, D. *Prog. Polym. Sci.* **2007**, *32*, 799.

(3) Whitehead, K. A.; Langer, R.; Anderson, D. G. *Nat. Rev. Drug. Discov.* **2009**, *8*, 129.

(4) Ferraro, B.; Morrow, M. P.; Hutnick, N. A.; Shin, T. H.; Lucke, C. E.; Weiner, D. B. *Clin. Infect. Dis.* **2011**, *53*, 296.

(5) Breaker, R. R. *Nature* **2004**, *432*, 838.

(6) Oh, J. K.; Drumright, R.; Siegwart, D. J.; Matyjaszewski, K. *Prog. Polym. Sci.* **2008**, *33*, 448.

(7) Kesharwani, P.; Gajbhiye, V.; Jain, N. K. *Biomaterials* **2012**, *33*, 7138.

(8) Ahmed, M.; Narain, R. *Prog. Polym. Sci.* **2013**, *38*, 767.

(9) Kesharwani, P.; Jain, K.; Jain, N. K. *Prog. Polym. Sci.* **2014**, *39*, 268.

(10) Li, W.; Zhan, P.; De Clercq, E.; Lou, H.; Liu, X. *Prog. Polym. Sci.* **2013**, *38*, 421.

(11) Wei, H.; Zhuo, R.-X.; Zhang, X.-Z. *Prog. Polym. Sci.* **2013**, *38*, 503.

(12) Ramos, J.; Forcada, J.; Hidalgo-Alvarez, R. *Chem. Rev.* **2013**, *114*, 367.

(13) Forbes, D. C.; Peppas, N. A. *ACS Nano* **2014**, *8*, 2908.

(14) Sunasee, R.; Wattanaarsakit, P.; Ahmed, M.; Lollmahomed, F. B.; Narain, R. *Bioconjugate Chem.* **2012**, *23*, 1925.

(15) Raemdonck, K.; Demeester, J.; De Smedt, S. *Soft Matter* **2009**, *5*, 707.

(16) Kabanov, A. V.; Vinogradov, S. V. *Angew. Chem. Int. Ed.* **2009**, *48*, 5418.

(17) Forbes, D. C.; Creixell, M.; Frizzell, H.; Peppas, N. A. *Eur. J. Pharm. Biopharm.* **2013**, *84*, 472.

(18) Nuhn, L.; Braun, L.; Overhoff, I.; Kelsch, A.; Schaeffel, D.; Koynov, K.; Zentel, R. *Macromol. Rapid Commun.* **2014**, *35*, 2057.

(19) Averick, S. E.; Magenau, A. J. D.; Simakova, A.; Woodman, B. F.; Seong, A.; Mehl, R. A.; Matyjaszewski, K. *Polym. Chem.* **2011**, *2*, 1476.

(20) Urakami, H.; Hentschel, J.; Seetho, K.; Zeng, H.; Chawla, K.; Guan, Z. *Biomacromolecules* **2013**, *14*, 3682.

(21) Ryu, J.-H.; Jiwpanich, S.; Chacko, R.; Bickerton, S.; Thayumanavan, S. *J. Am. Chem. Soc.* **2010**, *132*, 8246.

(22) Gratton, S. E. A.; Pohlhaus, P. D.; Lee, J.; Guo, J.; Cho, M. J.; DeSimone, J. M. *J. Control. Release* **2007**, *121*, 10.

(23) Cunningham, M. F. *Prog. Polym. Sci.* **2008**, *33*, 365.

(24) Min, K.; Matyjaszewski, K. *Central European Journal of Chemistry* **2009**, *7*, 657.

(25) McAllister, K.; Sazani, P.; Adam, M.; Cho, M. J.; Rubinstein, M.; Samulski, R. J.; DeSimone, J. M. *J. Am. Chem. Soc.* **2002**, *124*, 15198.

(26) Oh, J. K.; Tang, C.; Gao, H.; Tsarevsky, N. V.; Matyjaszewski, K. *J. Am. Chem. Soc.* **2006**, *128*, 5578.

(27) Zetterlund, P. B.; Kagawa, Y.; Okubo, M. *Chem. Rev.* **2008**, *108*, 3747.

(28) Sogabe, A.; McCormick, C. L. *Macromolecules* **2009**, *42*, 5043.

(29) Averick, S. E.; Paredes, E.; Irastorza, A.; Shrivats, A. R.; Srinivasan, A.; Siegwart, D. J.; Magenau, A. J.; Cho, H. Y.; Hsu, E.; Averick, A. A.; Kim, J.; Liu, S.; Hollinger, J. O.; Das, S. R.; Matyjaszewski, K. *Biomacromolecules* **2012**, *13*, 3445.

(30) Shrivats, A.; Hsu, E.; Averick, S.; Klimak, M.; Watt, A. S.; DeMaio, M.; Matyjaszewski, K.; Hollinger, J. *Clin. Orthop. Relat. Res.* **2015**, *473*, 2139.

(31) Nuhn, L.; Tomcin, S.; Miyata, K.; Mailänder, V.; Landfester, K.; Kataoka, K.; Zentel, R. *Biomacromolecules* **2014**, *15*, 4111.

(32) Hong, C. A.; Eltoukhy, A. A.; Lee, H.; Langer, R.; Anderson, D. G.; Nam, Y. S. *Angew. Chem.* **2015**, *127*, 6844.

(33) Anton, N.; Benoit, J.-P.; Saulnier, P. *J. Control. Release* **2008**, *128*, 185.

(34) Solans, C.; Izquierdo, P.; Nolla, J.; Azemar, N.; Garcia-Celma, M. J. *Curr. Opin. Colloid Interface Sci.* **2005**, *10*, 102.

(35) Pham, B. T. T.; Zondanos, H.; Such, C. H.; Warr, G. G.; Hawkett, B. S. *Macromolecules* **2010**, *43*, 7950.

(36) Durand, A.; Marie, E. *Adv. Colloid Interface Sci.* **2009**, *150*, 90.

(37) Asua, J. M. *Prog. Polym. Sci.* **2002**, *27*, 1283.

(38) Smith, M. H.; Lyon, L. A. *Acc. Chem. Res.* **2012**, *45*, 985.

(39) Shen, W.; Chang, Y.; Liu, G.; Wang, H.; Cao, A.; An, Z. *Macromolecules* **2011**, *44*, 2524.

(40) Oishi, M.; Nagasaki, Y. *React. Funct. Polym.* **2007**, *67*, 1311.

(41) Li, X.; Zuo, J.; Guo, Y.; Yuan, X. *Macromolecules* **2004**, *37*, 10042.

(42) Kuckling, D.; Vo, C. D.; Wohlrab, S. E. *Langmuir* **2002**, *18*, 4263.

(43) Min, K.; Gao, H. *J. Am. Chem. Soc.* **2012**, *134*, 15680.

(44) Convertine, A. J.; Benoit, D. S. W.; Duvall, C. L.; Hoffman, A. S.; Stayton, P. S. *J. Control. Release* **2009**, *133*, 221.

(45) Rieger, J.; Osterwinter, G.; Bui, C.; Stoffelbach, F.; Charleux, B. *Macromolecules* **2009**, *42*, 5518.

(46) Li, W.; Yoon, J. A.; Matyjaszewski, K. *J. Am. Chem. Soc.* **2010**, *132*, 7823.

(47) Xia, F.; Zuo, X.; Yang, R.; Xiao, Y.; Kang, D.; Vallée-Bélisle, A.; Gong, X.; Heeger, A. J.; Plaxco, K. W. *J. Am. Chem. Soc.* **2010**, *132*, 1252.

(48) Nel, A. E.; Madler, L.; Velegol, D.; Xia, T.; Hoek, E. M. V.; Somasundaran, P.; Klaessig, F.; Castranova, V.; Thompson, M. *Nat Mater* **2009**, *8*, 543.

(49) Verma, A.; Stellacci, F. *Small* **2010**, *6*, 12.

(50) Hillaireau, H.; Couvreur, P. *Cell. Mol. Life. Sci.* **2009**, *66*, 2873.

(51) Karmali, P. P.; Simberg, D. *Expert Opin. Drug. Deliv.* **2011**, *8*, 343.

(52) Aggarwal, P.; Hall, J. B.; McLeland, C. B.; Dobrovolskaia, M. A.; McNeil, S. E. *Adv. Drug Deliv. Rev.* **2009**, *61*, 428.

(53) Cho, H. Y.; Srinivasan, A.; Hong, J.; Hsu, E.; Liu, S.; Shrivats, A.; Kwak, D.; Bohaty, A. K.; Paik, H.-j.; Hollinger, J. O.; Matyjaszewski, K. *Biomacromolecules* **2011**, *12*, 3478.

(54) Tyeklar, Z.; Jacobson, R. R.; Wei, N.; Murthy, N. N.; Zubieta, J.; Karlin, K. D. *J. Am. Chem. Soc.* **1993**, *115*, 2677.

(55) Ali, M. M.; Stöver, H. D. H. *Macromolecules* **2004**, *37*, 5219.

Chapter VII. Stackable, Covalently Fused Gels: Repair and Composite Formation[§]

VII.1.Preface

This project was conducted in collaboration with the group from University of Pittsburgh led by Prof. Anna Balazs. Research in her group is focused on theoretical and computational modelling of thermodynamic and kinetic behavior of various polymer systems and composites. Together with their group's modelling data and experimental work, we created multilayered gels where each layer was "stacked" on top of the other and covalently interconnected to form mechanically robust materials, which could integrate the properties of the individual layers. This type of multilayered gels can be applied in areas such as drug delivery, wound healing, and could be used as soft actuators. In order to prepare such materials, a solution of new initiator, monomer, and cross-linker was introduced on top of the first gel and these new components underwent (co)polymerization to form the subsequent layer. Our collaborators simulated this process using dissipative particle dynamics (DPD) to isolate factors that affect the formation and binding of two chemically identical gel, as well as the formation of two incompatible stacked layers. Analysis indicated that the covalent bond formation between the different layers was primarily due to reactive chain-ends, rather than residual cross-linkers, demonstrating a potential advantage of CRP method vs FRP. In the experimental part, I had synthesized

[§] Part of this Chapter includes work, which was published and reformatted: Yong X., **Simakova A**., Averick S., Gutierrez J., Kuksenok O., Balazs A., Matyjaszewski K. Stackable, Covalently Fused Gels: Repair and Composite Formation. *Macromolecules* 2015, 48 , 1169-1178

multilayered gels using either free radical (FRP) or atom transfer radical polymerization (ATRP) methods. Polymerization results demonstrated that chemically identical materials preserved their structural integrity independent of the polymerization method. For gels encompassing incompatible layers, the contribution of reactive chain-ends plays a particularly important role in the integrity of the material, as indicated by the more mechanically robust systems prepared by ATRP. Furthermore, the integrity of materials prepared from incompatible layers can be improved by the application of amphiphilic copolymers, such as mikto-arm stars. These studies point to a new approach for combining chemically distinct components into one coherent, multi-functional material, as well as an effective method for repairing severed gels.

I would like to acknowledge everyone who participated in this collaborative work: Dr. Xin Yong and Dr. Olga Kuksenok, who conducted computational modelling and calculations, Dr. Saadyah Averick, who started experimental investigation of such materials synthesis and passed it to me, Dr. Junkal Gutierrez, who helped to generate materials and conduct mechanical testing, Dr. Hangjun Ding, who synthesized the miktoarm star copolymer, Dr. Awaneesh Singh, who studied the miktoarm stars organization on the gels interface, and Dr. Antoine Beziau and Rafael Natal for synthesis of hydrid ATRP/FRP gels.

VII.2. Introduction

Multi-functional materials address a number of vital technological needs since they allow one material to provide a range of properties and behavior. A challenge in creating these desirable materials is devising an approach for integrating the different components into one cohesive system. Conceptually, one would like to stack the components with different functionalities on top of each other to form the desired product. This approach would have the distinct advantage that it permits new functionalities to be added at will to improve or tailor the utility of the material. To date, however, it remains a considerable challenge to create "stackable materials" that would form a mechanically robust structure. As a step in addressing this challenge, herein we use computational modeling and experimental studies to design multi-layered, "stackable" gels, where one layer is effectively "stacked" on top of another. Each gel layer is covalently bound to the neighboring gels and hence, the system displays considerable mechanical integrity.

It is important to recall that researchers have devised means of "gluing" together separated pieces of polymer gels.[1-3] Recently, Leibler *et al.*, used nanoparticles as a binding agent to successfully attach two severed gels,[2] and in this way, could heal broken samples. Rather than binding separated sections, our aim is to grow one gel layer on top of another, and thereby, unite chemically distinct gels into a coherent material. Through this approach, we can, for example, stack a hydrophobic gel on top of a hydrophilic one, and thus, form multilayer amphiphilic gel composites, where a hydrophilic layer can alternate with a hydrophobic one. Researchers have created hybrid materials comprising two different types of gels by bringing two high-viscosity pre-gel mixtures into contact and then polymerizing the system[4]. While this method yields two-layered gels, it has not been

extended to creating multi-layered polymer networks. As we show below, our approach involves no inherent limitation on the number gel layers that can be created. We also note that two-dimensional, multi-layered hydrogel sheets can be created by photo-initiated polymerization through a photomask[5] or multi-step photolithography[6]. The advantage of our approach is that it does not impose any restrictions on the thickness of the samples, and while it can be used to create two-dimensional, multi-layered sheets, it can also be utilized to grow bulk, multi-layered gels of various shapes.

To create these materials, we took full advantage of atom transfer radical polymerization (ATRP)[7-10] to effectively add one layer on top of the other through successive polymerization reactions.[11-14] In particular, a solution of new initiator, monomer, and cross-linkers was introduced on top of the first gel and these new components then undergo living copolymerization to form the new second layer. Importantly, living polymerization preserves reactive species in the underlying gel, including active ends and partially-reacted cross-linkers with dangling vinyl groups.[14,15] These species can participate in successive reactions and form chemical cross-links that bind chains from different layers. In this manner, the layers become covalently linked and this multi-step living polymerization protocol enables the formation of multiple layers of covalently-fused gels.

The approach described herein introduces two advantageous features. As indicated above, it permits one to formulate completely new gels where each layer encompasses a distinct property and thus, the composite gel can exhibit a range of novel features. In other words, we can compartmentalize different functionalities into the different layers and incorporate a new functionality by simply adding a new gel layer. Second, as we discuss

further below, the approach allows us to repair the gel, if layers are severed. Notably, the new layer can be grown from the living chain ends in the existing underlying layer. This process ensures the formation of covalent bonds between the different layers, and thus, the creation of strong interfaces between the different layers.

Below, we describe both the computational and experimental approaches that allow us to formulate this system. Using both these approaches, we then characterize the physical features of these ‘stackable gels”. We particularly highlight the interfacial properties and pinpoint conditions that lead to mechanically robust materials.

VII.3. Results and discussion

VII.3.1. Formation of two-layer hydrophilic-hydrophilic gels and repair of damaged gels.

Simulation results. We first illustrate the proposed approach by forming a covalently-linked two-layer gel. As mentioned above, the polymerization process consists of two steps. In the first step, we initiated the living copolymerization in a solution to form the first (green) layer of the gel shown in Figure 1a-c. The ratios of the initiator, monomer and cross-linker concentrations in the solution are $[\mathrm{Ini}]_0/[\mathrm{X}]_0/[\mathrm{M}]_0 = 1/10/150$ and the gel is hydrophilic. The monomer conversion of the first-step polymerization reached 0.95 (i.e. 95%) (Figure 1c). In the second step, a solution with the same $[\mathrm{Ini}]_0/[\mathrm{X}]_0/[\mathrm{M}]_0$ ratio was introduced on top of the first gel layer and allowed to undergo living copolymerization to form the second gel layer, which is indicated in blue in **Figure VII.1d-f**. Notably, the chemical species in the green and blue layers are identical, and thus, the final product is a two-layer hydrophilic-hydrophilic gel prepared in the same solvent. The different colors for the two layers are used to aid in the visualization of the interface between the layers.

Because the two layers are completely compatible, we observe a relatively wide interface induced by the mutual diffusion of green and blue polymer (a quantitative analysis of the interface is discussed below). The inter-gel cross-links that connect chains grown from different layers are marked in red in **Figure VII.1f**; the high concentration of these inter-gel cross-links within the interfacial region indicates that the two layers are covalently fused.

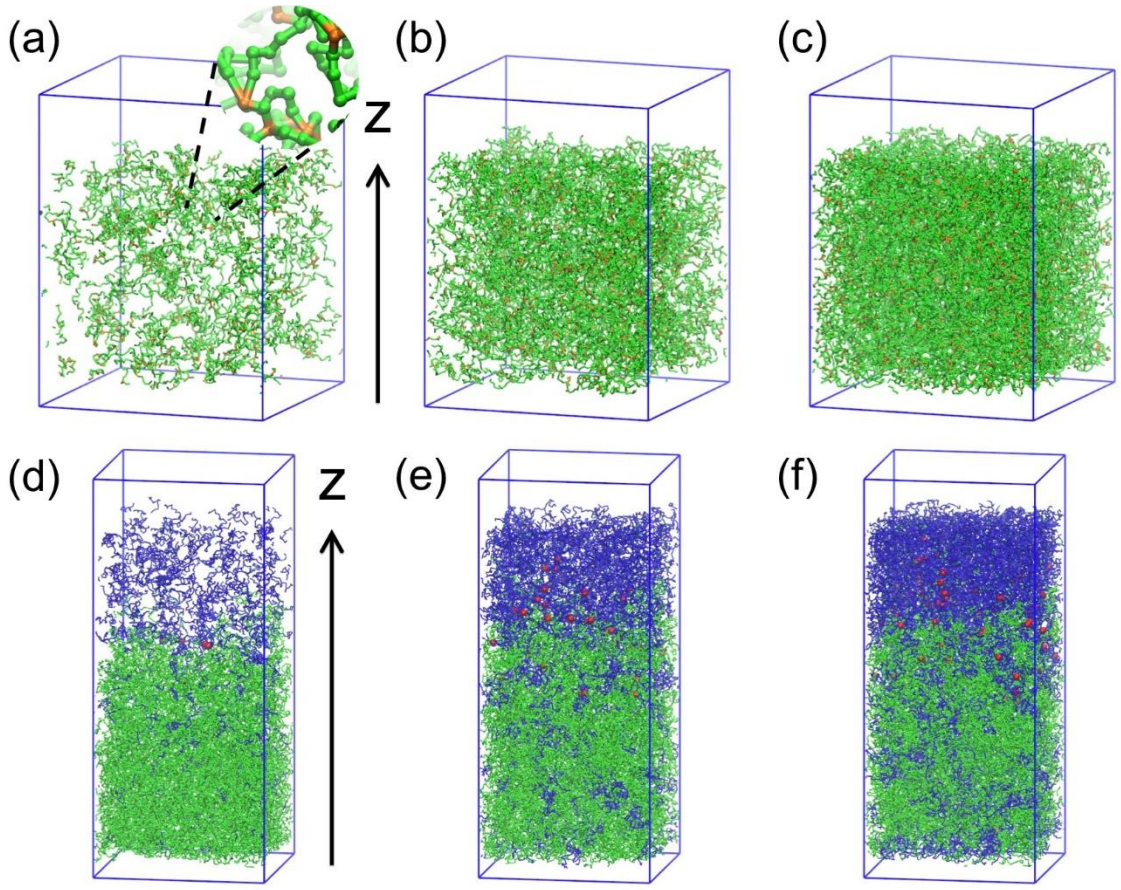

Figure VII.1. (a-c) Solution polymerization to form the first layer of a covalently-linked two-layer hydrophilic-hydrophilic gel. Snapshots taken at the following monomer conversions: (a) 0.19, (b) 0.57, and (c) 0.95. The green lines represent the polymer strands and the orange beads are formed cross-links (see enlargement in the inset in (a)). The ratio of the initial concentration of initiator to that of cross-linker is $[Ini]_0/[X]_0 = 1/10$. (d-f) Snapshots of the growth of the second gel layer (in blue) on top of the first layer are taken at the monomer conversions: (d) 0.19, (e) 0.57, and (f) 0.95. The red beads are the inter-gel cross-links connecting chains grown from different gel layers. The top and bottom substrate beads are not shown in the snapshots.

To probe the gelation process within each layer, we measured the reduced degree of polymerization (RDP) during the polymerization.[11,16] The RDP is the weight-averaged degree of polymerization (DP) of all macromolecules except the chain with the highest DP.[16] The gel point has been defined as the monomer conversion at which the RDP reaches the peak value.[11,16] **Figure VII.2a** shows the RDP of the first layer of the gel as a function of the monomer conversion in the first-step polymerization. Here, we consider two systems

with different ratios of initiator to cross-linker concentrations, $[\mathrm{Ini}]_0/[\mathrm{X}]_0$. In both systems, the RDP exhibits a peak value as the monomer conversion increases monotonically, indicating the successful gelation of the first layer. By comparing the two systems with different ratios $[\mathrm{Ini}]_0/[\mathrm{X}]_0$, we observe a gel point at a lower monomer conversion (and hence, earlier gelation) in the system with $[\mathrm{Ini}]_0/[\mathrm{X}]_0 = 1/10$ than in the system with $[\mathrm{Ini}]_0/[\mathrm{X}]_0 = 1/5$; this behavior agrees with trends seen in previous simulations and experiments.[11,12,16]

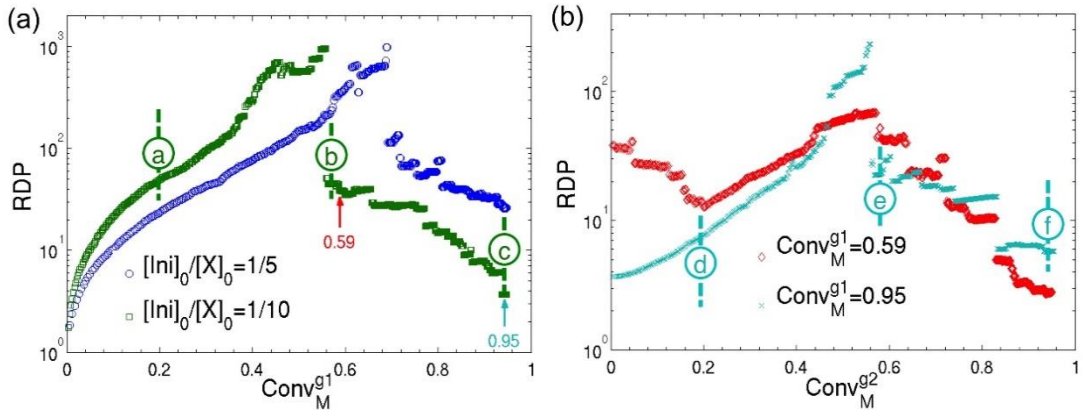

Figure VII.2. (a) Evolution of the reduced degree of polymerization (RDP) of the first layer of the gel as a function of the monomer conversion for different $[\mathrm{Ini}]_0/[\mathrm{X}]_0$. (b) Evolution of the RDP of the two-layer gel as a function of the monomer conversion of the second layer. The first layers in the two systems reach different monomer conversions. The annotations with the letters a-f represent the frames Figure 1a-f, respectively.

Following the same procedure, we then monitor the gelation of the second layer. For this process, we fix $[\mathrm{Ini}]_0/[\mathrm{X}]_0 = 1/10$, and examine the evolution of the upper gel for two different values of the monomer conversion in the lower layer: $\mathrm{Conv}_{\mathrm{M}}^{g1} = 0.59$ and 0.95. At different monomer conversions, the gels exhibit different polymer volume fractions and densities. Correspondingly, the number of primary chains (i.e., chains that are not incorporated into the network) remaining in the solution depends on the final monomer

conversion. Namely, the first layer with a monomer conversion of 0.59 (slightly beyond the gel point) contains more primary chains than the one reaching a monomer conversion of 0.95. Hence, the evolution of the RDP of the two-layer gel will exhibit different behavior for different $\mathrm{Conv}_{\mathrm{M}}^{g1}$, as seen in **Figure VII.2b**.

As one might have anticipated, a monomer conversion of 0.95 in the original layer results in a much closer resemblance of an RDP as a function of the conversion rate in the second layer (cyan curve in **Figure VII.2b**) than that of 0.59 to the same curve for the bottom layer (green curve in **Figure VII.2a**). For the system where the monomer conversion in the first layer is 0.59, the RDP of the two-layer gel first decreases then increases until it reaches a peak in the second-step polymerization. This non-monotonic behavior arises from a competition between two effects. With the onset of polymerization in the second layer, the remaining primary chains within the first layer that encompass large DP are rapidly incorporated into the gel network. Thereafter, they are excluded from the RDP calculation. Simultaneously, the DP of primary chains that later form the second layer is slowly increasing. This increase is overwhelmed by the decrease attributed to the removal of large DP primary chains in the first layer, leading to the decrease of RDP of the whole system. When most remaining primary chains in the first layer have been incorporated into the gel network, the trend is reversed and the RDP starts to increase. Due to the limited number of residual primary chains when the first layer reaches a monomer conversion of 0.95, the cyan curve in **Figure VII.2b** displays an immediate increase of the RDP at the start of the second-step polymerization. From the measurement of RDP in the multi-step living polymerization, we confirm the successful gel formation in each layer.

Note that the gel point remains the same for both examples in Figure 2b as well as for the original first gel layer (green curve) in **Figure VII.2a**.

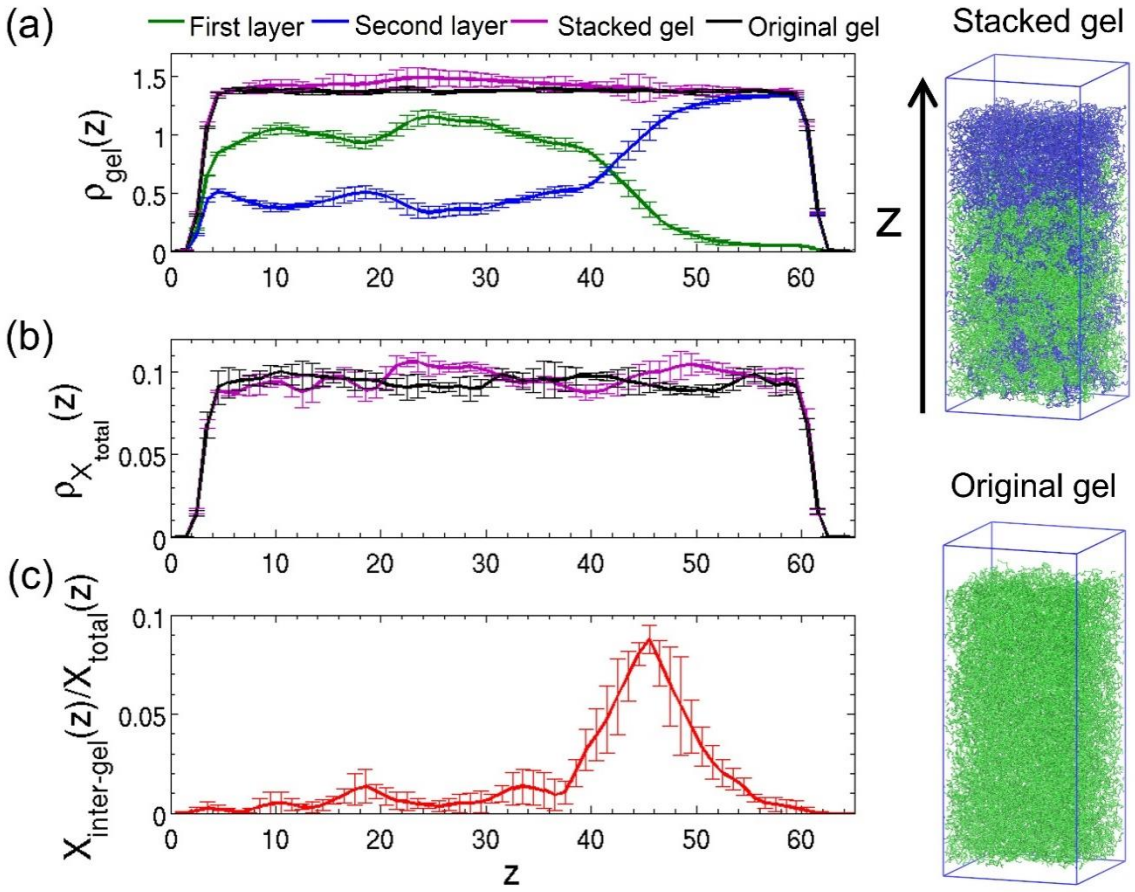

Figure VII.3. (a) Number density profiles of the first (green), second (blue) layers of the gel, the total density of the stacked two-layer gel (magenta), and the density of the original gel (black). (b) Number density profiles of cross-links formed (including inter- and intra-gel cross-links) in the repaired two-layer gel and original gel. (c) Fraction of the number of inter-gel cross-links with respect to the total number of cross-links formed as a function of the position in the *z* direction. Insets are the snapshots of the stacked two-layer and original gel. All conditions are the same as those of the simulation shown in Figure 1. Error bars arise from averaging over four independent runs.

Because the two-layer gel encompasses the same type of monomers in both layers, the process described above can also be considered as repairing a green gel that has been cut. To create a reference system for assessing the degree of repair, we conducted a one-step polymerization to form an uncut green gel with the same size as the two-layer system

$(30 \acute{} \ 30 \acute{} \ 60)$ (see **Figure VII.3**). Note that the green layer of size $30 \acute{} \ 30 \acute{} \ 30$ formed *via* the two-step polymerization has the same density and cross-link distribution as the bottom half of the uncut green gel shown in **Figure VII.3**.

To achieve successful healing, the repaired gel must resemble the original material. The density profiles in Figure 3a reveal that the curves for the repaired two-layer gel and the original uncut gel effectively lie on top of each other. The spatial distributions of cross-links formed in the gel along the transverse (z) direction are plotted for both gels in **Figure VII.3b**; the distribution and densities of the cross-links for the repaired and uncut gels show essentially identical values (within the error bars). We also examine the fraction of inter-gel cross-links with respect to all cross-links (including inter-gel and intra-gel cross-links) in the repaired two-layer gel as a function of position in the z direction. The plot in Figure 3c exhibits a localization of inter-gel cross-links near the interfacial region in **Figure VII.3a**. This peak is shifted from the center of the system towards the blue gel because the green layer undergoes a degree of swelling when the compatible solution of blue components was introduced on top of the "cut" layer. (Recall that before adding the fresh solution for the second layer, the gel was bounded by the repulsive layer[17]). Overall, the results reveal that the multi-step living polymerization approach provides a robust means to repair damaged gels.

After the repair is complete, the strength of the interface can be estimated by the relative number of inter-gel cross-links with respect to all cross-links.[18,19] We hypothesize that the monomer conversion of the first layer is the critical parameter that affects the number of inter-gel cross-links formed in the system, and consequently, influences the interfacial strength of the two-layer gel. **Figure VII.4** shows the fraction of inter-gel cross-

links as a function of the monomer conversion of the first layer. As the first-layer monomer conversion varies from 0.59 to 0.95, the fraction of inter-gel cross-links exhibits a monotonic decrease for the system with $[\mathrm{Ini}]_0/[\mathrm{X}]_0 = 1/10$. When initiator concentration is increased and the ratio is set to $[\mathrm{Ini}]_0/[\mathrm{X}]_0 = 1/5$, the fraction of inter-gel cross-links does, however, become relatively insensitive to the change of the first-layer monomer conversion.

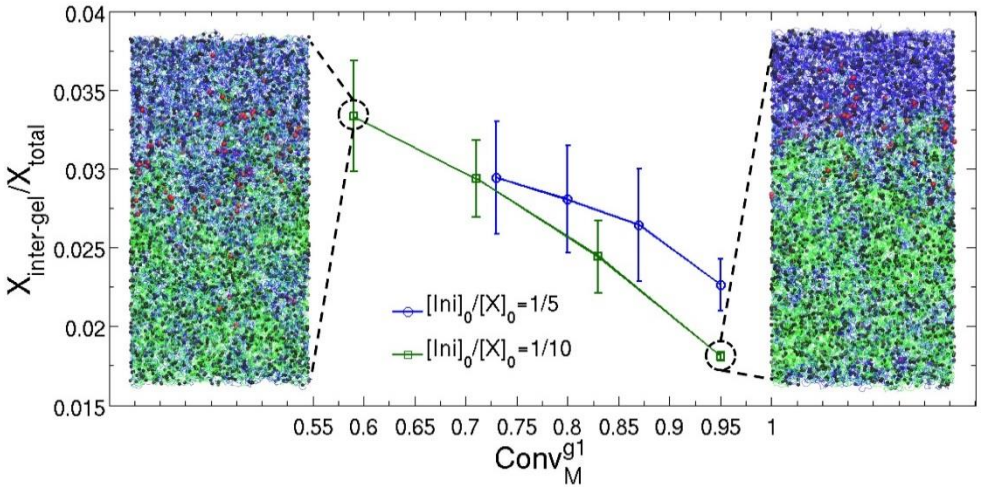

Figure VII.4. Fraction of the inter-gel cross-links as a function of the monomer conversion in the first layer. The monomer conversion in the second layer always reaches 0.95. The insets show the spatial distributions of the cross-links at the first-layer monomer conversions of 0.59 and 0.95. Black beads are the intra-gel cross-links connecting chains from the same layer. Error bars indicate the variations among four independent runs.

To understand the correlation between the first-layer monomer conversion and the fraction of inter-gel cross-links, as well as the distinct behavior at the higher value of $[\mathrm{Ini}]_0/[\mathrm{X}]_0$, we examined the reaction events of cross-link formation at the individual bead level. **Figure VII.5** highlights two possible scenarios for forming an inter-gel cross-link. Namely, an inter-gel cross-link can form either when an active chain end from the first (green) layer encounters a partially-reacted cross-linker bead in the second (blue) gel network, or when the active end of a blue chain reacts with a residual (partially-reacted)

cross-linker in the green layer. Thus, the numbers of active ends and residual cross-linkers in the first layer influence the total number of inter-gel cross-links formed.

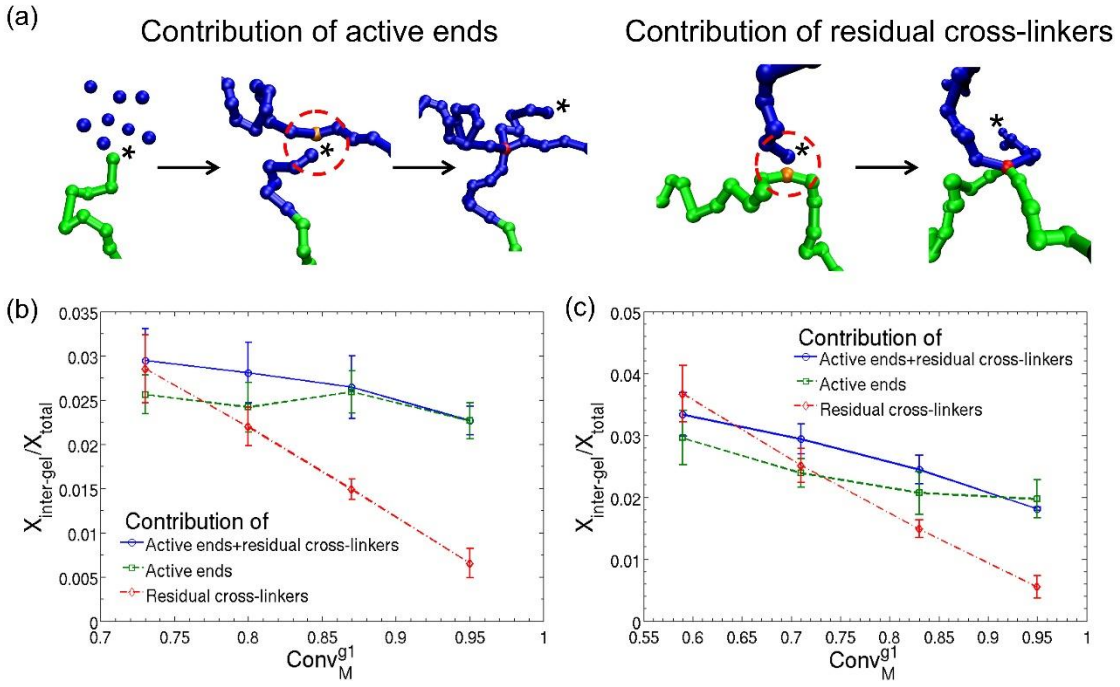

Figure VII.5. (a) Schematics show two possible scenarios of the formation of the inter-gel cross-link, where the orange bead represents partially reacted cross-linker with pendent functional group and the asterisk represents active radical. (b-c) Fraction of the inter-gel cross-links as a function of the monomer conversion of the first layer for (b) $[Ini]_0/[X]_0$ = 1/5 and (c) $[Ini]_0/[X]_0$ = 1/10. Contribution of active ends (residual cross-linkers) to the formation of inter-gel cross-links is demonstrated by removing residual cross-linkers (active ends) in the first layer of the gel.

We conducted two separate simulations to elucidate the contributions of the active ends and residual cross-links in the first layer. These systems are different from the original reference material since we "inactivated" either the active ends or the residual cross-linkers in the first layer. In particular, we switched off the elemental reactions involving the corresponding beads. The fraction of the inter-gel cross-links for these systems are plotted in **Figure VII.5b** and **c**, which also show the corresponding values for the reference systems having both active ends and cross-linkers. If the residual cross-linkers are solely responsible for the formation of inter-gel cross-links, then the fraction of the cross-links

decreases as the first-layer monomer conversion is increased. The number of residual cross-linkers scales inversely with the monomer conversion, leading to less inter-gel cross-link formation at higher monomer conversion.

In contrast, for systems with only active ends, the number of active ends remains constant during the polymerization reaction due to the absence of termination reactions. Hence, there is no significant correlation between the number of inter-gel cross-links formed and the monomer conversion.

Notably, there are more initiators in the system with $[\mathrm{Ini}]_0/[\mathrm{X}]_0 = 1/5$ than in the system with $[\mathrm{Ini}]_0/[\mathrm{X}]_0 = 1/10$. Thus, the contribution from the active ends overwhelms that of the residual cross-linkers for the systems at $[\mathrm{Ini}]_0/[\mathrm{X}]_0 = 1/5$. This leads to the observed insensitivity of the fraction of inter-gel cross-links to the monomer conversion in the first layer for the reference system with $[\mathrm{Ini}]_0/[\mathrm{X}]_0 = 1/5$ (as seen in Figure 4). However, for the system with $[\mathrm{Ini}]_0/[\mathrm{X}]_0 = 1/10$, we do observe a significant contribution from residual cross-linkers at low conversion rates; moreover, both contributions (from active ends and from residual cross-linkers) to the formation of inter-gel cross-links decrease with an increase of the conversion rate (**Figure VII.5c**). This functional dependence is consistent with the dependence of the fraction of the inter-gel cross-links as a function of the first layer monomer conversion observed in Figure 4 for the same initial values of $[\mathrm{Ini}]_0/[\mathrm{X}]_0 = 1/10$. We note that our experimental system corresponds to the $[\mathrm{Ini}]_0/[\mathrm{X}]_0 = 1/5$ case (**Figure VII.5b**). Hence, our simulation studies predict a dominant contribution of active chain ends to the strength of interface with respect to that of residual cross-linkers. In other words, at high conversion rates the number of inter-gel cross-links

and correspondingly the strength of the interface decreases drastically if there is no contribution from the active ends.

Experimental results. ATRP[7-9] was used to experimentally realize the process of formation of a two-layer gel system[12,14] predicted in the above computer simulation studies. The gels were prepared by first synthesizing a base layer (monomer conversion > 95%) and subsequently adding the next layer of the gel precursor solution (**Figure VII.6a**). To prepare a two-layer hydrophilic-hydrophilic gel, an aqueous gel precursor solution of N,N-dimethylaminoethyl methacrylate (DMAEMA), poly(ethylene glycol) dimethacrylate (PEGDM, crosslinker) and a poly(ethylene glycol) methyl ether 2-bromoisobutyrate (PEG-iBBr) ATRP macroinitiator with a copper catalyst and an azo-initiator as a reducing agent for the ICAR process[20] were added to a mold (**Scheme VII.1, Figure VII.7**) and polymerized *in situ*. To form the second layer, the identical gel precursor solution was added on top of the formed gel and polymerized. In order to better visually distinguish the gel layers, methacrylate monomers containing two different dye moieties were added into layers to show the stratification of material. Thus, methacrylates with either rhodamine or fluorescein moieties were used. Upon completion of the polymerization, the stacked gel was taken out of the mold and its integrity was inspected visually and mechanically (i.e. bending) (**Figure VII.6b-d**).

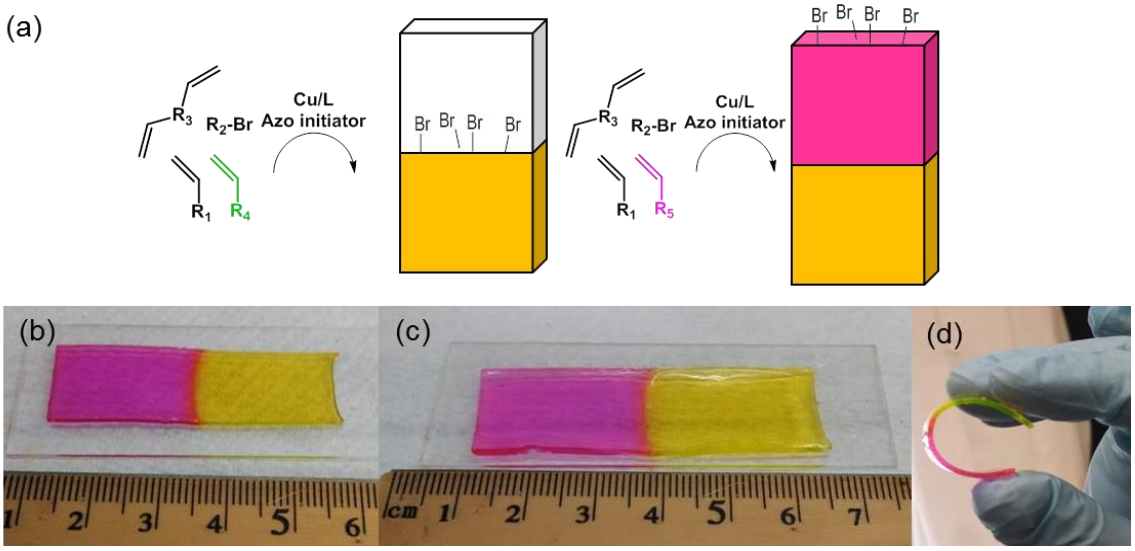

Figure VII.6. (a) Two layer hydrophilic-hydrophilic pDMAEMA gel prepared by ATRP of DMAEMA in water for both layers. Images of the gel (b) right out of the mold, (c) swollen in water, and (d) bent. R_1 – DMAEMA, R_2 – $PEG_{2k}iBBr$, R_3 – $PEGDMA_{750}$, R_4 – fluorescein methacrylate, R_5 - rhodamine methacrylate. Polymerization conditions for both layers: [DMAEMA]:[$PEG_{2k}iBBr$]:[$PEGDMA_{750}$]:[$CuBr_2$]:[TPMA]:[VA-044] = 75:1:5:0.1:0.8:0.1; either fluorescein or rhodamine methacrylate were added in one of the layer at the 0.02:75 molar ratio to DMAEMA.

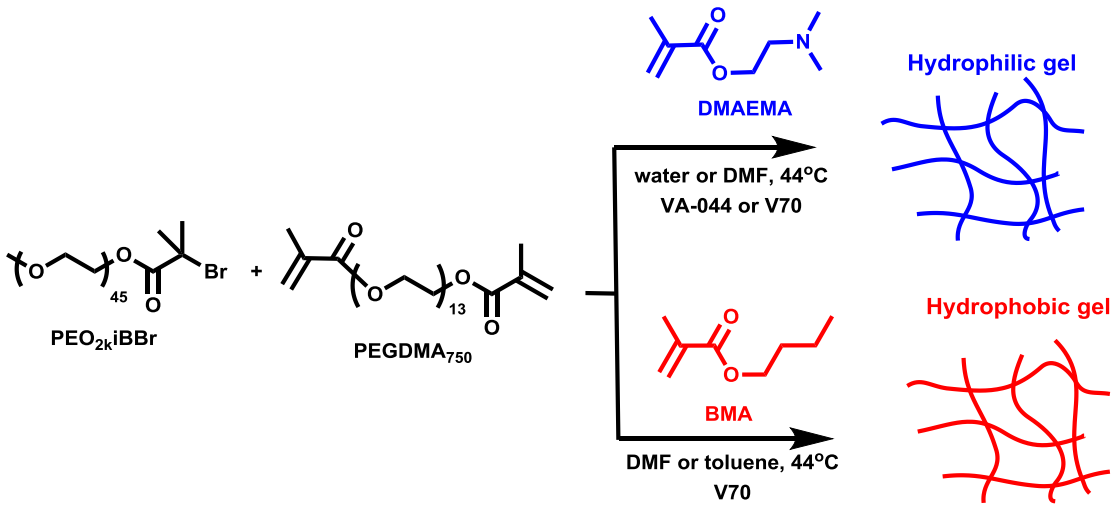

Scheme VII.1. Preparation of pDMAEMA and pBMA gels.

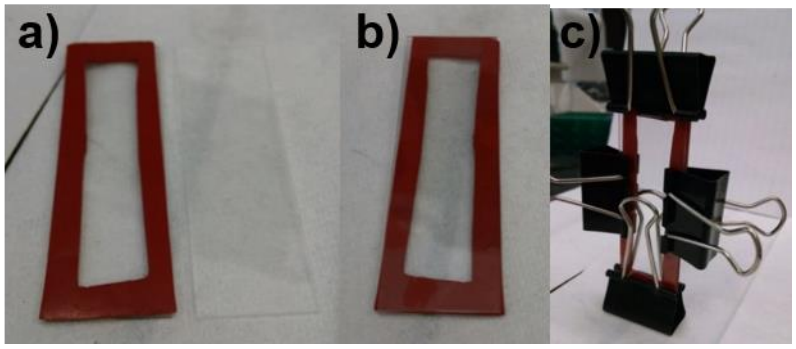

Figure VII.7. Mold used to prepare stacked gels by either ATRP or FRP. Mold consisted of PDMS frame between two glass slides (a, b) fixed by paper clips (c) to provide stability and anaerobic conditions.

Two-layer gels prepared by ATRP should share connecting bonds at the interface, from both reactive chain-ends and residual cross-linkers (see schematic in **Figure VII.5a**). This is in contrast to two-layer gels prepared by free radical polymerization (FRP) where the only available inter-gel linking sites come from unreacted cross-linkers in the first layer. Visual inspection and mechanical manipulations (bending) of the two-layer FRP and ATRP gels demonstrated similar properties when prepared in the same solvent (**Figure VII.8**). Tensile testing was used to provide quantitative assessment of the gel interface integrity. Due to the difference in properties of gels prepared by ATRP and FRP, the results were compared to a single-layer pDMAEMA gels prepared by each respective method (**Figure VII.9, Table VII.1**). Both the two-layer ATRP and FRP gels had ca. 20% lower elongation at break, as compared to the single layer gels. Gels prepared by ATRP were softer than those prepared by FRP due to a different network structure and higher swelling.[15,21,22] Gels prepared by ATRP displayed more than 3 times higher swelling ratio than FRP gels (**Table VII.1**). Half of the classical dog-bone samples prepared for the mechanical testing by either ATRP or FRP did not break at the interface (**Figure VII.10**). This indicates a relatively strong bonding between two parts of the bilayer gel prepared by

both methods. Therefore, experiments run at macroscopic scale for the multi-layered, chemically identical gels suggested that diffusion of the second layer gel precursor solution into the first layer is quite significant. Thus, it resulted in a strong interface even for gels where only residual vinyl bonds contributed to the formation of the inter-gel crosslinks.

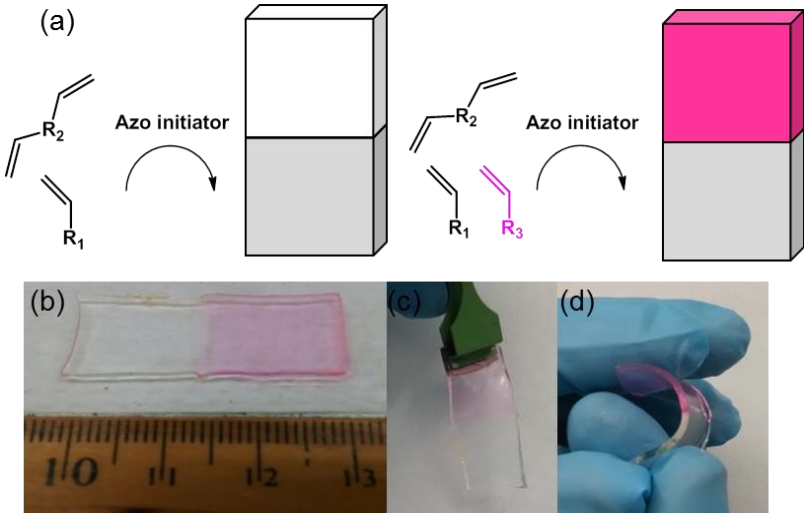

Figure VII.8. (a) Two layer hydrophilic-hydrophilic pDMAEMA gel prepared by FRP. Images of the gel (b) right out of the mold, (c) lifted, and (d) bent. R_1 – DMAEMA, R_2 – $PEGDMA_{750}$, R_3 – rhodamine methacrylate. Polymerization conditions for both layers: [DMAEMA]:[$PEGDMA_{750}$]:[VA-044] = 75:5:0.1. Rhodamine methacrylate was added into the second layer (pink) at the 0.02:75 molar ratio to DMAEMA

Table VII.1. Elongation at break and swelling ratios for single and two-layer gels prepared by ATRP and FRP

Sample	Elongation at break, %	Swelling ratio
ATRP DMAEMA single	188.0±22.2	5.5
ATRP DMAEMA double	153.5±20.2	5.6
FRP DMAEMA single	266.9±26.1	1.7
FRP DMAEMA double	222.3±15.0	1.9

Tensile elongation was averaged from at least of 3 samples. Swelling in water was measured at room temperature and calculated as $(W_s - W_d)/W_d$, where W_s is swollen gel and W_d is dried gel.

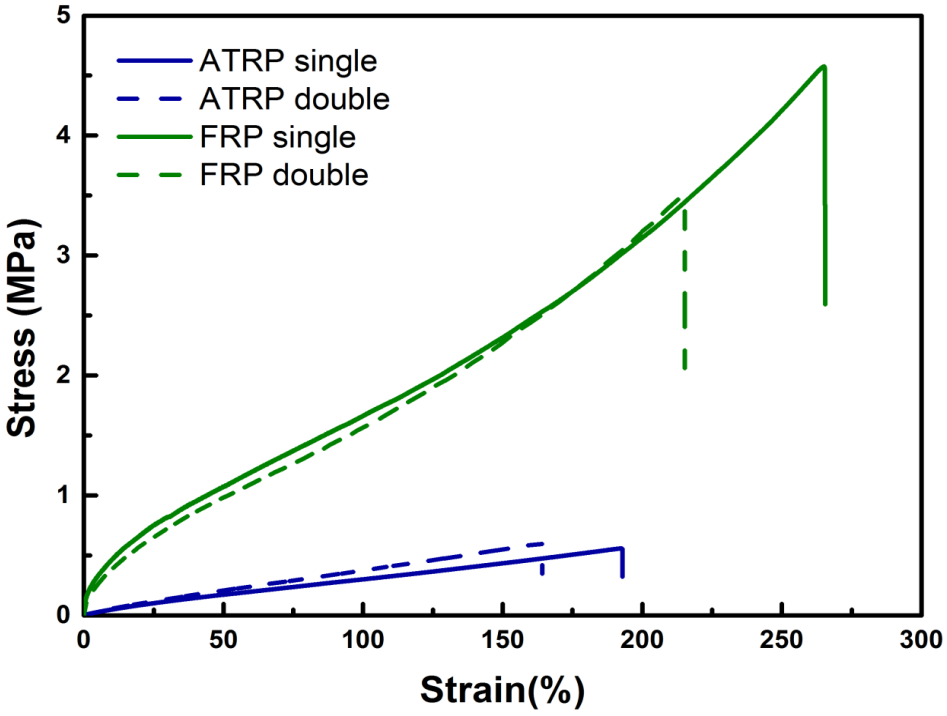

Figure VII.9. Stress – strain curve for pDMAEMA single and double gels prepared by either ATRP or FRP. Average size of a specimen 0.08x0.5x0.03 in (width x length x thickness of the narrow part of a dogbone shaped specimen).

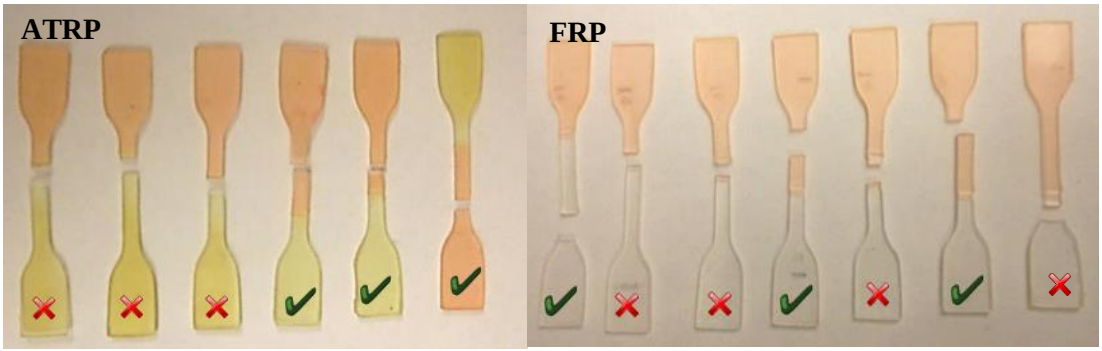

Figure VII.10. Samples after tensile test of pDMAEMA double gels prepared either by ATRP or FRP from the same monomer in the same solvent (DMF) used for both layers. Polymerization conditions for ATRP gels: [DMAEMA]:[PEG_{2k}iBBr]:[$PEGDMA_{750}$]:[$CuBr_2$]:[TPMA]:[VA-044] = 75:1:5:0.1:0.8:0.1; rhodamine methacrylate were added into the second layer at the 0.02:1 molar ratio to PEG_{2k}iBBr. Polymerization conditions for FRP gels: [DMAEMA]:[$PEGDMA_{750}$]:[VA-044] = 75:5:0.1. Rhodamine methacrylate was added into the second layer (pink) at the 0.02:75 molar ratio to DMAEMA. Dog bone shape specimen were cut after polymerization was completed and samples were dried.

VII.3.2. Preparation of multi-layered composite gels.

The simulations and experiments described above provided insight and guidelines for preparation of a two-layer gel with layers either chemically identical or highly compatible and synthesized in the same solvent. This compatibility, however, restricts the choice of constituent monomers, and thus, limits the selection of functionalities that can be incorporated into the gel. In this section, we extend the multi-layer gel formation to create composite systems with chemically incompatible polymers. Here, we first considered the same mutual solvent for both hydrophilic and hydrophobic polymers (i.e., DMF in the experiment), and set all the constituent initiator, monomer, and cross-linker of the different layers to be mutually incompatible (i.e. hydrophilic DMAEMA and hydrophobic n-butyl methacrylate (BMA).

Simulation results. **Figure VII.11a** shows a snapshot from the simulations of a two-layer amphiphilic composite gel where the first layer is hydrophilic and the second is hydrophobic ($a_{\mathrm{P1-P2}} = 35$). Because the two layers have the same solvent, the monomer of the blue gel can diffuse into the green layer, facilitated by the solvent exchange. During the polymerization of the second layer, the solvent shields the blue polymer from incompatible green gel. Hence, the system exhibits a broad interface between the incompatible layers (**Figure VII.11b**). It should be stressed that the blue and green monomers are relatively weakly incompatible. We anticipate that taking strongly incompatible layers (i.e., increasing the repulsion parameter $a_{\mathrm{P1-P2}}$) could result in a less diffuse, sharper interface between the layers. Notably, blue polymer in the green layer forms a connected cluster structure, indicating a weak phase separation with the mutual solvent.

The inter-gel cross-links in the composite gel have a somewhat narrower spatial distribution than that of the two-layer gel with compatible layers (**Figure VII.11c**). Nevertheless, the system encompasses a considerable number of inter-gel cross-links and thus, contains a significant fraction of covalent links between the incompatible layers. We observe that most inter-gel cross-links form in the second layer beyond the interface (see **Figure VII.11a, c**). To gain further insight into the formation of inter-gel cross-links, we recall that the dominant mechanism of forming inter-gel cross-links in our system is associated with the active ends in the first layer (see above). Even though the monomers in the second layer are incompatible with the polymer chains in the first layer, the solvent freely exchanges between the layers; hence, Brownian motion can cause the hydrophobic monomers to come in contact with active ends (note the relatively high fraction of the blue polymer within the green layer, see **Figure VII.11b**). Thus, the hydrophilic active chains eventually connect to hydrophobic blocks. This process is essentially similar to the polymerization of block copolymers from chemically incompatible monomers.[23] The active chains, originating from the first layer, slowly extend into the second layer due to the polymerization of the hydrophobic monomers and then form inter-gel cross-links with chains in the second layer. Notably, the density of active ends in the composite gel (see **Figure VII.11d**) exhibits a salient dip right below the interface, followed by an increase right above the interface. We attribute the inter-gel cross-links created above the interface to this depletion of active ends within the green portion of the interfacial region and an enrichment within the blue side of this region.

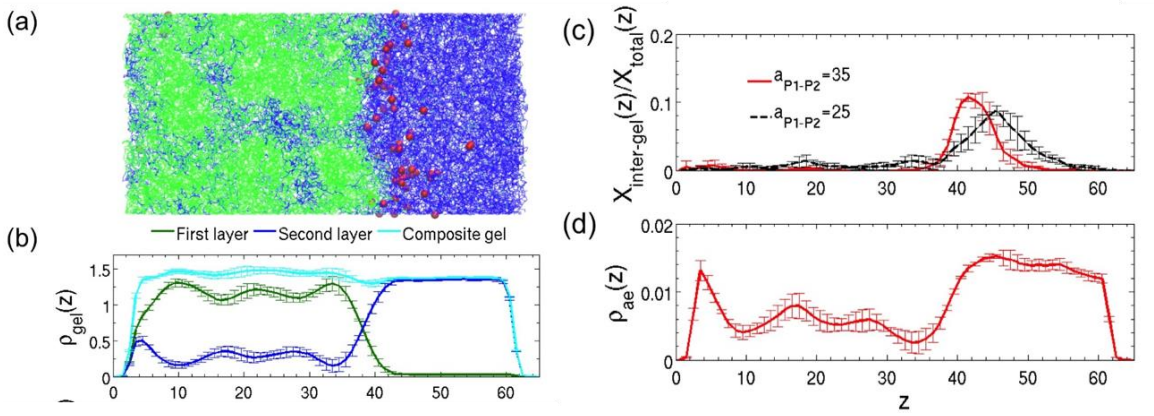

Figure VII.11. (a) Snapshot of the composite gel for $a_{\mathrm{P1-P2}} = 35$. (b) Number density profiles of the first (green), second (blue) layer of the gel, and the total density of the composite gel (cyan) for $a_{\mathrm{P1-P2}} = 35$. The orange arrow indicates the position of the interface. (c) Comparison of fractions of the number of inter-gel cross-links with respect to the total number of cross-links formed as a function of the position in the *z* direction between the composite gel (red solid line) and the repaired gel (black dashed line). (d) Spatial distributions of active chain end in the *z* direction for the composite gel.

Finally, utilizing the same procedure, we created a sandwich-like three-layer composite gel, where the top and bottom layers are hydrophilic and the mid layer is hydrophobic (the interaction parameters between incompatible polymers, cross-linkers, and initiators are set to a_{ij} =35, while the solvents in all three layers are the same). Similar to the two-layer composite gel, the two interfaces are wide and the inter-gel cross-link distributions span approximately 10 units in width, as shown in **Figure VII.12**. When monomers diffuse into incompatible layers, they form clusters to minimize the unfavorable enthalpic interaction with the incompatible environment. The number of inter-gel cross-links formed at the newest interface (between the second and third layer) remains the same as that of the original interface (between the first and second layer). This feature ensures that the protocol developed in this study can be readily extended to make composite gels with the multiple gel layers.

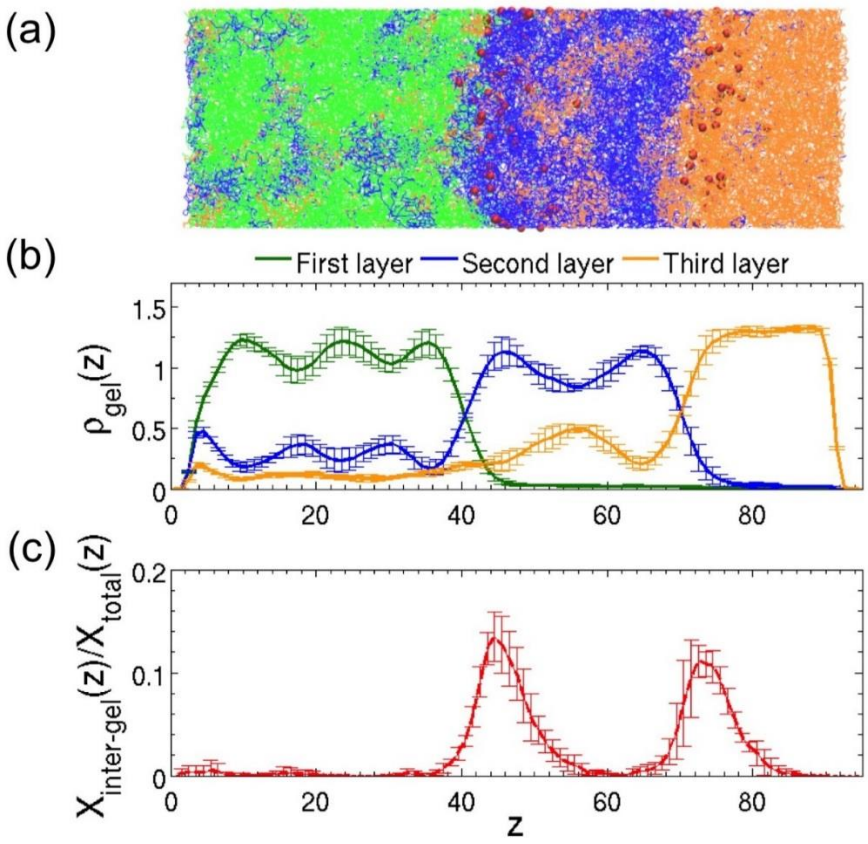

Figure VII.12. (a) Snapshot of the three-layer composite gel. All layers reach monomer conversion 0.95. (b) Number density profiles of the first (green), second (blue), and third (orange) layer of the three-layer A-B-A composite gel. Different colors for the two A layers are used merely for visualizing the layered structure. The repulsion parameter *a* is set to 35 between A and B polymers. (c) Fractions of the number of inter-gel cross-links with respect to the total number of cross-links formed as a function of the position in the *z* direction.

Experimental results. A three-layer hydrophilic-hydrophobic-hydrophilic gel was prepared to investigate how the reactive chain-ends and residual cross-linkers at the interface could be used to covalently link incompatible gels. The precursor solutions the same cross-linker and the same ATRP initiator were used in both layers (PEGDM and PEG-iBBr). The hydrophilic DMAEMA and hydrophobic n-butyl methacrylate (BMA) were used as monomers. Dimethylformamide (DMF) was used as a common solvent for all three layers. Three-layer gel was synthesized by adding a gel precursor solution on top of the previously formed gel layer (**Figure VII.13a**) using either ATRP or FRP,

respectively. Although gels prepared by both ATRP and FRP appeared intact after polymerization (**Figure VII.13b, e**), the gels prepared by FRP broke upon bending (**Figure VII.13f**) whereas gels prepared by ATRP remained intact (**Figure VII.13c-d**). These results showed that the composite gel prepared by ATRP had a stronger interface than the composite gel prepared by FRP. Thus, contribution of the reactive chain-ends towards linking incompatible gels resulted in materials with stronger interface.

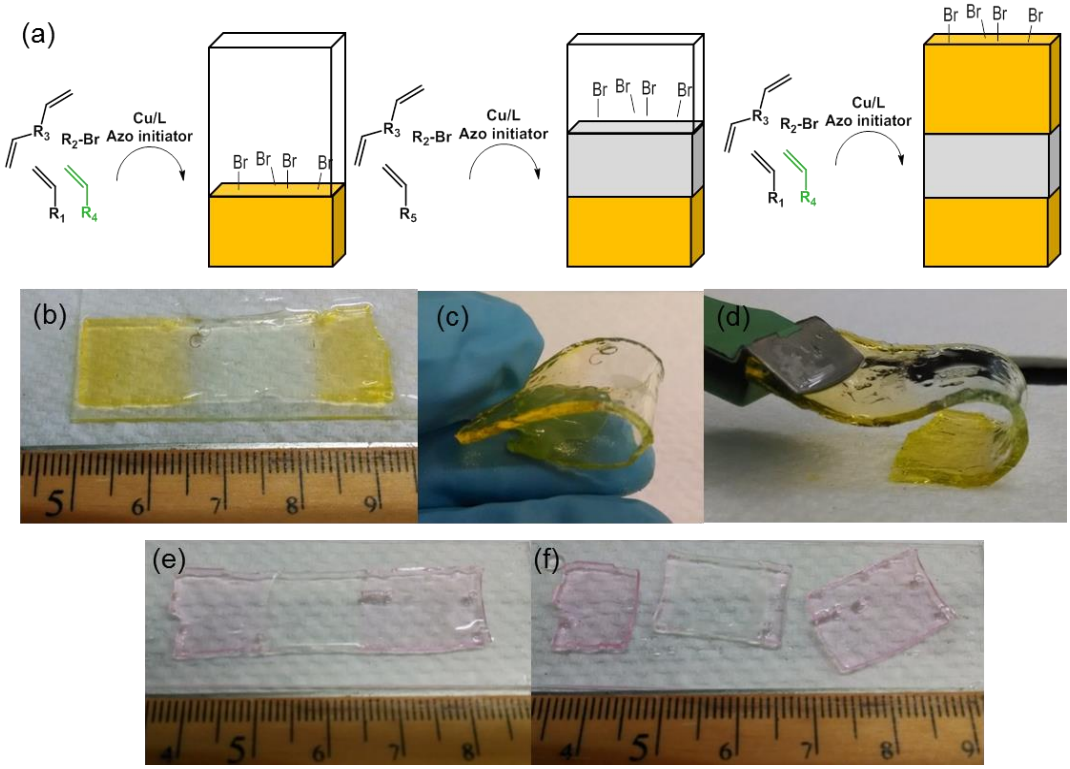

Figure VII.13. (a) Three-layer hydrophilic-hydrophobic-hydrophilic pDMAEMA-pBMA-pDMAEMA gels prepared by ATRP (a – d) and by FRP (e – f) in the same solvent (DMF) used for all layers. Images of the gel (b) right out of the mold, and (c-d) bent. R_1 – DMAEMA, R_2 – $PEG_{2k}iBBr$, R_3 – $PEGDMA_{750}$, R_4 – fluorescein methacrylate, R_5 - BMA. Polymerization conditions for first and third layers prepared by ATRP: [DMAEMA]:[$PEG_{2k}iBBr$]:[$PEGDMA_{750}$]:[$CuBr_2$]:[TPMA]:[VA-044]:[Fluorescein methacrylate] = 75:1:5:0.1:0.8:0.1:0.02. Fluorescein methacrylate were added at the 0.02:75 molar ratio to DMAEMA. Polymerization conditions for middle layer prepared by ATRP: [BMA]:[$PEG_{2k}iBBr$]:[$PEGDMA_{750}$]:[$CuBr_2$]:[TPMA]:[V70]= 75:1:5:0.1:0.8:0.3. For gels prepared by FRP conditions were similar, but ATRP initiator and catalyst were not included in the solutions, and rhodamine methacrylate was used instead of fluorescein methacrylate.

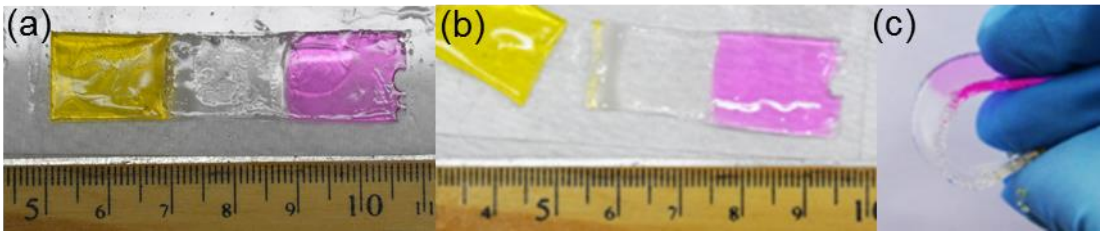

Figure VII.14. Three-layer hydrophilic-hydrophobic-hydrophilic pDMAEMA-pBMA-pDMAEMA gel prepared by ATRP in miscible solvents. Images of the gel (a) right out of the mold, (b) after mechanical manipulation, and (c) bent. Polymerization conditions for first and third layers: [DMAEMA]:[PEG_{2k}iBBr]:[$PEGDMA_{750}$]:[$CuBr_2$]:[TPMA]:[VA-044] = 75:1:5:0.1:0.8:0.1 in water. The first layer contained fluorescein methacrylate and the third layer contained rhodamine methacrylate at the 0.02:75 molar ratio to DMAEMA. Polymerization conditions for the middle layer: [BMA]:[PEG_{2k}iBBr]:[$PEGDMA_{750}$]:[$CuBr_2$]:[TPMA]:[V70]= 75:1:5:0.1:0.8:0.3 in DMF.

To investigate the limits of how incompatibility influences gels fusion, two additional composite gels were prepared by ATRP. First, the solvent for hydrophilic layer was changed to more polar (water), but still miscible with solvent that was used in hydrophobic layer (DMF). Three-layer gel prepared in different but miscible solvents had weaker links between layers. Interestingly, 1st and 2nd layer separated upon mechanical manipulations (**Figure VII.14a-b**), but 2nd and 3rd layer stayed connected even after bending (**Figure VII.14c**). This difference could be explained by the insolubility of BMA in water, which creates more heterogeneous and weaker interface. On the other hand, DMAEMA and pDMAEMA are well soluble in DMF, resulting in more pronounced diffusion of the hydrophilic monomer/polymer into hydrophobic layer. These results suggest that by increasing incompatibility between layers the interface between layers was weakened. Nevertheless, it was still possible to preserve certain integrity of gel.

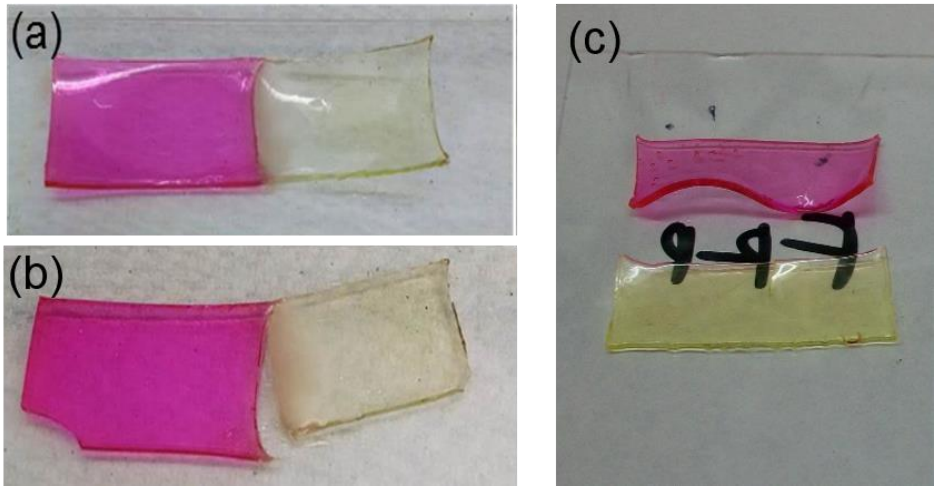

Figure VII.15. Three-layer hydrophilic-hydrophobic-hydrophilic pDMAEMA-pBMA-pDMAEMA gel prepared by ATRP (a, b) and FRP (c) in immiscible solvents. Images of the gel (a) right out of the mold, (b) after mechanical manipulation, and (c) right out of the mold. ATRP conditions for first layer: [DMAEMA]:[PEG_{2k}iBBr]:[$PEGDMA_{750}$]:[$CuBr_2$]:[TPMA]:[VA-044] = 75:1:5:0.1:0.8:0.1 in water. The first layer contained rhodamine methacrylate at the 0.02:75 molar ratio to DMAEMA. ATRP conditions for the second layer: [BMA]:[PEG_{2k}iBBr]:[$PEGDMA_{750}$]:[$CuBr_2$]:[TPMA]:[V70]= 75:1:5:0.1:0.8:0.3 in toluene. For FRP conditions of the composition was similar to ATRP conditions, but ATRP initiator and catalyst were not added to a solution.

Further increasing of the incompatibility by using two immiscible solvents resulted in separation of the layers after removal of the gel from a mold (**Figure VII.15**). Such a two-layer hydrophilic-hydrophobic gel was synthesized using toluene instead of DMF for pBMA layer by both ATRP and FRP. Under these conditions, the two-layer gel had a very weak bonding at the interface. Hence, the experimental results indicate that it is necessary to use mutually compatible solvent to create a sufficiently strong interface between the incompatible gel layers formed from two different monomers.

One approach to disperse/solubilize one phase into a second non-compatible phase is through the use of surfactants. Polymeric surfactants are especially efficient in dispersing one phase in another, due to their strong affinity towards the interface between the two phases.[24] Our group previously reported applications of miktoarm star copolymers for the

stabilization of Pickering emulsions.[25] It was shown that the stars consisting of hydrophilic PEO arms and hydrophobic PBA arms could efficiently disperse water-in-oil and form stable emulsion, even at exceptionally low concentrations (<0.01 wt. % vs. the total emulsion). We thus hypothesized that a similar miktoarm star with PEGMA and PBA arms (**Figure VII.16**) could improve connectivity of the final heterogeneous material, by locating at the interface and enhancing surface area between the prepared gel and precursor solution for the second gel. In order to investigate this hypothesis, we synthesized miktoarm star copolymer from $PEGMA_{2k}$ macromonomer, which contained 45 repeating units of ethylene glycol, and pBA_{20} macroinitiator, which consisted of ~20 repeating units. $PEGMA_{2k}$ macromonomer and pBA_{20} macroinitiator were crosslinked with divinylbenzene (DVB) to form the miktoarm star copolymer. Resulting star contained on average at least 10 arms based on apparent MW obtained from PMMA-based calibration.

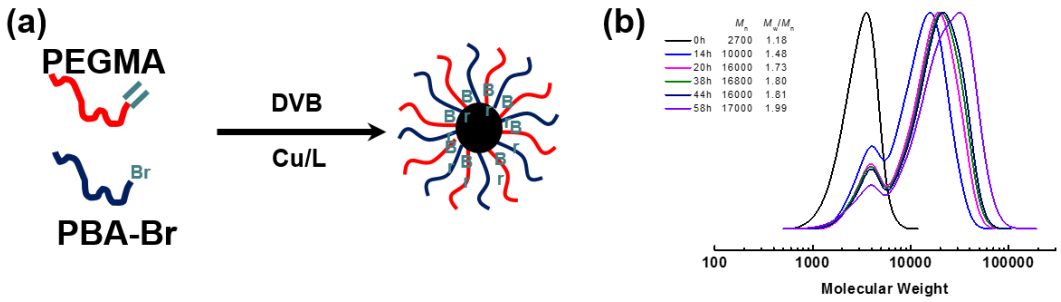

Figure VII.16. Preparation of miktoarm $PEGMA_{2k}$-pDVB-pBA_{20} (a), and its GPC traces (b). [PBA-Br]/[$PEGMA_{2k}$]/[DVB]/[$Sn(EH)_2$]/[$CuBr_2$]/[TPMA] = 0.5/0.5/14/0.2/0.01/0.1, [MI] = 0.02 M, 110°C, in anisole.

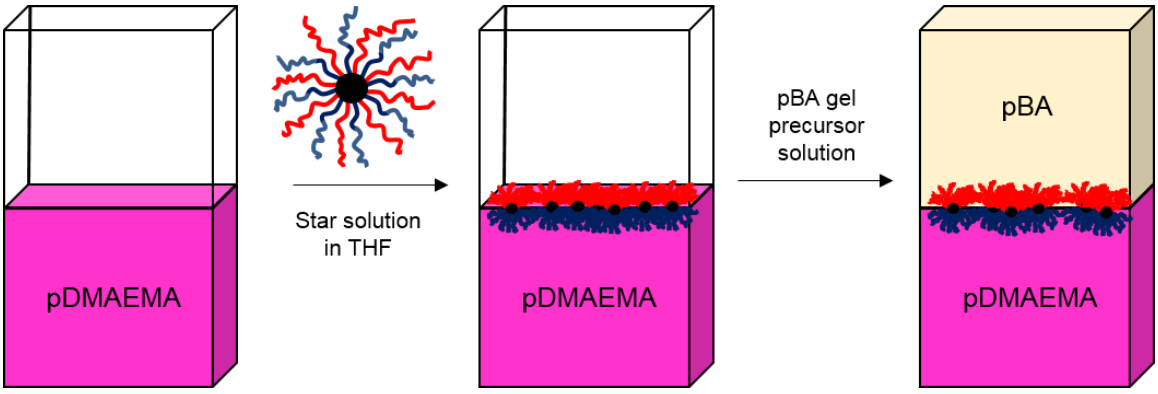

Scheme VII.2. Preparation of stackable gels with application of miktoarm star solution.

In the next set of experiments, we prepared the gels in immiscible solvents with the mikto-arm star copolymers at the interface of the hydrophilic PDMAEMA gel and BA/toluene gel solution for both ATRP and FRP. The star copolymer solution in THF, at a concentration 80 mg/mL, was added on top of first gel layer, a pDMAEMA gel that was formed in water (**Scheme VII.2**). THF was chosen as a solvent for the stars, due to good solubility of both arms in it, for addition at the interface. Arm solubility was confirmed by size distribution analysis by dynamic light scattering (DLS) technique (**Figure VII.17**), which showed that the star polymer's hydrodynamic radius in THF was around 10 nm. When star polymer was dissolved in toluene it experienced shrinking, which is indicative of the arms collapsing (green trace in **Figure VII.17),** and aggregated in aqueous solution (blue trace in **Figure VII.17).**

Previously reported coarse-grained molecular simulations showed that amphiphilic block copolymer grafted particles prefer to organize at the interface between two incompatible phases, with every block separating from each other into chemically identical area.[26,27] For the case of miktoarm star copolymers, we monitored how they would behave at the interface of a prepared hydrophilic gel and a solution of hydrophobic gel precursor (**Figure VII.18a**). For this modelling we used miktoarm stars consisting of 8 arms, each arm

consisting of 20 beads representing monomer units. The repulsion parameter was set to 60. According to the model, the mikto-arm star should prefer to stay at the interface between the two incompatible layers, segregating its arms from each other and solubilizing them in the compatible layer (i.e. PBA to the hydrophobic solution and PEGMA to the hydrophilic gel). It was concluded from the theoretical simulations, that it is possible for the mikto-arm stars to compatibilize hydrophilic and hydrophobic gels.

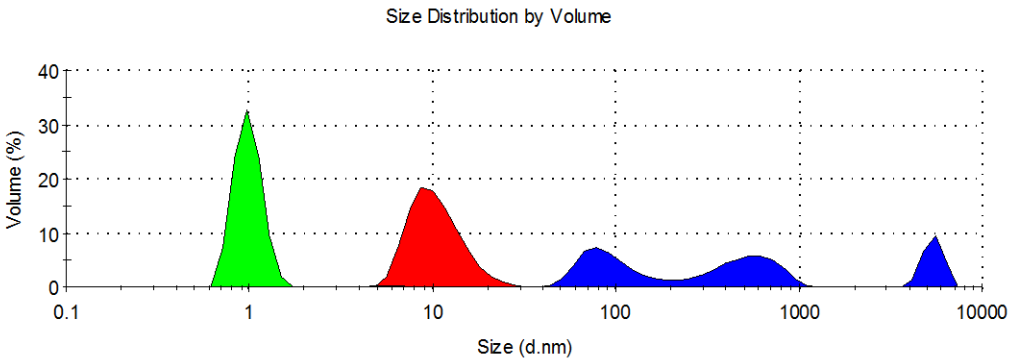

Figure VII.17. Size distribution of miktoarm PEGMA-PDVB-PBA star in different solvents: 1 mg/ mL in THF (red), 1 mg/mL in toluene (green), and 0.1 mg/mL in water (blue).

Experimental evaluation of the mikto-arm star copolymers as a "gluing" component for pDMAEMA and pBA gels demonstrated that such approach did not provide well-connected gels by the ATRP method, but resulted in formation of a sufficiently strong interface for gel prepared by FRP (**Figure VII.18b-c**). The gel prepared by FRP exhibited a strongly connected interface, which could withstand bending without damage (**Figure VII.19**). Such a drastic difference in integrity of the gels prepared by ATRP versus FRP could be potentially explained by the difference in the structure of the two gels. Gels prepared by RDRP methods are more homogeneous and exhibited a strongly delayed gel point compared to the FRP gels.[22,28-30] This results in a significant structural difference between the two gels prepared by these two methods. During the gelation process in FRP,

microgels are formed at an early stage of polymerization, resulting in heterogeneous material with higher number of crosslinks.[29] Gels prepared by ATRP have much smaller number of crosslinks per primary chain (much more initiator used) and consequently have looser structure and a higher swelling ratios.[22,29] They also have slower deswelling kinetics, explained by so-called "skin layer" effect, when gel surface collapses and acts as a barrier for transporting small molecules like water (or monomer and oligomers).[31] Thus, it is possible that a more homogeneous structure of ATRP gels hinders entanglement between two layers and star copolymers, and consequently prevents formation of an interconnecting interface.

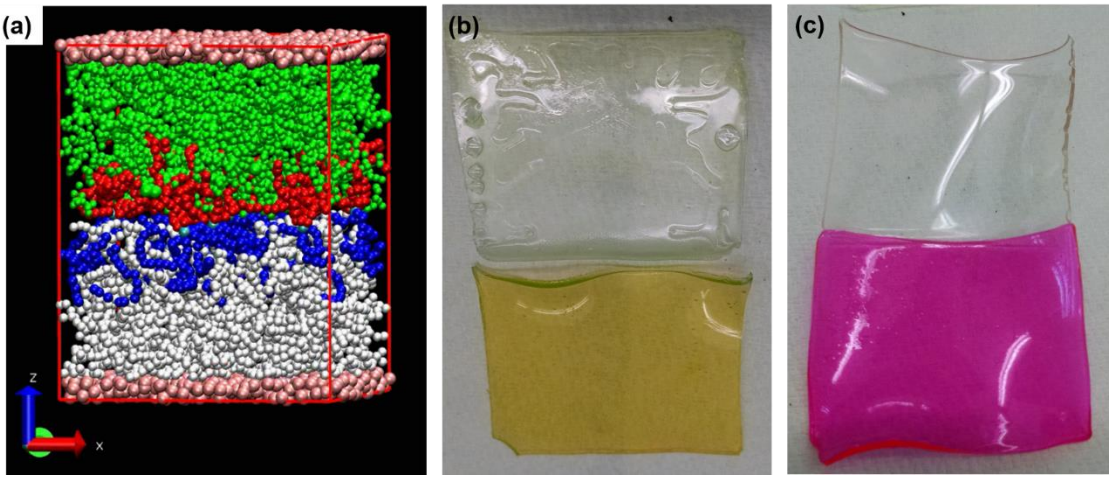

Figure VII.18. Star copolymer application to the interface between pDMAEMA in water – pBMA in toluene by ATRP and FRP. (a) Snapshot of the two-layer composite gel with stars arranged on the interface. The repulsion parameter *a* is set to 60 between A and B polymers. Blue arms are chemically identical to white layer, and red arms are chemically identical to green layer. (b) Heterogeneous gel synthesized by ATRP: [DMAEMA]:[PEG_{2k}iBBr]:[$PEGDMA_{750}$]:[$CuBr_2$]:[TPMA]:[VA-044]= 75:1:5:0.1:0.8:0.1 in water. The first layer contained fluorescein methacrylate at the 0.02:75 molar ratio to DMAEMA. ATRP conditions for the second layer: [BMA]:[PEG_{2k}iBBr]:[$PEGDMA_{750}$]:[$CuBr_2$]:[TPMA]:[V70]= 75:1:5:0.1:0.8:0.3 in toluene. (c) Heterogeneous gel synthesized by FRP: conditions of the composition were similar to ATRP conditions, but ATRP initiator and catalyst were not added to the solution. The first layer contained rhodamine methacrylate at the 0.02:75 molar ratio to DMAEMA.

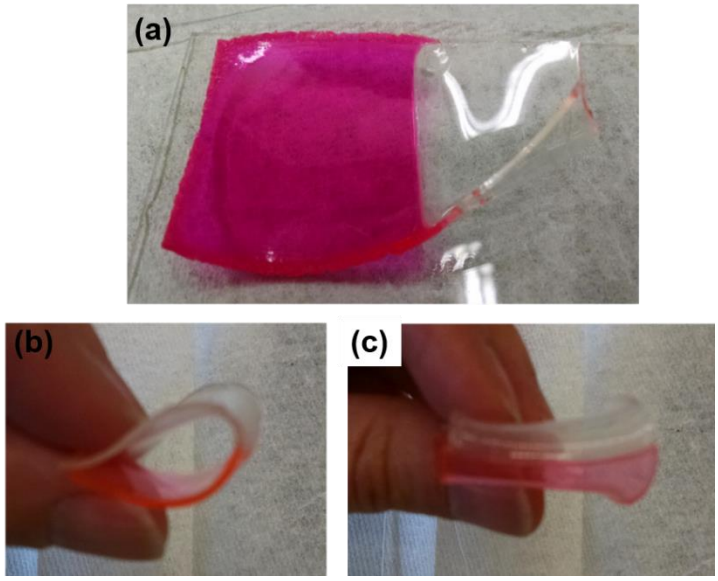

Figure VII.19. Mechanical stability of pDMAEMA in water gel – pBMA in toluene gel with miktoarm star copolymer in between prepared by FRP: (a) directly from the mold, (b, c) upon bending. Conditions for first layer: [DMAEMA]:[$PEGDMA_{750}$]:[VA-044] = 75:5:0.1 in water. The first layer contained rhodamine methacrylate at the 0.02:75 molar ratio to DMAEMA. Conditions for the second layer: [BMA]:[$PEGDMA_{750}$]:[V70]= 75:5:0.3 in toluene.

In the final set of experiments the combination of both ATRP and FRP synthesized gels was tested. In this case one layer was synthesized by ATRP and another layer was prepared by FRP. Both combinations where pDMAEMA gel was synthesized in water by ATRP and pBA gel was prepared in toluene on top of it by FRP and reverse order were tested. Solution of stars were applied in between two layers as in the previous experiment. Interestingly, after polymerization was complete both layers appeared to be glued to each other (**Figure VII.20**). In both cases, whether one began with either ATRP (**Figure VII.20a**) or FRP layer (**Figure VII.20b**), final gels were characterized by sufficiently strong interface between pDMAEMA and pBA layer demonstrated by their preserved integrity. This results suggested that combination of both methods can be used to create layered connected gel materials utilizing monomers polymerizable by either method.

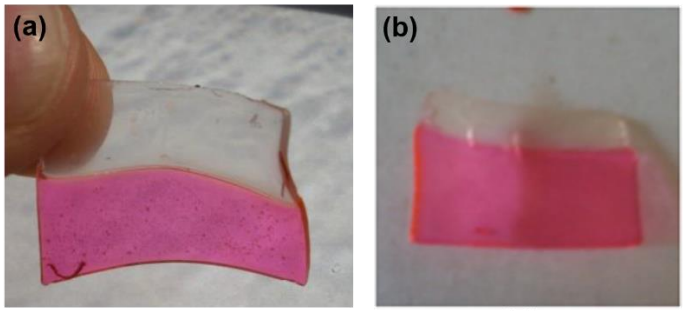

Figure VII.20. Star copolymer application to the interface to form ATRP/FRP hybrid gels between pDMAEMA in water – pBMA in toluene. (a) Heterogeneous gel, where first layer is synthesized by ATRP: [DMAEMA]:[PEG_{2k}iBBr]:[$PEGDMA_{750}$]:[$CuBr_2$]:[TPMA]:[VA-044]= 75:1:5:0.1:0.8:0.1 in water. The first layer contained rhodamine methacrylate at the 0.02:75 molar ratio to DMAEMA. Second layer was synthesized by FRP: [BMA] [$PEGDMA_{750}$]:[V70]= 75:5:0.3 in toluene. (b) Heterogenious gels, where first layer of pDMAEMA was synthesized in water by FRP, and second layer of pBA was synthesized by ATRP in toluene.

It must be stressed that simulations are limited to a relatively small area (ca. tens of nm) of the interface and experiments refer to macroscopic samples (ca. a few mm). Nevertheless, both simulation and experimental studies suggest that the presented approach can be utilized to prepare composite gels with the multiple stackable gel layers.

VII.4. Conclusions

Herein, we devised a novel approach to create stackable gels via successive polymerization reactions. In particular, a gel precursor solution consisting of initiator, monomer, and cross-linker was introduced on top of the underlying gel and underwent living copolymerization to form the new layer. The reactive species preserved in the living polymerization form chemical cross-links that covalently linked chains from different layers.

Using our recently developed DPD models, we first investigated the polymerization kinetics and gelation processes of the two-layer hydrophilic-hydrophilic gels. We characterized the interfacial strength between the layers by calculating the number of inter-gel cross-links. The findings indicate that the contribution of the active chain ends to the binding of the two layers at high conversion is dominant, as compared to that of residual cross-links with dangling vinyl groups. Following the prediction from the computational modeling, we experimentally realized the two-layer gel system by the multi-step polymerization. Mechanical evaluation of the materials showed that both multi-layered gels prepared either by ATRP or FRP preserved their integrity. Their mechanical properties were slightly reduced in comparison with single layered gels. Experiments suggest that interpenetration between chemically identical layers created a sufficiently strong interface even in the gels with only residual vinyl bonds contributing to the inter-gel cross-links (FRP). Simulations suggest that gels with chemically incompatible layers prepared by ATRP in the same solvent should have a strong interface between the layers. This behavior is attributed to the formation of inter-gel cross-links between the first and second layer due to the preserved active chain ends from the first layer. Results of experimental studies

support this mechanism. Namely, the three-layer composite gels prepared by ATRP preserved their connectivity upon bending, while the samples prepared by FRP broke. Thus, multi-layered gels prepared by ATRP are characterized by a stronger interface between layers than gels prepared by FRP.

Finally, we explored the application of a mikto-arm star copolymer as a compatibilizing agent at the interface between hydrophobic and hydrophilic gels prepared in immiscible solvents. Simulation results indicated that miktoarm stars prefer to organize at the interface with their arms segregating from each other into each layer forming dynamic Janus particles. This approach was successfully demonstrated with gels prepared by FRP, but failed to connect the two gels when the ATRP method was utilized. This can be explained by a significant difference in the structure of the ATRP gels versus the FRP gels. However, additional experimentation exploring combination of gel layers synthesized by consecutive ATRP and FRP revealed that such type of stackable gels were fully connected and preserved their integrity. Further studies elucidating the influence of the differences of polymerization method on the gels formation should be conducted to evaluate the effect on the connectivity between the two incompatible gels.

Overall, our approach provides a robust route for designing multi-layered, "stackable" gels, where each subsequent layer is effectively "stacked" on top of the previous layer. With each gel layer being covalently bound to the neighboring layers, the system displays considerable mechanical integrity and has the potential to compartmentalize distinct functionalities into the different layers for creating a range of multi-functional materials.

VII.5. Experimental section

VII.5.1. Materials.

2-(Dimethylamino)ethyl methacrylate (DMAEMA, 98%, Aldrich), n-butyl methacrylate (BMA, 99%, Aldrich), and poly(ethylene glycol) dimethacrylate ($PEGDMA_{750}$, average molecular weight 750, Aldrich) were passed over a column of basic alumina (Fisher Scientific) prior to use. Copper (II) bromide (99.999%, Aldrich), azo initiators 2,2'-Azobis[2-(2-imidazolin-2-yl)propane] dihydrochloride (VA-044, Wako) and 2,2'-Azobis(4-methoxy-2,4-dimethyl valeronitrile) (V70, Wako), methacryloxyethyl thiocarbamoyl rhodamine B (rhodamine methacrylate, Polysciences Inc.), fluorescein methacrylate (Sigma Aldrich), water (HPLC grade, Fisher Scientific), N,N-dimethylformamide (DMF, ACS grade, Fisher Scientific) were used as received. Tris(pyridin-2-ylmethyl)amine (TPMA)[32,33] and poly(ethylene glycol) isobutyryl bromide[34] ($PEG_{2k}iBBr$, average molecular weight 2000) were prepared as previously reported in literature.

VII.5.2. Instrumentation and characterization.

Monomer conversion was measured using ^1H NMR spectroscopy in D_2O using a Bruker Avance 500 MHz spectrometer at 44 °C. Elongation at break of prepared gels was measured on Instron 5943 equipped with a 50 N load cell.

VII.5.3. Gel synthesis.

Hydrophilic-hydrophilic two-layer gel by ATRP. DMAEMA stock solution was prepared from $PEG_{2k}iBBr$ (200 mg, 0.1 mmol), $PEGDMA_{750}$ (375 mg, 0.5 mmol), DMAEMA (1.178 g, 7.5 mmol), and 1.753 g of water. After that 1 ml of this stock solution was mixed with solution containing 20 mM $CuBr_2$ and 160 mM TPMA (150 µl), 60 mg/ml solution

of azo initiator VA-044 (17 µl), and 10 mg/ml solution of fluorescein or rhodamine methacrylate in DMF (50 µl). The solution was degassed, injected in a mold, and incubated at 44°C for 3h. The second solution was prepared with rhodamine methacrylate instead of fluorescein methacrylate and was injected on the top of layer 1. The gel was removed from the mold and dried under vacuum for 48 h before mechanical testing and swelling experiment. The sample was then swollen in water for 1 hour. The swelling ratio was calculated as: $swelling\ ratio = \frac{w_s - w_d}{w_d}$ where w_s and w_d are the weights of the swollen and dried hydrogels.

Hydrophilic-hydrophilic two-layer gel by FRP. This gel was synthesized similarly to the gel prepared by ATRP method, but contained only DMAEMA, $PEGDMA_{750}$, water, and VA-044 azoinitiator.

Hydrophilic-hydrophobic-hydrophilic three-layer composite gel by ATRP. DMAEMA stock solution was prepared from PEG_{2k}iBBr (200 mg, 0.1 mmol), $PEGDMA_{750}$ (375 mg, 0.5 mmol), DMAEMA (1.178 g, 7.5 mmol), and 1.753 g of DMF. After that 1 ml of this stock solution was mixed with solution containing 20 mM $CuBr_2$ and 160 mM TPMA in DMF (150 µl), 10 mg of azo initiator V70 (17 µl), and 10 mg/ml solution of fluorescein methacrylate in DMF (20 µl). The solution was degassed and 0.3 ml of it was injected in a mold, and incubated at 44°C for 3h.

BMA stock solution was prepared from PEG_{2k}iBBr (100 mg, 0.05 mmol), $PEGDMA_{750}$ (186 mg, 0.25 mmol), BMA (533 mg, 3.7 mmol), and 820 mg of DMF. After that 1 ml of this stock solution was mixed with solution containing 20 mM $CuBr_2$ and 160 mM TPMA (147 µl), azo initiator V70 (10 mg). The solution was degassed, 0.3 ml of it was injected in a mold, and incubated at 44°C for 3h.

The third layer was prepared in the same way as the first layer.

Hydrophilic--hydrophobic-hydrophilic three-layer composite gel by FRP. This gel was synthesized similarly to the gel prepared by ATRP method, but without ATRP initiator and catalyst. It contained only monomer, $PEGDMA_{750}$, solvent, and either VA-044 or V70 azoinitiator for water or DMF as a solvent respectively.

VII.5.4. Computational Model.

We use dissipative particle dynamics (DPD)[35-37] to model the formation of stackable, multi-layered gels. DPD is a coarse-grained, particle-based computational method that provides an effective means to simulate the time evolution of a many-body system governed by Newton's equation of motion, $m\,d\mathbf{v}_i/dt = \mathbf{f}_i$. An advantage of DPD over more the atomistic molecular dynamics (MD) is the ability to model physical phenomena occurring at relatively large length and time scales within computationally reasonable time frames.[35-37] In the DPD model, each bead represents a cluster of molecules. Moreover, each bead experiences a force $\mathbf{f}_i(t)$ that is the sum of three pair-wise additive forces: $\mathbf{f}_i(t) = \sum\left(\mathbf{F}_{ij}^{\mathrm{C}} + \mathbf{F}_{ij}^{\mathrm{D}} + \mathbf{F}_{ij}^{\mathrm{R}}\right)$. All pair-wise forces are truncated at a certain cutoff radius r_{c}. We describe these different pair-wise forces below.

The conservative force is a soft, repulsive force given by $\mathbf{F}_{ij}^{\mathrm{C}} = a_{ij}(1 - r_{ij})\hat{\mathbf{r}}_{ij}$, where a_{ij} is the maximum repulsion between beads i and j, $r_{ij} = \left|\mathbf{r}_i - \mathbf{r}_j\right| / r_{\mathrm{c}}$, and $\hat{\mathbf{r}}_{ij} = \mathbf{r}_{ij} / \left|\mathbf{r}_{ij}\right|$. This soft-core force leads to a degree of overlap between neighboring beads and permits the use of larger time steps than those commonly used in MD simulations. The drag force is $\mathbf{F}_{ij}^{\mathrm{D}} = -\gamma\omega_{\mathrm{D}}(r_{ij})(\hat{\mathbf{r}}_{ij} \cdot \mathbf{v}_{ij})\hat{\mathbf{r}}_{ij}$, where γ is a simulation parameter related to viscosity, ω_{D} is a weight function that goes to zero at r_{c}, and the relative velocity is $\mathbf{v}_{ij} = \mathbf{v}_i - \mathbf{v}_j$. The random

force is $\mathbf{F}_{ij}^{\mathrm{R}} = \sigma \omega_{\mathrm{R}}(r_{ij}) \xi_{ij} \hat{\mathbf{r}}_{ij}$, where ξ_{ij} is a zero-mean Gaussian random variable of unit variance and $\sigma^2 = 2k_{\mathrm{B}}T\gamma$. Here, k_{B} is the Boltzmann constant and T is the temperature of the system. We select weight functions to take the following form: $\omega_{\mathrm{D}}(r_{ij}) = \omega_{\mathrm{R}}(r_{ij})^2 = (1 - r_{ij})^2$ for $r_{ij} < r_{\mathrm{c}}$.

The time evolution of the system is captured by integrating the equation of motion via the modified velocity-Verlet algorithm.[38] In our simulations, we take r_{c} and $k_{\mathrm{B}}T$ as the characteristic length and energy scales, respectively. The characteristic time scale is then defined as $t = \sqrt{m r_{\mathrm{c}}^2 / k_{\mathrm{B}}T}$. By setting $g = 4.5$, we obtain a relatively rapid equilibration of the temperature in the system and the numerical stability of the simulations with a time step $\Delta t = 0.02\tau$.[37]

To simulate the ATRP process of forming a polymer gel, we utilize our recently developed, DPD-based living copolymerization reaction scheme.[39] The reactive components in the system are the initiator, monomer, and bifunctional cross-linker, which are all modeled as DPD beads. The bifunctional cross-linker encompasses two reactive cross-linking units, but is modeled by one DPD bead with five different "states", which indicate the effective reactivity of the cross-linker (i.e. the extent to which it has reacted).[39] The reaction kinetics for the ATRP are simulated by a set of elemental reactions and coupled to the dynamics of the system. Due to the characteristic of the living polymerization, we exclude termination and chain transfer reactions in the simulations.[9,39]

The polymerized chains are simulated with a bead-spring model, with a harmonic bond potential given by: $E_{\mathrm{bond}} = \frac{1}{2} K_{\mathrm{bond}} (r - r_0)^2$. Here, $K_{\mathrm{bond}} = 128$ is the elastic constant and $r_0 = 0.5$ is the equilibrium bond distance.[39] Other details of the simulated ATRP reaction

scheme can be found ref. [39]. In the current work, we form multi-layered gels by adding new layers on top of the existing ones through successive polymerization reactions. Namely, a solution of new initiator, monomer, and cross-linkers is injected on top of the old gel and these new components then undergo living copolymerization to form a new layer. Unless otherwise stated, the polymerization of each step reaches a monomer conversion of 0.95, which requires approximately $1x10^6$ simulation time steps. Living polymerization preserves reactive species in the old gel, including active ends and partially-reacted cross-linkers. These species can participate in successive reactions and form chemical cross-links that bind chains from different layers. In this manner, the layers are covalently linked and this multi-step living polymerization protocol enables the formation multiple layers of covalently-fused gels.

The size of our primary simulation box is $30 \times 30 \times (30N+10)$, where N is the number of layers. Periodic boundary conditions are imposed in all three directions. Each layer with a size $30 \times 30 \times 30$ is polymerized from a solution of initiator, monomer and cross-linkers. The ratio of the initial concentrations of these respective species is $[\mathrm{Ini}]_0/[\mathrm{X}]_0/[\mathrm{M}]_0 = 1/5/75$ or $1/10/150$ and the corresponding solvent concentration is $[\mathrm{S}]_0 = 50\%$. In other words, the ratio of initiator to cross-linker concentrations $[\mathrm{Ini}]_0/[\mathrm{X}]_0$ is varied while the ratio of cross-linker to monomer concentrations is held constant at $[\mathrm{X}]_0/[\mathrm{M}]_0 = 1/15$. We chose these respective concentrations to match corresponding values used in our experimental studies. Specifically, our reference case of $[\mathrm{Ini}]_0/[\mathrm{X}]_0/[\mathrm{M}]_0 = 1/5/75$ corresponds to values used in our experiments in sections A2 and B2 below. When the polymerization reaches full conversion, the polymer volume fraction of the gel f_p is 0.5.

The initial configuration of each new solution with the dissolved components is generated by randomly placing beads in a different box of size $30 \times 30 \times 30$.[17] The solution has been pre-equilibrated for 5×10^4 simulation time steps to reach equilibrium before being introduced into the primary simulation box. This process ensures that the diffusion between the existing gel layer and the new solution is not influenced by the initial configuration of the solution. To model gels with finite heights, we introduce top and bottom bounding layers of height 5 that effectively repel the gel and all the rest of the beads in the system.[17] The upper bounding layer is introduced into the system before the polymerization of the first gel layer to confine the solution to its defined size of $30 \times 30 \times 30$. When a new gel layer is added, the top bounding layer is moved above the new layer accordingly. Thus, the multi-layered gel is bounded by the layer of repulsive beads (which could represent the surrounding air[17]) in the transverse (z) direction, while the system is periodic in the lateral directions (x and y). The total bead number density of the system is $\rho = 3$.

The beads in the system can be categorized as hydrophilic or hydrophobic monomers, solvent, and moieties that form bounding (surface) layers. The interaction parameters between the components, a_{ij}, is set to $a_{ij} = 25$ for any two beads of the same moiety (in units of $k_B T / r_c$).[37] The values of the interaction parameters between chemically compatible and incompatible moieties are set to 25 and 35, respectively. The interaction between a bead within the bounding layer and all other beads is set to 60 to ensure separation between this bounding layer and all the other moieties within the simulation box.

ATRP Reaction Scheme. We model the ATRP process in the framework of DPD by introducing a set of elemental reactions. These reactions are coupled to the dynamics of the

system as we describe below. Like other non-reactive species in the system, the reactive components are also modeled as coarse-grained DPD beads, including the initiator, monomer, and bifunctional cross-linker.[39] In the simulation, we use different bead types to represent the "state" of the reactive species. For example, an unreacted monomer is specified as type "a", but this monomer changes to type "b" when it is added to a growing chain and becomes the new active end. Once the monomer has fully reacted, it is labeled as type "c". Similarly, we represent the "state" of the bifunctional cross-linker by the bead type, which indicates the extent to which the cross-linker has reacted. Namely, the bifunctional cross-linker encompassing two reactive cross-linking units can have five different "states" once it is activated.[16] These "states" for the cross-linker are as follows: one cross-linking unit being activated while the other remains unreacted, one cross-linking unit being fully reacted while the other remains unreacted, one cross-linking unit being fully reacted, while the other is activated, both cross-linking units being activated, and both cross-liking units being fully reacted. The result of the specific chemical reaction is modeled by updating the bead types after the reaction has occurred.[11,16,40]

The elemental reactions are the same as those considered in our previous work involving DPD simulations of ATRP.[39] ATRP is a living polymerization process, in which the chains continue to grow due to the low probability of termination reactions.[9] To model this process, we neglect chain termination reactions in the simulation.[11,16,41-43] Because the reactive species are coarse-grained, the reversible activation and deactivation processes of the active chain terminus in ATRP are not explicitly modeled here.[16,41] Thus, the corresponding equilibrium between dormant and active chains[9] is not considered in our model. Here, all chain ends remain active during the polymerization. In other words, our

reaction scheme only includes the initiation, propagation and cross-linking reactions, and we describe the details of the reaction steps below.

The reaction steps in our model is similar to several previous reaction models applied in coarse-grained MD and MC simulations.[11,16,40,42-46] First, a bead with free radical is randomly selected and serves as the reaction center. Once we pick the reaction center, we then check whether there are other reactive beads within an interaction radius r_i of this center. Following our previous work, we set $r_i = 0.7$ to obtain gel points consistent with experimental data and to reproduce linear first-order kinetics of ATRP.[39] If multiple reactive beads are located within the interaction range, one of them is picked at random. Between the selected reactive bead and the reaction center bead encompassing a radical species, a reacting pair is formed. Given the reacting pair, the elemental reaction involving the pair is determined according to the types of the two reacting beads.

Reaction probabilities $0 < P_r^x < 1$ are assigned in the simulation to characterize the reaction kinetics,[41-43,46] where the superscript x stands for the type of reaction. Namely, a random number between 0 and 1 is generated for each reaction. The number is then compared to the corresponding reaction probability. The reaction is accepted if the number is smaller than P_r^x, and is denied if the number is larger than P_r^x. A successful reaction changes the type of the reacting beads accordingly. Depending on the type of reaction, an irreversible bond may form between the reacting pair of beads.[39]

Within every reaction time step, the above steps are conducted for every bead with free radicals. But each bead is only allowed to go through the reaction procedure once per reaction step, no matter whether the reaction is accepted or denied, which is dictated by the

relevant reaction probability. The reaction steps are separated by a reaction interval $\tau_r = 0.2\,\tau$. In effect, the reactions are performed every 10 time steps.[41] By choosing different probabilities for the reactions, P_r^i, $P_r^{p,M}$, $P_r^{p,X}$, and $P_r^{p,P}$, we can effectively adjust the rate constants of the respective reactions: initiation, propagation with monomer, propagation with unreacted cross-linker, and propagation with partially reacted cross-linker.[46]

Relationship between Simulation Parameters and Experimental Values. We can relate the simulation parameters to physical length and time scales using the volume of water molecule and the self-diffusion coefficient of bulk water. If we assume that each solvent bead represents a volume of water consisting of 10 molecules,[47,48] we will obtain the characteristic length scale in our simulation of r_c = 0.97 nm[39] because 10 water molecules occupy a volume of 300 Å^3.[49] Once we know the characteristic length scale, the characteristic time τ can be determined as 0.21 ns by matching the diffusion constant of the DPD simulation to the self-diffusion coefficient of water.[37,49] Hence, the DPD simulation is capable of capturing behavior of complex fluid systems that are up to 100 nm in linear dimension during time frames up to tens of microseconds. While the simulation focuses on the nanoscale features of the interfacial region (i.e., details that are on the order of tens of nanometers as shown in Figs 3, 7, and 8), the experimental results shown in Figs. 6 and S4 highlight the macroscopic features of the interfacial region. By combining the simulation and experimental studies, we demonstrate the ability of forming covalent bonds across the interfaces in multi-layered gels formed through successive ATRP processes and can gain insight into the nanoscopic behavior that gives rise to the macroscopic interfacial properties. We note that the width and the density profiles within the interfacial region

depend on the diffusion rate of the monomers into the underlying gel and the polymerization rate in the solution above the gel.

The experimental values of the diffusion constant for a monomer within a gel is typically on the order of 10^{-6} to 10^{-7} cm^2/s.[50] The corresponding diffusion length is $2\sqrt{Dt}$,[51] and over the course of three hours (the time scale for the polymerization of the second layer), this length is equal to a few millimeters. The latter value is consistent with the width of the interfacial region in our experiments, as shown in Figs. 6 and S4.

In the simulation, we can estimate the diffusion constant for "type 2" monomers in the direction perpendicular to the interface. Namely, we assume the evolution of the density profile follows the 1D diffusion equation for interdiffusion, which gives the formula: $n(z,t) = \frac{n_0}{2}\left\{1 + erf\left[\left(z - z_i\right)/2\sqrt{Dt}\right]\right\}$.[51] Here, n is the concentration of "type 2" monomer as a function of time t and position in the z-direction, n_0 is the initial concentration of "type 2" monomer in the stock solution, z_i is the z position of the top surface of the first gel layer, and *erf* refers to the error function $erf\left(x\right) = \frac{2}{\sqrt{\pi}}\int_0^x e^{-t^2} dt$. From our simulations, we can obtain the density profile of "type 2" monomers in the first gel layer at some specific time t. We know the initial profile at $t = 0$. Hence, we can fit the density profile to the previous formula to get the value of D. From this estimate, we obtain a number that is on the order of 10^{-6} cm^2/s according to the above mentioned characteristic length and time scales, in agreement with experimental values.[50]

In terms of the polymerization rate, experiments have shown that the rate is approximately one monomer addition per second for the fastest ATRP process that preserves 90% of chain

end functionality.[52] In our experiments, the targeted degree of polymerization of primary chains is 75, which is defined by the ratio between the initial monomer concentration $[M]_0$ and initial initiator concentration $[Ini]_0$. The gel kinetics data shows that the polymerization reaches 88.6% conversion in two hours. We find that the experimental rate of polymerization is approximately one monomer per 100 seconds. In our polymerization scheme, monomer addition occurs every $\tau_r / P_r^{p,M}$ time interval. With the above characteristic time scale $\tau = 0.21\,\text{ns}$, the rate of polymerization in our simulations is one monomer addition per 8.4 ns. Thus, the rate of polymerization in the simulation is ten orders of magnitude faster than the corresponding experimental value. This indicates that the simulated polymerization process is highly accelerated compared to the experiments, while the simulated diffusion is consistent with the experiments. Hence, the accelerated polymerization results in the formation of a nanoscale interfacial region (compared with the millimeter-sized interface observed in the experiments), which contains covalent bonds across the interface to bridge the different gel layers. Notably, we previously validated that with sufficiently low reaction probability guaranteeing kinetically controlled reactions, our accelerated polymerization simulation is capable of accurately reproducing ATRP polymerization.[39]

VII.6. References

(1) Stukalin, E. B.; Cai, L.-H.; Kumar, N. A.; Leibler, L.; Rubinstein, M. *Macromolecules* **2013**, *46*, 7525.

(2) Rose, S.; Prevoteau, A.; Elziere, P.; Hourdet, D.; Marcellan, A.; Leibler, L. *Nature* **2014**, *505*, 382.

(3) Meddahi-Pellé , A.; Legrand, A.; Marcellan , A.; Louedec, L.; Letourneur, D.; Leibler, L. *Angew. Chem. Int. Ed.* **2014**, *53*, 6369.

(4) Banik, S. J.; Fernandes, N. J.; Thomas, P. C.; Raghavan, S. R. *Macromolecules* **2012**, *45*, 5712.

(5) Wu, Z. L.; Moshe, M.; Greener, J.; Therien-Aubin, H.; Nie, Z. H.; Sharon, E.; Kumacheva, E. *Nature Communications* **2013**, *4*.

(6) Wei, Z. J.; Jia, Z.; Athas, J. M.; Wang, C. Y.; Raghavan, S. R.; Li, T.; Nie, Z. H. *Soft Matter* **2014**, *10*, 8157.

(7) Matyjaszewski, K.; Tsarevsky, N. V. *J. Am. Chem. Soc.* **2014**, *136*, 6513.

(8) Matyjaszewski, K. *Macromolecules* **2012**, *45*, 4015.

(9) Matyjaszewski, K.; Xia, J. *Chem. Rev.* **2001**, *101*, 2921.

(10) Wang, J.-S.; Matyjaszewski, K. *J. Am. Chem. Soc.* **1995**, *117*, 5614.

(11) Gao, H.; Polanowski, P.; Matyjaszewski, K. *Macromolecules* **2009**, *42*, 5925.

(12) Gao, H.; Li, W.; Matyjaszewski, K. *Macromolecules* **2008**, *41*, 2335.

(13) Jiang, C.; Shen, Y.; Zhu, S.; Hunkeler, D. *J. Polym. Sci., Part A: Polym. Chem.* **2001**, *39*, 3780.

(14) Gao, H.; Matyjaszewski, K. *Prog. Polym. Sci.* **2009**, *34*, 317.

(15) Oh, J. K.; Tang, C.; Gao, H.; Tsarevsky, N. V.; Matyjaszewski, K. *J. Am. Chem. Soc.* **2006**, *128*, 5578.

(16) Polanowski, P.; Jeszka, J. K.; Matyjaszewski, K. *Polymer* **2010**, *51*, 6084.

(17) Esteves, A. C. C.; Lyakhova, K.; van der Ven, L. G. J.; van Benthem, R. A. T. M.; de With, G. *Macromolecules* **2013**, *46*, 1993.

(18) Aradian, K.; Raphael, E.; de Genness, P. G. *Macromolecules* **2000**, *33*, 9444.

(19) Lee, D. I. *Polymer* **2005**, *46*, 1287.

(20) Matyjaszewski, K.; Jakubowski, W.; Min, K.; Tang, W.; Huang, J.; Braunecker, W. A.; Tsarevsky, N. V. *Proc. Natl. Acad. Sci. U.S.A.* **2006**, *103*, 15309.

(21) Norisuye, T.; Morinaga, T.; Tran-Cong-Miyata, Q.; Goto, A.; Fukuda, T.; Shibayama, M. *Polymer* **2005**, *46*, 1982.

(22) Yoon, J. A.; Gayathri, C.; Gil, R. R.; Kowalewski, T.; Matyjaszewski, K. *Macromolecules* **2010**, *43*, 4791.

(23) Davis, K. A.; Matyjaszewski, K. *Adv. Polym. Sci.* **2002**, *159*, 1.

(24) Garnier, S.; Laschewsky, A.; Storsberg, J. *Tenside Surfact. Det.* **2006**, *43*, 88.

(25) Li, W.; Yu, Y.; Lamson, M.; Silverstein, M. S.; Tilton, R. D.; Matyjaszewski, K. *Macromolecules* **2012**, *45*, 9419.

(26) Estridge, C. E.; Jayaraman, A. *ACS Macro Letters* **2015**, *4*, 155.

(27) Seo, Y.; Brown, J. R.; Hall, L. M. *Macromolecules* **2015**, *48*, 4974.

(28) Yu, Q.; Xu, S.; Zhang, H.; Ding, Y.; Zhu, S. *Polymer* **2009**, *50*, 3488.

(29) Ide, N.; Fukuda, T. *Macromolecules* **1999**, *32*, 95.
(30) Scherf, R.; Müller, L. S.; Grosch, D.; Hübner, E. G.; Oppermann, W. *Polymer* **2015**, *58*, 36.
(31) Kaneko, Y.; Yoshida, R.; Sakai, K.; Sakurai, Y.; Okano, T. *Journal of Membrane Science* **1995**, *101*, 13.
(32) Tyeklar, Z.; Jacobson, R. R.; Wei, N.; Murthy, N. N.; Zubieta, J.; Karlin, K. D. *J. Am. Chem. Soc.* **1993**, *115*, 2677.
(33) Xia, J.; Matyjaszewski, K. *Macromolecules* **1999**, *32*, 2434.
(34) Lee, S. B.; Russell, A. J.; Matyjaszewski, K. *Biomacromolecules* **2003**, *4*, 1386.
(35) Hoogerbrugge, P. J.; Koelman, J. M. V. A. *Europhys. Lett.* **1992**, *19*, 155.
(36) Espanol, P.; Warren, P. *Europhys. Lett.* **1995**, *30*, 191.
(37) Groot, R. D.; Warren, P. B. *J. Chem. Phys.* **1997**, *107*, 4423.
(38) Plimpton, S. *J. Comput. Phys.* **1995**, *117*, 1.
(39) Yong, X.; Kuksenok, O.; Matyjaszewski, K.; Balazs, A. C. *Nano Lett.* **2013**, *13*, 6269.
(40) Polanowski, P.; Jeszka, J. K.; Li, W.; Matyjaszewski, K. *Polymer* **2011**, *52*, 5092.
(41) Liu, H.; Li, M.; Lu, Z.-Y.; Zhang, Z.-G.; Sun, C.-C. *Macromolecules* **2009**, *42*, 2863.
(42) Turgman-Cohen, S.; Genzer, J. *Macromolecules* **2010**, *43*, 9567.
(43) Turgman-Cohen, S.; Genzer, J. *J. Am. Chem. Soc.* **2011**, *133*, 17567.
(44) Akkermans, R. L. C.; Toxvaerd, S.; Briels, W. J. *J. Chem. Phys.* **1998**, *109*, 2929.
(45) Milchev, A.; Wittmer, J. P.; Landau, D. P. *J. Chem. Phys.* **2000**, *112*, 1606.
(46) Genzer, J. *Macromolecules* **2006**, *39*, 7157.
(47) Fuchslin, R. M.; Fellermann, H.; Eriksson, A.; Ziock, H.-J. *J. Chem. Phys.* **2009**, *130*.
(48) Spaeth, J. R.; Kevrekidis, I. G.; Panagiotopoulos, A. Z. *J. Chem. Phys.* **2011**, *134*.
(49) Groot, R. D.; Rabone, K. L. *Biophys. J.* **2001**, *81*, 725.
(50) Amsden, B. *Macromolecules* **1998**, *31*, 8382.
(51) Crank, J. *The Mathematics of Diffusion*; Second Edition ed.; Oxford University Press Inc.: New York, 1980.
(52) Zhong, M.; Matyjaszewski, K. *Macromolecules* **2011**, *44*, 2668.

Chapter VIII. Summary and Outlook

The goal of this thesis was to investigate how to control ATRP in aqueous media and apply the developed methods towards preparation of functional materials for a range of bio-applications. Prior art, reviewed in the Chapter I, had already indicated that aqueous ATRP could be used for preparation of various water-soluble polymers and hybrid materials such as bioconjugates, grafted particles and functional surfaces. However, many reported materials were characterized by relatively high dispersities, inefficient initiation or low retention of chain-end functionality. Furthermore, most of reports only focused on use of normal ATRP with high concentrations of catalyst. Such results suggested that additional systematic studies had to be conducted to evaluate the effect of different parameters on the level of control possible in ATRP when the reaction is conducted in water.

The synthesis of well-defined materials is especially important for the preparation of bioconjugates particularly because the uniformity of materials, which are intended to be used in bio-related settings, is extremely important for a reproducible biological response. Therefore, Chapters II – IV discuss the development of aqueous ATRP methods and application of the improved procedures towards controlled "grafting from" a protein under biocompatible conditions. Chapter II describes development of fundamental polymerization conditions to prepare protein-polymer hybrids with narrow molecular weight distribution (MWD) while attaining high monomer conversions. Both normal and AGET ATRP were investigated, and it was determined that slow feeding of a reducing agent during an AGET ATRP allowed preparation of well-defined protein-polymer hybrids utilizing active catalyst systems, like Cu/TPMA. The combination of an active

hydrolytically stable catalyst with slow feeding of ascorbic acid as the reducing agent resulted in development of a well-controlled polymerization reaching high monomer conversion, and producing polymers with low dispersity. This method was also successfully utilized for polymerization in buffered solutions, which is important for polymerization in the presence of biomolecules. Normal ATRP under such conditions provided only limited monomer conversion and formed polymers with broad MWDs. Chapter III took the developed aqueous AGET ATRP procedure one step further and described development of a well-controlled ARGET ATRP with low ppm (<300 ppm) concentrations of a copper catalyst. Such an improvement was important for grafting from proteins with limited stability, as well as for providing easier purification and reduced overall cost.

Chapter IV focused on the development of novel bio-inspired iron catalysts. A stable iron porphyrin based catalyst was utilized to successfully catalyze ATRP in aqueous media. It was additionally shown that this type of complex can potentially be useful for polymerization of acidic monomers.

The logical progress of these projects would result in the application of the developed methods for the preparation of functional bioconjugates. For instance, in our group, my collaborator Dr Saadyah Averick applied ARGET ATRP for grafting from a green fluorescent protein (GFP) and directly from a DNA macroinitiator. Similar methods could also be applied to direct synthesis of other interesting PPHs. Currently, very few protein-polymer hybrids have been commercialized by the pharmaceutical industry. One of the noted advantages of the "grafting from" method detailed in this work is easier purification procedures and more efficient selective modification of proteins. Application

of the grafting from method to one of the proteins, whose conjugate with a polymer is currently used commercially, could result in a higher quality and more uniform conjugate. Full chemical, biological, and economic analysis of this procedure for preparation of uniform protein-polymer hybrids by "grafting from" by RDRP methods would reveal the true potential of this approach.

Future improvements in the field would include polymerization of other bio-compatible responsive monomers, other than PEG-based monomers, in a well-controlled manner. Several publications demonstrated that sugar-functionalized polymers, zwitterionic copolymers, and some other functional polymers provide more stable conjugates. This current trend in this field is focused on development of bioconjugates that respond to specific environments with a living body and to external directed stimulation. Thus evaluating properties of such conjugates detailed herein for treatment of specific conditions would be fruitful for product development.

Grafting only one single polymer chain from a specific site in a complex protein is difficult due to concentration dependent solubility of proteins. Proteins and peptides tend to aggregate at concentrations higher than 2-3 mg/ml. Therefore the resulting ATRP initiator concentration for proteins, with only one attached initiating moiety, is quite low (~0.1 – 0.5 mM). This means that synthesis of PPHs with lower MW polymers can be especially difficult because a very dilute monomer solution has to be used to achieve the appropriate degree of polymerization. Preparation of various MW conjugated polymers under dilute initiator and monomer conditions should be investigated further in order to define conditions that allow one to obtain reproducible results.

Iron porphyrins were not evaluated for grafting from a protein in the work reported in this thesis. However, their high stability could be advantageous for such an application, particularly since copper complexes of medium or low stability can often cause protein denaturation due to interaction with copper ions. Additionally, iron porphyrin based catalyst, can be used for modification of proteins with acidic monomers like methacrylic acid. It was shown that such modifications produced high stability conjugates of interest in pharmaceutical areas and in biocatalysis.

In terms of catalyst development, there are several advances which could be targeted. Control over a copper mediated ATRP can be improved when the reaction is carried out under increased pressure. High pressure ATRP is characterized by faster and well-controlled reaction, when copper complexes were used as catalysts. But this approach failed to improve polymerization when iron was used as a catalyst due to formation of catalytically less active species. However, it would be interesting to investigate the influence of pressure on performance of a stable iron based complex such as iron porphyrins. Furthermore, easier removal and potential recycling of the catalyst would be beneficial for application of iron porphyrins. It was reported that catalysts with an attached temperature-sensitive polymer chain could be removed from solution and recycled. This approach could be tested for iron porphyrin complexes.

Biocatalysis is another area, which could benefit from continued development of protein-polymer conjugates. Several publications have disclosed modification of certain enzymes with polymers showing improved stability. However, this field remains highly dependent on protein-polymer hybrids prepared by “grafting from” by RDRP methods. Modifications of proteins with stimulus responsive polymers could influence not only

performance and stability of proteins, but the whole technological process. Easier separation procedures and recycling could be achieved. Additionally, in the current state of the art, proteins are immobilized on a resin for application as biocatalysts. However, certain valuable enzymes don't perform well under such conditions. Modification with polymers could be beneficial for improved stability and performance of such proteins in homogeneous media.

Chapter V explored preparation of ester-containing degradable copolymers by ATRP and it was demonstrated that copolymerization of vinyl monomers with a cyclic ketene acetal monomer (CKA) could successfully generated uniformly degradable polymers. However the copolymers produced by this preliminary approach were characterized by relatively broad MWDs and by limited efficiency of block copolymer synthesis. These product limitations could be due to inefficient ring-opening, resulting in formation of chain-ends, which can't be easily activated by the catalyst. Immediate future work should include optimization of conditions for attaining maximum ring-opening efficiency and measurement of reactivity ratios of different CKAs with both acrylates and methacrylates. Once satisfactory polymerization conditions are identified, this class of copolymers could be applied to the preparation of functional materials: block copolymers, star copolymers and brushes. Furthermore, radical ring-opening by ATRP should be explored for other cyclic monomers. For instance, lipoamide would be interesting candidate to incorporate sulfur into a backbone.

Chapter VI described ATRP of a hydrophilic inimer in inverse microemulsion to generate cationic nanogels with particle size control throughout the polymerization. The development of this method provides a convenient procedure for the synthesis of

hydrophilic cationic core-shell nanogels without Ostwald ripening. However, a big disadvantage of current microemulsion polymerization procedures is the use of high concentrations of surfactant. Many surfactants are highly toxic for cells, even at μg/ml concentrations, and have to be removed prior to biological testing. Therefore, purification is very costly and time consuming. Thus, future development of this project could include polymerization of inimers under miniemulsion conditions since miniemulsion procedures typically require 3 times less surfactant compared to microemulsion. Additionally, design of a reactive surfactant with better stabilization properties could provide additional advantages by creating a system where the surfactant is fully embedded in the nanogel, and purification is not required. Such types of nanogels could be potentially used for dual delivery of nucleic acids and hydrophobic drugs.

Chapter VII was focused on preparation of macrogels and how hydrophilic and hydrophobic gels could be merged into one material. Through combining computational modelling and experimentation, we showed that integrated heterogeneous gels could be efficiently prepared. Stackable gels, where each subsequent layer of gel was grown from a previously prepared gel, could be synthesized either by ATRP, FRP or combination of both radical polymerization procedures. The procedures disclosed in this Chapter could be further applied to the preparation of layered polymeric networks, and would allow for combination of a variety of polymers with differing properties. Such materials could be of interest in such areas as tissue engineering, wound healing, or soft actuators.

Overall, it was demonstrated in this Thesis that biocompatible aqueous ATRP can be efficiently conducted using various approaches and catalysts. Conditions were identified that allowed both homogeneous solution and dispersion polymerizations to be conducted,

yielding a diverse spectrum of materials including linear and block copolymers, bioconjugates, nanogels and macrogels. To date, a large body of literature reported successful preparation and analysis of similar types of materials. However, several hurdles had to be tackled for a viable application of material development specifically for the biomedical field. Efficient translation of biological results *in vitro* to *in vivo* is extremely important, but it still remains a very challenging target. Thus, continued collaborative efforts with chemical, material or biomedical engineers could result in further optimization of technology and cost-effective production.